Tracing carbon fluxes within two distinct microbial communities in anaerobically methane oxidising mats by stable isotope probing

Dissertation

Zur Erlangung des Doktorgrades der Naturwissenschaften

im Fachbereich Geowissenschaften der Universität Hamburg

vorgelegt von

Sebastian Bertram

aus

Dortmund

Hamburg
2012

Als Dissertation angenommen vom Fachbereich Geowissenschaften der Universität Hamburg

Auf Grund der Gutachten von Prof. Dr. Walter Michaelis
Dr. Martin Blumenberg

Hamburg, den 19.06.2012

Prof. Dr. Jürgen Oßenbrügge
Leiter des Department Geowissenschaften

“All truths are easy to understand once they are discovered; the point is to discover them.”

Galileo Galilei (1564 - 1642)

Table of content

Abbreviations

AAA - AOM-associated archaea
ai - *anteiso*
Ac - acetate
Ac-CoA - acetyl-coenzym A
Ac-Pi - phosphorylated
ANME - **AN**aerobic **ME**thanotrophic (archaea)
AOM - anaerobic oxidation of methane
approx. - approximate
apr - APS-reductase
APS - adenosine-5'-phosphosulfate
aps - ATP-sulfurylase
AQDS - anthraquinone-2,6-disulfonate
assim. - assimilation
ATP - adenosine-5'-triphosphate
BGR - Bundesanstalt für Geowissenschaften und Rohstoffe
(Federal Institute for Geosciences and Natural Resources)
BSTFA - N,O-bis(trimethylsilyl)trifluoroacetamide
b.p. - before present
c - *cis*
C_{t_x} - Concentration at the time x
CARD-FISH - catalyzed reporter deposition-fluorescence *in-situ* hybridisation
CHN - carbon, hydrogen, nitrogen
C/N - ratio of carbon to nitrogen
CNS - carbon, nitrogen, sulphur
CODH/ ACS - carbon monoxide dehydrogenase/ acetyl-CoA synthase
comp. - compound
Conc. - concentration
CsCl - caesium chloride
$C_{31:3}$ - hentriacontatrien
$C_{35:x}$ - isoprenoid hydrocarbon with 35 carbon atoms (with 5-7 double bonds)
$C_{40:x}$ - biphytane, (0-asaturated, 1 - monopentacyclic, 2 - dipentacyclic)
d - day
DAG - diacylglyceride
DAGE - dialkyl glycerol ether
DBB - Desulfobulbus
DCM - dichloromethane
derivat. - derivatised
dest. - distilled
DGGE - denaturing gradient gel electrophoresis
DIC - dissolved inorganic carbon
DMDS - dimethyl disulphide

DNA - desoxynucleic acid
dsr - dissimilatory sulphite reductase
dw - dry weight
EA - elemental analyser
Ech - energy-converting hydrogenase
EI - electron impact (ionisation)
e.g. - [*latin for exampli gratia*] for example
EPS - extracellular polymeric substance
eV - electron Volt
fa - fatty acid
Fd_{ox} - oxidised ferredoxin
Fd_{red} - reduced ferredoxin
FID - flame ionisation detector
FISH - fluorescence *in-situ* hybridisation
Fmd - formylmethanofuran dehydrogenase
Fpo - energy-converting $F_{420}H_2$ dehydrogenase complex
Frh - F_{420}-reducing hydrogenase
Ftr - formylmethanofuran:H_4SPT formyltransferase
FW - freshwater
g - gram
GC - gas chromatograph
GC-c-IRMS - gas chromatograph coupled isotope ratio mass spectrometry
GDGT - glycerol dialkyl glycerol tetraether
GoM Arc - Gulf of Mexico archaea
Gt - giga tones
GWP - global warming potential
h - hour
Hdr - heterodisulphide reductase
H_4MPT - tetrahydromethanopterin
H_4SPT - tetrahydrosarcinopterin
HSG - headspace gas
HSV - headspace volume
i - iso
i.d. - internal diameter
IPCC - Intergovernmental Panel on Climate Change
IPL - intact polar lipid
IS - internal standard
l - litre
K - kelvin
kj - kilo joule
M - molar
M^+ - molecule ion (positive)
m - meter
Ma - million years

MAGE - monoalkyl glycerol ether
Ma-Rnf - membrane-bound ferredoxin dehydrogenase
Mch - methenyl-H_4SPT cyclohydrolase
mcrA - methyl-coenzymeM reductase, subunit A
MePH - methanophenazine
Mer - methylene-H_4SPT reductase
MFR - methanofuran
mM - millimolar
mm - millimeter
mg - milligram
min - minute
ml - millilitre
MPa - mega pascal
MPR - methane production rate
MS - mass spectrometry
Mtd - methylene-H_4SPT dehydrogenase
Mtr - methyl-H_4SPT:HS-CoM methyltransferase
Mvh - methyl viologen hydrogenase
N - normality
n.a. - not analysed
NADH - nicotinamide adenine dinucleotide hydrogen
NADPH - nicotinamide adenine dinucleotide hydrogen phosphate
ng - nanogram
nM - nanomolar
n.m. - not measured
nuo - NADH:quinone oxidoreductase
Pa - pascal
PCA - principal compound analysis
PCR - polymerase chain reaction
PFOR - pyruvate ferredoxin:oxidoreductase
PLFA - phospholipid fatty acids
pg - picogram
PMI - pentamethylicosane/ -ene
ppb - part per billion
ppm - part per million
qPCR - quantitative polymerase chain reaction
RNA - ribonucleic acid
RT-qPCR - reverse transcriptase - quantitative polymerase chain reaction
RV - research vessel
$R_{v\text{-}PDB}$ - ratio of the Vienna Pee Dee Belemnite
SIP - stable isotope probing
SIMS - secondary ion mass spectrometry
SMTZ - sulphate methane transition zone
SR - sulphate reduction

SRB - sulphate reducing bacteria
SRR - sulphate-reduction rate
t - *trans*
t - time
TAG - triacylglyceride
TCA - tricarboxylic acid
TEA - terminal electron acceptor
THF - tetrahydrofolate
TMA - trimethyl ammonium
TMCS - trimethylchlorosilane
TOC - total organic carbon
T-RFLP - terminal restriction fragment length polymorphism
VFA - volatile fatty acid
Vho - methanophenazine reducing hydrogenase
V-PDB - Vienna Pee Dee Belemnite
vs. - versus
v/v - volume to volume
wt - weight
µg - micro gram
µl - micro litre
µM - micro molar
µmol - micro mol
µ - micro
µm - micrometer
µg - microgram
°C - grad Celsius

Vorwort und Zielsetzung

Methan ist ein bedeutendes Treibhausgas und beeinträchtigt das globale Klima. Die Konzentration in der Atmosphäre hat sich seit Beginn der Industrialisierung mehr als verdoppelt. Neben anthropogenen gibt es auch bedeutende natürliche Quellen. So werden beispielsweise in anoxischen marinen Sedimenten große Mengen an Methan gebildet, von denen jedoch nur ein kleiner Teil in die Wassersäule und die Atmosphäre emittiert wird. Jedoch vermindert die anaerobe Oxidation von Methan (AOM) bis zu 85% der Methanemission aus den marinen Sedimenten. Dieser Prozess ist damit im globalen Methankreislauf von erheblicher Bedeutung, da er letztlich die Methankonzentration in der Atmosphäre mit reguliert (del Giorgio und Duarte, 2002; Reeburgh, 2007).

Obwohl bereits Ende der siebziger Jahre durch Reeburgh (1976) sowie Barnes und Goldberg (1976) aufgrund von Porenwasserprofilen dieser Prozess als wahrscheinlich beschrieben wurde, gelang es erst 1999 Hinrichs et al., gefolgt von Boetius et al. (2000) entsprechende Euryarchaeota zu identifizieren und direkt mit biogener anaerober Methanoxidation in Verbindung zu setzen. Die identifizierten Archaeen werden in drei Gruppen aufgeteilt, ANME-1, -2 und -3 (**AN**aerobe **ME**thanotrophe Archaeen), die wiederum unterschiedliche Subgruppen enthalten. Diese methanotrophen Archaeen sind nah verwandt mit verschiedenen methanogenen Ordnungen, den Methanomicrobiales, Methanosarcinales und Methanococcales (Hinrichs et al., 1999; Boetius et al., 2000; Knittel et al., 2005). Wenngleich jüngst auch AOM unter Verwendung anderer Elektronenakzeptoren nachgewiesen wurde, so ist in marinen Sedimenten der Prozess der AOM mit an sulfatreduzierende Bakterien (SRB) gekoppelt. Deshalb wird er auch als sulfatabhängige AOM beschrieben. Unter Standardbedingungen liefert die sulfatabhängige AOM nur sehr wenig Energie (Barnes et al., 1976).

$$CH_4 + SO_4^{2-} \rightarrow HCO_3^- + HS^- + H_2O$$

$$\Delta G^0 = -22{,}8 \text{ kJ/mol}$$

Viele physiologische Details der AOM sind immer noch ungeklärt. Heute wird die sulfatabhängige AOM als reverser Prozess der Methanogenese betrachtet. Dies ist gestützt durch die Entdeckung eines neuen nickelbindenden Coenzyms F_{430} in ANME-1 und genomanalytische Untersuchungen von Umweltproben (Krüger et al., 2003; Hallam et al., 2004; Meyerdierks et al., 2005, 2010; Shima et al., 2011).

Bisher sind noch keine Isolate kultiviert worden, weder der ANME-1, -2 oder -3, noch der assoziierten sulfatreduzierenden δ-Proteobakterien. Neben ANME und SRB zeigten jüngere molekularbiologische Untersuchungen interessanterweise eine hohe mikrobielle Diversität an entsprechenden AOM Standorten. Jedoch blieben der Metabolismus und die Funktionsweise dieser Gemeinschaften immer noch ungeklärt. Frühere Studien demonstrierten ein methanogenes Potential mit unterschiedlichen Substraten (Seifert et al., 2006; Treude et al., 2007; Orcutt et al., 2008).

Eine Möglichkeit um Kohlenstoffflüsse in mikrobiellen Matten zu untersuchen, ist die Inkubation mit isotopisch markierten Substraten, sogenanntes (*englisch*) Stable Isotope Probing (SIP; Boschker et al., 1998). Neben der so erlaubten Verfolgung des Substratkohlenstoffs in die Gesamtbiomasse, können auch verschiedene organismenspezifische Lipidbiomarkermoleküle verwendet werden, die einen Einblick in die physiologische Strategie der Mitglieder dieser mikrobiellen Gemeinschaft ermöglichen.

In dieser Arbeit wurden vorherige Markierungsstudien (Methan, Bikarbonat; Blumenberg et al., 2005; Wegener et al., 2008a; Jagersma et al., 2009) um bislang nicht untersuchte ^{13}C-angereicherte Substrate (Acetat, Methanol) erweitert, um AOM abhängige und methanunabhängige Stoffwechsel zu untersuchen. Dazu wurden zwei AOM-basierte mikrobielle Lebensgemeinschaften aus dem Schwarzen Meer untersucht. Hierbei handelte es sich um ANME-1 oder ANME-2 dominierte Gemeinschaften (Michaelis et al., 2002; Blumenberg et al., 2004), so dass beide Vergesellschaftungen erstmals getrennt diesbezüglich analysiert werden konnten. Begleitend wurden die Raten des Methankonsums, der Methanbildung und der Sulfatreduktion bestimmt, um die Aktivitäten der jeweiligen untersuchten ANME-Archaeen und der entsprechenden sulfatreduzierenden Bakterien zu verfolgen. Die Methan- und Bikarbonatansätze ähneln dabei den entsprechenden *in-situ* Bedingungen. Mit Acetat wurden heterotrophe Eigenschaften der gesamten Gemeinschaft untersucht. Während der Inkubationen mit Methanol sollten methylotrophe Eigenschaften der Archaeen, sowie potentielle homoacetogene Stoffwechsel untersucht werden.

Mit Hilfe, der in dieser Arbeit eingesetzten ^{13}C-Markierungsexperimente, sollten neue Einsichten in die komplexen physiologischen Prozesse innerhalb der mikrobiellen AOM-Gemeinschaften gewonnen werden.

Preface and Objectives

Methane is a significant greenhouse gas that affects the global climate. The concentration in the atmosphere has more than doubled since the beginning of the industrialisation. Along with anthropogenic sources, there are also natural sources. For instance, high amounts of methane are formed in the anoxic marine sediments. However, only a minute part rises up into the water column and the atmosphere. The process of the anaerobic oxidation of methane (AOM) reduces its net emission from the sediments to the water body and atmosphere by more than 85 % and is therefore an important process in controlling the atmospheric concentration (del Giorgio and Duarte, 2002; Reeburgh, 2007).

Although AOM was described by Reeburgh (1976) as well as Barnes and Goldberg (1976) in the late seventies as a possible process, due to pore water profiles, it was not until 1999 that Hinrichs et al. followed by Boetius et al. (2000) connected euryarchaea with biogenic oxidation of methane under anoxic conditions. In the meantime, the identified clusters could be divided into three groups; ANME-1, -2 and -3 (**AN**aerobic **ME**thanotrophic archaea) with different subgroups. These methanotrophic archaea are closely affiliated to different methanogenic orders, Methanomicrobiales, Methanosarcinales and Methanococcales (Hinrichs et al., 1999; Boetius et al., 2000; Knittel et al., 2005). Although, recently AOM was also proven to be linked to other electron acceptors, the process of AOM in marine sediments is linked with sulphate reducing bacteria (SRB). Thus it is also considered as sulphate dependent AOM. It is a very low energy yielding process under standard conditions (Barnes et al.; 1976).

$$CH_4 + SO_4^{2-} \rightarrow HCO_3^- + HS^- + H_2O$$

$$\Delta G^0 = -22.8 \text{ kJ/mol}$$

Many physiological details of AOM are still unclear. Today the sulphate-related AOM is considered as a reverse process of the methanogenesis. This was supported by the finding of a new nickel binding coenzyme F_{430} in ANME-1, and genomic analysis of environmental samples (Krüger et al., 2003; Hallam et al., 2004; Meyerdierks et al., 2005, 2010; Shima et al., 2011).

There are still no isolated pure cultures from the ANME-1, -2, -3 or the involved sulphate reducing δ-proteobacteria. Interestingly, recent molecular biological investigations revealed that along with ANME-archaea and SRB, there exists a high microbial diversity in AOM-settings. However, the metabolisms and the function in those communities still remain unclear. Previous studies have already demonstrated methanogenic capabilities with different substrates (Seifert et al., 2006; Treude et al., 2007; Orcutt et al., 2008).

One approach to investigate the carbon fluxes in a microbial mat is an incubation technique with stable isotope labelled substrates – Stable Isotope Probing (Boschker et al., 1998). Along with the enabled tracing of the carbon flow into the total biomass, several specific lipid biomarker molecules can also be used to gain information on

the metabolic strategy of the prokaryotic members of such a microbial community. Within this work, previous labelling studies (methane, bicarbonate; Blumenberg et al., 2005; Wegener et al., 2008a; Jagersma et al., 2009) were extended with substrates which as of yet have not been investigated (acetate, methanol) to shed light on AOM-linked and other non-methane related metabolisms. Therefore, two different AOM-performing microbial mats from the Black Sea were investigated. These communities exhibit almost pure ANME-1 or ANME-2 dominated communities, respectively (Michaelis et al., 2002; Blumenberg et al., 2004), thus both communities were separated for the first time so that they could be analysed. Alongside this, the assimilation rates for ^{13}C from the labelled substrates (methane, bicarbonate, acetate, methanol) into archaeal and bacterial lipids were traced. In addition the rates of methane consumption, methanogenesis and sulphate reduction were determined to outline the activities of the respective ANME-archaea and sulphate reducing bacteria. The experiments with methane and bicarbonate are similar to the respective *in-situ* conditions. The experiments with acetate investigated the heterotrophic capabilities of the whole prokaryotic community. During the incubations with methanol, the methylotrophic capabilities of the archaea and potential homoacetogenic physiologies should be determined.

With the help of the conducted ^{13}C-labelling experiments during this work, new insights into the complex physiological processes within the microbial AOM-communities should be achieved.

1 Introduction

1.1 The global methane cycle

Methane (CH_4) is a strong greenhouse gas contributing to global warming in present and past geological times. In the recent atmosphere it reaches a mean concentration of 1.8 ppm (IPCC, 2007) and contributes with about 20 % to the recent greenhouse scenario, which is much lower than that of carbon dioxide (~400 ppm), another important greenhouse gas. Due to its high GWP (global warming potential) being 21 times that of carbon dioxide (IPCC, 2007), methane has a high relevance for climatic changes over relative short geological periods. In the geological past of the system earth, the atmospheric concentrations of methane and carbon dioxide had significant influences on climate, environmental and geochemical conditions, and thus on the evolution of organisms, as they adapted to altering environmental conditions. Hence, methane (and carbon dioxide) is also an important factor promoting evolutionary developments. For instance, dramatic increases in methane concentrations in the atmosphere from dissociated gas hydrates have been linked to mass extinctions during the Palaeocene-Eocene thermal maximum (~55 Ma before present (b.p.); Dickens et al., 1997) and the Permian-Triassic extinction event (~252 Ma b.p.; Krull and Retallack et al., 2000). Moreover, an elevated concentration of atmospheric methane during the Precambrian is considered to be responsible for a higher average global temperature, in spite of a fainted solar radiation (Kasting, 2005).

The global methane fluxes are mainly influenced by biogenic and anthropogenic sources. Consequences of the anthropogenic impact, since the beginning of the industrialisation at the end of the 19th century, are the dramatic increases of atmospheric concentrations of carbon dioxide and methane, from 280 ppm (pre-industrial) to 379 ppm (in 2005) for the first and from 0.715 ppm (pre-industrial) to 1.774 ppm (in 2005) for the latter, respectively (IPCC, 2007). Biological processes in anthropogenic defined habitats including rice paddies, soils, and livestock breeding, form the majority of methane. A lower, but still significant amount, however, is formed biologically without anthropogenic influence in wet lands, termite guts, freshwater and in marine sediments. Moreover, industrial influenced sources from landfills, oil and gas recovery, and coal mining are relevant (Kvenvolden and Rogers, 2005; Reeburgh, 2007). In addition, methane can be formed by geochemical alteration and thermal cracking in buried sediments, and released by volcanism (Horita and Berndt, 1999; Sherwood Lollar et al., 2002; Valentine et al., 2004). In marine sediments most methane is stored in clathrates – methane ice or gas hydrates (Kvenvolden, 1998). The stability of those hydrates depends on climate changes. Although still under debate, the dissociation of gas hydrates is considered as an important scenario promoting global warming and acidifying the oceans. Figure 1.1 illustrates methane as an intermediate of the global carbon cycle.

Biologically, methane can be aerobically oxidised by methanotrophic or methylotrophic bacteria and anaerobically by methanotrophic archaea (in syntrophy with

sulphate reducing bacteria). Nitrite driven bacterial methanotrophic oxidation of methane was also recently observed (Ettwig et al., 2008), although the importance of this process in nature is still unclear. The anaerobic oxidation of methane by closely phylogenetic relatives of the methanogens is considered as a reverse process of the methanogenesis (Krüger et al., 2003; Hallam et al., 2004). These ANME archaea use a similar set of enzymes (Hallam et al., 2003, 2004; Meyerdierks et al. 2005, 2010).

The half life time of methane is about 8 to 12 years in the atmosphere (Wahlen, 1993). The most important abiotic sink for methane is the photochemical oxidation with OH in the troposphere (Hanson and Hanson, 1996).

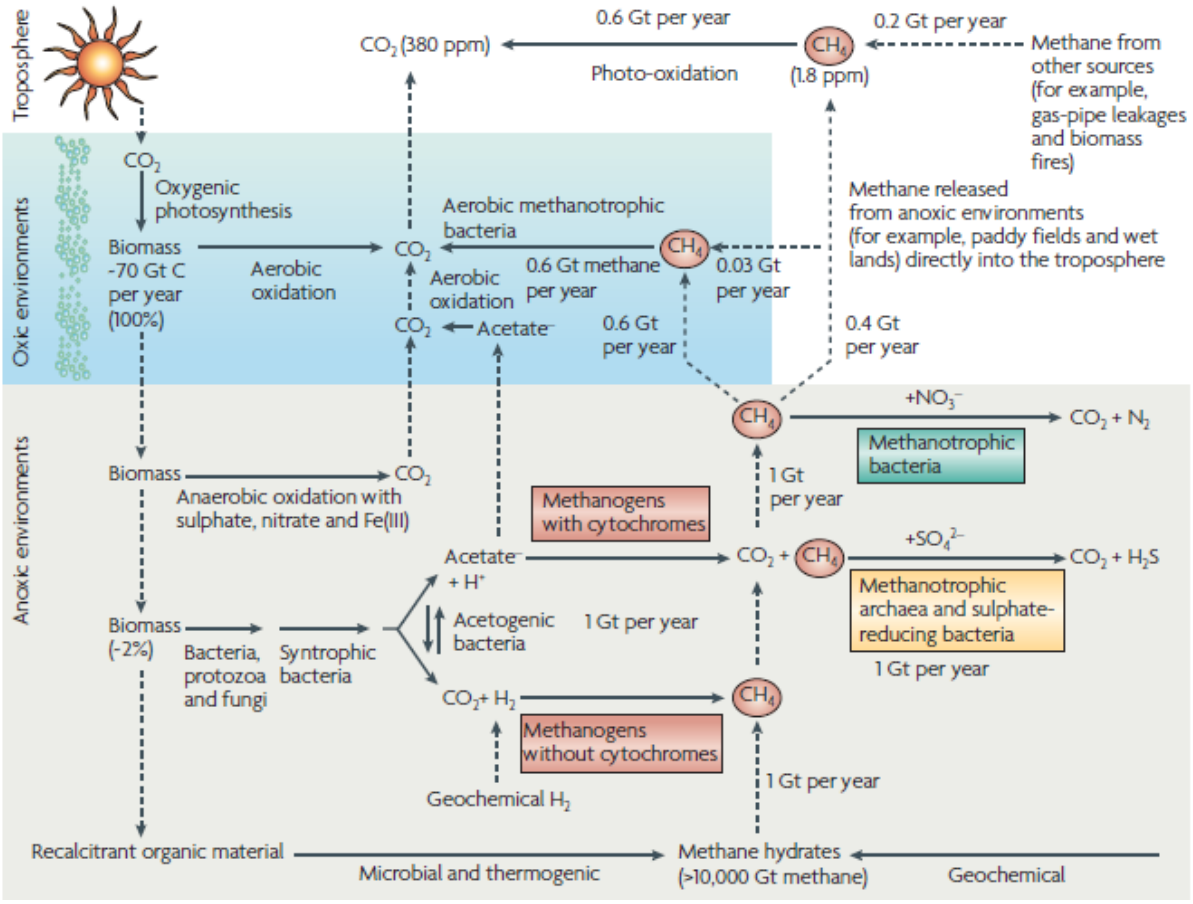

Figure 1.1: Methane as an intermediate in the global carbon cycle (Thauer et al., 2008a).
Gt - gigatons.

1.2 Anaerobic microbial methane metabolism

1.2.1 Methanogenesis

Methanogenesis is the final step in the anaerobic degradation of organic compounds. Methanogenic ecosystems are widespread in marine and freshwater systems (Deppenmeier, 2002a). After decomposition of the organic matter and the depletion of high energy yielding terminal electron acceptors (TEA) like oxygen, nitrate, ferric iron or sulphate, carbon dioxide is reduced anaerobically to methane. Beside the CO_2, acetate and methyl bearing compounds (e.g. methanol, trimethyl ammonium (TMA), and methyl sulfides) are substrates for methane generation by methanogenic archaea. Acetate in particular is an important substrate for

methanogens. It is estimated that up to 70 % of the microbial methane is formed from the methyl group of acetate in freshwater environments (Whiticar, 1999; Conrad, 1999).

Source organisms of almost all biologically formed methane are methanogenic archaea. Five orders belong to the kingdom Euryarchaeota (Deppenmeier, 2002a): Methanosarcinales, Methanobacteriales, Methanomicrobiales, Methanococcales and Methanopyrales. Recently a sixth order was proposed, the Methanocellales, isolated from rice paddy soils (Sakai et al., 2008, 2011). These five to six orders are not monophyletic (Woese and Olsen, 1986) and differ in their bio-chemistry, meaning the set of hydrogenases, dehydrogenases, heterodisulphide reductases, and the occurrence of cytochromes. Hence, different methanogens have different substrate spectra and are adapted to different hydrogen concentrations (Thauer et al., 2010). While members of the Methanosarcinales are able to grow with carbon dioxide, acetate, and methylotrophic substrates, all other orders are strongly adapted to CO_2-reduction under very low hydrogen pressure (Pa<10), with the exception of *Methanosphaera stadtmanae*. This species is only able to thrive on methanol and hydrogen as substrate, conducting a methanol reduction pathway. It is proposed that an electron bifurcation mechanism leads to the required reducing equivalents (Thauer et al., 2008a)[i].

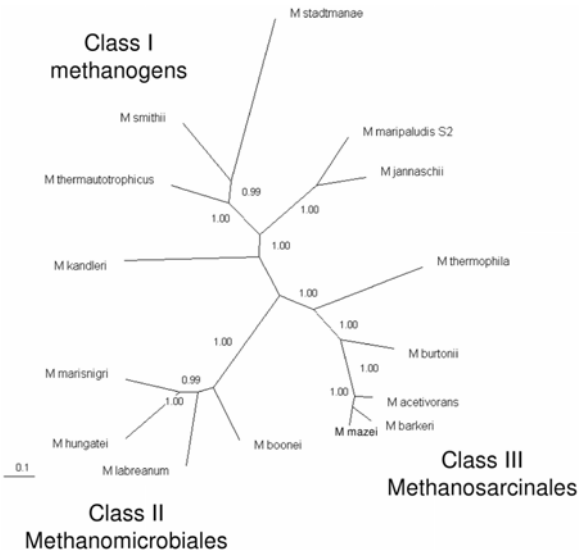

Figure 1.2: Phylogenetic relations between different species of methanogens; subdivided into three distinct groups according to Anderson et al. (2009).

Multiple ways are used to classify methanogens. Based on genomic investigations of enzymes involved in methanogenesis or cofactor synthesis, methanogens can be divided into two classes (Bapteste et al., 2005). While Class I methanogens comprise Methanobacteriales, Methanococcales and Methanopyrales, Class II methanogens are composed of the orders Methanomicrobiales and Methanosarcinales. Thauer et al. (2008a, 2010), in contrast, differentiate them into two classes, depending on the occurrence of cytochromes. Only Methanosarcinales are known to possess cytochromes. Anderson et al. (2009) extend the consideration of Bapteste et al. (2005) and divided the methanogens into three classes; Class I methanogens comprises Methanobacteriales, Methanococcales and Methanopyrales; Class II the Methanomicrobiales as a distinct group from the Class III methanogens - the Methanosarcinales (Figure 1.2).

[i] The electron bifurcation process is proposed to be the third type of energy conservation, in addition to substrate-level and electron transport phosphorylation. It is a separation of the two electrons from reducing equivalent (e.g. ferredoxin, NADH) of the respiratory chain, which leads to a bifurcation of the two electrons to a high and a low potential pathway (Stams and Plugge, 2009).

The exact methanogenic pathways vary between the genera and also on the strain level. They depend on the set of enzymes, the enzymatic set of subunits, and their location in the cell (e.g. the heterodisulphide reductase enzyme complex HdrABC/MvhADG in the cytoplasmatic lumen vs. the membrane-bounded heterodisulphide reductase HdrDE) and the occurrence of cytochromes.

Due to the complexity, the biochemistry of methanogenesis is only briefly and generalised described here, focusing on the order Methanosarcinales. For further readings about the physiological, biochemical, and ecological details publications by Deppenmeier (2002a, 2002b), Welander and Metcalf (2005), Thauer et al. (1998, 2008a, 2008b, 2010), and Ferry (1999, 2010) are recommended.

Several unique and specific cofactors are involved in the methanogenic pathway, e.g. methanofuran, tetrahydromethanopterin (H_4MPT), HS-CoM, HS-CoB (Deppenmeier, 2002a; Thauer et al., 2008a). Tetrahydromethanopterin (H_4MPT) and tetrahydrosarcinapterin (H_4SPT) are similar structural analogues with minor difference in their function (Ferry, 2010).

Figure 1.3 illustrates a simplified scheme for methanogenesis, with focus on CO_2-reduction. It has to be distinguished between three general pathways, depending on the substrate, the hydrogenotrophic methanogenesis with carbon dioxide, the methylotrophic methanogenesis with methylotrophic substrates, and the acetoclastic methanogenesis with acetate as substrate. Methanol can be introduced into the biochemical pathway over the coenzyme M, acetate over the acetyl-CoA.

The hydrogenotrophic methanogenesis with carbon dioxide as substrate begins with the reduction and binding to formylmethanofuran, catalysed by the formylmethanofuran dehydrogenase (Fmd; Deppenmeier, 2002b). Ferredoxin is most probably reduced by the H_2-oxidsing Ech hydrogenase (Ech) in cytochromes bearing Methanosarcinales (freshwater), or by analogues enzymes driven by a sodium gradient with a membrane-bound ferredoxin dehydrogenase (Ma-Rnf). In obligate CO_2-reducing methanogens the required electrons are supplied by a formate dehydrogenase (Ferry, 2010), or after an electron bifurcation within the cytoplasmatic MvhADG/HdrABC-complex (Thauer et al., 2008a). The formyl group is transferred with a formylmethanofuran transferase enzyme (Ftr) to the cofactor tetrahydrosarcinapterin (H_4SPT) and stepwise reduced to methyl-tetrahydrosarcinapterin (methyl-H_4SPT). The electrons are supplied by the reduced F_{420}:H_2 cofactor. F_{420} is reduced by the F_{420}-reducing hydrogenase (Frh). The methyl group is transferred to the cofactor HS-CoM by the methyl-H_4SPT:HS-CoM methyltransferase (Mtr). This step is coupled to an exergonic reaction and the formation of an electrochemical sodium gradient. The final step, conducted by the heterodisulphide reductase (Hdr), is the reaction with another cofactor HS-CoB, yielding methane and a heterodisulphide (CoM-S-S-CoB; Deppenmeier, 2002b). While the cytochromes bearing Methanosarcinales have a membrane bound heterodisulphide reductase (HdrDE) linked to a methanophenazine reducing hydrogenase (VhoACG), all other non-cytochromes bearing methanogens have a cytoplasmatic MvhADG/HdrABC (Thauer et al., 2008a).

During the second important methanogenic pathway, the methylotrophic methanogenesis, so-called methylotrophic substrates (e.g. methanol, methylamines, and methylated thiols) are converted to methane and carbon dioxide. This pathway starts with the formation of a methyl-CoM. The methyl group is transferred via methyl-H_4SPT:HS-CoM-methyltransferase to the cofactor H_4SPT. This endergonic step is driven by an electrochemical sodium ion gradient. From here two branches are possible, an oxidative and a reductive branch, respectively.

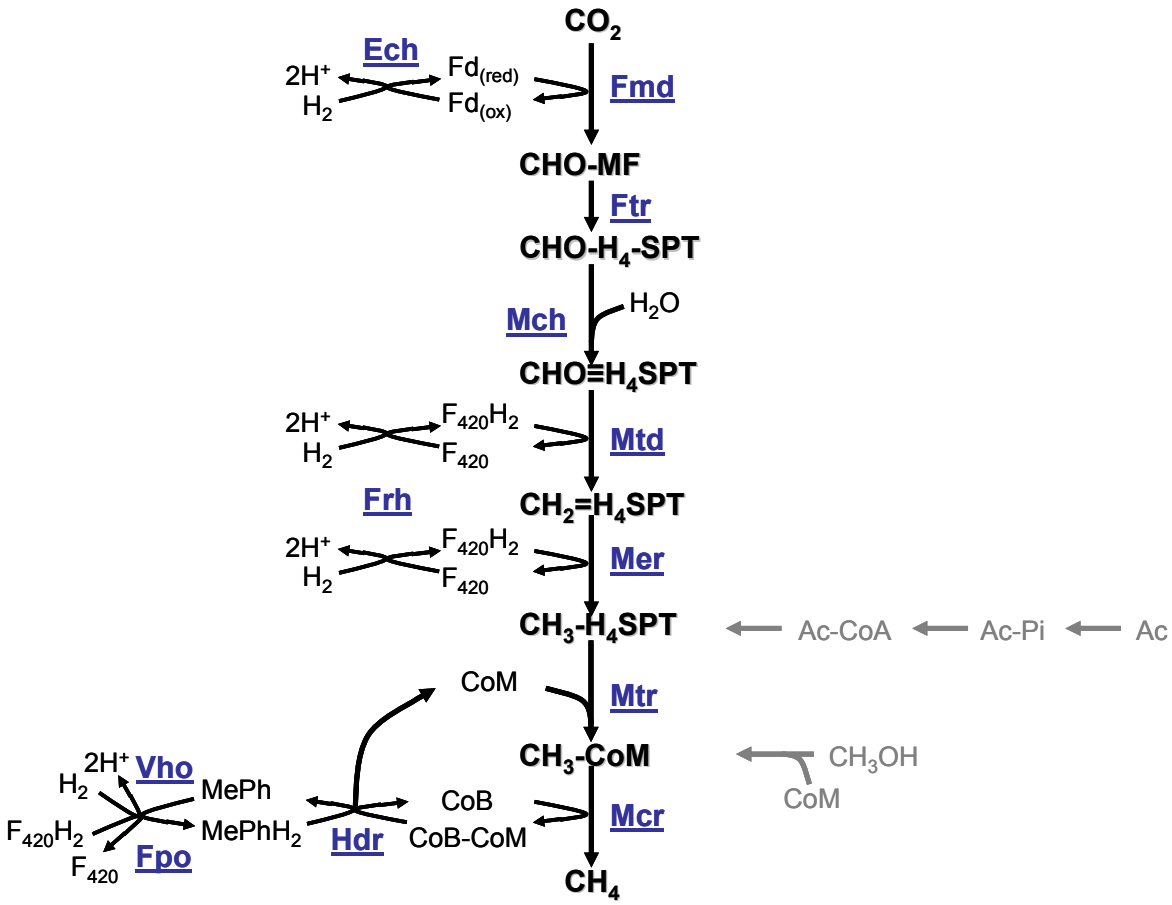

Figure 1.3: Simplified and generalised model of the biochemical conversion of carbon dioxide (after Welander et al., 2005), derived from *Methanosarcina barkeri* Fusaro. Methanol and acetate as alternative substrates for methanogenesis can be introduced at the coenzyme M for methanol and as acetyl-CoA. Ech - energy-converting hydrogenase, Ftr - formylmethanofuran:H_4SPT formyltransferase, Mch - methenyl-H_4SPT cyclohydrolase, Mtd - Methylene-H_4SPT dehydrogenase, Frh - F_{420}-reducing hydrogenase, Mer - methylene-H_4SPT reductase, Mtr - methyl-H_4SPT:HS-CoM methyltransferase, Mcr - methyl coenzym M reductase, Hdr - heterodisulphide reductase, Vho - methanophenazine reducing hydrogenase, Fpo - energy-converting $F_{420}H_2$ dehydrogenase complex, MePH - methanophenazine, Ac - acetate, Ac-Pi - phosphorylated, Ac-CoA - acetyl-coenzym A, Fd_{red} - reduced ferredoxin, Fd_{ox} - oxidised ferredoxin.

While the oxidative branch leads to stepwise oxidation to formyl-H_4SPT and reducing equivalents lead to the reduction of F_{420}, in the reductive branch three of four methyl groups are transferred to the cofactor HS-CoM by a specific methyltransferase. Again, the reduction of methyl-S-CoM with HS-CoB leads to methane and CoM-S-S-CoB. On the other end of the oxidative branch the formyl-methanofuran dehydrogenase catalysis the oxidation to carbon dioxide and methanofuran (Deppenmeier, 2002b). However, it is also possible, that

methylotrophic substrates are completely reduced to methane, e.g. *Methanosphaera stadtmanae* (Miller and Wolin, 1985).

During the third, the acetoclastic pathway, acetate is activated via an acetate kinase and a phosphotransacetylase (*Methanosarcina spp.*) or by an acetyl-CoA synthetase (*Methanosaeta spp.*), yielding acetyl-CoA. That is cleaved by the CO dehydrogenase/ acetyl-CoA synthase complex (CODH/ ACS). The resulting electrons reduce ferredoxin and the methyl is transferred to H_4SPT and finally converted to methane. The energy for this endergonic reaction is generated by a sodium-translocating methyl-H_4SPT:HS-CoM methyltransferase and a methyl-S-S-CoM reductase (Deppenmeier, 2002b).

1.2.2 Anaerobic oxidation of methane (AOM)

The process of the anaerobic oxidation of methane (AOM) was already inferred in 1976 from the observed loss of methane at the sulphate methane transition zones (SMTZ) in anoxic, marine sediments (Barnes and Goldberg, 1976; Reeburgh, 1976). About 20 years later syntrophic consortia responsible for the sulphate dependent anaerobic oxidation of methane were identified initiating intensive research of the AOM process (Hinrichs et al., 1999; Thiel et al., 1999; Boetius et al., 2000; Michaelis et al. 2002; Knittel et al., 2005; Lösekann et al., 2007).

Those syntrophic communities consist mainly of methanotrophic archaea belonging to the ANME-clusters (**AN**aerobic **ME**thanotrophic archaea) and often closely associated sulphate-reducing bacteria (SRB). Three clusters of ANME-archaea are known so far (ANME-1 to -3). In addition two subgroups, the so-called AAA-cluster (AOM-associated archaea) and the GoM Arc 1-cluster (Gulf of Mexico Archaea 1-cluster), affiliated to the ANME-2 cluster were identified. Additionally a thermophilic subgroup of ANME-1 was recently discovered (Teske et al., 2002; Schouten et al., 2003; Holler et al., 2011a). Furthermore, a freshwater adapted ANME-1 subgroup was described - ANME-1a FW (Takeuchi et al., 2011). While ANME-1 revealed a closer affiliation to Methanomicrobiales, ANME-2 archaea are closer affiliated to the Methanosarcinales (Blumenberg et al., 2004; Knittel and Boetius 2009). The members of the ANME-3 cluster are closely affiliated to the genus *Methanococcoides spp.* (Knittel et al., 2005). The sequence similarities (between 73 % and 92 %) indicate non-monophyletic relations between the three ANME-clusters and that the members probably belong to different orders or families which share similar physiological properties (Knittel and Boetius, 2009). Several differences between the investigated clusters were found, obtained by phylogenetic analysis and further epifluorescence micrographs of the archaea and associated bacteria. Both, the 16S-rDNA and the mcrA (methyl-coenzyme M reductase, subunit A) as a specific key enzyme were aligned to get information about the phylogenetic relations (Hallam et al., 2004; Nunoura et al., 2006). Those observations were also confirmed by investigations of the archaeal membrane lipids (Blumenberg et al., 2004; Niemann and Elvert, 2008; Rossel et al., 2008, 2011). Blumenberg assigned the three isomers of the biphytanes as specific lipid biomarkers for ANME-1 and *sn-2*-hydroxyarchaeol for ANME-2 (Blumenberg et al., 2004). Furthermore,

similarities of physiological capabilities, deduced from metagenomic analysis (Hallam et al., 2003; Meyerdierks et al., 2005, 2010), demonstrate the affiliation to methanogens. Based on these phylogenetic analyses ANME-1 showed two distinct subclusters (1a, b), and ANME-2 four subclusters (2a-d; Figure 1.4).

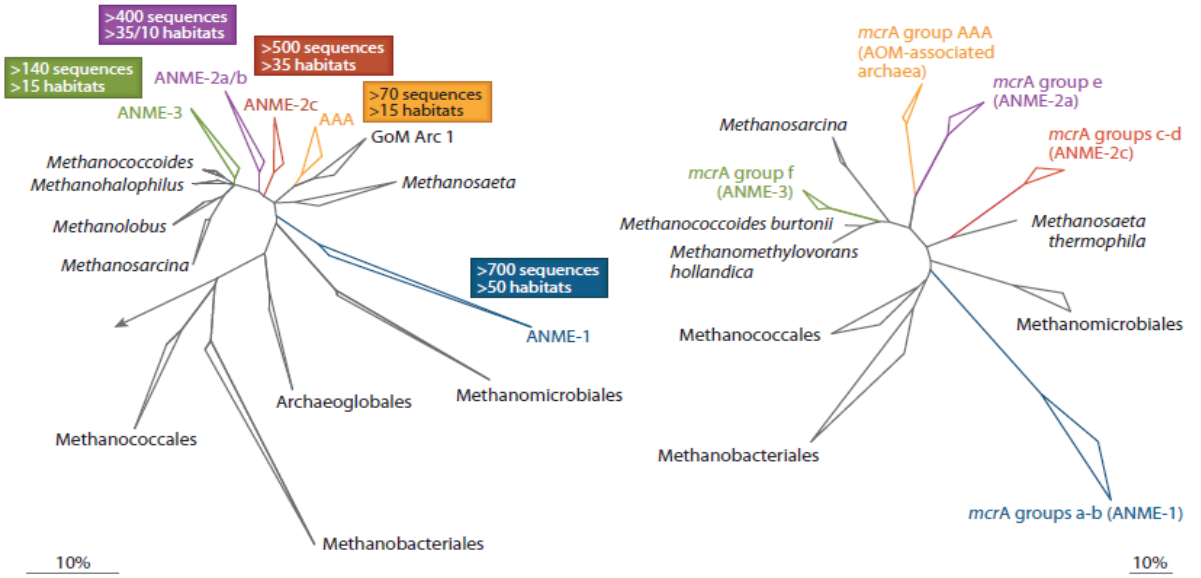

Figure 1.4: Phylogenetic relation between the three ANME-clusters; based on 16S-rDNA and mcrA genomic analysis (Knittel and Boetius, 2009).

The sulphate-related AOM is considered to be coupled with sulphate reducing bacteria. This syntrophic metabolism is a very low energy yielding process under atmospheric conditions (equation 1) (Barnes and Goldberg, 1976).

$$(1)\ CH_4 + SO_4^{2-} \rightarrow HCO_3^- + HS^- + H_2O \quad (\Delta G^0 = -22.8\ kJ/mol)$$

For most investigated communities, the pronounced occurrence of the SEEP-SRB1a-cluster was described (Boetius *et al.*, 2000; Orphan *et al.*, 2002; Knittel et al., 2005; Schreiber et al., 2010). But for most ANME-3 dominated samples, consortia with sulphate reducing bacteria of the DBB-cluster (Desulfobulbus) were identified (Niemann et al., 2006; Lösekann et al., 2007; Schreiber et al., 2010). According to the recently found thermophilic ANME-1 archaea, the associated SRB were named HotSeep-1 cluster (Holler et al., 2011a).

Figure 1.5 (Knittel and Boetius, 2009) illustrates a summary of the different consortia structures revealed by epifluorescence micrograph investigations with FISH and CARD-FISH probes from several sampling sites. These data are in accordance with those of other authors (Boetius et al., 2000; Michaelis et al., 2002; Orphan et al., 2002; Blumenberg et al., 2004; Lösekan et al., 2007; Pernthaler et al., 2008; Schreiber et al., 2010; Holler et al., 2011a). While ANME-1 revealed in most samples no close association to SRB (Figure 1.5a, b), ANME-2 samples showed different assembling of community structures. ANME-2a showed a mix-type structure with SRB (Figure 1.5c-e) and ANME-2c showed shell-type consortia (Figure 1.5f, g). ANME-2c were also observed as single cells (Figure 1.5h). Figure 1.5i shows an ANME-3/ Desulfobulbus consortia.

So far, no pure cultures of the ANME-clusters or the involved sulphate reducing δ-Proteobacteria exist, complicating the study of AOM. Previous assumptions for potential electron shuttles like hydrogen and acetate (Hoehler et al., 1994; Valentine and Reeburgh, 2000) could not be verified by experiments and also alternative electron shuttles were refuted (Nauhaus et al., 2005). Although still insufficiently understood, it is assumed that the process of AOM is a reverse biochemical process of the methanogenesis, which is supported by (i) the close affiliation of methanogens with ANME-archaea, and (ii) biochemical and molecular biological studies (Krüger et al., 2003; Hallam et al., 2004; Chistoserdova et al., 2005; Meyerdierks et al., 2005, 2010; Scheller et al., 2010; Shima et al., 2011).

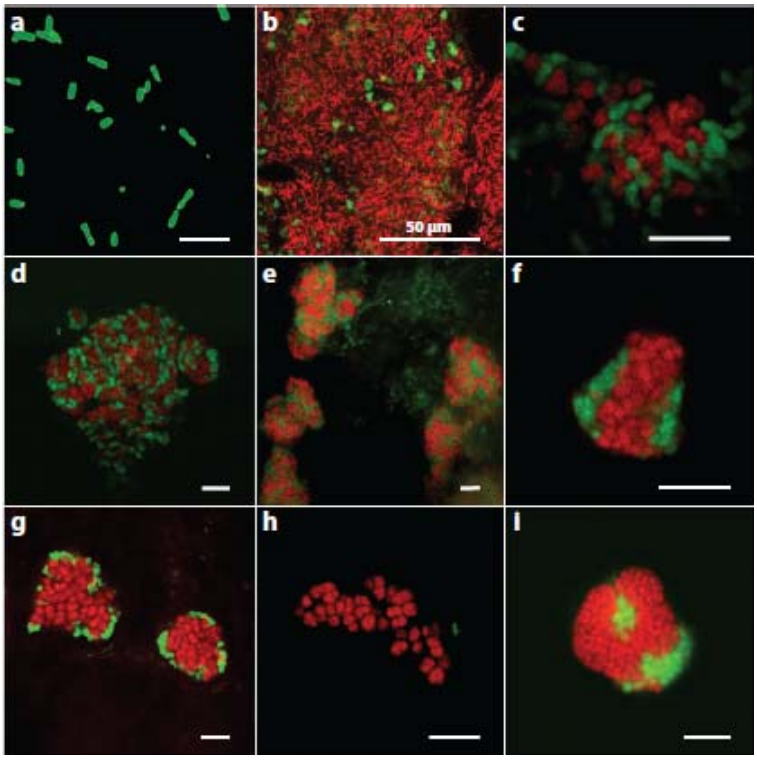

Figure 1.5: Epifluorescence micrographs of different ANME single cells and aggregates visualised by FISH or CARD-FISH.
(*a*) Single ANME-1 cells living in a microbial mat from the Black Sea. (*b*) Mat-type consortia formed by ANME-1 (*red*) and DSS cells (*green*). (*c-e*) Mixed-type consortia of ANME-2a (*red*) and DSS (*green*) cells observed in different seep sediments. (*f, g*) Shell-type consortia of ANME-2c (*red*) and DSS (*green*) cells and (*h*) single ANME-2c cells observed in different seep sediments. (*i*) ANME-3/*Desulfobulbus* consortia. Unless otherwise indicated, scale bar is 5 µm. Abbreviations: ANME, anaerobic methanotrophic archaea; CARD, catalyzed reporter deposition; DSS, *Desulfosarcina*; FISH, fluorescence in situ hybridization (Knittel and Boetius, 2009).

Hydrogen is a very important electron donor in methanogenic systems (Hoehler et al., 1994). Its concentration influences the bacterial composition and diversity (Hoehler et al., 1998; Conrad and Klose, 1999). In general, AOM is a microbial process based on diffusion of methane and sulphate in marine sediments. However, under specific, euxinic conditions with high methane fluxes mat structures (Treude et al., 2005; Krüger et al., 2008) or carbonated chimneys can be formed, e.g. in the Black Sea (Michaelis et al., 2002; Reitner et al., 2005). AOM in those mat ecosystems and sediments is coupled to the reduction of sulphate, and thus, might

be based on syntrophic metabolic interaction between ANME archaea and SRB. However, the nature of this process remains enigmatic, because intermediates and the assimilatory metabolic fluxes within the consortia are unclear. None of the proposed electron shuttles could be verified, yet. It was proposed, that AOM could be directly coupled to simultaneous sulphate reduction in ANME-archaea. However, neither Hallam et al. (2004) nor Meyerdierks et al. (2005, 2010) did find evidences for a dissimilatory sulphate reductase, based on any metagenomic approach. Several other mechanisms were proposed by Hoehler et al. (1994); nitrate, Mn(IV), and Fe(III) as electron acceptor or rather as hydrogen sink linked to AOM. A nitrite coupled AOM by bacteria was observed by Ettwig et al. (2008, 2010; see also Strous and Jetten, 2004; Raghoebarsing et al., 2006). Beal et al. (2009) described a higher abundance of ANME-1 within incubations with birnessite or Fe(III) as electron acceptors, indeed suggesting Fe(III) to be involved in AOM. Bacterial groups other than SRB have been reported to occur in AOM-performing communities as well (Heijs et al., 2006, 2007; Webster et al., 2007; Pernthaler et al., 2008; Beal et al., 2009; Pachiadaki et al., 2010; Bowles et al., 2010). These bacterial groups have metabolic capabilities, which are presumably not directly linked to AOM. Carbon dioxide is reduced directly by chemolithoautotrophic organisms, in such communities dominated by the sulphate-reducing bacterial cluster (Boetius et al., 2000; Orphan et al., 2002; Knittel et al., 2005; Niemann et al., 2006; Lösekann et al., 2007; Schreiber et al., 2010). Little is known about other chemolithoautotrophic organisms, using different terminal electron acceptors for their metabolism.

Based on combined geochemical studies and PCA (**P**rincipal **C**ompound **A**nalysis) of intact polar lipid biomarkers (IPLs), Rossel and colleagues (2011) showed that ANME-1 are more adapted to higher temperatures and lower sulphate concentrations as well as very low oxygen concentrations in bottom waters while ANME-2 dominated communities are viable at lower temperatures, higher oxygen content of bottom waters and higher sulphate-concentrations. These findings supported previous investigations by Krüger et al. (2008), and were also confirmed by Yanagawa et al. (2011). They imply a more versatile physiology of methanotrophic archaea, considering ANME-1 and ANME-2 archaea.

For AOM-communities, different stable isotope probing experiments with labelled methane and bicarbonate were already conducted (Blumenberg et al., 2005; Wegener et al., 2008a; Jagersma et al., 2009). These, and additional radioisotopic (Michaelis et al., 2002; Treude et al., 2007) and nanoSIMS-analyses (Orphan et al., 2001a, 2002) indicated the direct uptake of methane and bicarbonate carbon into archaeal lipids and subsequent incorporation of AOM-derived carbon dioxide into bacterial fatty acids. House and colleagues (2009) investigated *in-situ* the carbon isotopic composition and used radiotracer methods to study the relative activity of several metabolisms of ANME-clusters stratigraphically separated in the sediments at methane vents. Their results give evidence, in particular for ANME-1 phylotypes that they can switch between methanogenesis and methanotrophy. Furthermore, approaches by Seifert et al. (2006) and Treude et al. (2007) with either stable or

radioactive isotopes indicated such a process in AOM-performing microbial communities. Further, Krüger et al. (2008) determined directly rates of methanogenesis in AOM-performing mats from the Black Sea. Recently, Lloyd et al. (2011) detected a high abundance (16S by qPCR and RT-qPCR) of ANME-1 in methanogenic sediment layers and call obligate methanotrophic capabilities for ANME-1 in question.

Heterotrophic metabolisms in the often microbial complex AOM-setting are rarely investigated. Small organic intermediates of microbial transformations might feed these groups and by this also influence carbon fluxes in the AOM-consortia (Meulepas et al., 2010; Webster et al., 2011). For instance, the functions and impact of acetogenic organisms for the heterotrophic part of both mats respectively, is not completely answered. However, acetate is an important substrate for a multiplicity of organisms in marine sediments. In particular sulphate-reducing bacteria are known EPS-formers. This EPS (extracellular polymeric substance) is considered as a matrix for carbonate binding with its chemical properties (Dupraz and Visscher, 2005; Braissant et al., 2007), and as putative substrate to feed other heterotrophic organisms. Thus, the nature of the associations and the role of other prokaryotes, which are often also highly abundant, are still unresolved.

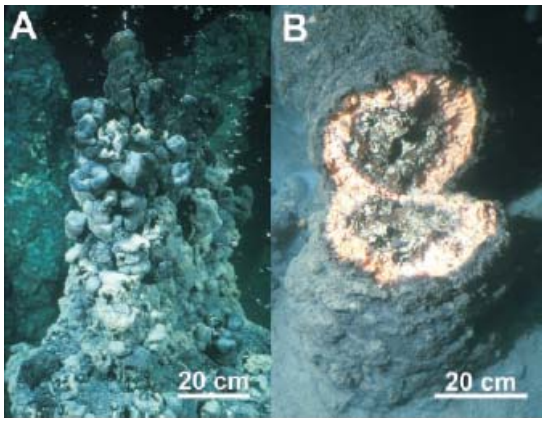

Figure 1.6: Carbonate chimneys from the anoxic waters of the Black Sea (Michaelis et al., 2002).

With respect to the study of AOM the Black Sea is unique due to its stable euxinic deeper water body and the high methane emissions from cold seeps. Here, reef-like carbonate structures (Michaelis et al., 2002) and surface layers of organic rich biofilms (Krüger et al., 2008), performing anaerobic oxidation of methane and reducing the emission of methane, grow on the seafloor. Although methane carbonates are also reported from other marine settings (e.g. Mediterranean mud volcanoes; Pachiadaki et al., 2010), only in the Holocene Black Sea massive, commonly structured microbial mats are formed by the activity of anaerobic methanotrophic communities (Figure 1.6). Due to the structured occurrence of ANME-1 and ANME-2 communities in the microbial mats from the Black Sea (Blumenberg et al., 2004; Krüger et al., 2008) they are excellently suitable for the investigation of AOM and other anaerobic processes directly or indirectly linked to AOM.

1.3 Biochemical pathways in complex anaerobic microbial communities

In anaerobic habitats the mineralisation of complex molecules with a high molecular weight works stepwise within several trophic levels. After the degradation of complex molecules by hydrolytic organisms, these monomeric compounds are degraded by anaerobically heterotrophic prokaryotes to volatile fatty acids (VFAs), followed by further syntrophic organisms to hydrogen and acetate. The hydrogen is consumed by other competitive microorganisms, e.g. SRB, methanogens and homoacetogens. The general anaerobic metabolism is mainly influenced by a couple of similar enzymes. Those enzymes involved in acetate-, sulphur-, and C_1-metabolism are dispersed within different phyla of prokaryotes, particularly in anaerobic lineages.

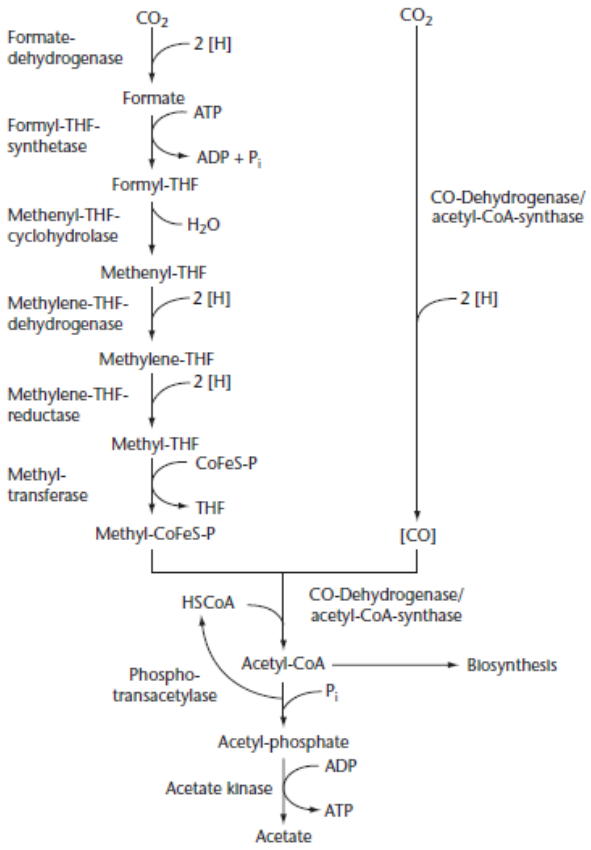

Figure 1.7: Wood-Ljungdahl pathway (Imkamp et al., 2007). THF - tetrahydrofolate

Within the trophic level of C_1- and C_2-metabolism, namely carbon dioxide, methyl compounds, methane, and acetate, the acetyl-CoA pathway (also called the Wood-Ljungdahl pathway; Figure 1.7), plays an important role in obligate anaerobic microorganisms. It is used assimilatory as well as dissimilatory. The use of acetyl-CoA is widespread over different prokaryotic phyla. The central compound in the acetyl-CoA pathway is acetate, which can be formed, depending on the organisms, from different substrates; for instance CO and H_2, CO_2 or methanol as electron donors and nitrate, nitrite, thiosulphate, or pyruvate as possible electron acceptors (Drake et al., 2008; Ragsdale and Pierce, 2008).

The two key enzymes of this metabolism are the formyl-THF-synthetase and the CO-dehydrogenase/acetyl-CoA synthase complex at the beginning of the two branches. The pyruvate ferredoxin:oxidoreductase (PFOR) links the degradation of more complex substrates (e.g. sugar monomers) to the Wood-Ljungdahl pathway. This pathway allows prokaryotes to grow autotrophically, heterotrophically and finally mixotrophically. Only homoacetogenic organisms form acetate by the reduction of CO_2 (Wood, 1991; Drake et al., 2008). However, also in methanogenic, methanotrophic, sulphate reducing archaea, Chloroflexi, Firmicutes and in SRB, this pathway has an anabolic function (Ragsdale and Pierce, 2008). Interestingly, tetrahydrofolate (THF), an involved cofactor (H_4MPT analogue) in the acetyl-CoA pathway was also identified in

the aerobic methanotrophic strain *Methylococcus capsulatus* (Bath) (Chistoserdova et al., 2005). The acetyl-CoA pathway is probably ancient (Ragsdale and Pierce, 2008; Martin, 2012). It is the only linear CO_2 fixing pathway with methyl as most complicated intermediate. This is also the only pathway which combines carbon fixation with energy generation. Interestingly, aerobic and anaerobic methane metabolisms are quite similar, at least on the genetic level encoding enzymes involved in part of the C_1-pathway and the presence of involved cofactors, namely methanofuran (MFR) and tetrahydromethanopterin (H_4MPT; Chistoserdova et al., 1998, 2004, 2005). Moreover, related nucleic acid sequences were found in some Planctomycetes, which are assumed to be a very ancient lineage of the domain bacteria. They probably use this pathway as a detoxification of formaldehyde (Chistoserdova et al., 2004).

Sulphate reducing bacteria and archaea share similar enzymes involved in the sulphur metabolism, namely the ATP-sulfurylase (aps), the APS-reductase (apr) and the dissimilatory sulphite reductase (dsr). Another interesting group of enzymes is involved in the sulphur metabolism. The heterodisulphide reductase was found in sulphate reducing bacteria (Strittmatter et al., 2009), as well as in methanogenic, methanotrophic (Thauer et al., 2008a) and in sulphate reducing archaea, e.g. *Archaeoglobus fuldigus* (Klenk et al., 1997). While the SRB link the sulphur metabolism for energy generation directly to sulphate reduction, methanogenic and methanotrophic archaea use sulphur-containing cofactors (CoM-S and CoB-S). Archaeoglobus link the sulphur metabolism when grown on acetate directly to methane oxidation (Vorholt et al., 1995), a process that is also feasible as being important in specific AOM-settings.

All these processes, relevant under anaerobic conditions may also affect the physiology in AOM-performing microbial systems. However, they are not further investigated so far. Particularly, the homoacetogenic capabilities may contribute to reduced hydrogen concentrations and thus favour methanotrophic conditions.

1.4 Lipid biomarkers

Several definitions for biomarkers coexist in the research field of natural and life sciences. Environmental studies have a focus on intact biomolecules in recent sediments, e.g. nucleic acid (Brocks et al., 2011). These life biomarkers have an important function, to detect and to visualise *in-situ* and *in-vitro* organisms and classify the source organisms phylogenetically. Furthermore, dependent on the ribonucleic (RNA) or desoxynucleic (DNA) acid they give information on the activity, e.g. for microorganisms in environmental samples but also in enrichment-cultures (Radajewski et al., 2000; Neufeld et al., 2007). In the research field of geobiology, mineralogical, elemental, isotopical and morphological indicators are investigated to find evidence in the geological record for life (Brocks et al., 2011). It is a great challenge in geomicrobiology to study those organisms in an environmental context, even more so in the past. However, biosphere and geosphere have evolved together. Lipid biomarkers as chemofossils or chemotaxonomical markers are organic

compounds from a biosynthetic origin, preserved in the sediments and sedimentary rocks. Compared to intact biomolecules they have some beneficial features; they can be preserved over long geological times, they are resident against diagenetic alterations, and their structure can still be related to the precursor lipid. Usually lipid biomarkers are much less specific such as, for instance nucleic acid. Some of those compounds are very specific down to the level of orders or family (Simoneit, 2002; Brocks and Pearson, 2005, 2011). Another advantage is that the function and metabolic capabilities can often be directly linked with the environment, e.g. the occurrence of AOM at marine seeps (Hinrichs et al., 1999; Michaelis et al., 2002; Blumenberg et al., 2004; Pancost and Sinninghe Damsté, 2003).

Lipid biomarkers can be distinguished into free and hydrolysed lipids (Figure 1.8) and IPLs (intact polar lipids). IPL are different to the residual lipids in that they are considered to be exclusively extracted from living cells (Sturt et al., 2004). All other lipids can also be found in soils and sediments as remnants of previous living cells. However, these compounds can open a window into a better understanding of former times, with ages up to several billion years. The carbon isotopic composition gives further information about the metabolism and the substrates used by the respective source organisms (e.g. Hayes, 2001).

All living cells have mainly intact polar lipids as compounds of their cell membranes (Figure 1.8). They consist of a polar group, for example containing a phosphate, sulphur or glycosidic moiety and a hydrophobic subunit. The hydrophobic part can be a straight or branched ester or ether linked alkyl chain. Diacylglycerides (DAGs) are ubiquitous in all eukaryotic and bacterial organisms. The alkyl and acyl chains differ in chain lengths, methyl branches and the amount of double bonds. The chain lengths are shorter and the fatty acids have fewer double bonds in bacteria compared to eukaryotes. Triacylglycerides (TAGs) consist also of fatty acids. However, ether linked alkyl moieties are also very common and plasmalogens consist of mixed ether, ester and a phosphor linked alkyl chain. Three groups of bacterial ethers can be distinguished, mono- and dialkyl glycerol ethers (MAGEs, DAGEs), and non-isoprenoidal glycerol dialkyl glycerol tetraethers (GDGTs). Mono- and dialkyl ethers were commonly found in extreme and anaerobic environments, like hot springs (Huber et al., 1992, 1996), AOM settings (Hinrichs et al., 2000; Pancost et al., 2001; Michaelis et al., 2002), and hydrothermal vents (Blumenberg et al., 2007). However, recently they were also reported from mesophilic environments (Schouten et al., 2000; Rütters et al., 2002; Oppermann et al., 2010). Specific MAGEs and DAGEs are attributed to SRB (Michaelis et al., 2002; Rütters et al., 2001; Pancost et al., 2001) and other obligate or facultative anaerobic species, e.g. Clostridia (Langworthy and Pond, 1986), *Streptococcus mutans* (Brissette et al., 1986), *Aquifex pyrophilus* (Huber et al., 1992), *Ammonifex degensii* (Huber et al., 1996). In addition aerobic Myxobacteria produce ether lipids during spore formation under unfavourable conditions (Caillon et al., 1983; Ring et al., 2006). The third group of bacterial ethers consists of branched GDGTs, found in anoxic soils and peat bogs, but the source organisms are still unknown (Pancost and Sinninghe Damsté,

2003; Weijers et al., 2007). Recently, soil-specific Acidobacteria were linked to the occurrence of bacterial GDGTs (Sinninghe Damsté et al., 2011).

Archaeal lipids consist of a glycerol backbone with a polar head group at the *sn-1*-position and two ether linked isoprenoid hydrocarbon chains. While the cell membranes of the eukaryotes and almost all known bacterial lineages consist of a semi permeable bilayer, archaeal mono layers consist of glycerol dialkyl glycerol tetraethers (GDGTs). However archaeal bilayer membranes are also widespread; they are composed of isoprenoid diether lipids (saturated [archaeol] and unsaturated; Sturt et al., 2004; Koga and Morii, 2005). Different a-, mono-, di- and tricyclic biphytanes with penta- or hexacyclic ring structures were identified. GDGTs were identified in methanogenic lineages (Michaelis and Albrecht, 1979; Chappe et al., 1980; Chappe et al., 1982; De Rosa and Gambacorta, 1988; Hoefs et al., 1997) and in *Thermoplasma acidophilum* (Langworthy, 1977). Furthermore GDGTs were found in many mesophilic Crenarchaeota (DeLong et al., 1998; Schouten et al., 2000; Biddle et al., 2006), in particular crenarchaeol is highly diagnostic for pelagic Crenarchaeota (Sinninghe Damsté et al., 2002; now classified as Thaumarchaeota).

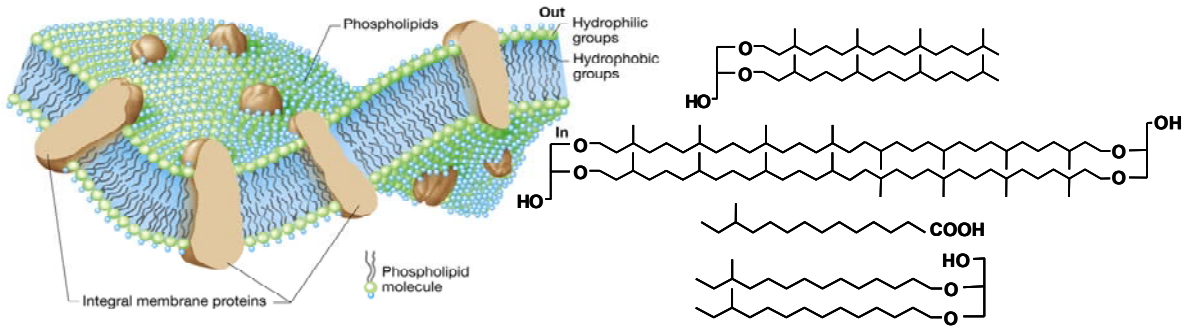

Figure 1.8: Phospholipid membrane (Madigan, 2002) and molecular structures of lipid biomarkers. Archaeol, biphytane ($C_{40:0}$), *anteiso*-pentadecanoic acid (*ai*fa15), a*i15/ai15* dialkyl glycerol ether (*ai*15DAGE).

1.5 Stable Isotope Probing (SIP)

Carbon has three isotopes, one radioactive (^{14}C) and two stable isotopes, ^{12}C and ^{13}C. ^{12}C is the most abundant isotope in natural systems (~98.89 %). The isotopic composition of a sample is compared to the Vienna Pee Dee Belemnite standard (V-PDB) with a known ratio of ^{13}C / ^{12}C ($R_{V\text{-}PDB}$ = 0.0112372). The deviation of the two ratios from the sample against the V-PDB is expressed in the $\delta^{13}C$-notation in ‰, +1 ‰ equals roughly a positive shift of the ^{13}C in a relative abundance of 0.001 % against the V-PDB. With equation (2) the $\delta^{13}C$-value can be calculated with the measured ratio of the sample against the V-PDB standard.

$$(2)\ \delta^{13}C\ [‰] = [(^{13}C / ^{12}C)_{Sample} / (^{13}C / ^{12}C)_{Standard} - 1] \times 1000$$

Due to the higher mass of ^{13}C, the respective energy needed to cleave a close electron binding with this isotope leads to a discrimination of ^{13}C against ^{12}C in biochemical processes. Hence, in non-equilibrium processes, biological products are slightly enriched in ^{12}C, while the educt remains enriched in ^{13}C. In environmental

samples this fractionation effect during biosynthesis can give information on the metabolism or rather the carbon fixation pathway (Craig, 1954; Sirevag et al., 1977; Hayes, 1993; Summons et al., 1994; Sakata et al., 1997).

A valuable technique in tracing the carbon flow in complex, slow growing microbial communities is lipid stable isotope probing, using isotopically labelled substrates (SIP; Boschker et al., 1998). This technique allows tracing the carbon flow without the safety requirements if using ^{14}C. Additionally, the incorporation of ^{13}C from labelled substrates into metabolic end products, e.g. the isotopic enrichment of methane can elucidate methanogenic capabilities directly. The label can also be traced into dissolved inorganic carbon (DIC; Meulepas et al., 2010). Dijkstra et al. (2011) modelled metabolic processes with isotopologue pairs of position-specific ^{13}C-labelled glucose and pyruvate. Nucleic acid, RNA as well as DNA (RNA-SIP, DNA-SIP) can be enriched by ^{13}C with specific labelled substrates and separated according to CsCl-density centrifugation. In combination with other sophisticated molecular biological techniques (T-RFLP, DGGE, microarrys, metagenomic approaches) a detailed analysis of complex microbial communities can be achieved (Manefield et al., 2002; Dumont and Murrell, 2005; Dumont et al., 2006; McDonald et al., 2005; Neufeld et al., 2007).

2 Materials and Methods

2.1 Sampling and sampling site

The microbial mat samples were obtained during a research cruise with the RV Poseidon (317/2) in September 2004 from anoxic waters at the north western shelf of the Black Sea. They were obtained at 180 meters below sea level by the submersible JAGO (Krüger et al., 2008). These mat samples were subdivided into two different types present in the microbial mats: a pink coloured mat, dominated by ANME-1 archaea and associated bacterial communities, and a black coloured mat, which is dominated by ANME-2 consortia (according to Blumenberg et al., 2004 and Krüger et al., 2008).

The samples were stored at 8 °C in the dark until the beginning of the incubation experiments. The medium was the same modified basal medium as used by Widdel and Bak (1992) described below. The exception was the lack of vitamine-solution and methane in the headspace.

2.2 Incubation experiments and experimental set-up

2.2.1 Incubation experiments - Medium composition

Mat samples were incubated with modified basal medium (16.23 mM sulphate, 4.67 mM ammonium, 1.47 mM phosphate, trace elements, vitamines, 30 mM bicarbonate and 0.5 mM sulphide) at 8 °C in the dark (Widdel and Bak, 1992; detailed mixture see appendix A.1). The initial pH was 7.5 and the salinity was adjusted to 24 ‰.

All incubation experiments were performed with pure methane or nitrogen in the headspace (0.2 MPa for ^{13}C-labelled methane and 0.1 MPa for all other experiments). The δ^{13}C-values were -37.7 ‰ for the unlabelled methane, and -51.0 ‰ for the buffer carbonate, respectively. Riboflavin, an ingredient of the vitamine solution was dissolved in 20 mM acetate resulting in a final acetate concentration of 20 nM. The δ^{13}C-value of this compound was not measured, but it should not have a significant influence on the results of the experiments, due to the higher concentrations of labelled substrates. The medium was supplemented with different ^{13}C-labelled substrates as sole or complimentary carbon source according to Table 2.1. According to Krüger et al. (2008) the amount of the EPS (extracellular polymeric substance) was 1.3 % (dry weight) and the δ^{13}C was about -72 ‰.

Table 2.1: Experimental set-up. Each experiment was applied in replicate for both, ANME-1 and ANME-2 dominated mat systems. See also appendix A.6.

Number of Experiments	Methane	Bicarbonate	^{13}C-Labelling	Concentration of Label	Inhibition	Sampling after [days]	Notation
3	2 bar	30 mM	Methane	25 %	-	64, 135, 378	ML
2	1 bar	30 mM	Bicarbonate	30 mM, 20 %	-	64	BcLM
2	-	30 mM	Bicarbonate	30, mM, 20 %	-	64	BcL
6	1 bar	30 mM	Na-Acetate	3 mM, 99.9 %	-	23, 26, 56	AcLM
4	-	30 mM	Na-Acetate	3 mM, 99.9 %	-	23, 56	AcL
2	1 bar	30 mM	Na-Acetate	3 mM, 99.9 %	CH_3F	26	AcLMI
2	-	30 mM	Na-Acetate	3 mM, 99,9 %	CH_3F	26	AcLI
2	1 bar	30 mM	Methanol	3 mM, 99.9 %	-	26	MeLM
2	-	30 mM	Methanol	3 mM, 99.9 %	-	26	MeL

2.2.2 Sulphate reduction rates

The sulphide content was determined using the formation of copper sulphide (Cord-Ruwisch, 1985) and reported by Siegert (2010). For this work, the sulphate reduction rates (SRR) were recalculated based on the TOC-content of the respective samples. Given sulphide concentrations were calculated per gram TOC and day [$\mu mol\, g_{TOC}^{-1} d^{-1}$] for both mat types (equation 3).

(3) $$\mathbf{SRR = (RGP_{Conc.\text{-}H_2S} \times 1000) \times (1000 / [\{1000/100\} \times dw])}$$

The sulphate reduction rates were calculated using the RGP algorithm yielding a linear regression with a maximal fitting for all measured data. The algorithm calculates iterative, based on the formula for the linear slope (y = ax + b), all square deviations for assumed values. The smallest fitting value determines the slope. Conc.-$_{H_2S}$ is the measured concentration of sulphide; TOC is the measured amount of total organic carbon in the sample [%]; dw gives the dry weight of the sample [mg].

AOM-dependent sulphate reduction rates were calculated by subtracting sulphate reduction rates in the absence of methane from those when methane was present.

2.2.3 Headspace sampling and concentration measurement of methane

The gas phase in the headspace of the incubation vessels was sampled with an air-tight syringe. It was rapidly transferred into air-tight glass vials, sealed with a stainless-steel clamp and a butyl-rubber, and filled up with a saturated solution of sodium chloride for subsequent isotopic measurements. Concentration of the head-space gas (CH_4) was taken from Siegert (2010). The samples were immediately measured in glass vials for quantifications. Before quantification of the samples, gas standards (1,000 ppm, 10,000 ppm, 100,000 ppm) were measured in triplicate. With this calibration, a slope and a respective correlation was calculated for further determination of the headspace concentrations.

The concentration of methane in the headspace of the samples was analysed by using a GC-FID with a nickel catalyst methaniser (gas chromatograph-flame ionisation detector; SRI 8610C, SRI Instruments, USA) equipped with a 6-foot HayeSep D column (SRI Instruments, USA) running continuously at 60 °C.

All rates, methane decrease and methane formation (for methane free incubations), were calculated based on concentration measurements and the respective TOC of the samples per day [$\mu mol\, g_{TOC}^{-1} d^{-1}$] for both mat types (equation 4).

(4) **$Conc._{HSG}$ = ([$RGP_{conc.-gas}$ /1000] x HSV) x (1000/ [{TOC/100} x dw]) x 1000**

The measured headspace concentrations of methane and carbon dioxide ($Conc._{HSG}$) were also calculated with the RGP algorithm. For details see above, section 2.2.2. (sulphate reduction rates), HSV (headspace volume) is the given volume [ml] in the headspace.

2.3 Pre-cleaning of the solvents and equipment

To remove organic compounds, all solvents used were distilled. The water was deionised, autoclaved at 121 °C, 2 bar and afterwards extracted with DCM three times. Glass equipment was heated for 5 hours at 500 °C, rinsed by acetone and hexane three times and dried with a cool air flow before use. Other (calibrated) glass equipment, for example graduated cylinder or pipettes, for exact measurements was only washed by acetone, methanol, and hexane three times to remove organic compounds.

2.4 Biomarker work-up

A detailed flow-sheet illustrating the individual procedures and measurements is given in Figure 2.1.

2.4.1 Determination of C/N and TOC from the bulk samples

Total carbon, total nitrogen and total organic carbon (in wt %) were determined by flash combustion using a Carlo Erba Science 1500 CNS Analyser (Erba Science, Italy). The carbonate was removed with 50 µl 1 N HCl and after the samples were dried on a 40 °C heating plate (repeated three times). The inorganic carbon was calculated as the difference between total carbon and organic carbon. Replicate analyses yield a standard deviation of 0.05 % for the carbon content.

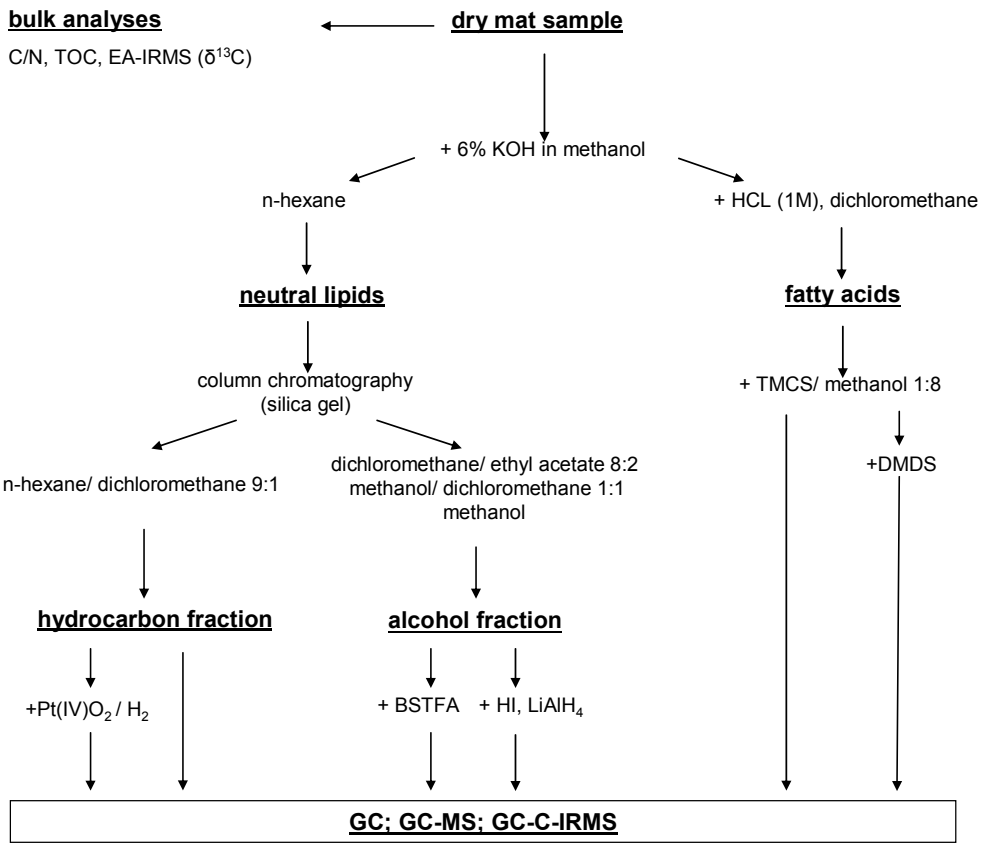

Figure 2.1: Procedure of the lipid and bulk work-up.

2.4.2 Extraction of the lipids

The mat-samples from parallel incubations of identical experimental set-up were pooled, freeze-dried and homogenised before extraction. Subsamples (approx. 10 mg) were subjected to bulk analysis (C/N, TOC; $\delta^{13}C$ see below). The extraction method was previously described (Michaelis et al., 2002). Briefly, alkaline hydrolysis with KOH (6 %) in methanol was conducted using a 100 - 300 mg dry weight mat sample for 3 h at 80 °C in a supersonic bath. The neutral lipids were extracted with n-hexane. Separation of the neutral lipid fraction was performed with a silica gel (mesh 60, Merck, Germany) column, into a hydrocarbon fraction with three column volumes of n-hexane/ dichloromethane (9:1), and a polar fraction (alcohol and ethers) with three columns of dichloromethane/ ethyl acetate (8:2), three column volumes of methanol/ dichloromethane (1:1), and six column volumes of methanol. After acidification (pH 1) with HCl (1 M), the free and liberated fatty acids were extracted with dichloromethane (Figure 2.1). To determine heterogeneities for each substrate-specific experiment, an autoclaved control was extracted (except for the experiments with ^{13}C-labelled methane).

2.4.3 Derivatisation of the lipids

Fatty acids were transferred to methyl esters with trimethylchlorosilane (TMCS) / methanol (1:8; v/v). The alcohols were silylated with N,O-bis(trimethylsilyl)trifluoroacetamide (BSTFA). Both derivatisations were conducted for 2 h at 80 °C. The double bond positions of the fatty acid methyl esters were determined through derivatisation with dimethyl disulphide (DMDS) (Buser et al., 1983).

Double bonds were also hydrogenated for selected compounds (e.g. hentriacontatriene) as described below. Respective lipids were dissolved in methanol, and incubated with a headspace with hydrogen over night at room temperature with small amounts of platinum-IV-oxide as a catalyst. The hydrogenated lipids were extracted three times with dichloromethane/ methanol (2:1) and dissolved in n-hexane followed by drying in a stream of argon.

Ether bound lipids from aliquots of the alcohol fraction were analysed after ether-bond cleavage by HI-treatment (2 h at 110 °C) and reduction of the resulting iodides using $LiAlH_4$ in dry n-hexane under an argon-atmosphere (after Kohnen et al., 1992).

2.4.4 Instrumental set-up

The compounds were quantified with an internal standard (5α-Cholestane) and analysed with a gas chromatograph equipped with a flame ionisation detector (Fisons HRGC Mega 2 series) and hydrogen as carrier gas (1.8 ml/min). The concentrations of lipids were calculated per gram TOC. The compounds were identified by a GC-MS (Thermo DSQ II quadrupol GC-mass spectrometer, ionisation was performed at -70 eV and helium was used as carrier gas (1.8 ml/min)). Samples for isotopic analyses were analysed by coupled gas chromatography-combustion-isotope spectrometry (GC-c-IRMS; Finnigan DeltaPlus XL mass spectrometer), using a GC (Hewlett-Packard 6890) with an on-column injection system. The carrier gas was helium (1.0 ml/min) with a constant flow. The compounds were oxidised via a CuO/Ni/Pt combustion furnace operated at 940 °C. For GC-FID, GC-MS and GC-C-IRMS analyses, compounds were separated with a DB5-MS-column (30 m x 0.32 mm i.d., fused silica 0.25 µm film thicknesses) and temperature program: 80 °C for 3 minutes, 6 °C/min up to 310 °C isotherm for 30 minutes. The precision of the IRMS was checked daily by a certified standard (Schimmelmann-mix B) of mixed alkanes (C_{15}-C_{29}, with increasing concentrations) and was generally better than ± 0.5 ‰.

2.4.5 Correction of the $\delta^{13}C$-values after derivatisation

The measured $\delta^{13}C$-values of the derivatised compounds (methylated fatty acids and silylated alcohols) were corrected. The carbon isotopic composition of the respective reagent (methanol or BSTFA) was determined as follows. About 0.1 mg BSTFA was given on 1.0 - 1.5 mg silica gel (mesh 60, Merck, Germany) in a silver-capsule. It was measured with a Finnigan MAT 252 mass spectrometer after high-temperature flash combustion in a Carlo Erba NA-2500 elemental analyser (Erba

Science, Italy) at 1020 °C. The $\delta^{13}C$-value of the methanol was determined by the injection of 0.05 - 0.1 µl directly on column, with an isotherm heating of 80 °C, helium as carrier gas with 1ml/min, constant flow. The $\delta^{13}C$-values of the derivatised compounds were corrected by equation (5) (Goñi and Eglinton, 1996) and expressed as [‰].

$$(5)\ \delta_{UD} = (\eta_D / \eta_{UD})\ \delta_D - (\eta_{derivat.\text{-}reagent} / \eta_{UD})\ \delta_{derivat.\text{-}reagent}$$

δ_{UD} is the isotopic ratio of the underivatised compounds, η_{UD} is the number of the carbon atoms in the underivatised compounds, $\eta_{derivat.\text{-}reagent}$ is the ratio of the derivatisation-reagent (methanol or BSTFA; measured off-line with CHN analyser, see above), $\eta_{derivat.\text{-}reagent}$ is the number of carbon atoms added from the derivatisation-reagent, δ_D is the isotopic ratio of the derivatised compound and η_D is the number of carbon atoms in the derivatised compound ($\eta_D = \eta_{UD} + \eta_{derivat.\text{-}reagent}$).

2.4.6 Correction of the concentrations of the biphytanes after ether cleavage (HI-treatment)

The efficiency of the ether cleavage was estimated by the release of phytane obtained after HI-treatment. No phytane was detected in the (alcohol) fraction before the HI-treatment. The theoretical concentration of the phytane, derived from the sum of archaeol and *sn-2*-hydroxyarchaol was calculated by the formula n = m / M. In which n x 2 is the (theoretical) concentration of phytane derived from the ether lipids, m is the weight of the respective compound in the sample (archaeol or *sn-2*-hydroxyarchaeol), M is the molecular weight of the ether lipids. The efficiency was calculated using equation (6).

(6) **Efficiency [%] = Conc. Phytane$_{measured}$ [ng/µl] / Conc. Phytane$_{cal.}$ [ng/µl] x 100**

2.4.7 Calculations of the ^{13}C-assimilation rates

2.4.7.1 Summation of the daily $\Delta\delta^{13}C$

The $\Delta\delta^{13}C$ of the depicted compounds (Section 3.3) were summarised for all archaeal and bacterial compounds and divided through the time of incubation. For experiments with labelled methane or bicarbonate, the label was calculated for 100 %.

2.4.7.2 Calculation of the total ^{13}C-assimilation rates, calculated for the total amount of the respective compound

The total ^{13}C-assimilation rates were calculated as follows. The carbon isotopic compositions were expressed in the δ-notation versus V-PDB in ‰, and the ^{13}C-content was calculated with equation (7), expressed as [$\mu g\, g_{TOC}^{-1}$].

$$(7)\ ^{13}C\text{-content} = C_{t_x} / \{1/ [(\delta^{13}C/1{,}000 +1) \times R_{V\text{-}PDB}] + 1\}$$

Where C_{t_x} is the concentration of the respective lipid at the sampling time t_x and $R_{v\text{-}PDB}$ is the $^{13}C/^{12}C$ ratio of the standard, ($R_{V\text{-}PDB}$ = 0.0112372 ± 0.0000090). The total ^{13}C-uptake was calculated for the respective lipids depending on the

concentrations of the compounds in the different samples with equation (7). The ^{13}C-uptake was also calculated per day to compare different incubation times.

2.4.7.3 Calculation of the total ^{13}C-assimilation rates, calculated for the total amount of the respective lipids and normalised to 1µg lipid fraction

The total ^{13}C-assimilation rates were calculated for selected lipids and normalised to 1 µg total lipid fraction per day [ng $\mu g_{\Sigma(\text{selected lipids})}^{-1} d^{-1}$]. The sum of the respective ^{13}C-uptake into individual compounds was calculated as daily rate (according to 2.4.7.2) and divided through the total quantity of the selected lipids. For experiments with labelled methane or bicarbonate, the label was calculated for 100 %.

For the ANME-1 dominated mat samples, the following bacterial and archaeal lipids were used for further calculations.

Compounds for ANME-1 associated bacteria (for abbreviations A.5):
16:1MAGE(a), *i*/*i*15DAGE, *i*/*ai*15DAGE, *ai*/*ai*15DAGE, *i*fa13, *ai*fa13, *i*fa14, fa14, *m*15:0ω8, *i*fa15, *ai*fa15, fa15, *i*fa16, fa16:1ω7c, fa16:1ω5, fa16, cyclohexyl, ifa17, *ai*fa17, fa17:1ω6c, fa17, *ai*fa18, fa18:1ω9c, fa18, diploptene

Compounds for ANME-1 associated archaea (for abbreviations A.5):
PMI:4, PMI:5, archaeol, archaeol:1, C_{35}(a-f), $C_{40:0}$, $C_{40:1}$, $C_{40:2}$

For the ANME-2 dominated mat samples, the following bacterial and archaeal lipids were used for further calculations.

Compounds for ANME-2 associated bacteria (for abbreviations A.5):
16MAGE(c), *i*/*i*15DAGE, *i*/*ai*15DAGE, *ai*/*ai*15DAGE, *i*fa14, fa14, *m*15:0ω8, *i*fa15, *ai*fa15, fa15:1ω6c, fa15, *i*fa16, fa16:1ω7c, fa16:1ω5c, fa16, cyclohexyl, *m*fa17:0ω7, *i*fa17, *ai*fa17, fa17:1ω6c, *cy*17:1ω5,6, fa17, fa18:1ω9c, fa18

Compounds for ANME-2 associated archaea (for abbreviations A.5):
PMI:4, PMI:5, archaeol, *sn-2*-hydroxyarchaeol

2.4.7.4 Calculation of the ^{13}C-assimilation rates

The assimilation of the ^{13}C was calculated according to 1 µg compound at the respective sampling time and was divided through the time of incubation [days]. Thus, the ^{13}C-assimilation rates were calculated for 1 µg compound per day.

2.4.8 Correction of the ^{13}C-assimilation rates for compounds with minor $\delta^{13}C$-shifts

Compounds with minor $\delta^{13}C$-shifts were corrected to the $\delta^{13}C$-values of the saturated *2,6,10,15,19*-pentamethylicosane, due to a high isotopic variance in the different samples. The corrected compounds were biphytanes (after ether cleavage of the glycerol dialkyl glycerol tetraethers) and C_{35}-isoprenoid hydrocarbons.

A mean difference ($\delta^{13}C_{\text{mean-value}}$) between the compounds and the *2,6,10,15,19*-pentamethylicosane was determined by the respective measurements for every

sample (before incubation). For the correction of the compounds from incubated samples, the difference between the respective compounds and the *2,6,10,15,19*-pentamethylicosane ($\delta^{13}C_{PMI\text{-}sample}$) was determined. For calculation of a corrected $\delta^{13}C$-shift, a theoretical $\delta^{13}C_{t_0}$ at the beginning of the incubation was calculated by equation (8).

(8) $$\textbf{Corrected } \delta^{13}C_{t_0}\ [‰] = \delta^{13}C_{comp.\text{-}sample} - (\delta^{13}C_{PMI\text{-}sample} + \delta^{13}C_{mean\ value})$$

Figure A.2a shows the variances within pink mat samples for the biphytanes, Figure A.2c for the six isomers of the C_{35}-isoprenoid hydrocarbons. Tables A.2b and A.2d illustrate the corrected $\delta^{13}C$-values for the biphytanes and the C_{35}-isoprenoid hydrocarbons.

2.5 Isotopic measurements of methane after labelling experiments with different substrates

2.5.1 Isotopic measurements of methane

Gas samples were obtained from the headspace of the respective incubation experiments as described above (section 2.2.3). The stable carbon isotopes of CH_4 were measured by GC-c-IRMS (ThermoScientific Delta V Plus) with a Carboxen 1010-Plot column (30 m x 0.32 mm, Supelco), using the following temperature program to separate CO_2 and CH_4: 4 minutes at 40 °C, 30 °C/min. to 240 °C, 10 minutes holding with a flow rate of 1.6 ml/minute. The injection system was an eight port Valco valve with a 100 µl column and a 20 µl column for different concentrations. Methane was equilibrated to approximate 1,600 ppm. Helium was used for flushing the syringe to avoid memory effects. A blank measurement of helium gas was conducted to check the equipment before analysis. The syringe and syringe tip were flushed several times with pure helium before and after injection. The equipment was tested with a gas standard mixture of methane (-59.3 ‰) and carbon dioxide (-26.9 ‰) to check the precision of the system and avoid memory effects within the measurements several times between sample measurements. Minor memory effects were observed after analysis of isotopic highly enriched samples (up to 10 ‰ for methane). In view of the strong ^{13}C-enrichment of the investigated samples, these memory effects had no significant impact on the obtained results.

2.5.2 Calibration of the IRMS for ^{13}C-enriched gas samples

The IRMS (ThermoScientific Delta V Plus) was calibrated with a standard of 100 % labelled methane. In this approach the pure methane standard was diluted with a methane standard with a $\delta^{13}C$ of -59.3 ‰ to achieve a defined isotopic composition. A factor for the correction of the measured $\delta^{13}C$-values to the theoretical $\delta^{13}C$-values was calculated by a regression between measured and theoretical $\delta^{13}C$-values. Thus, all measured $\delta^{13}C$-values were corrected with this factor (Figure A.3a). The linearity of the IRMS was determined up to 816‰ by a calibration with known isotopic $\delta^{13}C$-values of the diluted methane standard. All measured $\delta^{13}C$-values above 816 ‰ were corrected with this factor (2.1186). It was determined a R^2 = 0.9841 for the

regression (Figure A.3a). Figure A.3b shows the determined ^{13}C-content in %, calculated from the corrected $\delta^{13}C$-values.

2.5.3 Calculation of methane formation from isotopic measurements of methane

The $\delta^{13}C$-values of methane were used for calculations of the methane formation for both; incubation experiments (i) started with methane in the headspace and for those, (ii) started without methane in the headspace. The calculations were similar for both approaches according to equations (9.1) - (9.3). The formation of methane during the experiments with a headspace of pure methane was calculated based on the total amount of methane in the system and the $\delta^{13}C$-shift of the methane, assuming the newly formed methane to have the same isotopic composition as the labelled substrate.

The impact of the substrate on previous methane free incubation experiments was determined directly by the isotopic composition. Experiments with 20 % labelled bicarbonate were multiplied with a factor of 5.

An isotopic fractionation of the methane during anaerobic oxidation of methane was not considered in the calculations, as this effect is assumed to be negligible compared to the measured $\delta^{13}C$-shift.

(9.1) $\mathbf{Amount_{CH_4}\,[\mu mol] = (\,\{Conc._{HS}\,[ppm] / 10^6\}\,x\,HSV\,) / 22.4\ l/mol\ x\ 10^6}$

(9.2a) $\mathbf{Ratio_{CH_4} = 0.0112372\ x\ (1 + \delta^{13}C_{CH_4} / 1000)}$

(9.2b) $\mathbf{^{12}C_{CH_4}\,[\%] = 100/\ Ratio_{\,CH_4} + 1)}$

(9.2c) $\mathbf{^{13}C_{CH_4}\,[\%] = 100 - {}^{12}C_{CH_4}\,[\%]}$

(9.3) $\mathbf{formed\ CH_4\,[\mu mol] = {}^{13}C_{CH_4\,tx}\,[\%] - {}^{13}C_{CH_4\,t0}\,[\%] / 100\ x\ Amount_{CH_4}\,[\mu mol]}$

HSV is the headspace volume (26ml), 22.4 litre/mol for ideal gases under standard conditions (T =273 K, pressure = 1 bar, gas constant R = 8.3144621 $JK^{-1}\ mol^{-1}$), $\delta^{13}C_{CH_4}$ within experiments started with (unlabelled) methane in the headspace was -37.7‰.

2.5.4 Correction of the determined rates of methane decrease by isotopically determined formation of methane

The rates of methanogenesis were corrected by isotopically determination of newly formed methane during incubations started with methane in the headspace. The isotopically determined amount of newly formed methane was subtracted from the measured amount of methane in the headspace (equation 10). With this amount, the rates were calculated.

(10) $\mathbf{methane_{corrected}\,[\mu mol] = methane_{measured}\,[\mu mol] - methane_{\Delta\delta^{13}C}\,[\mu mol]}$

$Methane_{\Delta\delta^{13}C}$ is the isotopically determined newly formed methane (see also equations 9.1 - 9.3).

3 Results

Carbon fluxes within two phylogenetic distinct anaerobically methane-oxidising microbial mats were investigated, namely an ANME-1 archaea dominated community represented by pink (or orange) coloured samples and black coloured samples, dominated by ANME-2 archaea (Figure 3.1). Both samples were recovered at the north western shelf of the Black Sea during a research cruise in 2004 from the anoxic sediment surface at about 180 m water depth.

Subsamples of the two mat types were attributed to different carbon isotopic labelled substrates within incubation experiments. For these experiments, changes in the isotopic compositions of the lipid biomarkers were determined. In addition, methane decrease, methanogenesis and sulphate reduction were monitored.

For the following sections, the described notation according to table 2.1 (page 17) will be used. The concentrations and $\delta^{13}C$-values for all considered compounds within all incubation experiments are presented in the appendix; Tables A.4a-d (page 140-143).

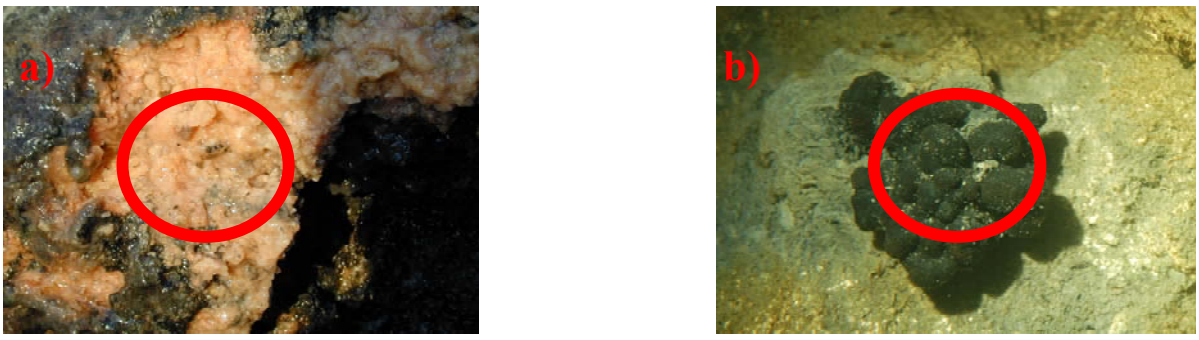

Figure 3.1: a) An **ANME-1 dominated pink coloured microbial mat sample** covered by a black coloured mat. b) A **nodule structure of black coloured ANME-2 dominated AOM-performing microbial communities** on the sea floor.

3.1 Methane decrease, methanogenesis, sulphate reduction, and methane-dependent sulphate reduction rates

During the incubation experiments with ^{13}C-bicarbonate, ^{13}C-acetate, and ^{13}C-methanol, concentrations and stable isotope compositions of methane in the headspace were investigated to get first information on the substrate specific physiological activities present in the two mat types. Additionally, total and methane-dependent sulphate reduction rates were calculated from sulphide concentrations.

3.1.1 Methane decrease

The decrease of methane was measured by headspace concentrations (Figure 3.2). After 10 days of incubation, the decrease was only between 1 and 6 % for all experiments (Figure 3.2), except for the pink mat amended with acetate (PAcLM) showing a decrease of about 32 %. For most experiments, the decrease was between 7 % and 17 % after 26 days of incubation (PBcLM, PAcLMI, PMeLM, BBcLM, BAcLMI, BMeLM). Considerable higher methane decreases of up to 42 % (PAcLM) and 32 % (BAcLM) were found for experiments supplemented with acetate

for both mat types. The methane decrease was lower in the presence of methyl fluoride for both mat types, about 10 % after 26 days (PAcLMI, BAcLMI). The methane decrease for incubation experiments with added methanol in ANME-2 dominated samples reached about 11 % (BMeLM; Figure 3.2) exceeding the respective decrease in pink mat samples considerably (PMeLM; about 7 %). For the time period between 26 and 64 days of incubation, analysed for the incubations with bicarbonate, no or only minor (BBcLM) methane decreases were observed.

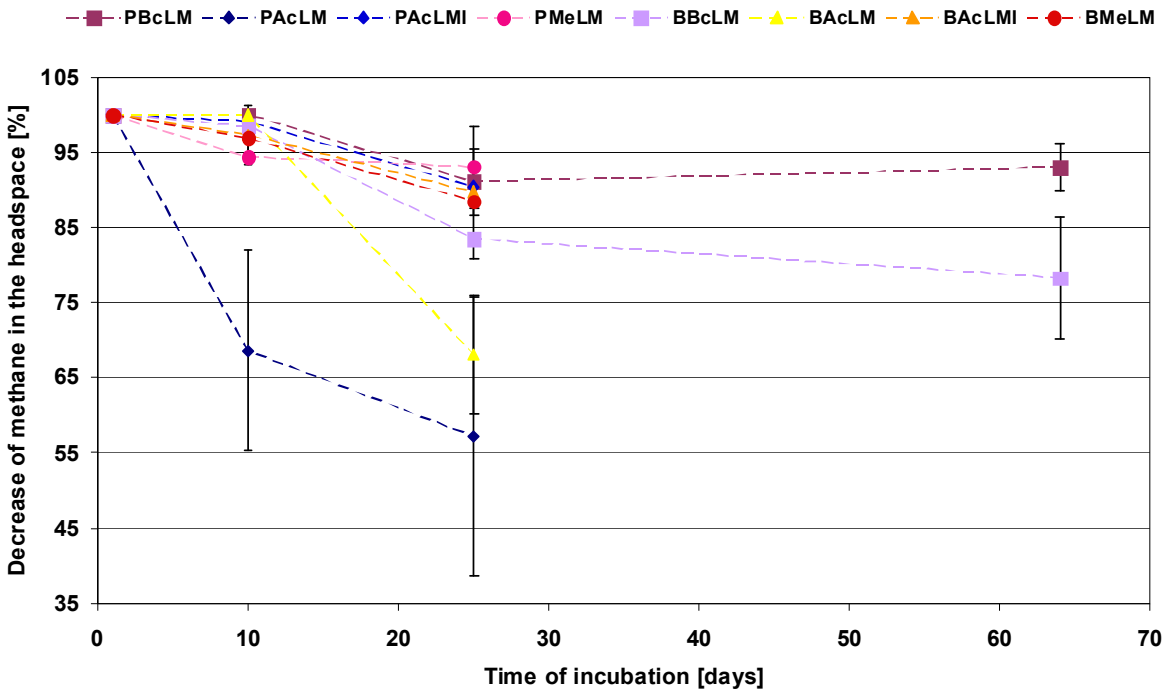

Figure 3.2: Total decrease of methane during incubation experiments with different substrates. Decreases were determined by headspace concentrations (measured by Siegert). The error bars result from replicate measurements.

3.1.2 Methanogenesis

The increases of methane for incubations started without methane in the headspace are illustrated in figure 3.3 for both mat types. Moreover, the isotopic composition of methane in the headspace was traced for all experiments to determine the methane generation from the carbon of the respective added substrates (Figures 3.4, 3.5). The rates of methanogenesis for incubations started with a methane free atmosphere were determined by the increase of methane in the headspace (black columns; Figure 3.6). For inhibition of the acetoclastic methanogenesis experiments with methyl fluoride were performed.

Only marginal increases of methane were observed for experiments with bicarbonate (~2 µmol) and acetate (~1 µmol), indicating a low methane generation from the respective substrates for pink mat samples (PBcL; PAcL; Figure 3.3). In contrast, black mat samples revealed considerable increases of methane after 56 and 64 days with acetate and bicarbonate (BAcL ~9 µmol; BBcL ~11 µmol).

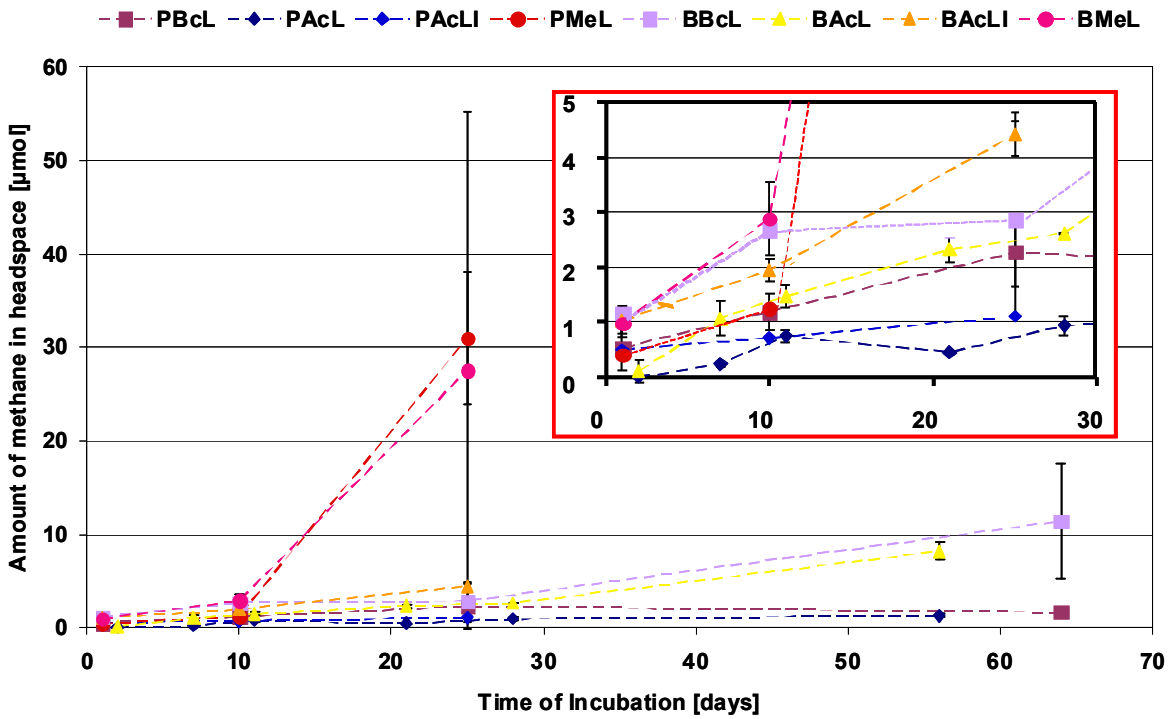

Figure 3.3: Methane increase during incubation experiments with different substrates. Amounts were determined by headspace measurements (measured by Siegert, 2011). The error bars result from replicate measurements.

Highest concentrations were observed with methanol in both mat types after 26 days (PMeL, BMeL). Independent of the presence of methane, up to 30 µmol methane were newly formed.

Figures 3.4 and 3.5 compare the impact of labelled carbon from bicarbonate and acetate on newly formed methane for pink and black mat types, respectively.

In pink mat samples, incubated with labelled bicarbonate in the presence of methane, the concentrations of newly formed methane reached up to 28 µmol after 64 days (PBcLM; Figure 3.4). In contrast, the increase of newly formed methane was marginal in all other experiments, and never exceeds 2 µmol (PBcL, PAcLM, PAcLMI, PAcL, PAcLI; Figure 3.4).

Black mat samples revealed a higher methanogenic activity during all experiments (Figure 3.5). Experiments with labelled acetate reached amounts of newly formed methane between 1 and 2 µmol after 26 days of incubation, independent of the presence of methane or methyl fluoride (BAcLM, BAcLMI, BAcL, BAcLI). After 56 days, incubation experiments methane free at the outset reached 4µmol (BAcL). Highest increase of methane was measured after 64 days with labelled bicarbonate and methane in the headspace (BBcLM). It was about 3 times higher, than in similar experiments with ANME-1 dominated samples. Interestingly, initially methane free incubations with labelled bicarbonate revealed relative low increase of labelled substrate derived methane with was up to 10 µmol after 64 (BBcL; Figure 3.5).

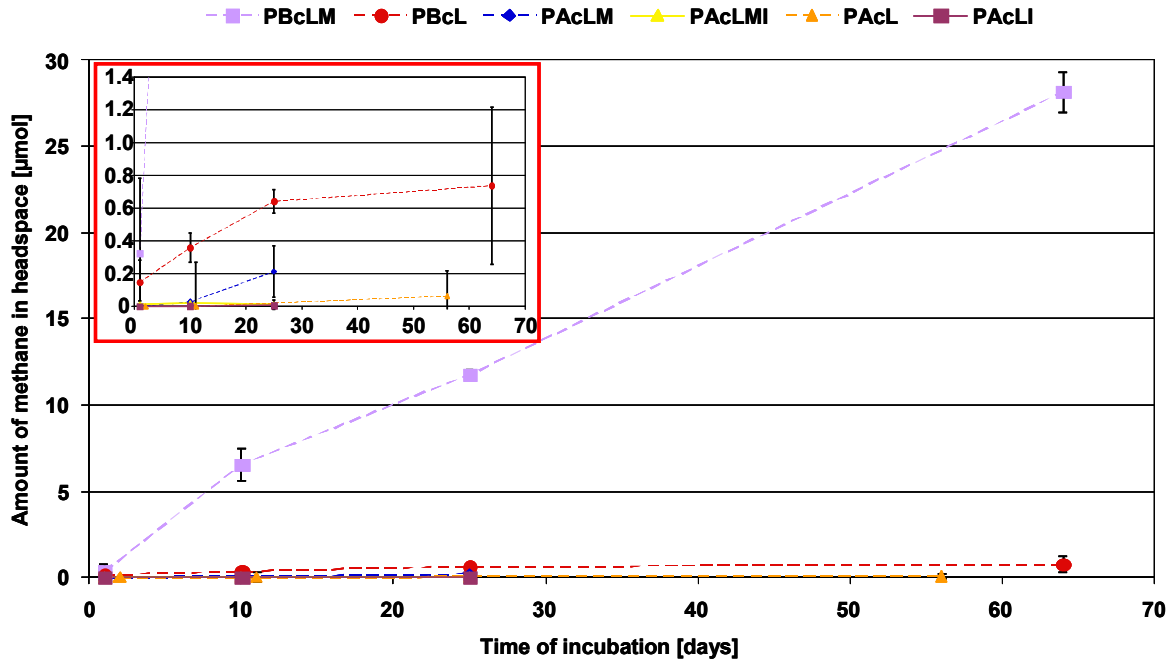

Figure 3.4: Methanogenesis of ANME-1 dominated samples determined based on the concentrations (measured by M. Siegert) and the isotopic compositions (this study) of the methane for incubation experiments with bicarbonate or acetate according to section 2.5.3. The error bars result from replicate measurements.

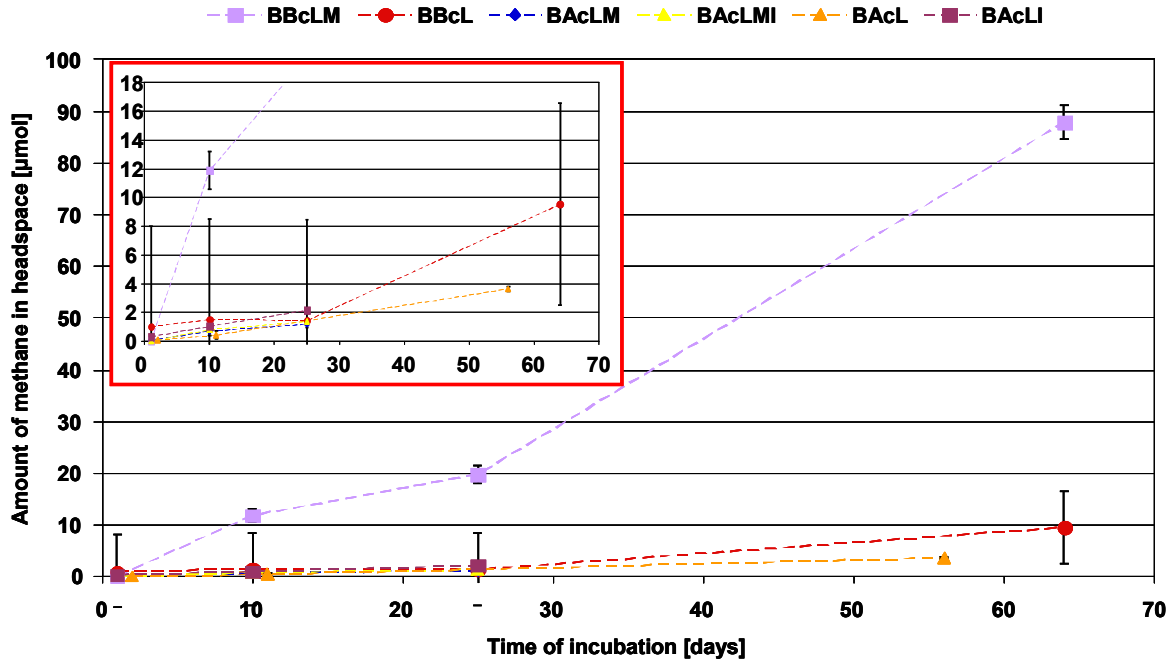

Figure 3.5: Methanogenesis of ANME-2 dominated samples determined based on the concentrations (measured by Siegert) and isotopic compositions (this study) of the methane for incubation experiments with bicarbonate or acetate according to section 2.5.3. The error bars result from replicate measurements.

The calculated rates of methanogenesis for the respective substrates are shown in figure 3.6. The black columns show the rates, only based on measurement of the headspace concentrations in initially methane free incubations. The white columns illustrate the rates, based on the isotopic composition of methane; (i) the portion of substrate derived ^{13}C of newly formed methane in initially methane free incubations, and (ii) the rates of methanogenesis during incubations with methane in the headspace. The isotopically determined rates of methanogenesis from labelled bicarbonate were multiplied with a factor of 5 (due to a 5 fold lower substrate label of bicarbonate, compared to the substrates acetate and methanol).

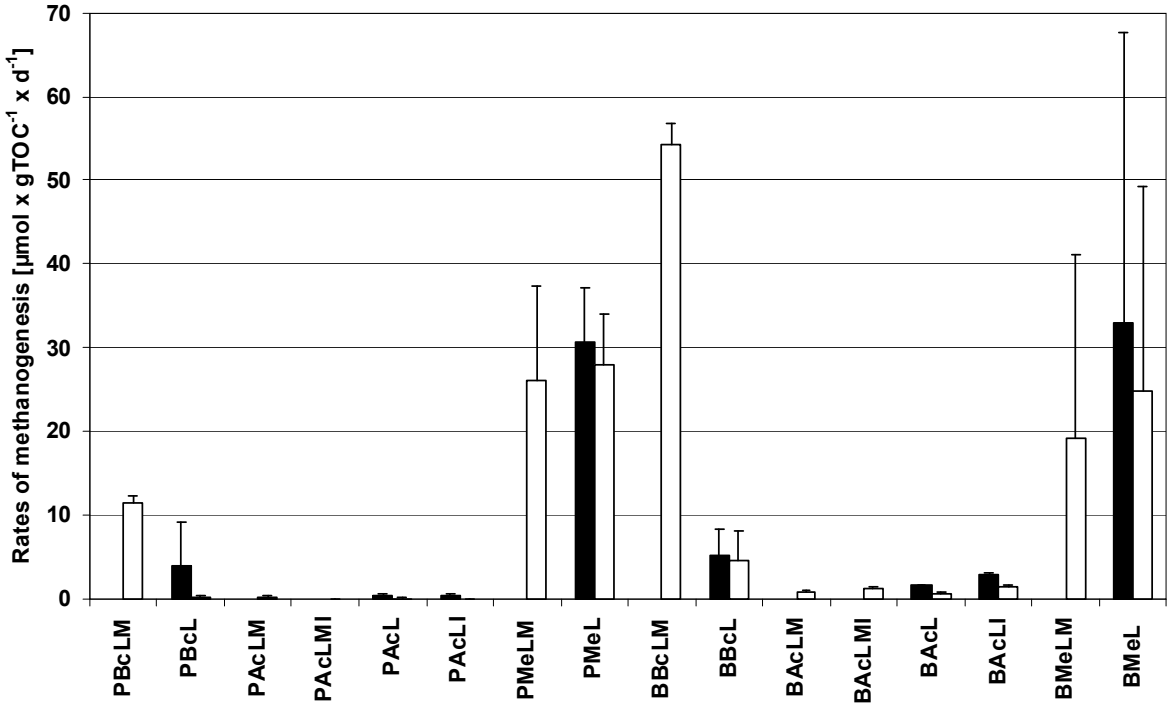

Figure 3.6: Rates of methanogenesis in incubation experiments with different substrates (with and without methane). Black columns: the rates were determined from methane concentrations in the headspace (measured by M. Siegert). White columns: the rates were determined based on the concentration and the isotopic composition of methane. For bicarbonate, the rates were multiplied with a factor of 5 due to respectively lower label concentrations. The error bars result from replicate measurements and show the maximum level of deviation of the rates.

The rates of methanogenesis during experiments with labelled bicarbonate (black columns - BBcL, PBcL) were similar for both samples in methane free incubations (~5 µmol $g_{TOC}^{-1} d^{-1}$), but significantly higher for ANME-2 dominated mat samples in the presence of methane (white columns - BcLM ~55 µmol $g_{TOC}^{-1} d^{-1}$). Within experiments with labelled acetate, only marginal rates of methanogenesis were determined for the pink mat whereby initially methane free experiments revealed slightly higher rates (black columns - PAcL, PAcLI) than those started with methane present (white columns - PAcLM, PAcLMI). In contrast, considerable rates of methanogenesis were generally detected within black mat samples (black columns - BAcL, BAcLI; white columns - BAcLM, BAcLMI). Very high rates of methanogenesis were determined for experiments with added methanol. These rates were nearly in the same range for

both mat types independent if methane was present or not. For the pink mat type, average rates of about 29 µmol $g_{TOC}^{-1} d^{-1}$ were measured. The rate of methanogenesis for black mat types was from 25 µmol $g_{TOC}^{-1} d^{-1}$ in the presence of methane to 32 µmol $g_{TOC}^{-1} d^{-1}$ during incubations without methane (black and white columns - MeLM, MeL; Figure 3.6).

3.1.3 Comparison of methane consumption and sulphate reduction rates

The rates of methane consumption were calculated from the data of methane decrease (see section 3.1.1), taking into account the data of (simultaneous) methane generation as determined by stable isotope composition. Therefore, they were corrected with additional isotopic measurements of the methane. The isotopically determined concentrations were added to the measured concentrations. Figure 3.7 shows these methane decrease rates together with the respective sulphate reduction and calculated methane-dependent sulphate reduction rates. For incubation experiments with 2bar pressure of ^{13}C-labelled methane (data not shown - ML; Table 2.1, page 17) only sulphate reduction rates were measured. However, the respective rates were similar to those of incubation experiments with 1bar methane pressure (BcLM) for both mat types.

The rates of methane consumption exceeded those of sulphate reduction for all experiments in both mat types but, much more pronounced in ANME-1 dominated mat samples (Figure 3.7). Both mat types revealed highest rates in the experiments with labelled acetate, whereby the addition of methyl fluoride as inhibition reagent for acetoclastic methanogenesis led to a lower methane consumption and methane-dependent sulphate reduction in both samples (PAcLMI, BAcLMI).

The sulphate reduction rates in ANME-1 dominated samples were relatively low compared to methane consumption (for all experiments; Figure 3.7). The sulphate reduction rates reached highest levels for ANME-1 dominated mat samples within incubations supplemented with ^{13}C-acetate (PAcLM). This holds true for the measured sulphate reduction as well as the calculated methane-dependent sulphate reduction (PAcLM). Very low methane-dependent sulphate reduction rates were determined for acetate incubation experiments with methane and methyl fluoride (PAcLMI). No sulphate reduction was measured in experiments with methanol and methane for pink mat samples (PMeLM), while methane consumption was occurring. In contrast, the rates of sulphate reduction and methane consumption were in about the same range for ANME-2 dominated samples amended with methanol (BMeLM).

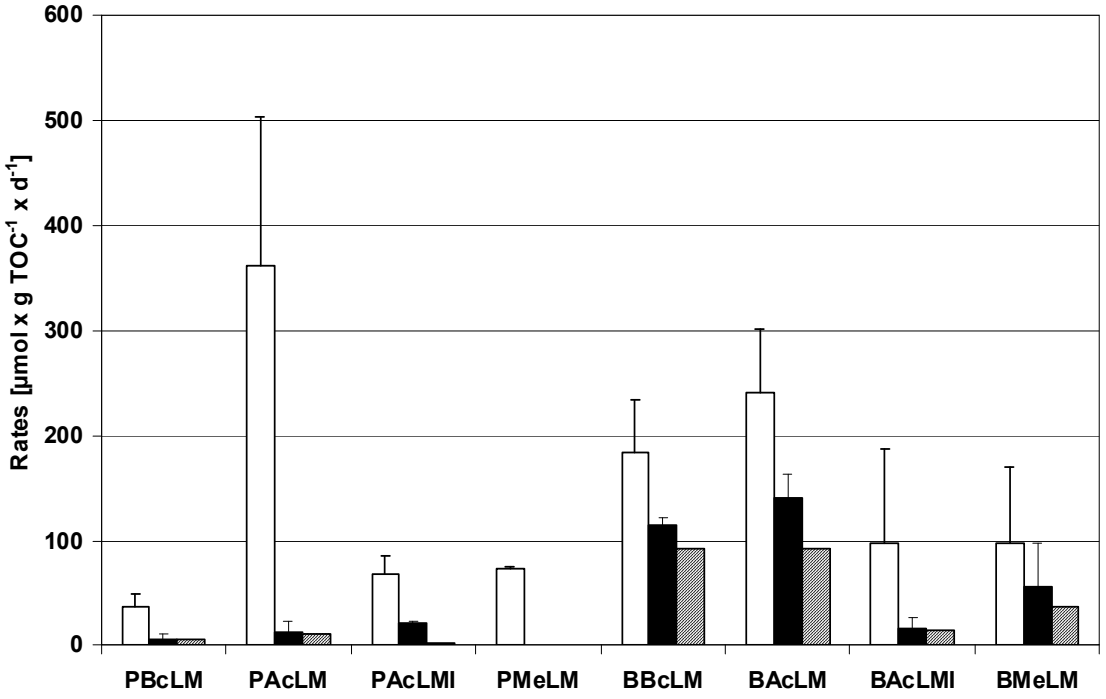

Figure 3.7: Methane consumption rates (white columns - measured) compared to sulphate reduction rates (black columns - measured) and methane-dependent sulphate reduction rates (striped columns - calculated) of incubation experiments with ANME-1 and ANME-2 dominated mat samples**.** The consumption of methane (white columns) was determined from the headspace concentrations (measured by M. Siegert)**.** The sulphate reduction rates (black columns) were determined from sulphide concentrations (measured by M. Siegert), and calculated rates of AOM-dependent sulphate reduction (black-white striped columns; calculated). The error bars result from replicate measurements and show the maximum deviation of the rates.

3.2 The lipid biomarker compositions of the communities

For all incubation experiments, the concentrations of most of the identified bacterial and archaeal lipids were determined. The relative distributions of the selected lipid biomarkers differ significantly between the two mat types. Figures 3.8 illustrate the average distribution of selected compounds attributed to the archaea in pink (orange columns) and black mat (black columns) samples, respectively. On the y-axis, the relative abundance of all compounds normalised to *sn-2*-hydroxyarchaeol (3.8) is depicted.

Archaeol (*2,3-di-O*-phytanyl-*sn*-glycerol) was a main compound in both mat types. The *2,6,10,15,19*-pentamethylicosane/enes (PMI) showed, with relative high amounts of PMI:3, similar patterns in both mat types (Figure 3.8).

A monounsaturated archaeol (Archaeol:1; *2-O-3*-phytenyl-*3-O*-phytanyl-sn-glycerol or *2-O*-phytanyl-*3-O-3*-phyentyl-sn-glycerol) and especially, among ether cleavage products, high amounts of a- ($C_{40:0}$ or *3,7,11,15,18,22,26,30*-octamethyl-dotriacontane), monopenta- ($C_{40:1}$ or *1*-(*1,5,8,12,16,20*-hexamethyldocosyl)-*3*-(*4*-methylhexyl)-cyclopentane) and dipentacyclic ($C_{40:2}$ or *1,1'*-(*1,5,8,12*-tetramethyl-*1,12*-dodecandiyl)-bis[*3*-(*4*-methylhexyl)]-cyclopentane) isomers of biphytanes were only found in ANME-1 dominated mat samples. These samples also revealed low

amounts of several isomers of a C_{35}-isoprenoid. The structural details are described below (Figure 3.9, 3.10).

Crocetane (*2,6,11,15*-tetramethylhexadecane) and *sn-2*-hydroxyarchaeol (*2-O-3*-hydroxyphytanyl-*3-O*-phytanyl-*sn*-glycerol) were only observed in ANME-2 dominated samples (Figure 3.8).

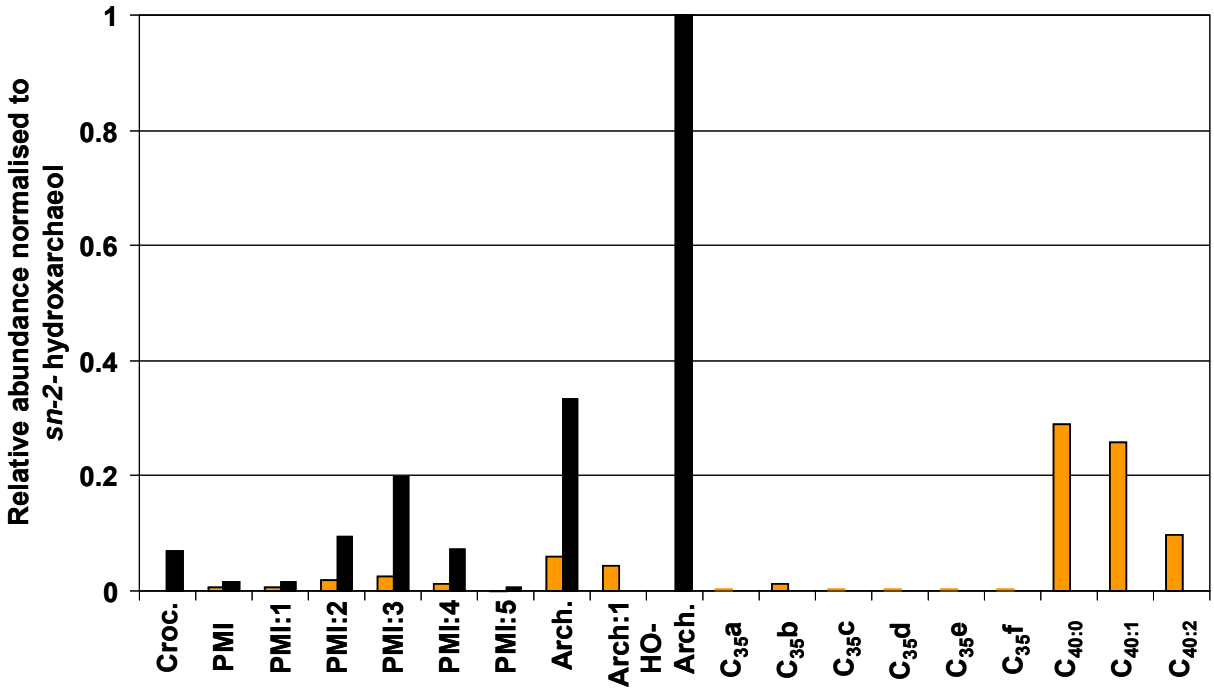

Figure 3.8: The composition and relative abundance of selected archaeal compounds in ANME-1 and -2 dominated samples; normalised to the concentrations of *sn-2*-hydroxyarchaeol.

The mass spectrometric analysis of the C_{35}-compounds revealed an isoprenoid structure for the six isomers of the C_{35}-isoprenoid hydrocarbons. The base peak with the mass of 69 represents a diagnostic isoprenoid fragment with one double bond. The molecular ion peaks of the isomers $C_{35:5}$a and $C_{35:5}$d are 482, which indicate five fold unsaturated structures. The isomers $C_{35:6}$b and $C_{35:6}$e have a mass of 480, thus they have six unsaturations. For the isomers $C_{35:7}$c and $C_{35:7}$f the mass of 478 was identified, which indicates an isoprenoid hydrocarbon molecule with seven unsaturations. They were tentatively identified as five (C_{35} a, d), six (C_{35} b, e) and seven (C_{35} c, f) fold unsaturated isomers (Figure 3.8).

The isomers $C_{35:5}$a and $C_{35:5}$d are further described in detail to elucidate more structural details (Figures 3.9, 3.10). All other structures ($C_{35:6}$b, $C_{35:7}$c, $C_{35:6}$e, $C_{35:7}$f) are described in detail in the appendix (A.7).

The spectrum of the C_{35}-ioprenoid hydrocarbon isomer $C_{35:5}$a shows the fragments with a m/z of 137, 205, and 275 which implicate an arrangement of up to four isoprenoid fragments with three double bonds. The mass 345 implicates an arrangement of five isoprenoid fragments with 3 double bonds. The mass 413 indicates a fragment of six isoprenoid building blocks with 4 double bonds (Figure 3.9).

The isomers $C_{35:5}$a, $C_{35:6}$b, and $C_{35:7}$c only differ in their amount of double bonds. They were tentatively identified as constitutional isomers of *2,6,10,14,18,22,26*-heptmethyloctacosene, respectively. The carbon backbones of all of these C_{35}-isoprenoids were most probably assembled with a head-to-tail condensation.

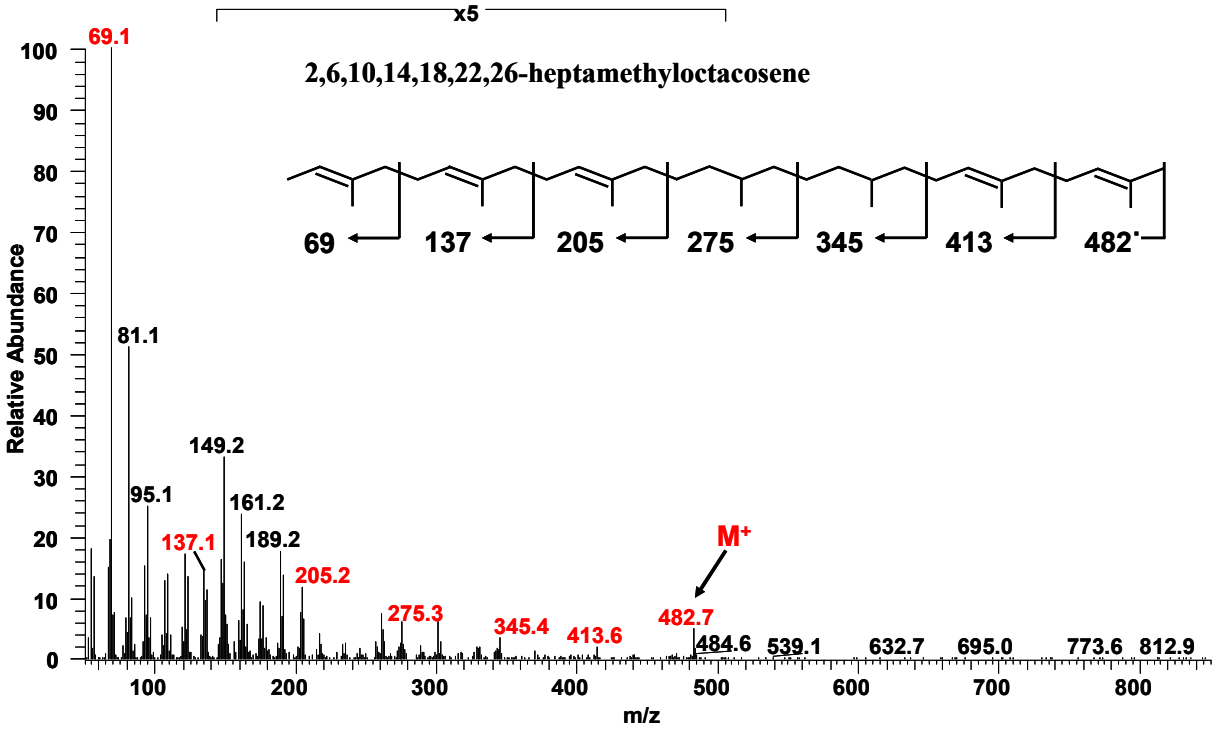

Figure 3.9: Spectrum of the C_{35}-isoprenoid hydrocarbon isomer $C_{35:5}$a with five double bonds. The spectrum was revealed with a GC-MS in the EI modus with -70 eV.

The structural analysis of the isomers $C_{35:5}$d, $C_{35:6}$e, and $C_{35:7}$f revealed slightly structural differences from those of the isomers $C_{35:5}$a, $C_{35:6}$b, $C_{35:7}$c. The spectrum of $C_{35:5}$d shows two fragments with the mass 123 and 149, which could be tentatively explained with an internal pentacyclic ring structure, linked to the fifth carbon atom. The same masses but later retention times underline such a consideration of an internal ring structure (Figure 3.10). However, the mass spectra give no detailed resolution of the molecules. They are only tentatively identified as *5*-pentacyclopentyl-*3,12,16,20,24,28*-hexamethylnonacosene ($C_{35:5}$d), with four to six undersaturations.

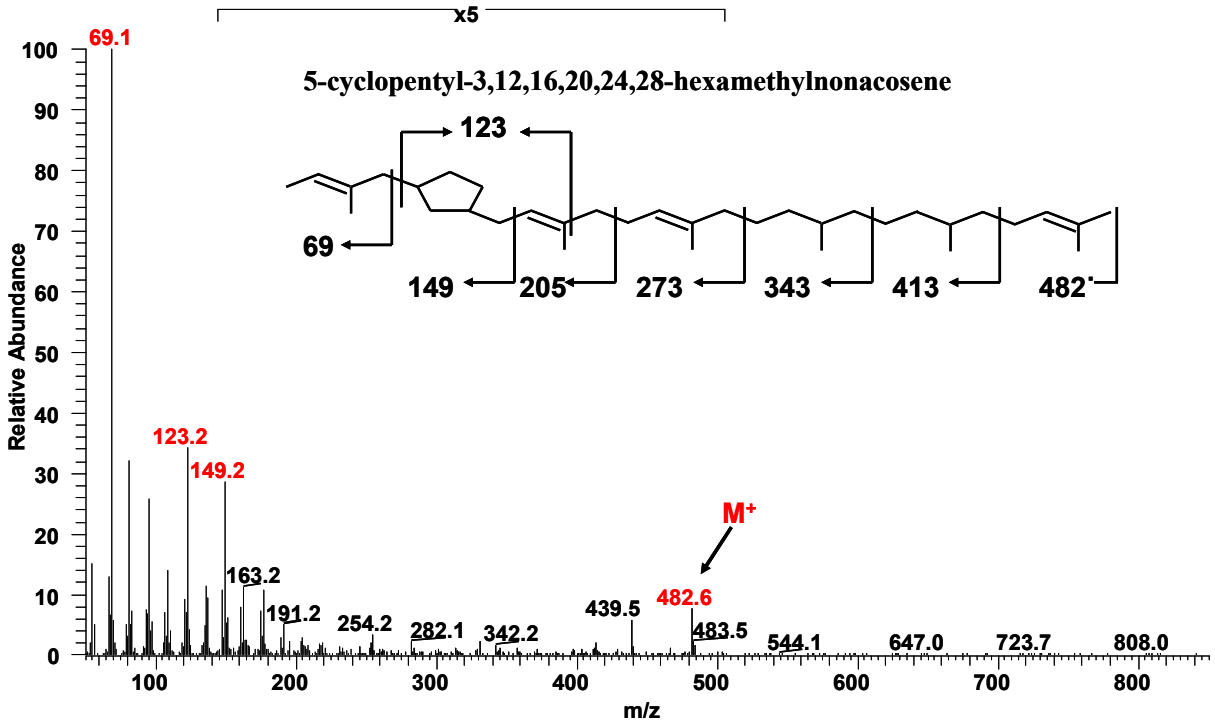

Figure 3.10: Spectrum of the C_{35}-isoprenoid hydrocarbon isomer $C_{35:5}$d with four double bonds, bearing one additional pentacyclic ring structure. The spectrum was revealed with a GC-MS in the EI modus with -70 eV.

For the bacterial lipids (Figure 3.11, normalised to *cis-ω5*-hexadecenoic acid), in particular *ω12*-methyl tetradecanoic acid (*ai*fa15:0), assigned to SRB in AOM-performing settings (Michaelis et al., 2002), and 17α(H),21α(H)-bishomohopanoic acid (hopanoic acid) were predominant in the fatty acid fraction of the ANME-1 dominated mat samples.

The composition of the fatty acids in ANME-2 dominated mat samples (Figure 3.11) was strongly dominated by *cis-ω7*- and *cis-ω5*-hexadecenoic acid (fa16:1ω7c, fa16:1ω5c), and the cyclopropyl-containing *ω5,6*-heptadecanoic acid (*cy*fa17:1ω5,6). *cis-ω5*-hexadecenoic acid was attributed to SRB in AOM-settings (Elvert et al., 2003).

In pink and black mat samples, different patterns of several monoalkyl glycerol ethers (MAGEs) and dialkyl glycerol ethers (DAGEs) with different alkyl chains were also found. These compounds were most abundant in respective ANME-1 samples. The constitutional isomers of *1,2-di-O*-pentadecyl-*sn*-glycerol ethers (15DAGEs) were major bacterial compounds in the alcohol fraction of the ANME-1 dominated mat samples. Here, only the unsaturated isomer of the *1-O*-hexadecyl-*sn*-glycerol ether lipids (16:1MAGE) of three detected isomers will be considered as representative compound for all other monoalkyl ethers (ranging between C_{14}-C_{18}) in the pink mat samples. For ANME-2 dominated samples, only one isomers of *1-O*-hexadecyl-*sn*-glycerol (16MAGEc) and the three constitutional isomers of terminally branched *1,2-di-O*-pentadecyl-*sn*-glycerol ethers (15DAGEs) will be described in the following sections. While the isomers of the *1,2-di-O*-pentadecyl-*sn*-glycerol ethers revealed in similar concentrations in both mat types, the isomers of *1-O*-hexadecyl-*sn*-glycerol were rather dominant in the pink mat samples.

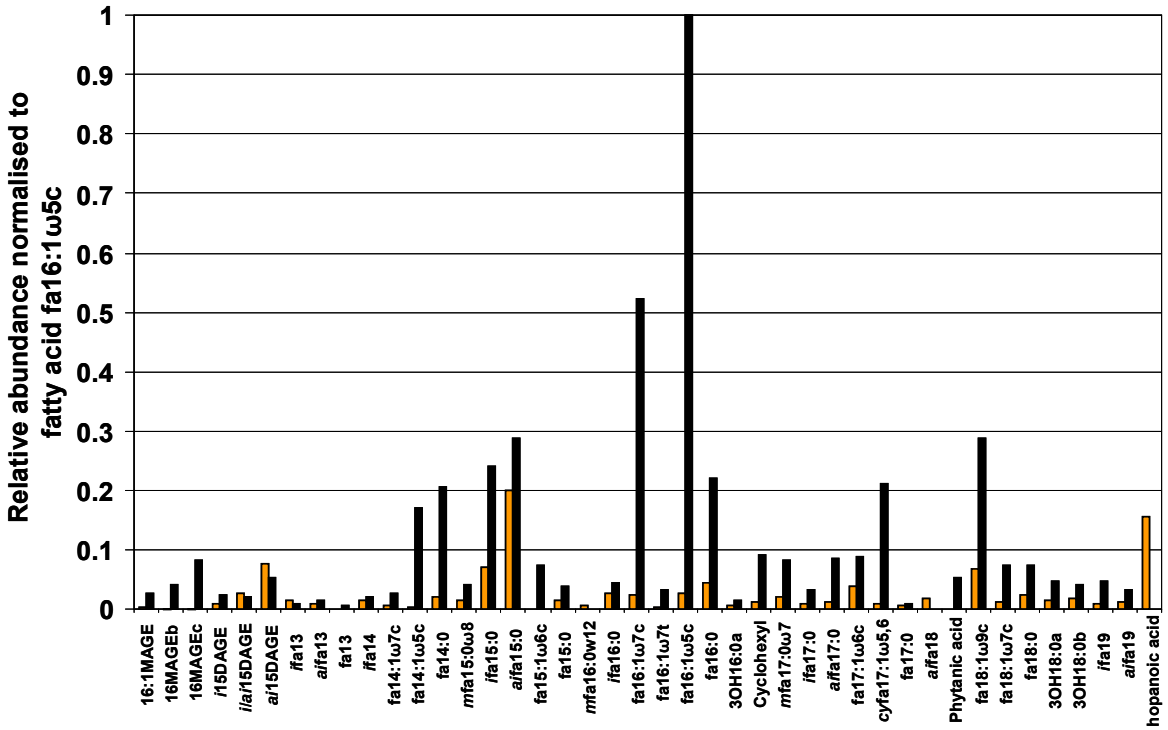

Figure 3.11: The composition and relative abundance of selected bacterial compounds in the ANME-1 and -2 dominated samples; normalised to *cis-ω5*-hexadencenoic acid.

3.3 Daily $\delta^{13}C$-shifts of individual lipids and daily total $\delta^{13}C$-shifts

The daily assimilation as $\Delta\delta^{13}C$ was determined to compare the assimilation rates for archaeal and bacterial lipids. The assimilation rates correspond to the synthesis rates for specific compounds with different substrates; Figures 3.12 and 3.13. The degradation of those compounds is assumed to be very slowly within the experimental set up. The daily total $\delta^{13}C$-shifts were expressed in the δ-notation and summarised for most compounds (listed in Section 2.4.7.3, p.22); illustrated in Table 3.1. The uptake is calculated per day to compare different incubation times for different experiments, independent of the individual concentrations. For the nomenclature of the bacterial compounds the abbreviations according to the appendix (A.5, page 144) are used in the following description of the results.

3.3.1 Daily $\delta^{13}C$-shifts of individual archaeal lipids

3.3.1.1 Daily $\delta^{13}C$-shifts of selected archaeal lipids in ANME-1 dominated mats

The assimilation patterns differ strongly between all incubation experiments within the archaeal lipids for ANME-1 dominated mat types (Figure 3.12a, c, e, g). Highest assimilation rates of substrate derived ^{13}C were determined after the addition of methanol (Figure 3.12g), particularly in the absence of methane (MeL; Figure 3.12g). The uptake of ^{13}C-labelled acetate (99.9 %) derived carbon was up to 8 times higher than that of bicarbonate (e.g. for PMI:5; Figure 3.12c, e). However, the bicarbonate used was only labelled with 20 % of ^{13}C.

Highest uptakes of ^{13}C into PMI:4 and PMI:5 were observed, compared to other compounds from ^{13}C-methane, ^{13}C-bicarbonate, and ^{13}C-acetate (Figure 3.12a, c, e). For the latter two they were slightly enhanced when methane was present (Figure 3.12c, e). Relatively low incorporation of ^{13}C from labelled methanol was determined for the PMIs compared to the isoprenoid glycerol ether lipids. For instance, PMI:5 revealed a daily shift up to 4 ‰ in the absence of methane (MeLM, MeL; Figure 3.12g).

The determined ^{13}C-assimilation rates for archaeol were enhanced compared to its unsaturated isomer in most incubation experiments (Figure 3.12a, c, g). By contrast, archaeol:1 showed slightly higher assimilation rates with ^{13}C-labelled bicarbonate in the absence of methane (BcL; Figure 3.12c). Generally very high assimilation rates were observed into archaeol (121 ‰) and its unsaturated isomer (32 ‰) with ^{13}C-labelled methanol in the absence of methane (MeL; Figure 3.12g).

C_{35}-isoprenoids revealed only uptake from ^{13}C-methane, ^{13}C-acetate, and ^{13}C-bicarbonate, especially for the 7 fold unsaturated hydrocarbon isomers (C_{35}c, C_{35}f; Figure 3.12a, c, e). For the latter two, it was diminished with acetate or almost absent with bicarbonate when methane was present. Despite the general very high uptake of ^{13}C from labelled methanol into other archaeal lipids, no considerable assimilation into the C_{35}-isoprenoids was observed (MeLM, MeL; Figure 3.12g).

In general, the determined assimilation rates for constitutional isomers of the biphytanes ($C_{40:0}$, $C_{40:1}$, $C_{40:2}$) as products after ether cleavage of the glycerol dialkyl glycerol tetraethers (GDGTs) were very low (Figure 3.12a, c, e, g). The $\delta^{13}C$-values of these compounds were not analysed for experiments with bicarbonate only (BcL; Figure 3.12c). The rates from labelled methane and bicarbonate were nearly in the same range, e.g. from labelled bicarbonate between 0.03 ‰ d^{-1} and 0.05 ‰ d^{-1}. Daily rates from labelled acetate, independent of the presence of methane, were measured about 0.4 ‰, 0.5 ‰, and 0.5 ‰ for $C_{40:0}$, $C_{40:1}$, and $C_{40:2}$, respectively (Figure 3.12e). Similar ^{13}C-incorporations were observed with labelled methanol, into the $C_{40:1}$ and $C_{40:2}$ (MeL; $C_{40:1}$ ~0.2 ‰ d^{-1}, $C_{40:2}$ ~0.4 ‰ d^{-1}).

3.3.1.2 Daily $\delta^{13}C$-shifts of selected archaeal lipids in ANME-2 dominated mats

The assimilation patterns of ANME-2 specific archaeal lipids were similar for experiments with methane, bicarbonate, and acetate in the presence of methane (ML, BcLM, AcLM; Figure 3.12b, d, f). But those rates differ strongly from incubation experiments with methanol, which demonstrated also the highest changes, particularly in the absence of methane (MeLM, MeL; Figure 3.12h). The assimilation rates in the presence of methane were significantly higher in experiments with bicarbonate and acetate, also if compared with ANME-1 mats (BcLM, BcL, AcLM, AcL, AcLMI, AcLI; Figure 3.12d, f). Very high rates were observed within experiments with methanol (MeLM), and in particular in the absence of methane (MeL; Figure 3.12h). Also very high assimilation rates were observed with ^{13}C-labelled acetate (Figure 3.12f).

For crocetane, a very low ^{13}C-shift (0.02 ‰ d^{-1}) was observed from ^{13}C-methane only (ML; Figure 3.12b).

The four and five fold unsaturated pentamethylicosenes, however, revealed very high assimilation rates compared to other compounds from ^{13}C-methane, ^{13}C-bicarbonate, and ^{13}C-acetate (Figure 3.12b, d, f). For the latter two, they were strongly enhanced when methane was present (Figure 3.12d, f). A δ^{13}C-shift per day about 12 ‰ was measured for PMI:5 from incubations with labelled acetate and methane in the headspace. No isotopic values were analysed for PMI:5 in experiments with labelled bicarbonate and methane, due to low concentrations (BcM; Figure 3.12d). Similar to ANME-1 dominated samples; relatively low ^{13}C-assimilation rates into the PMIs from labelled methanol were observed (MeLM, MeL; Figure 3.12h) compared to those of the isoprenoid glycerol ethers. However, the daily ^{13}C-shift were higher in the absence of methane and reached a rate up to 8 ‰ d^{-1} (MeL; Figure 3.12h).

For archaeol and *sn-2*-hydroxyarchaeol similar observations as for the pentamethylicosenes were made (Figure 3.12b, d, f). Considerable ^{13}C-assimilation rates from labelled bicarbonate in the presence of methane took place into archaeol with lower extent in the absence of methane (BcLM, BcL; Figure 3.12d). *sn-2*-hydroxyarchaeol showed only uptake from labelled acetate and methane in the headspace. The measured $\Delta\delta^{13}$C was 0.3 ‰ d^{-1} (AcLM; Figure 3.12f). Nonetheless, the dialkyl glycerol ethers revealed slightly lower rates but exceptionally high ^{13}C-assimilation rates from labelled methanol (MeLM, MeL; Figure 3.12h). Here, the ^{13}C-assimilation rates were much higher in the absence of methane, for archaeol as well as for *sn-2*-hydroxyarchaeol 47 and 18 ‰ d^{-1}, respectively (MeL; Figure 3.12h).

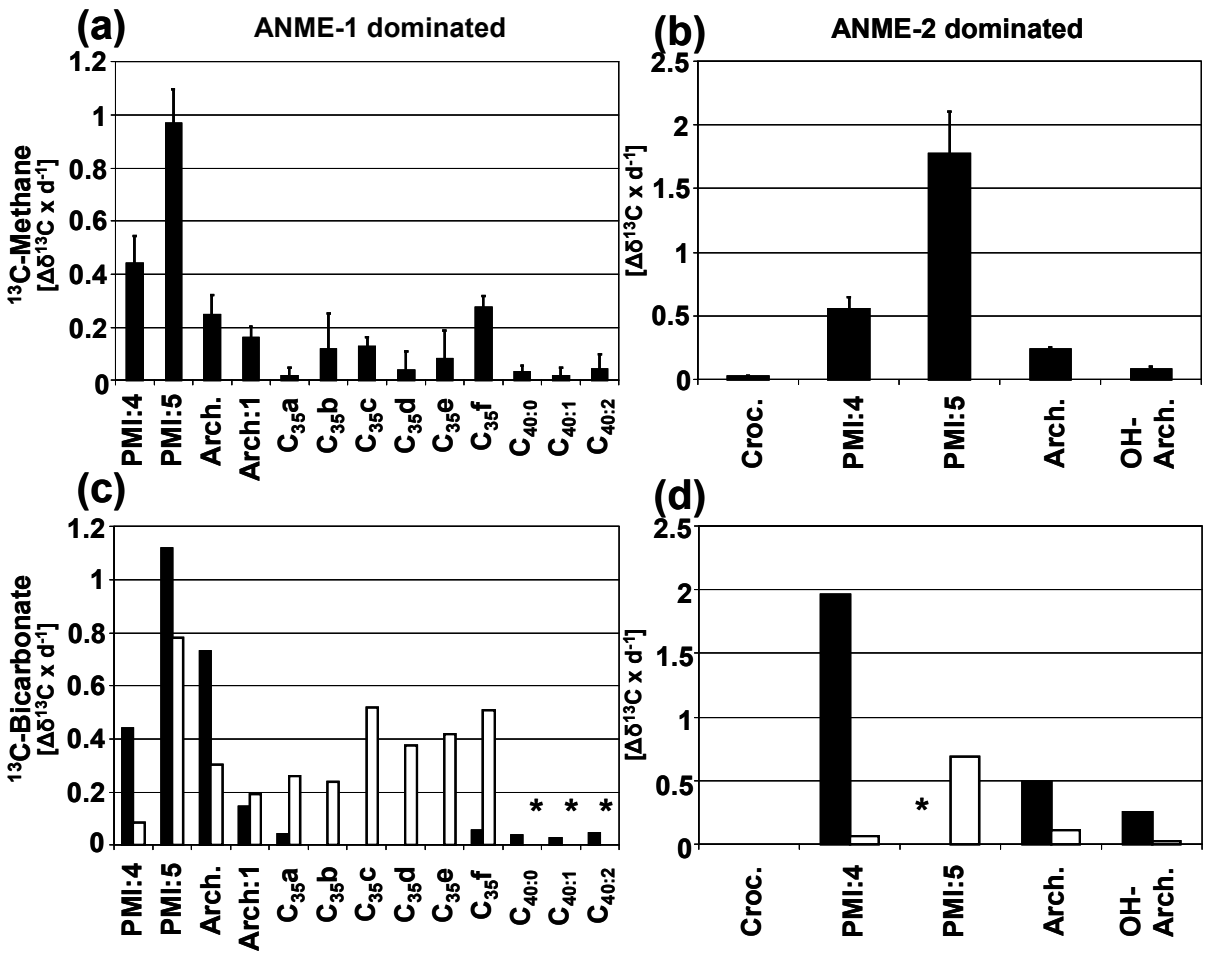
(a)
ANME-1 dominated
(b)
ANME-2 dominated
(c)
(d)
13C-Methane
[Δδ13C x d-1]
13C-Bicarbonate
[Δδ13C x d-1]
PMI:4
PMI:5
Arch.
Arch:1
C35a
C35b
C35c
C35d
C35e
C35f
C40:0
C40:1
C40:2
Croc.
OH-Arch.
*

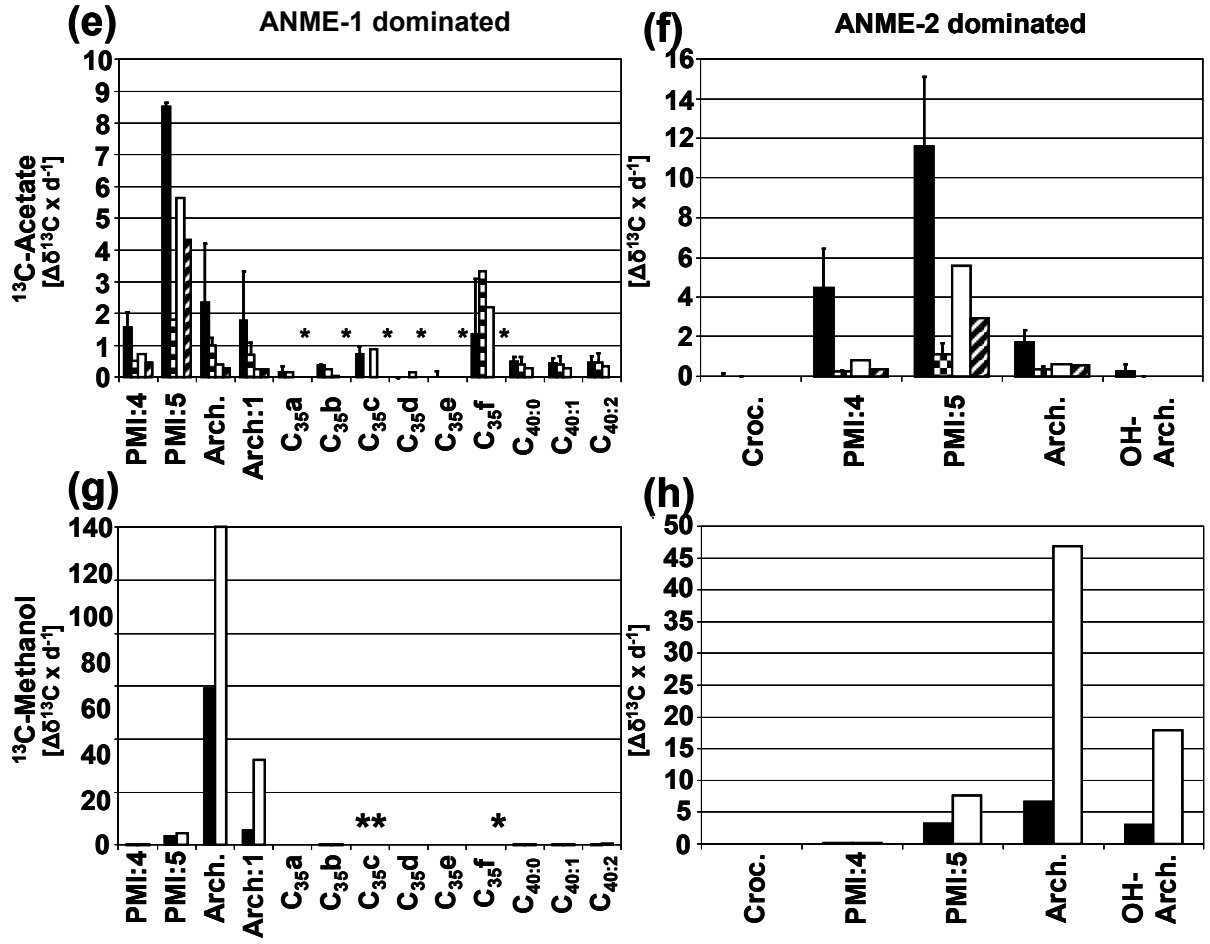

Figure 3.12: Daily ^{13}C-shifts of archaeal lipid biomarker compounds of ANME-1 (left) and -2 (right) dominated communities incubated with different ^{13}C-labelled substrates under different conditions. (a, b) ^{13}C-methane - ML, (c, d) ^{13}C-bicarbonate (black columns with methane - BcLM, white columns without methane in the headspace - BcL), (e, f) ^{13}C-acetate (black columns with methane - AcLM, chequered columns without methane in the headspace - AcL, white columns with methane and methyl fluoride - AcLMI, black-white stripped columns with methyl fluoride and without methane in the headspace - AcLI), (g, h) ^{13}C-methanol (black columns with methane - MeLM, white columns without methane in the headspace - MeL). The error bars result from replicate or triplicate measurements and show the maximum level of deviation of the rates. For experimental details see methods and table 2.1. * not analysed.

3.3.2 Daily $\delta^{13}C$-shifts of individual bacterial lipids

The compound specific ^{13}C-assimilation rates per µg compound are shown in Figure 3.13 for selected bacterial compounds. The $\Delta\delta^{13}C$ were distinct for both bacterial mat communities, but they were generally similar within each experiment independent of methane was present or not. Only the ^{13}C-assimilation rates differed in their range between incubation experiments with different ^{13}C-labelled substrates (Figure 3.13a - h). Highest ^{13}C-assimilation rates were observed with labelled acetate (AcLM, AcL, AcLMI, AcLI; Figure 3.13e, f). There was obviously no considerable influence from the presence of methane or methyl fluoride in all incubation experiments with acetate (AcLM, AcL, AcLMI, AcLI; Figure 3.13e, f).

3.3.2.1 Daily $\delta^{13}C$-shifts of selected bacterial lipids in ANME-1 dominated mats

The assimilation patterns were distinct in all incubation experiments. For instance, slight differences were observed between experiments with labelled methane (ML; Figure 3.13a) and labelled bicarbonate (BcLM, BcL; Figure 3.13c). The patterns were similar for experiments with labelled bicarbonate (BcLM, BcL; 3.13c), labelled methanol (MeLM, MeL; 3.13g), and acetate (AcLM, AcLMI, AcL, AcLI; Figure 3.13e).

Highest ^{13}C-assimilation rates derived from labelled methane were observed for fa16:1ω7c, fa16:1ω5c, fa16:0, and fa18:0 (ML; Figure 3.13a), e.g. for the fa16:1ω7c a daily rate of 0.5 ‰ was measured. Highest rates were observed for fa16:1ω7c and fa16:0 from experiments with labelled bicarbonate. Here, the fa16:1ω7c revealed an average $\delta^{13}C$-shift of about 3 ‰ d^{-1}, independent of the presence of methane (BcLM, BcL; Figure 3.13c). Lower assimilation rates were observed for fa14:0 and *ai*fa15 from samples with labelled bicarbonate only. The fa14:0 showed a daily shift of 0.25 ‰, when no methane was present (BcL; Figure 3.13c). Low but considerable ^{13}C-uptake into diploptene (AcLM, AcL, AcLMI, AcLI; Figure 3.13e) has been observed after the addition of acetate, rates up to 9 ‰ d^{-1} were determined for incubations with labelled acetate in the presence of methane and methyl fluoride (AcLMI; Figure 3.13e).

Notably, relative low assimilation rates were also observed for fa14:0, *i*fa15, *ai*fa15, and fa18:0 within experiments with labelled acetate (AcLM, AcL, AcLMI, AcLI; Figure 3.13e), e.g. for the fa14:0 37 ‰ d^{-1} (AcL) and for the fa18:0 9 ‰ d^{-1} (AcL) were measured. In the same experiments relatively high assimilation rates were determined for fa16:1ω7c, fa16:1ω5c and fa16:0 (AcLM, AcL, AcLMI, AcLI; Figure 3.13e). For instance, after incubations with acetate only the fa16:1ω7c reached an average shift of 431 ‰ per day (AcL). Relative low ^{13}C-assimilation rates were observed after addition of labelled methanol into fa14:0, *i*fa15:0, *ai*fa15:0, fa16:1ω5c, and fa18:1ω9c (MeLM, MeL; Figure 3.13g). The shift for the fa16:1ω7c was 2.7 ‰ per day, during incubations with methanol in the absence of methane (MeL; Figure 3.13g). Noticeable, assimilation of ^{13}C into fa18:1ω9c (0.3 ‰ d^{-1}) was only observed in the presence of methane (MeLM; Figure 3.13g). In the methanol experiments for

most compounds the rates were slightly reduced in the presence of methane (MeLM; Figure 3.12g).

In none of the incubations, uptakes into bishomohopanoic acid were observed.

3.3.2.2 Daily δ^{13}C-shifts of selected bacterial lipids in ANME-2 dominated mats

The patterns of daily ^{13}C-shift into the lipids of ANME-2 associated bacteria were similar for incubations with carbon isotopic labelled methane (ML; Figure 3.13b) and labelled bicarbonate, particularly when methane was present (BcLM, BcL; Figure 3.13d). However, they differ strongly when the samples were incubated with labelled acetate or methanol (AcLM, AcL, AcLMI, AcLI, MeLM, MeL; Figure 3.13f, h). While the assimilation patterns from labelled acetate apparently were not affected by the presence or absence of methane or methyl fluoride for most of the compounds (AcLM, AcL, AcLMI, AcLI), the patterns, particularly the assimilation of some specific fatty acids were mainly influenced by the presence of methane (MeLM). Remarkable, enhanced assimilation rates for fa16:1ω7c, fa16:0, fa18:1ω7c, fa18:1ω9c and fa18:0 were measured (MeLM; Figure 3.13h), for instance the fa16:1ω7c revealed a daily shift of 5.9 ‰.

During incubations with labelled methane, lowest assimilation rates were found for *cy*fa17:1ω5,6 (0.1 ‰ d^{-1}), fa18:1ω9c, fa18:1ω7c (0.1 ‰ d^{-1}) and highest ^{13}C-incorporation into fa14:0 (0.4 ‰ d^{-1}), *i*fa15:0, *ai*fa15:0, fa16:0 (0.6 ‰ d^{-1}), fa16:1ω7c (0.3 ‰ d^{-1}), fa16:ω5c (0.3 ‰ d^{-1}), and fa18:0 within incubations with labelled methane (ML, Figure 3.13b). Considerable assimilation rates into all MAGEs and DAGEs were found in incubation experiments with labelled methane, for instance a daily shift of 0.2 ‰ for 16MAGE(c) (ML; Figure 3.13b). Incubation experiments with labelled bicarbonate (BcL, BcLM; Figure 3.13d) revealed very low uptakes into fa16:1ω5c (0.2 ‰ d^{-1}; BcL; Figure 3.13d). The fa14:0 and fa16:1ω5c revealed no or marginal assimilation rates without methane in the headspace. Otherwise *cy*fa17ω5,6 showed only marginal assimilation rates without methane (BcLM, BcL; Figure 3.13d), e.g. 0.05 ‰ d^{-1} without methane in the headspace.

Highest assimilation rates were determined after incubations with acetate, when methane was present for *i*fa15:0, fa16:1ω7c (27.7 ‰ d^{-1}), fa16:0 (36 ‰ d^{-1}), and fa18:1ω9c (40.2 ‰ $d^{-1;}$ AcLM; Figure 3.13f). Enhanced assimilation rates into fa16:0 (48.2 ‰ d^{-1}), fa16:1ω7c (32.7 ‰ d^{-1}), and fa18:1ω9c were shown without methane and/ or methyl fluoride (AcLM, AcL, AcLI; Figure 3.13f).

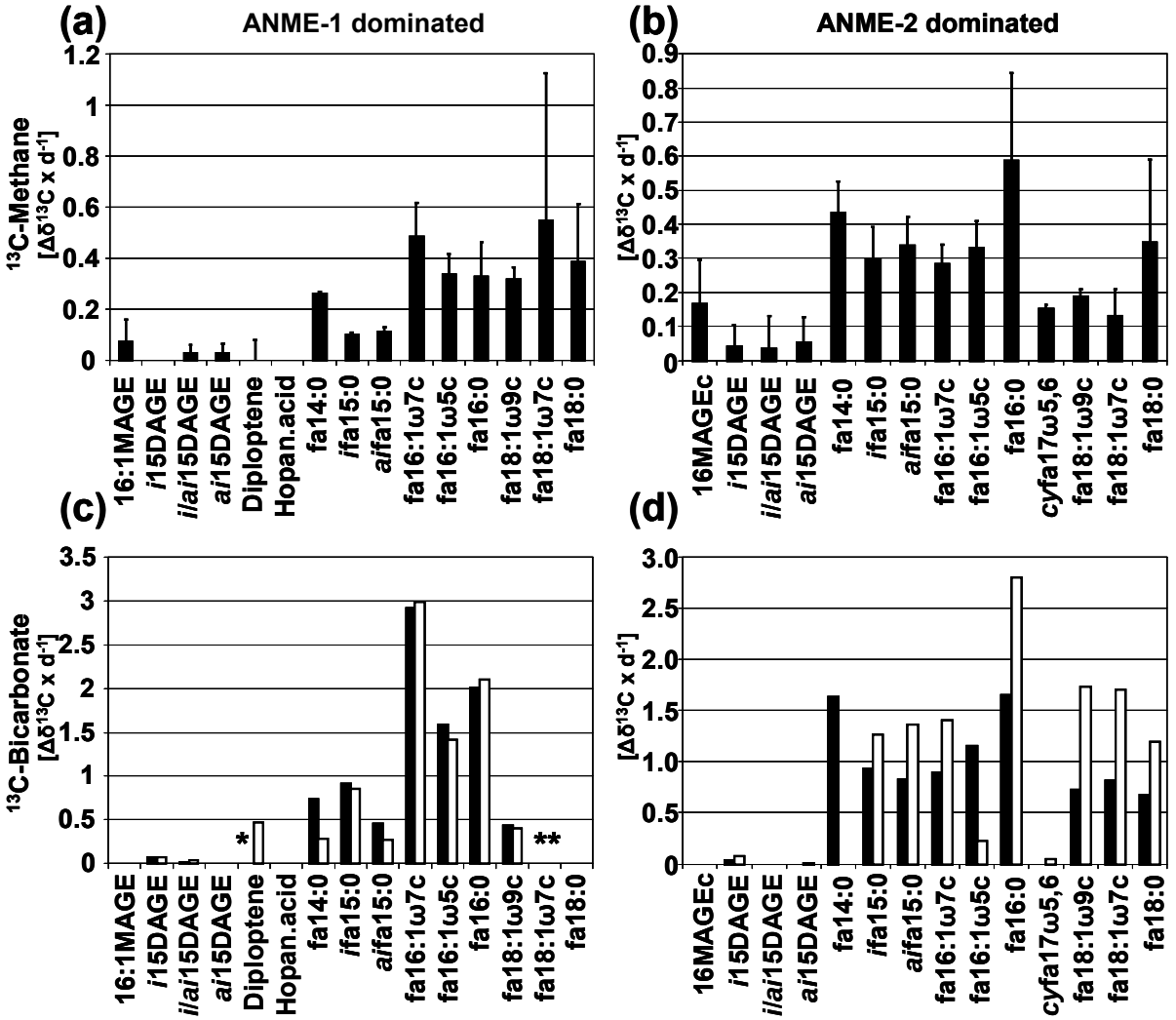
(a)
ANME-1 dominated
13C-Methane
[Δδ13C x d-1]
1.2
1
0.8
0.6
0.4
0.2
0
16:1MAGE
i15DAGE
il/ai15DAGE
ai15DAGE
Diploptene
Hopan.acid
fa14:0
ifa15:0
aifa15:0
fa16:1ω7c
fa16:1ω5c
fa16:0
fa18:1ω9c
fa18:1ω7c
fa18:0
(b)
ANME-2 dominated
[Δδ13C x d-1]
0.9
0.8
0.7
0.6
0.5
0.4
0.3
0.2
0.1
0
16MAGEc
i15DAGE
il/ai15DAGE
ai15DAGE
fa14:0
ifa15:0
aifa15:0
fa16:1ω7c
fa16:1ω5c
fa16:0
cyfa17ω5,6
fa18:1ω9c
fa18:1ω7c
fa18:0
(c)
13C-Bicarbonate
[Δδ13C x d-1]
3.5
3
2.5
2
1.5
1
0.5
0
*
**
16:1MAGE
i15DAGE
il/ai15DAGE
ai15DAGE
Diploptene
Hopan.acid
fa14:0
ifa15:0
aifa15:0
fa16:1ω7c
fa16:1ω5c
fa16:0
fa18:1ω9c
fa18:1ω7c
fa18:0
(d)
[Δδ13C x d-1]
3.0
2.5
2.0
1.5
1.0
0.5
0
16MAGEc
i15DAGE
il/ai15DAGE
ai15DAGE
fa14:0
ifa15:0
aifa15:0
fa16:1ω7c
fa16:1ω5c
fa16:0
cyfa17ω5,6
fa18:1ω9c
fa18:1ω7c
fa18:0

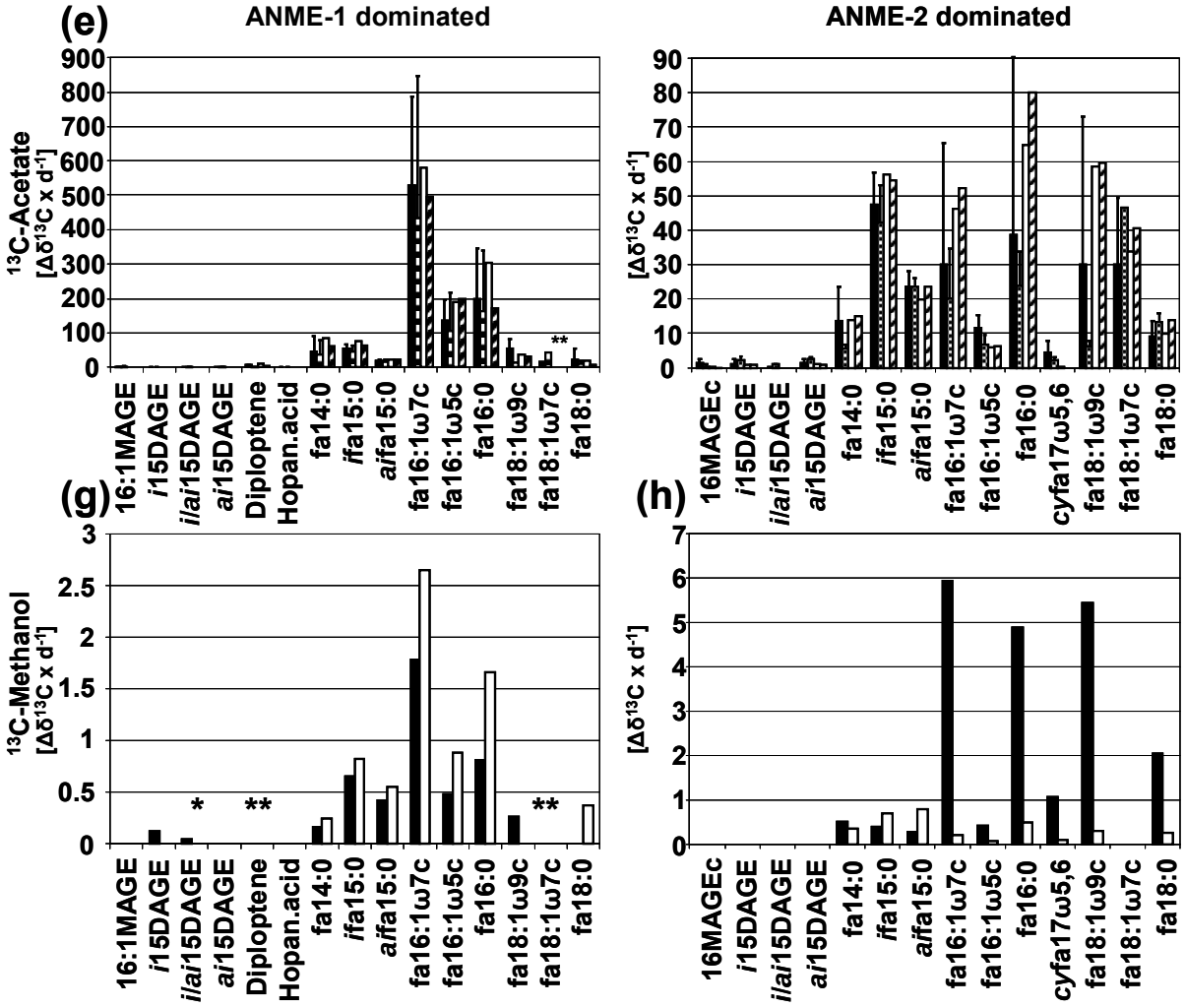

Figure 3.13: Daily ^{13}C-shifts of bacterial lipid biomarker compounds of ANME-1 (left) and -2 (right) dominated communities incubated with different ^{13}C-labelled substrates under different conditions. (a, b) ^{13}C-methane - ML, (c, d) ^{13}C-bicarbonate (black columns with methane - BcLM, white columns without methane in the headspace - BcL), (e, f) ^{13}C-acetate (black columns with methane - AcLM, chequered columns without methane in the headspace - AcL, white columns with methane and methyl fluoride - AcLMI, black-white stripped columns with methyl fluoride and without methane in the headspace - AcLI), (g, h) ^{13}C-methanol (black columns with methane - MeLM, white columns without methane in the headspace - MeL). The error bars result from replicate or triplicate measurements and show the maximum level of deviation of the rates. For experimental details see methods and table 2.1. * not analysed.

3.3.3 Daily total $\delta^{13}C$-shifts of archaeal and bacterial lipids

The bacterial and archaeal activity was determined by the daily $\delta^{13}C$-shift and summarised to compare the two communities (Table 3.1), the archaeal as well as the bacterial part.

The daily total $\delta^{13}C$-shifts of archaeal compounds were remarkable higher for ANME-1 and -2 in most experiments, particularly within those, incubated with methane (Table 3.1). Relative high total daily incorporations were found within experiments with acetate; in particular in the presence of methane (AcLM; 18 ‰ d^{-1}), they were slightly reduced with added methyl fluoride (AcLMI; 11.2 ‰ d^{-1} for pink mats, 7 ‰ d^{-1} for black mats). For ANME-1 associated compounds, the daily incorporations were in the same range with labelled methane (2.7 ‰ d^{-1}), compared to incubations with labelled bicarbonate (2.6 ‰ d^{-1} with methane and 3.7 ‰ d^{-1} without methane). The incorporation rates were similar for experiments with labelled bicarbonate (BcLM, BcL), slightly enhanced without methane (BcL). Very high assimilation rates were observed with methanol, especially in the absence of methane (68 ‰ d^{-1}). Interestingly the rates were considerable higher without methane in the headspace (171 ‰ d^{-1}; MeL). The observations of compounds, associated to ANME-2 are quite similar. Interestingly, incubations with bicarbonate (BcL; 0.9 ‰ d^{-1}) and acetate (AcL; 1.7 ‰ d^{-1}; Table 3.1) without methane in the headspace, revealed only low assimilation rates. They were also lower for ANME-2 associated compounds with methanol compared to ANME-1, whereby they were reduced in the presence of methane (MeLM; 13 ‰ d^{-1}; Table 3.1).

The total incorporation rates for compounds of associated bacteria within different ^{13}C-labelled substrates are depicted in Table 3.1. Lowest rates were observed after the addition of isotopically labelled methane (ML; 3 ‰ d^{-1} within the pink mat; Table 3.1). Incubations with labelled bicarbonate revealed similar incorporation rates within both mat types (BcLM, BcL; 8.9 - 12 ‰ d^{-1}; Table 3.1). They were significant higher compared to those with labelled methane (ML), respectively. Relative high rates were found within experiments with labelled methanol (MeLM, MeL). However, they were considerable higher in the presence of methane (MeLM) compared to those with labelled methanol only (MeL; Table 3.1) for compounds of the ANME-2 associated bacterial community. Highest rates, however, were found within all incubation experiments with acetate. For all experiments with acetate and for both mat types total daily shifts were between 132 and 1317 ‰ d^{-1} (AcLM, AcL, AcLMI, AcLI; Table 3.1).

Table 3.1: Daily total $\delta^{13}C$-shift [‰ d^{-1}] of selected lipid biomarkers of ANME-1 and -2 dominated consortia under different conditions. [a] no biphytanes were analysed, [b] PMI:5 was not analysed, [c] the hydrocarbon fraction was not analysed.

	ML	BcLM	BcL	AcLM	AcL	AcLMI	AcLI	MeLM	MeL
Archaeal lipids-ANME1	**2.7**±0.3	**2.6**	**3.7**[a]	**18.3**±2.5	**9**±8	**11.2**	**5.3**[a/c]	**68.2**	**171.4**
Archaeal lipids-ANME2	**2.7**±0.4	**2.7**[b]	**0.9**	**18**±4.7	**1.7**±0.5	**7**	**3.8**	**13**	**72.4**
Bacterial lipids-ANME1	**3**±1	**9.1**	**8.9**	**1071**±569	**839**±800	**1317**	**1050**	**4.7**	**7.2**
Bacterial lipids-ANME2	**5.4**±3.6	**9.3**	**12**	**209**±160	**132**±21	**292**	**313**	**21**	**3.2**
Total lipids ANME-1	**5.7**	**11.7**	**12.6**	**1089**	**848**	**1328**	**1055**	**72.9**	**179**
Total lipids ANME-2	**8**	**12**	**12.9**	**227**	**133.7**	**299**	**317**	**34**	**75.6**

3.4 Total ^{13}C-assimilation rates into individual lipids and daily total ^{13}C-uptake

To obtain an overview on substrate incorporation during the different experiments, the rates of ^{13}C-uptake, were calculated for selected individual lipids, given in Figures 3.14 and 3.15. They illustrate the total ^{13}C-assimilation rates [$\mu g\,^{13}C\,g_{TOC}^{-1}\,d^{-1}$] into some representative compounds for archaea and bacteria, according to the individual concentration of the lipids. They are summarised for archaea and bacteria for a total ^{13}C-uptake, respectively (Table 3.2; see section 2.4.7.3, p.22 for details).

3.4.1 Total ^{13}C-assimilation rates into selected archaeal lipids

3.4.1.1 Total ^{13}C-assimilation rates into selected archaeal lipids in ANME-1 dominated mats

For putative ANME-1 associated archaeal compounds, the uptakes into the isoprenoid alkyl glycerol ethers were relatively low in experiments with labelled methane (ML; Figure 3.14a), but significantly higher within all experiments with bicarbonate and acetate when methane was present (BcLM, AcLM, AcL; AcLMI, AcLI; Figure 3.14c, e). Interestingly, very low ^{13}C-uptake was observed into archaeol (1.0 $\mu g\,^{13}C\,g_{TOC}^{-1}\,d^{-1}$) from bicarbonate in experiments without methane (BcL; Figure 3.14c). The uptakes for archaeol:1 were similar, independent of the presence of methane (BcLM, BcL; ~0.5 $\mu g\,^{13}C\,g_{TOC}^{-1}\,d^{-1}$; Figure 3.14c). Highest rates were observed for isoprenoid dialkyl glycerol ethers with labelled methanol (MeLM, MeL; Figure 3.14g). Remarkably, they were up to four times higher without methane in the headspace for archaeol:1 (MeL; Figure 3.14g), and reached daily shifts for archaeol between 197 when methane was present (MeLM) to 387 $\mu g\,^{13}C\,g_{TOC}^{-1}\,d^{-1}$ in the absence of methane (MeL).

Only minor uptakes were observed for the six isomers of the C_{35}-isoprenoid alkenes from labelled methane, and from labelled bicarbonate when methane was present (ML, BcL; Figure 3.14a, c). Slightly higher uptakes from labelled acetate were observed (AcLM, AcL, AcLMI; Figure 3.14e). Only uptake into isomer C_{35}b was detected for incubation experiments with labelled methanol (MeLM, MeL; Figure 3.14g), e.g. 0.2 $\mu g\,^{13}C\,g_{TOC}^{-1}\,d^{-1}$ in the absence of methane (MeL). Similar to the isoprenoid dialkyl glycerol ethers (archaeol and archaeol:1), the biphytanes revealed lowest uptakes within the experiments with ^{13}C-labelled methane, and labelled methanol when methane was present (ML, MeLM; Figure 3.14a, g), and highest total assimilation rates within incubation experiments with labelled acetate (AcLM, AcL, AcLMI; Figure 3.14e). They were slightly reduced with added (unlabelled) methane for the isomers of the biphytanes $C_{40:1}$ (2.6 $\mu g\,^{13}C\,g_{TOC}^{-1}\,d^{-1}$) and $C_{40:2}$ (0.8 $\mu g\,^{13}C\,g_{TOC}^{-1}\,d^{-1}$; AcLM; Figure 3.14e). Moreover, they revealed considerable uptakes with labelled methanol in the absence of methane (MeL; Figure 3.14g). No corrected assimilation rates (see section 2.4.8, p.22) were determined for experiments with labelled acetate in the absence of methane and methyl fluoride. For incubation experiments with labelled bicarbonate (BcL; Figure 3.14c) no δ^{13}C-values were measured due to a contamination of the sample.

3.4.1.2 *Total ^{13}C-assimilation rates into selected archaeal lipids in ANME-2 dominated mats*

Crocetane revealed very low uptake from labelled methane (ML; Figure 3.14b) and acetate (0.1 $\mu g\,^{13}C\,g_{TOC}^{-1}\,d^{-1}$; AcLM, AcL; Figure 3.14f). No considerable uptake was determined within other experiments.

The unsaturated pentamethylicosenes revealed relatively low but similar uptake rates among almost all experiments (Figure 3.14b, d, f, h). However, they exhibited noticeable lower uptakes with bicarbonate in the absence of methane, e.g. for PMI:5 0.4 $\mu g\,^{13}C\,g_{TOC}^{-1}\,d^{-1}$ from bicarbonate only (BcL; Figure 3.14d). The patterns within experiments with acetate, independent of the presence or absence of methane or methyl fluoride were similar (AcLM, AcL, AcLMI, AcLI; Figure 3.14f). Very low uptakes were observed from labelled methanol, especially with methane in the headspace, e.g. for PMI:5 0.2 $\mu g\,^{13}C\,g_{TOC}^{-1}\,d^{-1}$ from methanol when methane was present (MeLM; Figure 3.14h).

For most experiments the uptakes into the isoprenoid dialkyl glycerol ethers were higher for compounds in ANME-2 dominated microbial mats compared to ANME-1 specific lipids (Figure 3.14a-f). The exception was found for compounds in experiments with labelled methanol (MeLM; Figure 3.14g). Here, the rates for archaeol were up to two fold higher in the presence of methane (MeLM; Figure 3.14g). Within experiments with labelled bicarbonate and methane (BcLM; Figure 3.14d) or labelled methanol (MeLM, MeL; Figure 3.14h) *sn-2*-hydroxyarchaeol revealed significantly higher uptakes compared to archaeol, e.g. after incubations with methanol and methane in the headspace 121 $\mu g\,^{13}C\,g_{TOC}^{-1}\,d^{-1}$ for *sn-2*-hydroxyarchaeol versus 65 $\mu g\,^{13}C\,g_{TOC}^{-1}\,d^{-1}$ for archaeol (MeLM). Within the experiment without methane the two glycerol ether lipids were found to show highest uptakes (MeL; Figure3.14h), up to 782 $\mu g\,^{13}C\,g_{TOC}^{-1}\,d^{-1}$ for *sn-2*-hydroxyarchaeol. In all experiments, the isoprenoid dialkyl glycerol ethers revealed highest uptakes (Figure 3.14b, d, f, h).

With labelled methane (ML; Figure 3.14b) the uptakes were similar for both compounds and were about 3.5 $\mu g\,^{13}C\,g_{TOC}^{-1}\,d^{-1}$. The ^{13}C-incorporation into compounds, extracted from experiments with labelled bicarbonate without methane in the headspace was considerably low, for instance the average uptake per day was about 1.1 $\mu g\,^{13}C\,g_{TOC}^{-1}\,d^{-1}$ for both isoprenoid dialkyl glycerol ethers (BcL; Figure 3.14d). Distinct uptake patterns were found for experiments with acetate (Figure 3.14f). Only in the presence of methane, ^{13}C derived by acetate was incorporated into *sn-2*-hydroxyarchaeol (3.1 $\mu g\,^{13}C\,g_{TOC}^{-1}\,d^{-1}$; AcLM; Figure 3.14f). The uptakes were higher for archaeol in those experiments, in particular with methane and added methyl fluoride (31 $\mu g\,^{13}C\,g_{TOC}^{-1}\,d^{-1}$; AcLMI; Figure 3.14f).

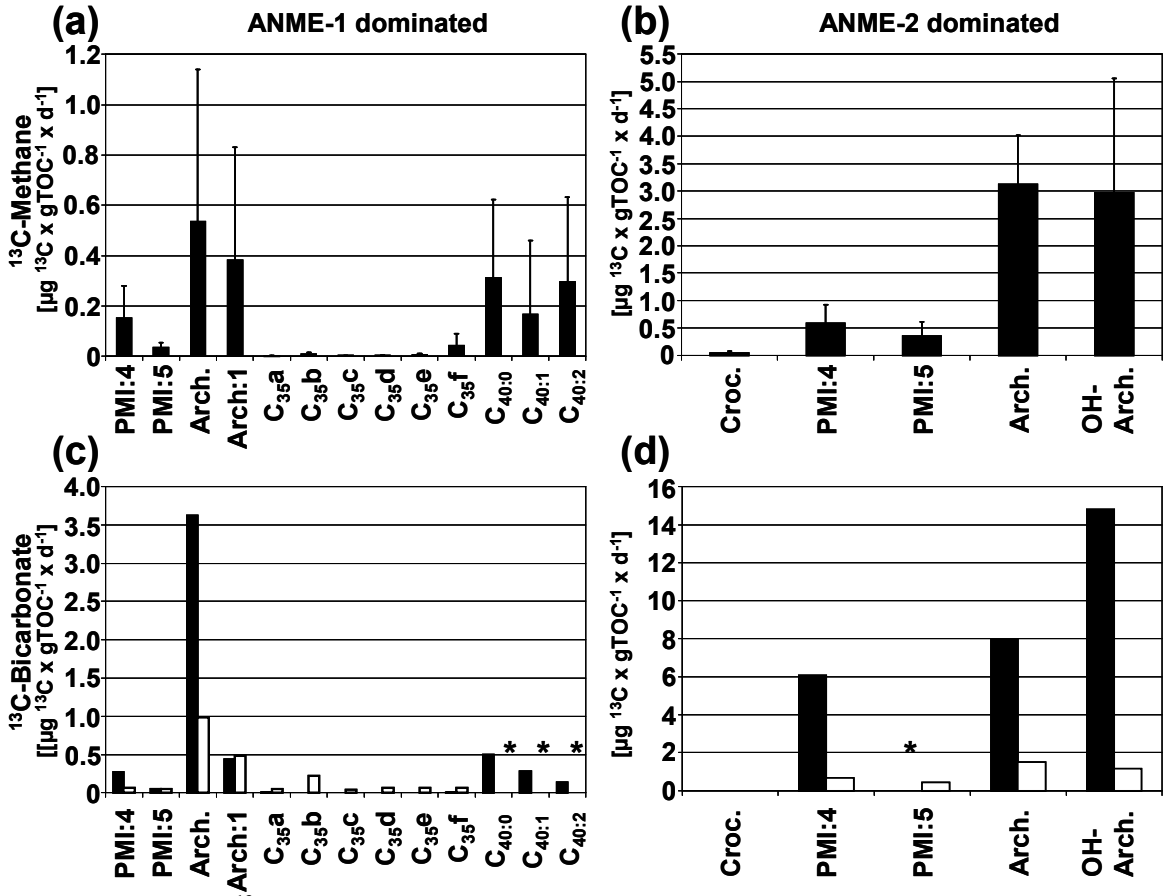

Figure 3.14: Total ^{13}C- assimilation rates for archaeal lipid biomarker compounds of ANME-1 (left) and -2 (right) dominated communities incubated with different ^{13}C-labelled substrates under different conditions. (a, b) ^{13}C-methane - ML, (c, d) ^{13}C-bicarbonate (black columns with methane - BcLM, white columns without methane in the headspace - BcL).The error bars result from replicate or triplicate measurements and show the maximum level of deviation of the rates. For experimental details see methods and table 2.1. * not analysed.

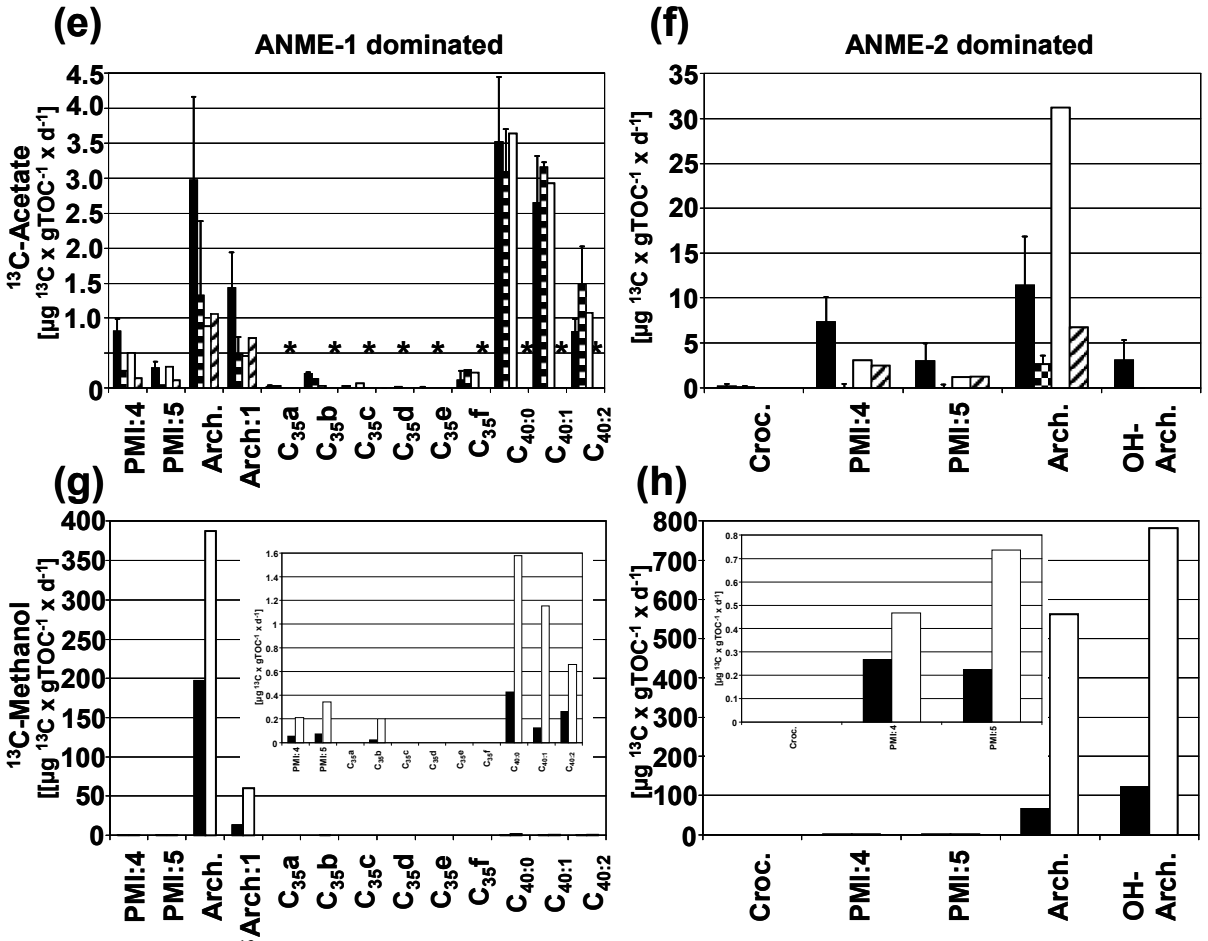

Figure 3.14: Total ^{13}C-assimilation rates for archaeal lipid biomarker compounds of ANME-1 (left) and -2 (right) dominated communities incubated with different ^{13}C-labelled substrates under different conditions. (e, f) ^{13}C-acetate (black columns with methane - AcLM, chequered columns without methane in the headspace - AcL, white columns with methane and methyl fluoride - AcLMI, black-white stripped columns with methyl fluoride and without methane in the headspace - AcLI), (g, h) ^{13}C-methanol (black columns with methane - MeLM, white columns without methane in the headspace - MeL). The error bars result from replicate or triplicate measurements and show the maximum level of deviation of the rates. For experimental details see methods and table 2.1. * not analysed

3.4.2 Total ^{13}C-assimilation rates into selected bacterial lipids

3.4.2.1 Total ^{13}C-assimilation rates into selected bacterial lipids in *ANME-1 dominated mats*

For ANME-1 dominated samples, the ^{13}C-incorporation patterns were slightly different between experiments with labelled methane (ML; Figure 3.15a) or labelled bicarbonate (BcLM, BcL; Figure 3.15c). The ^{13}C-incorporation patterns with labelled methanol (MeLM, MeL; Figure 3.15g) resemble those with labelled bicarbonate (BcLM, BcL; Figure 3.15c). The occurrence of methane in the headspace had apparently no significant effect. The incorporation patterns from labelled acetate showed strong differences compared to all other experiments as well as the by far highest uptakes. However, they exhibit only marginal changes under varied conditions (presence or absence of methane or methyl fluoride; Figure 3.15e). Lowest uptakes were found into the bacterial MAGEs and DAGEs within all experiments (Figure 3.15a, c, e, g).

For bacterial compounds, associated with ANME-1 dominated mats, very high ^{13}C-uptake was observed for *ai*fa15 within experiments (1.3 $\mu g\,^{13}C\,g_{TOC}^{-1}\,d^{-1}$; ML; Figure 3.15a), labelled bicarbonate and (unlabelled) methane (4.6 $\mu g\,^{13}C\,g_{TOC}^{-1}\,d^{-1}$; BcLM; Figure 3.15c) and methanol, independent of the presence or absence of methane (~2.9 $\mu g\,^{13}C\,g_{TOC}^{-1}\,d^{-1}$ for both; MeLM, MeL; Figure 3.15e). High uptakes were also observed for hexadecanoic acid and fa16:1ω7c within incubation experiments with labelled bicarbonate or methanol (BcLM, BcL, MeLM, MeL; Figure 3.15c, g). The hexadecanoic acid reached an average uptake of about 3.3 $\mu g\,^{13}C\,g_{TOC}^{-1}\,d^{-1}$ from bicarbonate (BcLM, BcL) and between 1.0 from methanol with methane (MeLM) and 1.4 $\mu g\,^{13}C\,g_{TOC}^{-1}\,d^{-1}$ in the absence of methane (MeL).

3.4.2.2 Total ^{13}C-assimilation rates into selected bacterial lipids in ANME-2 dominated mats

For ANME-2 dominated mat type associated bacterial lipids the ^{13}C-incorporation patterns with labelled bicarbonate (BcLM, BcL; Figure 3.15d) resemble those with labelled methane (ML; Figure 3.15b). However, the ^{13}C-uptakes were slightly enhanced without methane in the headspace (BcL; Figure 3.15d). Some exceptions were observed. Tetradecanoic acid revealed only ^{13}C-uptake in the presence of methane (~9 $\mu g\,^{13}C\,g_{TOC}^{-1}\,d^{-1}$; BcLM) and the ^{13}C-uptake into fa16:1ω5c was considerable enhanced in the presence of methane (43 $\mu g\,^{13}C\,g_{TOC}^{-1}\,d^{-1}$; BcLM; Figure 3.15d). Generally low uptakes were observed for *cyfa*17:1ω5,6 in the absence of methane (0.3 $\mu g\,^{13}C\,g_{TOC}^{-1}\,d^{-1}$; BcL; Figure 3.15d). The incorporation patterns with labelled acetate differed significant to experiments with labelled methane or bicarbonate (AcLM, AcL, AcLMI, AcLI; Figure 3.15f). Nonetheless, they revealed similar patterns under different conditions within experiments with acetate, independent of the presence of methane or methyl fluoride (AcLM, AcL, AcLMI, AcLI; Figure 3.15f). The fa16:1ω7c revealed highest acetate derived ^{13}C-uptake, e.g. during incubations with acetate, methane and methyl fluoride an uptake per day

about 730 $\mu g^{13}C\,g_{TOC}^{-1}d^{-1}$ (AcLMI). Distinct incorporation patterns for experiments with methanol were observed. The uptake was exceedingly higher in the presence of than in the absence of methane. In particular fa16:1ω7c (30 $\mu g^{13}C\,g_{TOC}^{-1}d^{-1}$; MeLM) was strongly enriched in ^{13}C, while most other considered fatty acids showed relative low incorporations. Noticeable, are the enhanced uptakes of fa16:0, fa18:1ω9c (9 $\mu g^{13}C\,g_{TOC}^{-1}d^{-1}$, respectively), fa16:1ω5c, fa18:1ω7c (4$\mu g^{13}C\,g_{TOC}^{-1}d^{-1}$, respectively), and fa18:0 (2 $\mu g^{13}C\,g_{TOC}^{-1}d^{-1}$; MeLM; Figure 3.15h). Similar to ANME-1 samples, all bacterial glycerol ether lipids showed only very low or no uptake of substrate derived ^{13}C from any labelled substrate (Figure 3.15b, d, f, h).

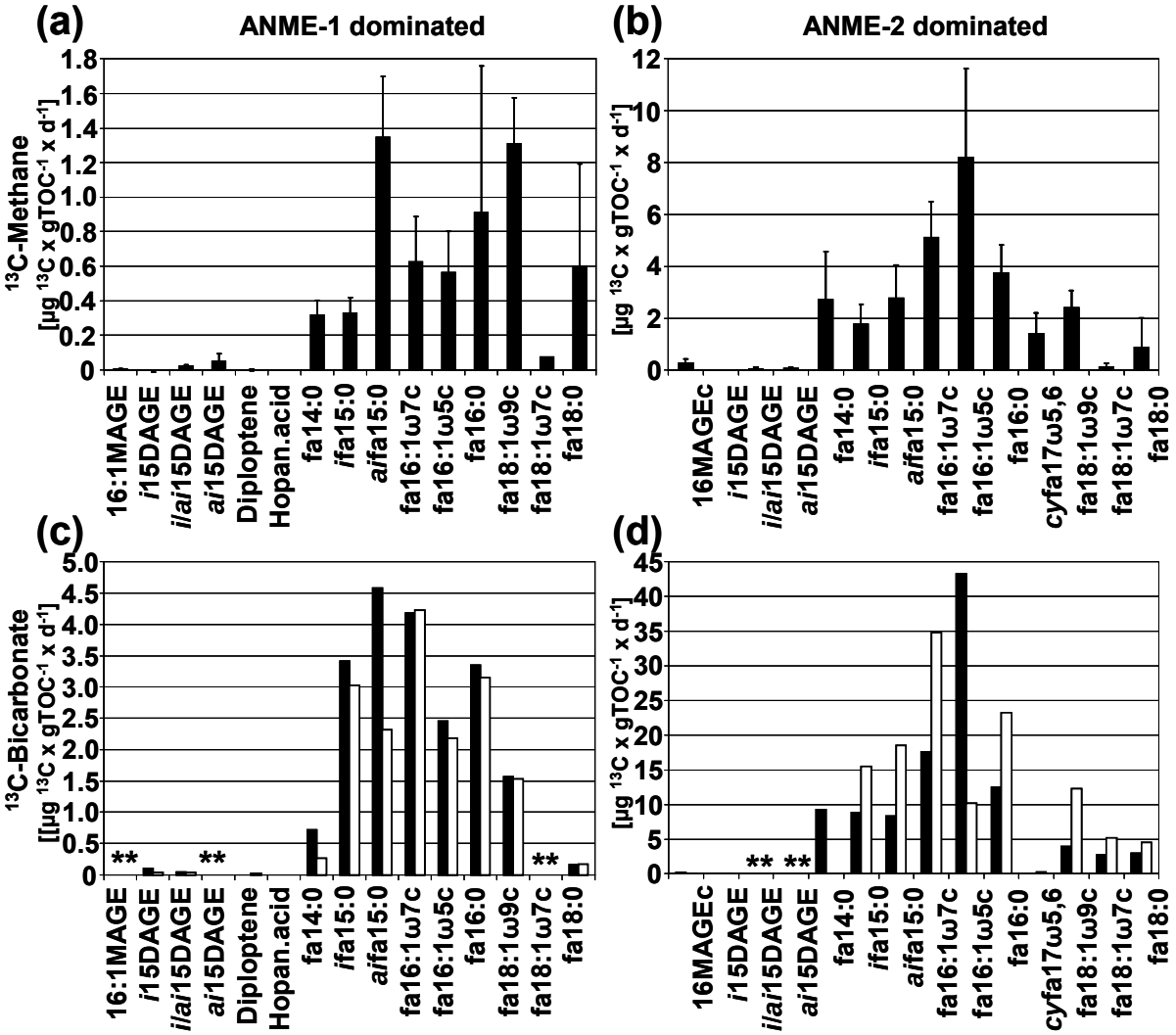

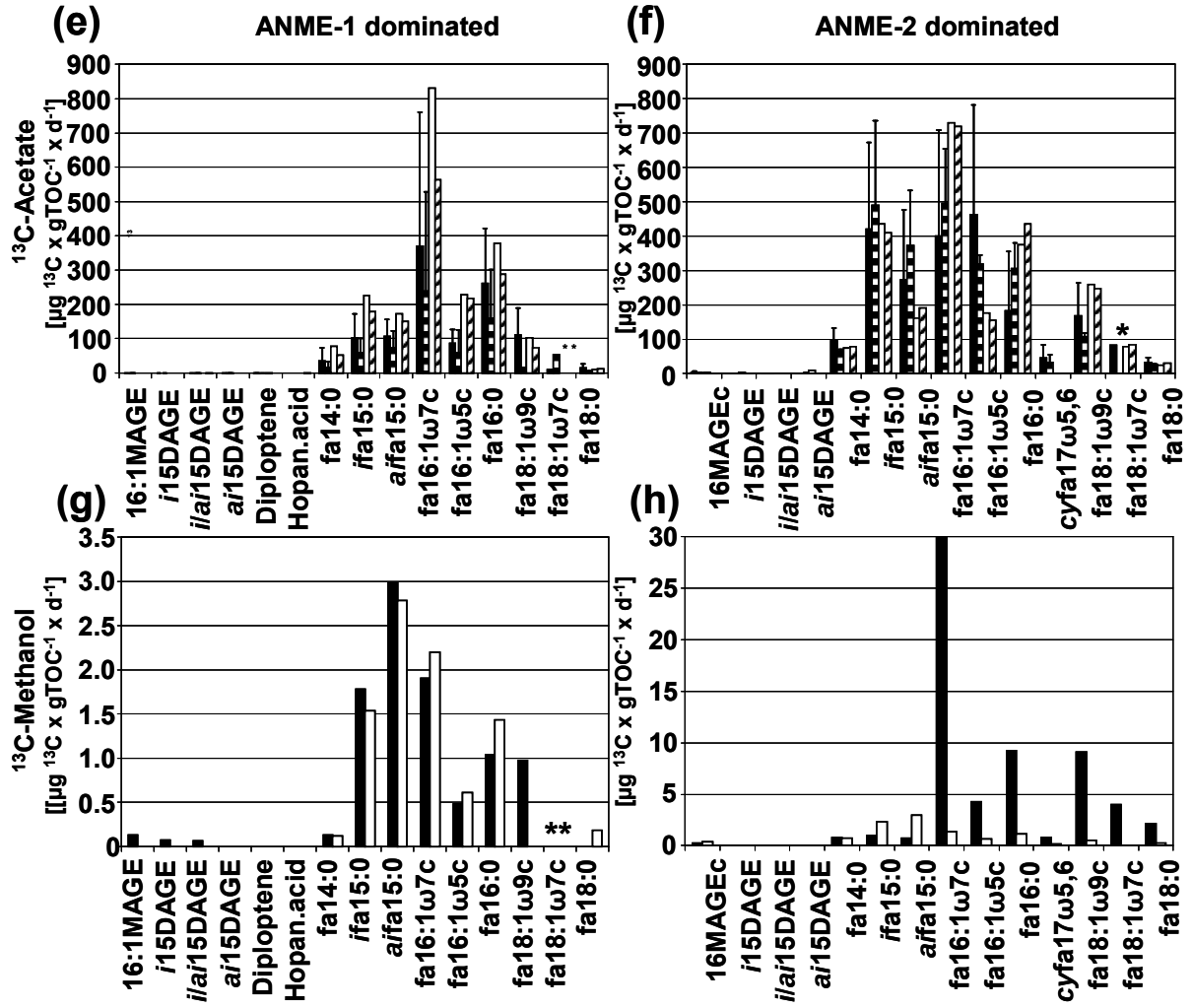

Figure 3.15: Total ^{13}C-assimilation rates for bacterial lipid biomarker compounds of ANME-1 (left) and -2 (right) dominated communities incubated with different ^{13}C-labelled substrates under different conditions. (a, b) ^{13}C-methane - ML, (c, d) ^{13}C-bicarbonate (black columns with methane - BcLM, white columns without methane in the headspace - BcL), (e, f) ^{13}C-acetate (black columns with methane - AcLM, chequered columns without methane in the headspace - AcL, white columns with methane and methyl fluoride - AcLMI, black-white stripped columns with methyl fluoride and without methane in the headspace - AcLI), (g, h) ^{13}C-methanol (black columns with methane - MeLM, white columns without methane in the headspace - MeL). The error bars result from replicate or triplicate measurements and show the maximum level of deviation of the rates. For experimental details see methods and table 2.1. * not analysed.

3.4.3 Daily total ^{13}C-uptake

The daily total ^{13}C-uptake differs significantly between ANME-1 and -2 archaea for different substrates (Table 3.2). Relative low incorporations were observed with labelled methane and acetate for both mat samples (ML, AcLM, AcL, AcLMI, AcLI; Table 3.2). Among these, the ANME-2 dominated samples for incubations with labelled acetate and methane (AcLM) are set apart by enhanced rates (6 and 11 ng^{13}C $\mu g_{\Sigma(\text{selected lipds})}^{-1} d^{-1}$ for ANME-1 and -2 respectively). The assimilation rates were slightly higher from labelled bicarbonate (BcLM, BcL; Table 3.2). Especially for ANME-1 dominated samples, total ^{13}C-assimilation rates within experiments with labelled bicarbonate (BcLM, BcL) were considerably higher than those observed in experiments with acetate (AcLM, AcL, AcLMI, AcLI). Interestingly, the uptakes of ^{13}C, derived from methane and from bicarbonate (in the presence of methane) were higher for ANME-2 compared to ANME-1 associated compounds (ML, BcLM), while the opposite was found for incubations with bicarbonate in the absence of methane (BcL). By far the highest uptakes for archaeal lipids were observed in incubation experiments with methanol for both mat types (MeLM, MeL), this in particular for incubations without methane in the headspace (253 ng^{13}C $\mu g_{\Sigma(\text{selected lipds})}^{-1} d^{-1}$; MeL; Table 3.2).

The uptake of ^{13}C derived from methane was slightly higher for ANME-2 than for ANME-1 associated bacteria (ML; Table 3.2). The total ^{13}C-uptakes per day from labelled bicarbonate were in the same range, independent of the presence of methane (BcLM, BcL) and they were significantly higher for lipids of ANME-2 associated bacterial communities. For selected lipids of ANME-1 associated bacteria the total uptakes were about 32 ng^{13}C $\mu g_{\Sigma(\text{selected lipds})}^{-1} d^{-1}$ and for ANME-2 associated about 56 ng^{13}C $\mu g_{\Sigma(\text{selected lipds})}^{-1} d^{-1}$ (BcLM, BcL; Table 3.2). The total ^{13}C-incorporations rates for the selected bacterial compounds were highest for all experiments with acetate, especially for ANME-1 dominated mats (AcLM, AcL, AcLMI, AcLI), up to 849 ng^{13}C $\mu g_{\Sigma(\text{selected lipds})}^{-1} d^{-1}$ with methane and methyl fluoride (AcLMI). Lowest rates were observed from labelled methanol (MeLM, MeL), which holds true for both mat types (MeL). However, while methane had no influence on methanol derived ^{13}C-uptakes among ANME-1 mats, assimilation rates from methanol were significant higher with methane (MeLM; Table 3.2) for ANME-2 communities.

Table 3.2: Daily total ^{13}C-uptake [ng^{13}C $\mu g_{\Sigma(\text{selected lipids})}^{-1} d^{-1}$] for a normalised fraction of selected lipids, of ANME-1 and ANME-2 dominated consortia under different conditions. [a] no biphytanes were analysed, [b] PMI:5 was not analysed, [c] the hydrocarbon fraction was not analysed. The given errors in parenthesis result from replicate or triplicate measurements.

	ML	BcLM	BcL	AcLM	AcL	AcLMI	AcLI	MeLM	MeL
Archaeal lipids-ANME1	3 (±0.5)	8.5	14[a/]	6 (± 3)	2 (± 2)	4	3[a/c]	131	195
Archaeal lipids-ANME2	6 (± 1)	20[b]	3	11 (± 7)	1 (± 0.1)	2	2	40	253
Bacterial lipids-ANME1	8 (± 2)	31	33	535 (± 270)	463 (±443)	849	624	4	5
Bacterial lipids-ANME2	13 (± 4)	55	57	201 (± 153)	133 (± 29)	199	271	19	4
Total lipids ANME-1	11	40	46	541	465	853	627	135	200
Total lipids ANME-2	19	75	60	212	134	201	273	59	257

3.5 Daily ^{13}C-assimilation rates of hentriacontatrien

In almost all samples, dominated by ANME-2, three isomers ($C_{31:3}$a - c) of hentriacontatrien were found. None of these compounds could be identified in any ANME-1 dominated sample.

The M^+ of these three isomers were determined with a mass of 430. The three isomers showed similar fragmentation (Figure 3.16). The base peaks are 67, 79, and 91. The fragment of 91 masses indicates four double bonds. However this can not be confirmed by the mass of the molecular ion. Moreover, the hydrogenisation of the double bonds revealed a mass of 436 for the molecular ion. Thus, these three isomers are identified as a hydrocarbon with three double bonds.

However, the precise positions of the double bonds could not be determined. The derivatisation with DMDS did not reveal clear structural details.

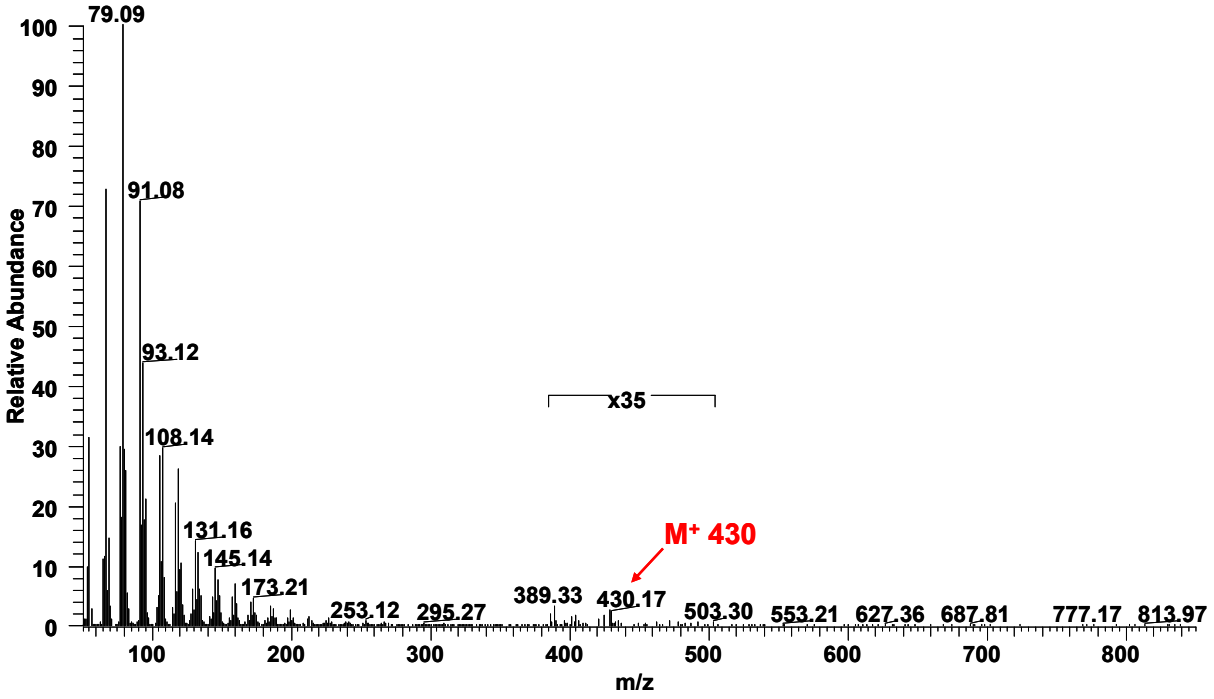

Figure 3.16: **Fragmentation pattern of hentriacontatrien in the GC-MS after EI-ionisation (-70 eV).**

These compounds showed minor but considerable uptake of ^{13}C from different labelled substrates. Table 3.3 illustrates the daily assimilation rates, also compared to some other representative bacterial lipids (16MAGE, *i/i*15DAGE, *i/ai*15DAGE, *ai/ai*15DAGE, fa14:0, fa16:1ω5c, fa16:0).

In most incubation experiments, the assimilation rates of the three isomers were significant higher than those of the mono- and dialkyl glycerol ether lipids.

For incubation experiments with labelled methane, the assimilation rates for all three isomers were quite similar (ML). They were also in the same range with other bacterial compounds (e.g. fa14:0, fa16:1ω5c). The ^{13}C-assimilation rates were slightly enhanced within experiments with labelled bicarbonate (BcLM, BcL; Table 3.3), particularly during experiments with methane in the headspace (BcLM).

Whereby the rates were significant higher as well as other considered fatty acids (e.g. fa14:0, fa16:1ω5c) during incubations without methane (BcL). Furthermore, the lowest rates were observed for the isomer $C_{31:3}$(c).

Highest assimilation rates have been observed into the isomer $C_{31:3}$(c) during incubation experiments with acetate. For most experiments the assimilation rates of the alkenes were considerable low compared to tetradecanoic and *cis-ω5*-hexadecenoic acid. No δ^{13}C-values could be measured for samples with methanol.

Table 3.3: The daily δ^{13}C-shift [‰ d^{-1}] of the three isomers of hentriacontatrien ($C_{31:3}$a-c) during experiments with different ^{13}C-labelled substrates.

The table compares the assimilation rates of the three constitutional isomers of hentriacontatrien with other bacterial compounds. The notation of the samples is explained in Table 2.1. Numbers represent days of incubation. n.a. - not analysed

	Experiments									
Compounds	**ML64**	**ML135**	**BcLM**	**BcL**	**AcLM23**	**AcL23**	**AcL56**	**AcLM26**	**AcLMI26**	**AcLI26**
C31:3(a)	0.2	n.a.	n.a.	n.a.	0.22	0.32	n.a.	n.a.	n.a.	n.a.
C31:3(b)	0.27	0.21	n.a.	0.59	1.94	1.46	n.a.	4.83	2.41	2.06
C31:3(c)	0.12	0.15	0.71	0.58	3.01	2.55	2.77	7.68	3.64	3.28
16MAGE(c)	0.07	0.31	0.33	0.12	0.29	-0.3	0.31	2.37	0.12	0.02
i15DAGE	0.11	0.01	0.04	0.08	0.16	1.12	1.09	0.65	0.69	0.59
i/ai15DAGE	0.15	-0.02	-0.4	-0.3	-0.16	0.65	0.4	-0.28	-0.26	-0.39
ai15DAGE	0.14	0.001	-0.1	0.01	0.64	1.76	1.06	0.75	0.93	0.71
fa14:0	0.50	0.47	1.63	0.0	8.35	4.37	5.75	22.92	12.69	13.7
fa16:1ω5c	0.41	0.33	1.16	0.23	8.06	4.15	7.87	14.45	5.35	5.7
fa16	0.86	0.55	1.66	2.0	13.16	15.41	38.52	91.23	69.93	74.24

4 Discussion

Only a few previous studies on the carbon flow in anaerobic methanotrophic consortia using ^{13}C-labelled substrates exist (Blumenberg et al., 2005; Wegener et al., 2008a; Jagersma et al., 2009). They showed the uptake of carbon from methane and bicarbonate into archaeal and associated bacterial lipids, presumably with a predominance of ANME-archaea and SRB.

This work extends these previous studies with other substrates (acetate, methanol) applied on almost pure mat samples obtained from the Black Sea. These mat samples are dominated by ANME-1 or ANME-2. Among the incubations performed, those with labelled methane or labelled bicarbonate when methane was also present should most likely mimic the *in-situ* conditions. However, the methane pressure and thus the concentration of dissolved methane in the basal medium is much lower than in water depths of about 200 m from where the samples were derived. The incubation experiments with only labelled bicarbonate were conducted to prove the methanogenic and autotrophic potential of the investigated community. Incubation experiments with labelled acetate, with and without methane in the headspace, were conducted to determine heterotrophic capabilities. In addition, the archaeal metabolism was investigated with focus on acetoclastic methanogenic capabilities. Incubation experiments with methanol, also in the presence and absence of methane, demonstrate methylotrophic methanogenic capabilities of the investigated archaea and also potential acetogenic metabolism of associated bacteria.

Along with these stable isotope experiments, the rates of methane consumption, methane formation, and sulphate reduction were determined to get deeper insights into physiological properties of the investigated communities. Furthermore, the isotopic composition of newly formed methane was measured in both, incubations started without methane in the system and incubations started with a nearly pure methane atmosphere. With this approach the methanogenic capabilities with different substrates were investigated for both AOM-performing communities.

Table 4.1 gives a short overview on the abbreviations used in the following discussion for the respective experiments and mat types.

Table 4.1: The abbreviations of the experiments.
mM - millimolar, CH_3F - methyl fluoride

Methane	^{13}C-Labelling	Concentration of Label	Inhibition	Notation
2 bar	Methane	25 %	-	ML
1 bar	Bicarbonate	30 mM, 20 %	-	BcLM
-	Bicarbonate	30 mM, 20 %	-	BcL
1 bar	Na-Acetate	3 mM, 99.9 %	-	AcLM
-	Na-Acetate	3 mM, 99.9 %	-	AcL
1 bar	Na-Acetate	3 mM, 99.9 %	CH_3F	AcLMI
-	Na-Acetate	3 mM, 99,9 %	CH_3F	AcLI
1 bar	Methanol	3 mM, 99 %	-	MeLM
-	Methanol	3 mM, 99 %	-	MeL

4.1 Lipid biomarker compositions of the prokaryotic communities

The distributions of bacterial and archaeal compounds are in agreement with data of other AOM-site studies (Blumenberg et al., 2004; Niemann and Elvert, 2008 and references therein) and support a predominance of ANME-1 or ANME-2 archaea in the pink and black mats studied respectively. The lipid biomarker patterns are diagnostic for both mat communities and support a distinct microbial composition for each mat type. This includes a predominance of glycerol dialkyl glycerol tetraether (GDGTs) derived biphytanes in ANME-1 or *sn-2*-hydroxyarchaeol and crocetane in ANME-2 archaea (according to Blumenberg et al., 2004). In the following discussion, the respective mat types will be considered to consist of mainly ANME-1 archaea for the pink mat and ANME-2 archaea for the black mat. Similarly, a predominance of *anteiso*-C_{15}-dominated structures (fatty acids, dialkyl glycerol diethers) in ANME-1 associated bacteria and e.g. *cis-ω5*-hexadecenoic acid (fa16:1ω5c) in ANME-2 associated bacteria (Elvert et al., 2003; Blumenberg et al., 2004) demonstrate two distinct associated bacterial communities in the samples. They also indicate a stable community structure for all samples, despite small variances (Figure 3.8).

In addition, a series of unsaturated isoprenoid C_{35}-alkanes showing highly depleted $\delta^{13}C$-values indicative of a source organism thriving on methane were found in ANME-1 mat samples. Unsaturated isoprenoid C_{35}-alkanes were described by Holzer et al. (1988) and were taken from a thermophilic methanogen, isolated from a hydrothermal vent site of the Guaymas basin (Gulf of California), but also from AOM-sites in the Mediterranean Sea (Bouloubassi et al., 2006) and the Black Sea (Stadnitskaia et al., 2005; Roberts et al., 2008). The lack of these compounds in ANME-2 mats suggests C_{35}-isoprenoids as facultative additional biomarkers of ANME-1 archaea.

Considering the respective stable isotope experiments, the assimilation rates within the archaeal lipids are mainly influenced by the ANME-1 and -2 archaea in the pink and black mats respectively. Moreover, the assimilation rates into the fatty acids also mirror the physiological capabilities of the bacterial community. The molecular biological analysis revealed high amounts of δ-Proteobacteria, which comprise mainly SRB in AOM-settings and additional other bacterial phyla (Figure 4.1). These observations are consistent with investigations of different authors (Heijs et al., 2006, 2007; Pernthaler et al., 2008; Bowles et al., 2011). The physiological capabilities of the bacterial phyla in the two mat systems have to date not been very well investigated. These physiological properties can be only tentatively deduced by known phylogenetically relatives. Friedrich et al. (2007, AGU) showed the bacterial activity and composition by 16S rRNA and DNA analysis (Figure 4.1) for both sample types. SRB are dominant with regard to biomass and activity in both associated bacterial communities. For the pink mat type, the 16S rDNA analysis showed in particular two dominant bacterial groups resembling the community. SRB contributed up to 40 % and Caldithrix about 35 % to the bacterial composition. Additionally, Planctomycetes, Caldithrix and members of the candidate phylum WS-3 were active

members. In black mats, δ-Proteobacteria only made up to 30 % of the whole community (revealed by 16S rDNA - Figure 4.1). Bacteroidetes, Chloroflexi and Planctomycetes together revealed up to 45 %. In the black mat, the δ-Proteobacteria made up more than 80 % of the active bacterial community, while the Planctomycetes were the second dominant group with about 9 % activity (Figure 4.1 - 16S rRNA). Nonetheless, Chloroflexi, Clostridia and Bacteroidetes were also active in the black mat samples. The composition and activity may be affected by different substrates during the experiments.

Different phyla typically for the sulphate methane transition zone (SMTZ) were described by several authors. Worth mentioning are the relatives which belong to the phyla of the α-, β-, γ-, δ-Proteobacteria, Planctomycetes, Chloroflexi, JS-1, Clostridia, Firmicutes, Bacteroidetes, and Spirochetes (e.g. Inagaki et al., 2006; Heijs et al., 2007; Jagersma et al., 2009; Bowles et al., 2011; Webster et al., 2011).

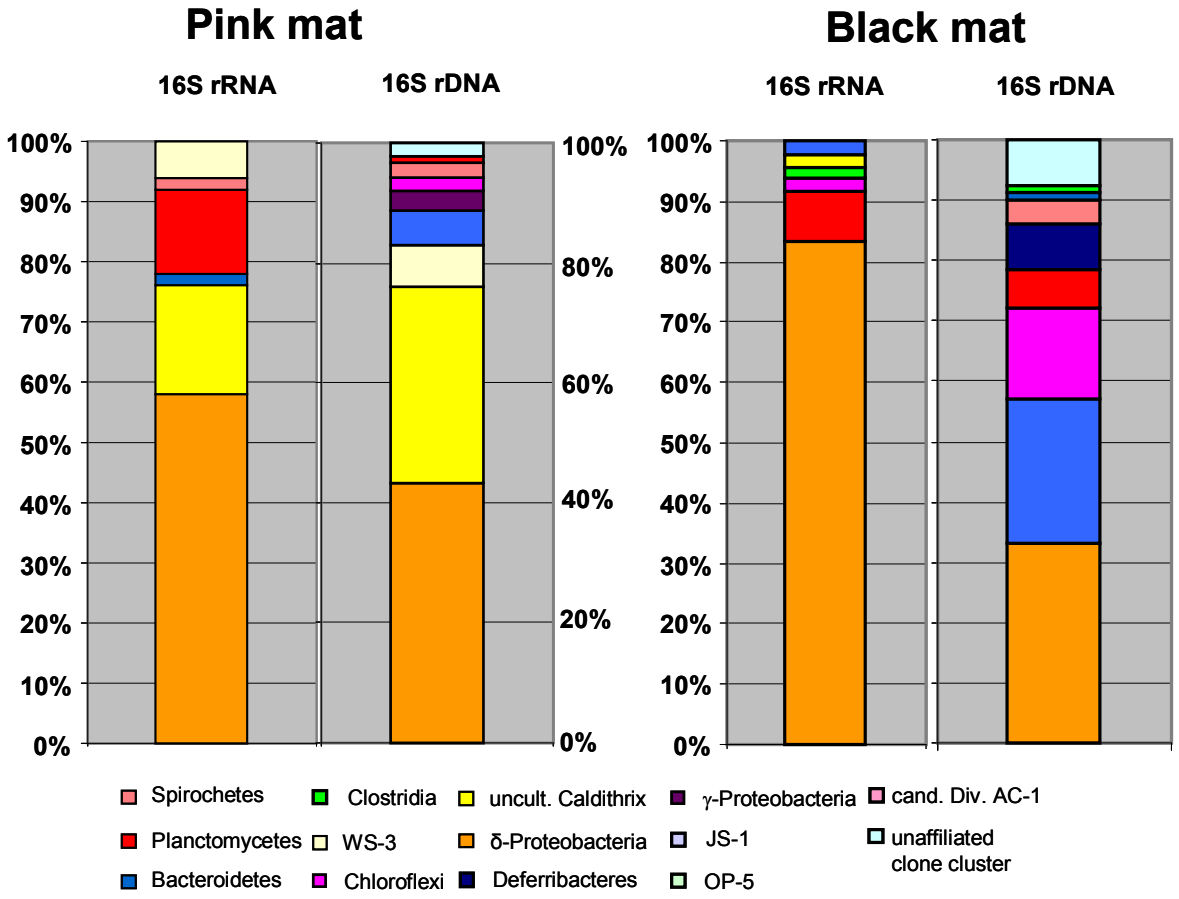

Figure 4.1: Bacterial composition and activity in ANME-1 (*left* diagrams) and ANME-2 (*right diagrams*) dominated mat samples from the Black Sea.

Composition of the 16S rRNA and the 16S rDNA clone libraries from pink and black mats (Bacteria). The samples were incubated for 2 years in the laboratory prior to analysis (Friedrich et al., 2007, AGU).

4.2 General methodological considerations

The carbon flows were traced in the two different AOM-performing microbial communities (ANME-1 and -2 dominated) by compound-specific stable isotope probing using different ^{13}C-labelled substrates (see Table 4.1). The $\Delta\delta^{13}C$ (Figures 3.12, 3.13, pages 38 and 41) were recalculated to daily ^{13}C-assimilation rates, and illustrate similar patterns as the $\Delta\delta^{13}C$ do. The $R_{V\text{-}PDB}$ is adapted to the isotopic ratio of environmental samples. Using the δ-notation for very high ^{13}C-incorporation has the disadvantage that the $\delta^{13}C$-shift increases exponentially but the amount of ^{13}C increases linear. This makes it difficult to derive directly the assimilation, especially for values higher than 20,000 ‰.

Since the respective ^{13}C-assimilation rates are independent of the concentrations of the individual compounds in the different samples, they allow the metabolic activity and rates of synthesis to be determined. The degradation of the lipids has apparently no considerable effect, due to the long residence time of the compounds and relative short incubation times. A higher assimilation rate of substrate derived ^{13}C means better conditions to grow for respective source organisms due to the presence of (i) favoured electron donors and acceptors (ii) a higher energy yield. Those considerations are constrained in general by very low synthesis rates for respective compounds under given experimental conditions and respective substrate availability. In addition, very high concentrations of investigated compounds can affect ^{13}C-assimilation rates. Thus the synthesis rate can be underestimated. The assimilation rates are also influenced by the composition of the bacterial community. Hence, it is important to compare these data with the total ^{13}C-uptakes per day (Figures 3.14, 3.15, 4.4, 4.11; Table 3.2); otherwise the anabolic capabilities of involved source organisms influence the uptake of labelled substrate derived carbon.

The total daily ^{13}C-assimilation rates into selected compounds calculated per gram TOC are depicted in figures 3.14 (archaeal compounds) and 3.15 (bacterial compounds) for the different incubation experiments. Figure 4.4 illustrates the total ^{13}C-uptake from the different labelled substrates into lipids attributed to archaea (see section 2.4.7.3, page 22). These data were extrapolated to 100 % label for experiments with methane (ML, 25 % ^{13}C) and bicarbonate (BcLM, BcL, 20 % ^{13}C) to facilitate the direct comparison of ^{13}C-incorporation rates between all experiments. Generally, total ^{13}C-uptake into lipids from a labelled substrate should increase along with the usability of the respective substrate for the prokaryotic community. For example, ^{13}C from methanol was highly incorporated into the archaeal biomass, demonstrating a considerable capability of the archaea to metabolise methanol (Figure 4.4). Archaea of pink mat samples revealed ^{13}C uptakes of 131 and 195 ng^{13}C $\mu g_{\Sigma(\text{selected lipds})}^{-1} d^{-1}$, with and without methane respectively. On the other hand, only minor uptake of about 5 ng^{13}C $\mu g_{\Sigma(\text{selected lipds})}^{-1} d^{-1}$ into the bacterial lipids during the same experiments demonstrates a minor suitability of methanol as substrate for the associated bacteria under given experimental conditions (Figure 4.11).

The respective rates of methane consumption, methane generation, and sulphate reduction (Figures 4.25) as well as ^{13}C-assimilation (Figures 4.5, 4.12) and total

^{13}C-assimilation rates (Figures 3.14, 3.15), were all calculated per gram TOC to directly compare the two different sample types. The TOC content in % for the ANME-1 dominated mat is slightly higher (about 35 % of dry weight) than the ANME-2 dominated mat type (about 20 %). The TOC content was in the same range for similar mat samples from the Black Sea with 34 % (ANME-1 dominated) and 19 % (ANME-2 dominated) (Roberts et al., 2008).

The methane decrease will be considered as methane consumption in further sections of this discussion. From there it is also equivalent to anaerobic oxidation of methane (Barnes and Goldberg, 1976; Hoehler et al., 1994; Boetius et al., 2000; DeLong et al., 2000). Nevertheless, it has to be considered that even a marginal theoretical artificial loss of methane during the incubations (leakages) and sampling leads to overestimations of the methane consumption rates.

For further investigations of acetoclastic methanogenic capabilities, experiments were performed with methyl fluoride as inhibition reagent. The addition of methyl fluoride should inhibit the acetoclastic pathway in archaea (Conrad and Klose, 1999; AcLMI, AcLI; Figure 3.6). However, incubations with methyl fluoride revealed rates of methanogenesis similar to those without methyl fluoride (AcLM, AcL; Figure 3.7) and the daily assimilation into archaeal lipids was reduced in the presence of methane and methyl fluoride (AcLM, AcLMI; Figure 3.12e, f), e.g. in black mat samples archaeol revealed a daily assimilation of ^{13}C during incubations with acetate and methane of 1.7 ‰, whilst in experiments with added methyl fluoride and methane the measured rate was of 0.6 ‰ per day. Interestingly, the addition of methyl fluoride led also to lower methane consumption and methane-dependent sulphate reduction rates for both sample types (Figure 3.7). That indicates an impact on the archaeal metabolism. Remarkable are the slightly higher assimilation rates into the archaeal lipids with methyl fluoride and without methane (AcL, AcLI; Figure 3.12e, f). Hence, methyl fluoride seems to have had a slight effect on the lipid synthesis. An effect on the proliferation and growth for acetoclastic *Methanosarcinales spp.* was already observed in anoxically incubated rice roots by qPCR and T-RFLP analysis (Penning and Conrad, 2006). Since the biochemical effect of methyl fluoride is not well understood, the lipid biomarker data can only be hardly explained. As expected, no considerable effect was observed for associated bacteria (AcLM, AcL, AcLMI, AcLI; Figure 4.13e, f). The total rates were in the same range with 849 ng ^{13}C $\mu g_{\Sigma(\text{selected lipds})}^{-1} d^{-1}$ during incubations with acetate, methane and methyl fluoride (AcLMI) whilst experiments only with acetate revealed total assimilations of about 463 ng ^{13}C $\mu g_{\Sigma(\text{selected lipds})}^{-1} d^{-1}$ (AcL). It is assumed, that no inhibition of methanogenesis with methyl fluoride occurred. Thus, these data will not be further discussed.

In this study the sulphate related AOM was investigated. The monitoring of methane consumption and methane-dependent sulphate reduction revealed interesting stoichiometric characteristics. The sulphate related AOM, in case of ANME-2 archaea, seems to depend on a close consortia structure with SRB (Boetius et al., 2000; Orphan et al., 2002; Knittel et al., 2005). This could not be confirmed for ANME-1 associations (Michaelis et al., 2002; Blumenberg et al., 2004; Takeuchi et

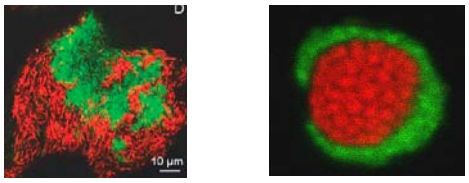

Figure 4.2: FISH-micrography of ANME-1 and ANME-2 dominated communities. ANME-1 and -2 archaea are labelled with red fluorescent probes, respectively. SRB are labelled with green fluorescent probes (Pictures: Michaelis et al., 2002; Boetius et al., 2000).

al., 2011), though a very high abundance of SRB was also observed in ANME-1 dominated communities (Michaelis et al., 2002; Blumenberg et al., 2004; Krüger et al., 2008). Hence, it has to be distinguished between facultative and obligate syntrophic communities (Stams and Plugge, 2009), with regard to the community structure within ANME-1 and ANME-2 dominated samples.

According to the ^{13}C-incorporation, the community structure also has to be considered. ANME-1 dominated systems exhibit generally no close association between archaea and bacteria but rather mono-specific clusters of ANME-1 cells (Figure 4.2; Orphan et al., 2001a, 2001b; Michaelis et al., 2002; Knittel et al., 2005). With respect to the carbon flow, this means that the carbon dioxide derived from methane oxidation will be isotopically diluted with the buffer carbonate in the medium (isotopic medium dilution effect). Thus, the uptake of ^{13}C into bacterial compounds will be diminished during incubations with labelled methane. In contrast, ANME-2 communities exhibit a rather close consortia structure between ANME-2 archaea and SRB (Figure 4.2; Boetius et al., 2000; Orphan et al., 2001b; Knittel et al., 2005; Orcutt et al., 2005). In addition, other bacterial members of this community, which are often also present in ANME-communities in general (Heijs et al., 2006, 2007; Friedrich et al., 2007, AGU; Pernthaler et al., 2008; Bowles et al., 2011) are far apart from most ANME-2/DSS-consortia. ^{13}C-labelled substrate, which is directly oxidised (e.g. methane to CO_2) by ANME-2 will be incorporated by the archaea itself and directly associated SRB (Boetius et al., 2000; Hinrichs and Boetius, 2002). In this case bacterial lipids of non-active or non-assimilating organisms dilute the lipid enrichment of ^{13}C (isotopic lipid dilution effect). Noticeable, the determined assimilation rates into bacterial lipids are mainly influenced by the associated SRB. This was also demonstrated with nanoSIMS techniques by Orphan et al. (2001a). The dominance of associated SRB was shown by several authors (Boetius et al., 2000; Orphan et al., 2002; Knittel et al., 2005; Niemann et al., 2006; Lösekann et al., 2007; Schreiber et al., 2010). The molecular biological analysis by Friedrich et al. (2007, AGU) clearly shows the high activity of SRB in both mat samples (Figure 4.1). Blumenberg et al. (2005) observed uptakes of ^{13}C into bacterial lipids, assigned to ANME-2 associated SRB in a mixed sample of ANME-1 and ANME-2 communities. They estimated, based on the uptakes of methane-derived ^{13}C into bacterial lipids, that ANME-2 associated SRB were two times more biosynthetically active than SRB typically associated to ANME-1. This could be an effect by direct uptake of closely associated SRB in those ANME-2/DSS consortia, mirroring an isotopic medium dilution effect within these experiments for ANME-1 associated bacteria.

These observations by Blumenberg et al. (2005) were similar to the results of the experiments with ^{13}C-labelled methane in this study (Figure 4.3). The daily $\Delta\delta^{13}C$ and total assimilation into the bacterial compounds were slightly enhanced for bacterial lipids in ANME-2 dominated samples within experiments with ^{13}C-labelled methane (ML; Tables 3.1, 3.2). On the one hand, a closer association of the respective SRB to ANME-2 can explain this higher uptake of methane derived ^{13}C (relative low isotopic lipid dilution effect), on the other hand a higher metabolic activity of associated bacteria can be responsible for a higher uptake of ^{13}C. Although, the rates of methane consumption and sulphate reduction are significantly higher within incubations with labelled bicarbonate for ANME-2 (PBcLM: 5 $\mu mol\, g_{TOC}^{-1} d^{-1}$, BBcLM: 115 $\mu mol\, g_{TOC}^{-1} d^{-1}$; Figures 4.25), the activity deduced from the ^{13}C-assimilation rates (BcL, BcLM; Figure 4.11) are quite similar for both mat types. For instance the rates for bacterial lipids in pink mat samples were about 32 pg ^{13}C $\mu g_{comp.}^{-1} d^{-1}$ (PBcLM, PBcL) and about 56 pg ^{13}C $\mu g_{comp.}^{-1} d^{-1}$ for bacterial compounds in black mat samples.

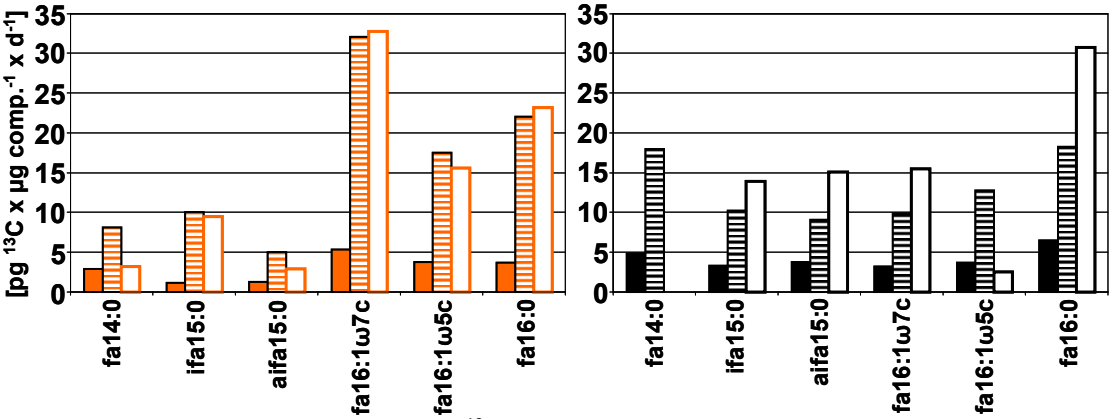

Figure 4.3: Comparison between the ^{13}C-assimilation patterns of the associated bacterial communities of both mat samples. Left figure: pink mat, incubations with ^{13}C-labelled methane (orange coloured columns), ^{13}C-labelled bicarbonate in the presence of methane (orange-white striped columns), and ^{13}C-labelled bicarbonate in the absence of methane (white columns framed orange). **Right figure**: black mat, incubations with ^{13}C-labelled methane (black coloured columns), ^{13}C-labelled bicarbonate in the presence of methane (black-white striped columns), ^{13}C-labelled bicarbonate in the absence of methane (white columns framed black).

The results from experiments with labelled bicarbonate support such consideration of the isotopic dilution effects (BcLM, BcL; Figure 4.3). The assimilation rates were slightly higher for bacterial lipids within experiments with methane in the headspace for ANME-1 dominated samples (BcLM, BcL; Figure 4.4), demonstrating an AOM-influenced anabolism. But, for most individual compounds, the rates were similar (BcLM, BcL; Figure 4.3), demonstrating an isotopic medium dilution effect with unlabelled buffer carbonate. In a similar manner dilution effects of unlabelled methane, after its oxidation, may have occurred (BcLM; Figure 4.3), leading to an underestimation of the assimilation rates. Nonetheless, the activity of most source organisms for these compounds was interestingly not directly influenced by methane (e.g. is the $\Delta\delta^{13}C$ for hexadecanoic acid ~2 ‰ d^{-1} independent of the presence of methane). This clearly shows the existence of rather AOM-independent, other autotrophic source organisms in the ANME-1 mats (Figure 4.3). SRB and

homoacetogenic bacteria are plausible source organisms. Furthermore, no sulphate reduction was measured, when methane was absent in pink mat samples. That demonstrates a sulphate-independent autotrophic metabolism during incubations without methane (PBcLM; Figure 3.7).

Besides the fact of there being a loose association between SRB and ANME-1, enhanced assimilation rates into the SRB-specific *anteiso*-pentadecanoic acid (*ai*fa15) during experiments with labelled bicarbonate in the presence of methane (BcLM 5 $pg^{13}C$ $\mu g_{comp.}^{-1} d^{-1}$; Figures 4.3), supports (i) the assignment of this compound to ANME-1 associated SRB (Blumenberg et al., 2004) and (ii) the presence of methane-related SRB in the community.

On the other hand, for most bacterial compounds in ANME-2 dominated samples, enhanced assimilation rates occurred in the absence of methane, during experiments with labelled bicarbonate (BcLM, BcL; Table 3.1, Figures 4.3). This observation hints to a slight isotopic dilution effect with CO_2 derived from unlabelled methane for most compounds. The metabolisms of most source organisms were apparently influenced by AOM. In this case, two effects influence the ^{13}C-assimilation rates. An isotopic dilution by the CO_2 from methane oxidation, and the isotopic lipid dilution effect led to lower ^{13}C-assimilation rates. The isotopic lipid dilution effect was increased by other AOM-independent autotrophic source organisms, which was demonstrated by the very low assimilation rates for most compounds during experiments with labelled bicarbonate in the presence of methane (BcLM; Figure 4.3). The tetradecanoic (fa14:0) and *cis*-*ω5*-hexedecenoic acid (fa16:1ω5c) revealed considerably high assimilation rates in the presence of methane (BcLM; Figure 4.3). The fa16:1ω5c was assigned to SRB, associated to ANME-2 consortia (Elvert et al., 2003). In this case, it is expected that the respective source organisms are indeed closely associated to ANME-2 archaea and depend directly on AOM.

For substrates not exclusively oxidised by ANME-archaea, the ^{13}C-label of the bacterial and archaeal lipids is strongly affected by a medium dilution effect and other substrates within the medium (e.g. bicarbonate or newly formed metabolites like acetate). These effects depend on (i) which organisms are able to oxidise a given substrate, (ii) which organisms can grow on the produced metabolites, (iii) the synthesis rates and concentrations of metabolites, (iv) which other metabolites are present in the medium under given conditions, and (v) how the respective organisms are locally related to each other. Further considerations to be accounted for are how active involved microorganisms are and how fast they grow under the adjusted experimental conditions, which also depends on the available energy yield. The synthesis rates and respective concentrations of metabolites, other than the added labelled substrates in these experiments were not considered. However, these effects probably play a minor role within the experiments due to high concentrations of labelled substrates (Table 2.1).

Among the investigated archaea, no methanogens were detected by primer sets specific for *mcrA* genes during PCR-analysis (data not shown; Friedrich M.W., personal communication). However, the occurrence of methanogenic species other

than ANME-1 or -2 cannot be totally excluded, due to general methodological biases, e.g. due to low primer specificity (Nunoura et al., 2008). Knittel et al. (2005) detected high proportion of ANME-1 and further molecular biological evidence for crenarchaeal benthic group (MBGB) in carbonate reef structures from the Black Sea (230 m). Beside the indications from molecular biological data there is further evidence for the absence of non-ANME-methanogens (e.g. Methanosarcinales). During incubation experiments with labelled acetate in the absence of methane, the ^{13}C-uptake into the archaeal lipid biomarkers was relatively low (Figure 4.3). In particular for *sn-2*-hydroxyarchaeol no uptake was observed during experiments without methane in the headspace (AcL; Figures 4.5f). A significant uptake would be expected if members of the Methanosarcinales were active, since they are well known to thrive on acetate (Deppenmeier, 2002a). However, it has to be considered that the acetoclastic methanogenesis could be inhibited by SRB under such sulphate reducing conditions. The rates of methane consumption (PAcLM: 362 µmol $g_{TOC}^{-1} d^{-1}$ vs. PBcLM: 37 µmol $g_{TOC}^{-1} d^{-1}$ and BAcLM: 241 µmol $g_{TOC}^{-1} d^{-1}$ vs. BBcL: 184 µmol $g_{TOC}^{-1} d^{-1}$) were enhanced compared to those of methanogenesis (PBcL: 4 µmol $g_{TOC}^{-1} d^{-1}$ and BBcL: 5 µmol $g_{TOC}^{-1} d^{-1}$) for both ANME-communities, demonstrating the dominance of an oxidative pathway (Phelps et al., 1985; Achtnich et al., 1995; Fukui et al., 1997), leading to an enhanced methane oxidation. Although methanogenesis also occurred, the rates of methanogenesis never exceeded those of methane consumption. However, the rates of methanogenesis were considerably high (Figure 4.25). The measured methane consumption rates were about three to five times higher than the rates of methanogenesis for experiments with bicarbonate and methanol. It was expected that methanogenesis was completely inhibited or at least strongly restricted by SRB under sulphate reducing conditions. Contrarily, the rates of methylotrophic methanogenesis appear to be decoupled from sulphate. Methanol is no adequate substrate for most SRB, as was also shown for other environments (e.g. Oremland and Polcin, 1982). For other methylotrophic archaea, which do not directly belong to the ANME-clusters, higher rates of methanogenesis would be expected to occur in the experiments, especially in the absence of methane would be expected. Thus, it is assumed that the investigated samples are by far or even completely dominated by ANME-1 or -2 archaea, respectively.

For the first time, the carbon flow and the rates of methanogenesis from ^{13}C-labelled acetate was tested in AOM-communities. Acetate might be incorporated directly as a building block for lipids via acetyl-CoA. However, it has to be considered that the direct assimilation requires ATP for acetate activation (Deppenmeier, 2002b). Thus, a higher incorporation of acetate could be constrained by energetic limitations. Anyway, apparently acetate has very little relevance for the methanogenic pathway for both ANME-clusters under the sulphate reducing conditions adjusted. Only marginal methane formation (AcLM, AcL; Figure 4.25) was measured within the experiments with acetate. In addition, the isotopic composition of the newly formed methane during ^{13}C acetate labelling experiments showed no considerable ^{13}C-incorporation. This indicates a predominance of an autotrophic pathway (CO_2-reducing methanogenesis) even during incubations with acetate. The minor ^{13}C

uptake in the newly generated methane from labelled acetate can be explained with a marginal relevance of the acetoclastic pathway (minor acetoclastic methanogenesis). Otherwise the ^{13}C comes from acetate-derived CO_2 after bacterial acetate oxidation (CO_2-reduction). The very low rates of methanogenesis and the very low incorporation of ^{13}C from acetate (AcLM, AcL; Figure 4.25; BcL, AcL; Figures 3.4, 3.5) indicate a rather autotrophic metabolism under experimental conditions in the AOM-mats studied. Moreover, acetate even seems to reduce the capabilities of CO_2-reduction of both ANME-clusters, and led obviously to enhanced methane consumption within incubations with methane, especially in ANME-1 dominated samples (AcLM; Figure 4.25). Since bicarbonate was the buffer of the incubation medium, at least similar rates of autotrophic methanogenesis were expected, but not observed (Figure 4.25). The rates of methanogenesis were significantly reduced in incubations with acetate, compared to experiments with bicarbonate as labelled substrate. For pink mats the daily rates of methanogenesis were 4 $\mu mol\, g_{TOC}^{-1} d^{-1}$ within incubations with bicarbonate only, in samples with added acetate the rates of methanogenesis revealed 0.5 $\mu mol\, g_{TOC}^{-1} d^{-1}$.

Molecular biological investigations by Meyerdierks et al. (2010) revealed nucleic acid sequences, assigned as putative acetate decarboxylase/ synthase and enzymes of an incomplete tricarboxylic acid cycle (TCA) and reductive TCA. They suggested that these enzymes are more involved in an anabolic pathway. This is also underlined by the data of this study which support a rather anabolic impact of acetate on archaea in AOM settings than the use of acetate as substrate for methanogenesis. Although an uptake into the lipid biomass was measured from labelled acetate, no effect of acetoclastic methanogenesis was determined by isotopic analysis. This refutes a catabolic role of acetate under given experimental conditions.

Considering an autotrophic anabolism, the uptake of acetate derived ^{13}C after bacterial acetate oxidation might be isotopically diluted by the buffer bicarbonate.

A preferred uptake of acetate via a mixotrophic metabolism of associated bacteria (probably SRB) and a direct incorporation into bacterial lipids (Figures 4.11) would be responsible for reduced substrate availability, followed by lower assimilation rates into archaeal lipids. Calculating that the labelled acetate would be completely oxidised to CO_2, the buffer carbonate would have a final $\delta^{13}C$-value of about 17,227 ‰. The assimilation rates of the archaeal lipids would be at least five fold lower than observed if CO_2 was assimilated instead of acetate.

Finally, a mixed incorporation, CO_2-incorporation after acetate oxidation and a direct uptake via acetyl-CoA, was probably responsible for the measured ^{13}C-uptake into the archaeal lipids (e.g. ANME-1: archaeol 11 $pg^{13}C\ \mu g_{comp.}^{-1} d^{-1}$; AcL, Figure 4.5). Acetate has obviously no catabolic relevance for both investigated ANME-clusters.

Formate might be also relevant, but was not tested in this study. Although Sørensen et al. (2001) postulated formate as the only thermodynamically relevant electron shuttle. They based their assumption on a study at shallow waters with very

low methane concentrations (0.02 mM). Valentine et al. (2002) provided acetate as electron shuttle at higher methane concentrations. However, none of the electron shuttles could be confirmed yet (Nauhaus et al., 2002, 2005). In the Black Sea the methane concentration is about 11 µM in the anoxic water body (Reeburgh et al., 1991). Krüger et al. (2008) measured concentrations of methane below the sediment mats of 3.7 mM and 3.1 µM in the surrounding seawater. The concentrations of dissolved methane in the medium during the experiments with a pressure of 0.2 MPa methane were about 0.55 µM, in all other experiments the concentrations were 0.33 µM. None of the substrates inhibited the methane consumption or had a considerable increasing effect on the sulphate reduction as was previously shown in other experiments by Nauhaus and colleagues (2002, 2005).

Summary

Methyl fluoride showed no significant inhibition effect on the acetoclastic methanogenesis.

Especially the incubation experiments with (labelled) bicarbonate underlines a facultative syntrophic consortia structure for ANME-1 compared to a more obligate consortia structure for ANME-2/DSS.

The composition and the ^{13}C-assimilation into the lipid biomarkers under the different experimental conditions give strong evidence for two distinct microbial mat systems, dominated by ANME-1 and -2, respectively.

The carbon derived from labelled acetate was most likely directly incurporated into the archaeal lipids as a building block via acetyl-CoA or after bacterial acetate oxidation as bicarbonate.

4.3 Archaeal and bacterial metabolisms among ANME-1 and -2 dominated mats

4.3.1 Archaeal metabolism among ANME-1 and -2 dominated mats

4.3.1.1 Assimilation rates and ^{13}C-uptake of the archaeal lipids in the ANME-systems

The metabolisms of the archaea were investigated though the addition of different ^{13}C-labelled substrates. Methane, bicarbonate, methanol, and acetate were tested for their impact on methanotrophy, methanogenesis, sulfate reduction and whether they are incorporated ^{13}C into the archaeal biomass. The latter experiments were also conducted with methane in the system.

The amount of most of archaeal lipids in the samples dominated by ANME-1 was relatively low compared to ANME-2 dominated mat samples (Figure 3.8; appendix Tables A.4c, d). Thus, the total ^{13}C-assimilation rates were also lower. Therefore, the ^{13}C-assimilation rates of the archaeal lipids were considered to mark the differences of the rates of lipid synthesis between the two samples, which is a concentration independent approach. The daily δ^{13}C-shifts (Figure 3.12) were recalculated into total ^{13}C-assimilation rates for 1µg lipid fraction of selected lipids (Figure 4.4) and the

^{13}C-assimilation rates for individual compounds (Figure 4.5). The total ^{13}C-assimilation rates during most incubation experiments were lower, than for archaeal lipids of ANME-2 dominated mat samples (Figure 4.4).

Similar to PMIs, ^{13}C-depleted archaeol, archaeol:1 and *sn*-2-hydroxyarchaeol can be attributed to ANME-archaea (Hinrichs et al., 1999; Blumenberg et al., 2004). Since the membrane of Methanosarcinales (Koga et al., 1993 and references therein) and probably ANME-2 consists mainly of isoprenoid dialkyl glycerol diether lipids (Blumenberg et al., 2004), the synthesis rate goes along with membrane maintenance or even active cell growth. The assimilation rates are influenced by the respective label of the substrate and the given growth conditions. Thus, the synthesis rates are mirroring the metabolic effect of the substrate in the presence and absence of the methane.

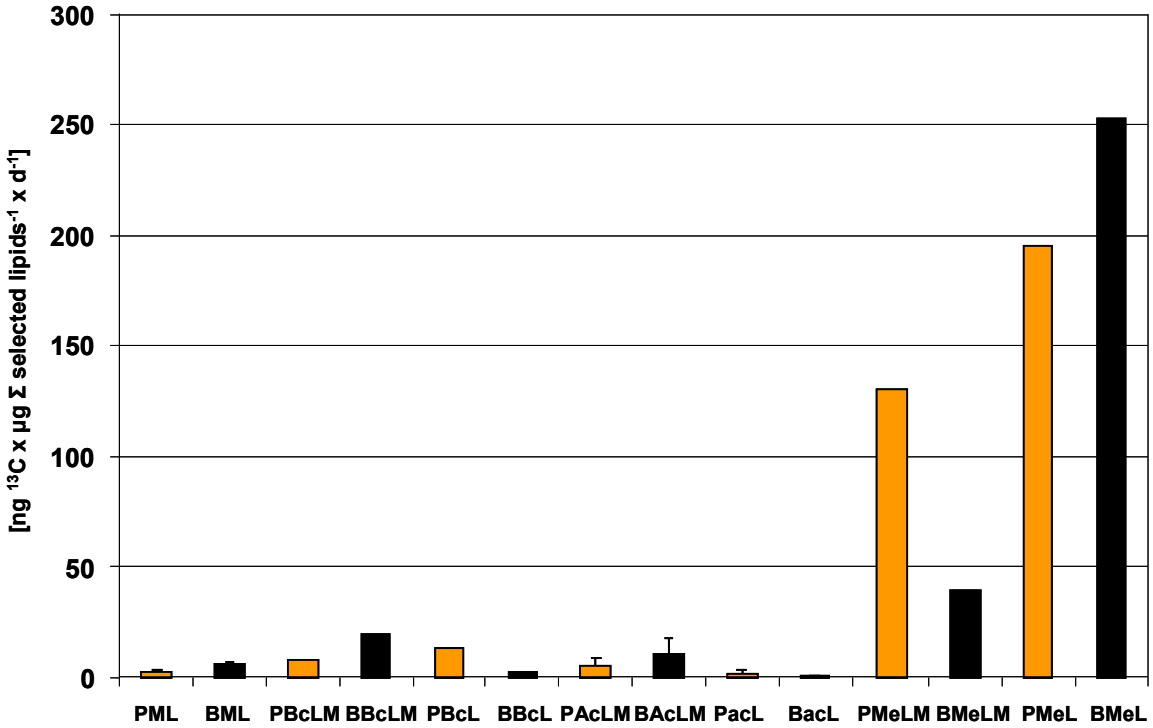

Figure 4.4: Total ^{13}C-assimilation rates into the archaeal lipids during the incubation experiments. The orange columns depict the pink mat samples, and the black columns the black mat samples. The rates were calculated for a 1µg fraction of selected (archaeal) lipids, for further details see also section 2.4.7.
Abbreviations: P - pink, B - black, ML - labelled methane, BcLM - labelled bicarbonate with methane, BcL - labelled bicarbonate, AcLM - labelled acetate with methane, AcL - labelled acetate, MeLM - labelled methanol with methane, MeL - labelled methanol

Among ANME-1 similar ^{13}C-assimilation rates were observed between incubation experiments with labelled bicarbonate, independent of the presence of methane (BcLM, BcL; Figure 4.5a, c), demonstrating a more versatile metabolism for ANME-1 archaea (BcLM, BcL; Figure 4.5c). This is also underlined by similar total ^{13}C-uptakes from methane and from labelled bicarbonate with and without methane (ML, BcLM, BcL; Figure 4.4). The ^{13}C-assimilation from labelled methane and labelled

bicarbonate (in the presence of methane) were slightly diminished, most likely due to an isotopic dilution effect from unlabelled bicarbonate or methane in the system, respectively (ML, BcLM; Figure 4.5a, c). The uptake of ^{13}C from bicarbonate apparently did not necessarily depend on the presence of methane. This implies that ANME-1 can easily switch between an autotrophic and methanotrophic metabolism. The ^{13}C-assimilation rates from labelled methane (ML; Figure 4.5a) were in the same range as those from acetate incubation experiments for ANME-1 dominated samples (AcL, Figure 4.5e). The total ^{13}C-assimilation rates from acetate were considerable higher in the presence of methane (AcLM; Figure 4.5e). This indicates a direct incorporation of acetate.

PMI:4 and PMI:5 revealed the highest incorporation during incubation experiments with labelled methane (~11 $pg^{13}C\ \mu g_{comp.}^{-1}d^{-1}$; ML; Figure 4.5a) or labelled bicarbonate (~12 and ~9 $pg^{13}C\ \mu g_{comp.}^{-1}d^{-1}$, respectively; BcLM, BcL; Figure 4.5c). Archaeol revealed considerable higher ^{13}C-incorporation compared to the unsaturated isomer in the same experiments, for instance during incubations with labelled bicarbonate and methane 8 (arch.) and 1.6 (arch:1) $pg^{13}C\ \mu g_{comp.}^{-1}d^{-1}$, respectively (BcLM, Figure 4.5c). The synthesis rates and probably the function are of these two compound groups may be different and depend apparently on the experimental conditions. The PMIs have obviously a higher turnover rate.

The total uptakes and especially the assimilation rates for the biphytanes were considerable low in most experiments compared to those of archaeol and its unsaturated isomer in ANME-1 dominated samples (Figure 4.5). This indicates a very low synthesis rate and will be further discussed in section 4.3.1.2.

The assimilation rates into the C_{35}-iosprenoids were significantly high during incubations with labelled bicarbonate, when methane was absent. For the isomer $C_{35:7}c$ a daily assimilation of 5.7 $pg^{13}C\ \mu g_{comp.}^{-1}$ was found (BcLM; Figure 4.5c). The anabolism seems to depend on the substrate or at least on the experimental conditions. This will be further discussed in section 4.3.1.3.

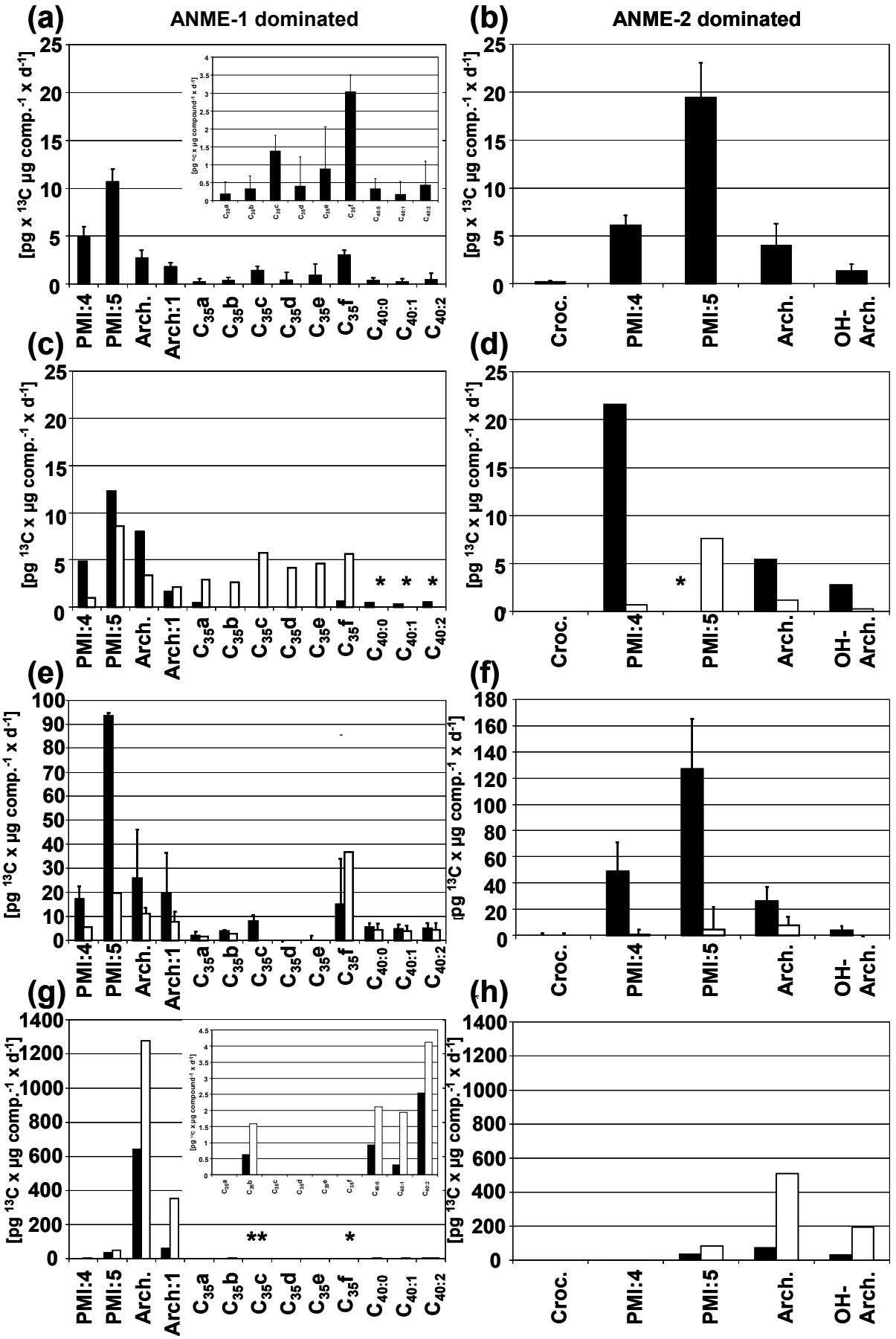
(a)
ANME-1 dominated
(b)
ANME-2 dominated
(c)
(d)
(e)
(f)
(g)
(h)
[pg x 13C µg comp.-1 x d-1]
[pg 13C x µg comp.-1 x d-1]
PMI:4
PMI:5
Arch.
Arch:1
C35a
C35b
C35c
C35d
C35e
C35f
C40:0
C40:1
C40:2
Croc.
OH-Arch.
*
**

Figure 4.5: ^{13}C-assimilation rates into the archaeal lipid biomarker compounds of ANME-1 (left) and -2 (right) dominated communities incubated with different ^{13}C-labelled substrates under different conditions. (a, b) ^{13}C-methane - ML, (c, d) ^{13}C-bicarbonate (black columns with methane - BcLM, white columns without methane in the headspace - BcL), (e, f) ^{13}C-acetate (black columns with methane - AcLM, chequered columns without methane in the headspace - AcL, white columns with methane and methyl fluoride - AcLMI, black-white stripped columns with methyl fluoride and without methane in the headspace - AcLI), (g, h) ^{13}C-methanol (black columns with methane - MeLM, white columns without methane in the headspace - MeL). The error bars result from replicate or triplicate measurements and show the maximum level of deviation of the rates. For experimental details see methods and table 2.1. * not analysed.

In contrast to ANME-1, the total ^{13}C-assimilation rates for archaeal lipids assigned to ANME-2 demonstrate a very strong adaptation to methane (ML, BcLM, BcL; Figures 4.4, 4.5). This is supported by the generally higher total ^{13}C-assimilation rates within experiments with (labelled) methane and with labelled bicarbonate in the presence of methane (ML, BcLM; Figure 4.4; 6 and 20 ng^{13}C $\mu g_{\Sigma(\text{selected lipids})}^{-1} d^{-1}$) compared to experiments with labelled bicarbonate or labelled acetate in the absence of methane (BcL, AcL; Figure 4.4; 3 and 1 ng^{13}C $\mu g_{\Sigma(\text{selected lipids})}^{-1} d^{-1}$). The observed ^{13}C-assimilation rates from labelled bicarbonate and (unlabelled) methane (BcLM; Figure 4.4) were higher than those from labelled acetate and (unlabelled) methane (AcLM; Figure 4.4; 11 ng^{13}C $\mu g_{\Sigma(\text{selected lipids})}^{-1} d^{-1}$). This also implies a stronger impact of bicarbonate than of acetate.

The assimilation patterns of ANME-1 and -2 were almost similar (Figure 4.5a, c, e and b, d, f). This demonstrates similarities in the metabolism of the two investigated ANME-clusters. However, the low assimilation rates into ANME-2 lipids during incubations without methane in the headspace demonstrate the strong adaptation to methane. For example, the assimilation rates of archaeol in the presence of methane from labelled bicarbonate (BcLM; Figure 4.5) or labelled acetate (AcLM; Figure 4.5) were 5 and 26 pg^{13}C $\mu g_{comp.}^{-1} d^{-1}$, respectively. In the case that methane was absent, the daily ^{13}C-incorporations were 1.2 from labelled bicarbonate (BcL; Figure 4.5) and 7 pg^{13}C $\mu g_{comp.}^{-1}$ from labelled acetate (AcL; Figure 4.5). The synthesis of these compounds, however, was apparently affected by the experimental conditions. Very low assimilation rates for methane and bicarbonate (BcLM; Figure 4.5d) derived ^{13}C into *sn-2*-hydroxyarchaeol were measured, though being much lower in the absence of methane (BcL; Figure 4.5d). These findings give further evidence for a methanotrophic source organism of *sn-2*-hydroxyarchaeol. At least under these conditions, the synthesis of *sn-2*-hydroxyarchaeol was influenced by the presence of methane. In addition, the relative high assimilation rates of the polyunsaturated PMI:4 and PMI:5 compared to those of the isoprenoid dialkyl glycerol ethers (archaeol, *sn-2*-hydroxarchaeol) demonstrate a very high turnover rate of those PMIs in most experiments (Figure 4.5a-f; discussed later in section 4.3.1.2). The assimilation rates and the total ^{13}C-uptake observed here were also increased in the presence of methane, indeed underlining their formation during methanotrophy.

In previous studies it was observed that CH_4 and HCO_3^- derived ^{13}C was incorporated into archaeal lipids of involved archaea (Blumenberg et al, 2005; Wegener et al., 2008a; Jagersma et al., 2009). This was in principal confirmed, but -

for the first time - tested for individual ANME-clusters (Figures 4.4, 4.5, 4.6). The calculated ^{13}C-assimilation rates from this study can be compared to published data (Blumenberg et al., 2005; Wegener et al., 2008a) of some archaeal compounds. In figure 4.6 the assimilation rates into the individual compounds are compared between the experiments of Blumenberg et al. (2005) and those of this study. Interestingly, similar assimilation patterns were found. They were in the same range, e.g. for PMI:5 15 pg^{13}C $\mu g_{comp.}^{-1} d^{-1}$. In their study the archaeol revealed a daily ^{13}C-incorporation about 0.8 pg^{13}C $\mu g_{comp.}^{-1}$, and thus much lower than the same compound in this study. While in ANME-1 dominated samples archaeol revealed an incorporation rate of 2.7 pg^{13}C $\mu g_{comp.}^{-1} d^{-1}$, the daily rates in ANME-2 dominated samples were up to 4 pg^{13}C $\mu g_{comp.}^{-1}$ (ML; Figure 4.6). Contrary to the findings of this study, the daily ^{13}C-incorporation into the unsaturated isomer of archaeol (arch:1: 3.6 pg^{13}C $\mu g_{comp.}^{-1}$) was higher compared to archaeol. Also the daily assimilation in this study was lower, about 1.8 pg^{13}C $\mu g_{comp.}^{-1}$ (ML; Figure 4.6). Nonetheless, the biphytanes showed a similar daily assimilation compared with those of this study. The rates were between 0.3 for $C_{40:1}$ and 0.7 pg^{13}C $\mu g_{comp.}^{-1} d^{-1}$ for $C_{40:0}$ measured by Blumenberg and colleagues (2005), and between 0.2 for $C_{40:1}$ and 0.4 pg^{13}C $\mu g_{comp.}^{-1} d^{-1}$ for $C_{40:2}$ in this study (ML; Figure 4.6).

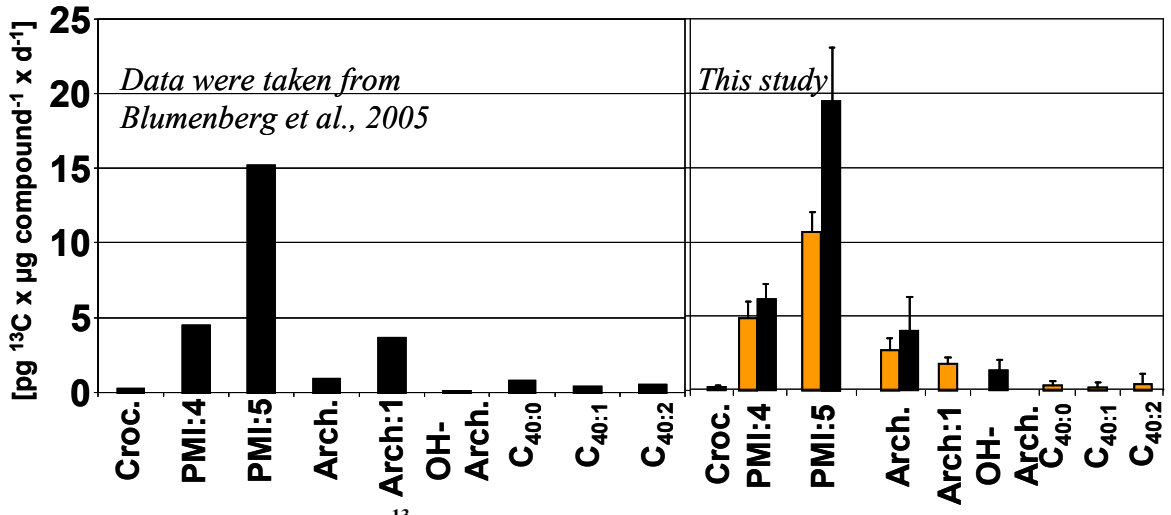

Figure 4.6: Comparison of the ^{13}C-assimilation rates into the archaeal lipids from Black Sea mat samples. Left side: The data were taken from a study by Blumenberg et al. (2005) with a mixed microbial mat sample from the Black Sea, incubated with 7 % ^{13}C-labelled methane. **Right side:** The data were taken from this study, ANME-1 (orange columns) and ANME-2 dominated (black columns) mat samples were incubated with 25 % ^{13}C-labelled methane, respectively. For the abbreviations see appendix A.5.

The assimilation rates differ for the respective archaeal compounds investigated by Wegener et al. (2008a). The calculated assimilation rates for archaeol and *sn-2*-hydroxyarchaeol were similar (~3.6 pg^{13}C $\mu g_{comp.}^{-1} d^{-1}$) for Black Sea samples in their long time studies (159 days, labelled methane; 176 days, labelled bicarbonate and methane). Within short batch experiments (50 days) with ^{13}C-labelled bicarbonate, in the presence and absence of (unlabelled) methane, archaeol revealed assimilation rates (~2.3 pg^{13}C $\mu g_{comp.}^{-1} d^{-1}$) similar to this study. The

assimilation rates into *sn-2*-hydroxyarchaeaol were lower (~1.3 pg^{13}C $\mu g_{comp.}^{-1} d^{-1}$) than in this study.

The ^{13}C-assimilation rates are in the same range for the described compounds and experiments, indicating similar activities deduced by the ^{13}C-enrichement. The slight differences between all experiments might be explained by the use of different samples, varying experimental set ups, particularly with the substrate label and natural fluctuations in the samples. Blumenberg et al. (2005) and Wegener et al. (2008a) obtained their data by mixed samples of ANME-1 and -2. Contrary the data of this study were obtained from two distinct mat samples, dominated by ANME-1 or -2, respectively. The concentrations and residence times of those compounds might also have affected the ^{13}C-assimilation rates.

There are apparently slight differences in the metabolisms between both ANME-clusters as discussed below (Sections 4.4, 4.5; Figure 4.25). This is also indicated by variations in the ^{13}C assimilation patterns of the archaeal lipids (compare BcLM, BcL, MeLM, MeL; Figure 4.5c, d and g, h).

Interestingly, the highest total ^{13}C-assimilation rates into ANME-1 and -2 specific lipids were not observed in AOM-approaches (addition of methane and bicarbonate), but from methanol-derived ^{13}C (MeLM, MeL; Figure 4.4). This clearly indicates a strong adaptation to methylotrophic substrates for both ANME-clusters. Furthermore, very high rates of methylotrophic methanogenesis were measured. Intriguingly, the rates were independent of the addition of methane (MeLM, MeL; black and white columns; Figure 4.25). Although the rates of methanogenesis were similar, the lipid uptakes from ^{13}C-methanol were different in both mat types. The lower assimilation rates observed for archaeal compounds of both mat samples in the presence of methane (Figure 4.4) can be best explained by either (i) an isotopic dilution effect with unlabelled methane, (ii) a competitive inhibition effect by (unlabelled) methane, or (iii) a preferred AOM-dependent metabolism under given experimental conditions. It appears that they exhibit under methylotrophic conditions they exhibit a different lipid anabolism than under methanotrophic conditions.

During incubation experiments with labelled methanol, archaeol revealed daily incorporations of 640 when methane was present and 1278 pg^{13}C $\mu g_{comp.}^{-1}$ in the absence of methane in ANME-1 dominated samples. The assimilation rate for PMI:5 during the same experimental set up was 35 pg^{13}C $\mu g_{comp.}^{-1} d^{-1}$ (MeLM; Figure 4.5). Considerable lower assimilation rates were measured for the same compounds during the respective experiment with ANME-2 samples. Archaeol revealed a ^{13}C-incorporation of 72 pg^{13}C $\mu g_{comp.}^{-1} d^{-1}$ during incubations with labelled methanol and methane. Nonetheless, the assimilation into archaeol was still higher than into PMI:5 (MeLM; Figure 4.5). The distinct assimilation patterns and the very high assimilation from methanol indicate strong methylotrophic capabilities of both inves-

tigated ANME-clusters (MeLM, MeL; Figure 4.5g, h). Very high synthesis rates of lipids were observed, indicating a very high activity of the ANME-archaea[ii].

4.3.1.2 Biosynthesis of the glycerol dialkyl glycerol tetraethers (GDGTs) in ANME-1

Probably the GDGTs comprise the majority of the lipids of the membrane of ANME-1. The ^{13}C-assimilation into the biphytanes within all incubation experiments (Figures 4.5, 4.6, 4.7) was also observed in previous studies by Blumenberg et al. (2005), who observed minor but appreciable ^{13}C-incorporation into the biphytanes. Blumenberg measured daily $\delta^{13}C$-shift for the $C_{40:0}$ of 0.06 ‰, for $C_{40:1}$ of 0.03 ‰ and for $C_{40:2}$ 0.06 ‰ after 316 days. The rates in this study were between 0.2 ‰ for $C_{40:1}$ and 0.4 ‰ per day for $C_{40:2}$ and thus considerable higher.

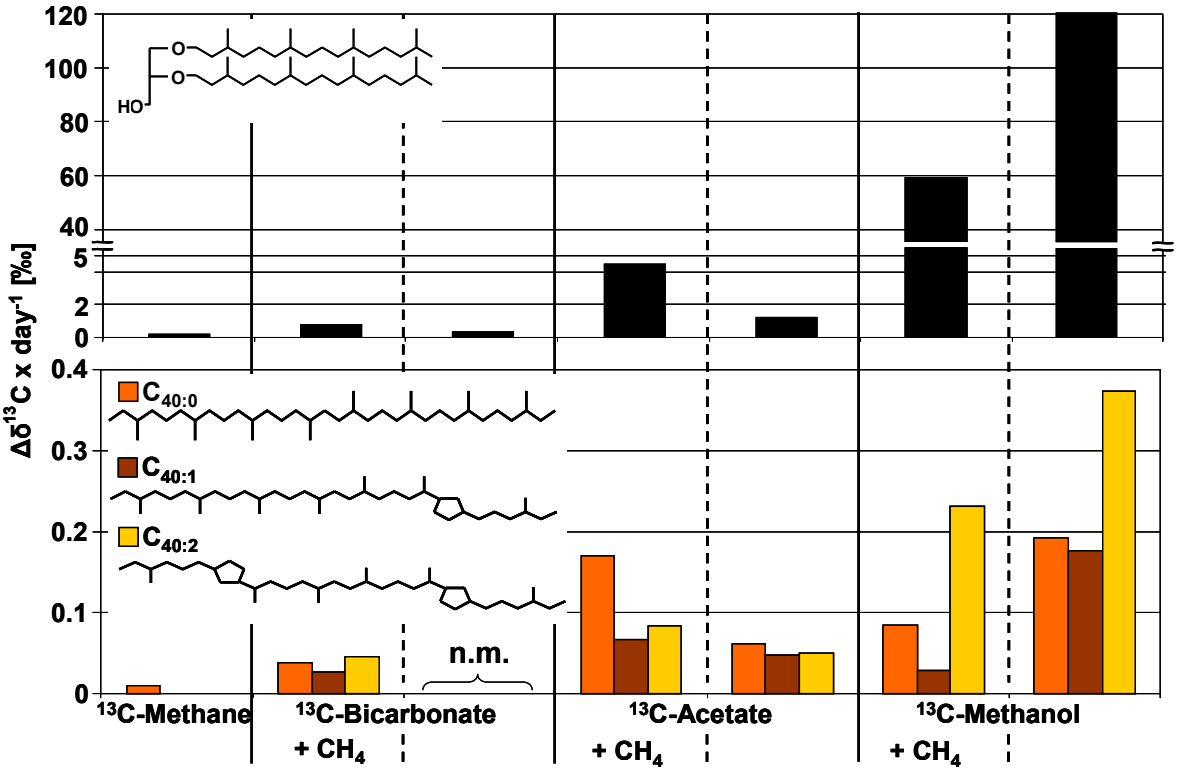

Figure 4.7: ^{13}C-assimilation rates into the dialkyl glycerol diethers and the biphytanes in ANME-1 dominated samples. The ^{13}C-assimilation rates for incubations with labelled methane after 378 days and labelled acetate after 56 days were illustrated. For abbreviations see also tables 4.1, A.6; n.m. - not measured.

Interestingly, similar assimilation patterns were obtained for the biphytanes and archaeol (Figures 4.7), though with considerably lower rates. The very high amount of the GDGTs, very low synthesis rates and long residence times can explain the marginal ^{13}C-uptake into the archaeal lipids, assigned to ANME-1.

[ii] Only species of the order Methanosarcinales and one exception in the order Methanobacteriales, *Methanosphaera stadtmanae,* are described to be capable to grow with methanol (Miller et al., 1983; Deppenmeier et al., 2002a). Here, different biochemical mechanisms lead to methanol disproportion or methanol reduction. These pathways are basically influenced by the composition and occurrence of hydrogenases (Thauer et al., 2010).

This observation supports the idea, that archaeol is a precursor compound in ANME-1 for the GDGTs (De Rosa et al., 1980; Figure 4.8). Kellermann et al. (2011, IMOG) measured the assimilation rates into the archaeal intact polar lipids from an ANME-1 dominated enrichment culture. They also showed that the isotopic label was higher in archaeol than in the GDGTs and came independently to the same conclusions.

Takano et al. (2010) showed a very low uptake into the biphytanes of benthic archaea, but a high uptake into the glycerol backbone of the glycerol dialkyl glycerol tetraethers (GDGTs) through sedimentary *in-situ* stable isotope experiments. The different assimilation patterns between both parts of the GDGTs suggest an anabolic recycling process for the isoprenoidal core lipids. This explains also the very low uptake into the biphytanes.

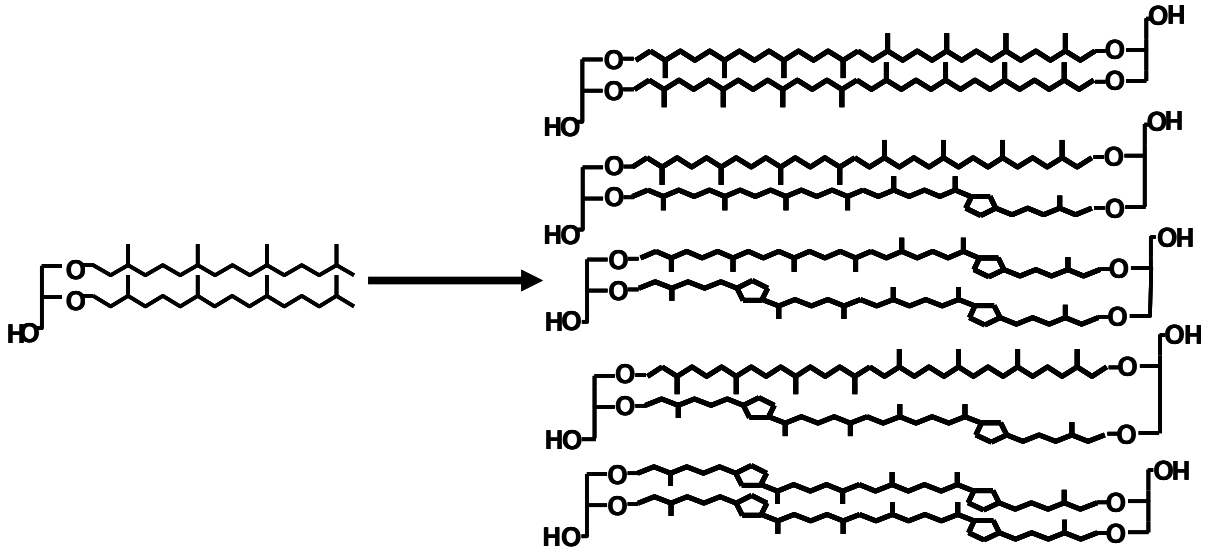

Figure 4.8: Archaeol as potential precursor molecule for the glycerol dialkyl glycerol tetraether lipids in ANME-1.

4.3.1.3 Putative functions of the archaeal isoprenoid hydrocarbons in ANME-systems

Crocetane (*2,6,11,15*-tetramethylhexadecane) was tentatively assigned to ANME-2 or other involved archaea in those AOM-settings, due to its high depletion in ^{13}C and occurrence in AOM-settings (Elvert et al., 1999; Blumenberg et al. 2004). Elvert et al. (2000) assumed that crocetane could be an ultimate product which is preserved in sediments and authigenic carbonates in ancient cold seep environments. Nonetheless, the source organism of crocetane still remains obscure. In the ^{13}C-labelling approaches of this study crocetane revealed only minor ^{13}C-uptake from labelled methane or labelled acetate (ML, AcLM, AcL; Figures 4.5b, f). Blumenberg et al. (2005) observed also only negligible $\delta^{13}C$-shifts for this compound during incubations with labelled methane. A very low assimilation rate within the experiments and a very long residence time of this compound could be responsible for those marginal uptakes from labelled substrates. Otherwise, this could also be an effect of isotopic heterogeneities within the samples.

^{13}C-depleted *2,6,10,15,19*-pentamethylicosane and -enes (PMI) are commonly reported from AOM settings and are attributed to both ANME-clusters (Thiel et al., 1999; Elvert et al., 1999; Blumenberg et al., 2004). The uptake of ^{13}C within all experiments, especially when methane was present, into the PMIs supports ANME-archaea as potential source organisms. The assimilation rates might be affected by the respective substrates and differ slightly. The very high assimilation rates into PMI:5 within all incubation experiments, especially in the presence of methane, imply a function in methanotrophy in both mat types. In particular for experiments with ANME-2 dominated samples, the assimilation rates were affected by the presence of methane. This observation underlines an assignment of these compounds to ANME-archaea. The ^{13}C-incorporations from methanol for unsaturated pentamethylicosenes were similar to those of the biphytanes. In all other experiments the ^{13}C-assimilation rates into the biphytanes were considerably lower compared to those of the PMIs. These findings imply a varied anabolism under given experimental conditions for investigated ANME-clusters (Figure 4.5g).

Constitutional isomers of unsaturated C_{35}-isoprenoid hydrocarbons have been found in all ANME-1 dominated samples (Figure 4.9). Tornabene et al. (1978) postulated a function as intracellular reversible hydrogen sink for isoprenoids in archaea (Figure 4.10). However, another function of such compounds could be the regulation of cell membrane fluidity (Sinensky et al., 1974) depending on varying pressure and temperature. PMIs and C_{35}-isoprenoids were originally found in methanogenic archaea (Holzer et al., 1979; Tornabene et al., 1979).

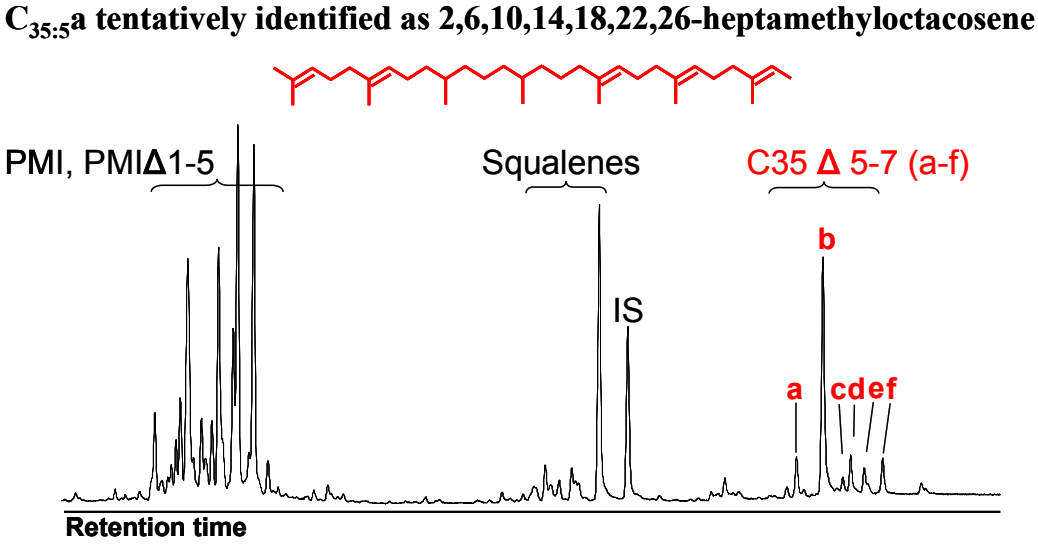

Figure 4.9: MS-chromatogram of a hydrocarbon fraction, ANME-1 dominated samples.
The chromatogram shows the isomers of pentamethylicosane, its mono- and poly unsaturated isomers (Δ1-5). After the squalenes six peaks represent the respective unsaturated isomers of the C_{35}-iosprenoid hydrocarbon. While the positions of the double bonds could be tentatively identified for the first three isomers (C_{35}a-c), the structural details of the last three isomers (C_{35}d-f) remain unresolved. A pentacyclic ring structure is assumed, deduced by the number of unsaturations and the later retention times. PMI – pentamethylicosane/ -ene, IS - internal standard (5α-cholestane), C_{35}Δ5-7 (a-f) - C_{35}-isoprenoid hydrocarbons.

Low ^{13}C-assimilation rates were observed within incubation with labelled methane (ML; Figure 4.5a). While only marginal ^{13}C-uptakes were observed from bicarbonate in the presence of methane, ^{13}C-uptakes into all isomers in the absence of methane were detected. The absence of ^{13}C-uptake into most isomers (exception $C_{35:5}$a and $C_{35:7}$f; Figure 4.5c) in the presence of methane during incubation experiments with labelled bicarbonate (BcLM) can be explained by an isotopic dilution effect by unlabelled methane. Otherwise, assuming that AOM and methanogenesis occur simultaneously in the microbial system (see also Figure 4.25), the hydrogen formed by AOM could be consumed by methanogenesis in adjacent ANME-1 cells. This process would maintain a low hydrogen partial pressure, supporting AOM. Consequently, the enhanced carbon assimilation into the C_{35}-isoprenoids indicates a rather methanogenic life style of the ANME-1 under methane free conditions. Hence, to avoid hydrogen loss by diffusion ANME-1 most likely use these isoprenoids as intracellular reversible hydrogen sinks (Figure 4.10). Manquin et al. (2004) investigated the effect of several factors for such irregular isoprenoid compounds in the thermophilic deep-sea methanogen *Methanococcus jannaschii*. They demonstrated that the availability of hydrogen significantly influences the production of C_{35}-isoprenoids. Usually, methanogens capable of acetoclastic methanogenesis are absent at high temperature methanogenic sampling sites (Thauer et al., 2010). Consequently, this leads to the assumption that these compounds have also a function as hydrogen storage in ANME-1.

Low rates of ^{13}C-incorporation were observed within incubations with labelled acetate, considering the high label of the substrate (AcLM, AcL; Figure 4.5e). These patterns, and the remarkable high assimilation rate into the isomer $C_{35:7}$f, cannot be explained. Since acetate most likely has no catabolic effect to ANME-1, these signals could be influenced by an acetate-independent metabolism, e.g. by CO_2-reduction (compare to section 4.2, Figure 4.25). However, during the synthesis of these compounds the labelled acetate was incorporated as building blocks, and thus leading to the observed labelling of these compounds.

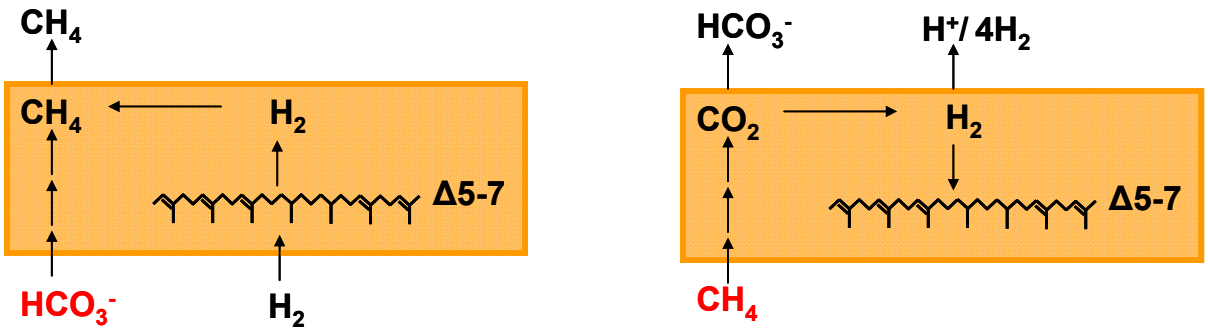

Figure 4.10: C_{35}-isoprenoid hydrocarbon in ANME-1 as hypothesised, reversible, intracellular hydrogen sink, involved in autotrophic methanogenesis. This scheme explains a putative function of the C_{35}-isoprenoids as reversible hydrogen sink during two different metabolic stages of ANME-1. When methane is produced from bicarbonate, the isomers supply the reaction in a hydrogen depleted environment. In case that methane is present, leading to a favoured energy supply from the disequilibrium of a methane rich environment, hydrogen produced after methane oxidation is stored reversible with those compounds. The concentration of hydrogen and sulphate trigger the respective metabolism.

The assimilation patterns of the C_{35}-isoprenoids are apparently affected by the experimental conditions and were distinct from those observed for archaeol and the biphytanes with very low uptakes from methanol (MeLM, MeL; Figure 4.5g). Only marginal incorporation could be determined for one isomer ($C_{35:6}$b) in both methanol incubation experiments, respectively. The lack of ^{13}C-uptake into most compounds during experiments with methanol (MeLM, MeL; Figure 4.5g) supports a function as reversible hydrogen sink. These data further support a direct relation between hydrogen metabolism and the synthesis of these C_{35}-isoprenoids in that they function as a store for hydrogen, since the needed hydrogen could be supplied by methanol itself after a disproportion reaction (Deppenmeier, 2002b). Hence, no hydrogen must be stored.

Summary

Similar total daily $\Delta\delta^{13}$C of the archaeal lipids during incubation experiments with labelled methane and labelled bicarbonate in the presence of methane and slightly enhanced total daily δ^{13}C-shifts with labelled bicarbonate (when no methane was present) demonstrate methane independent autotrophic capabilities for ANME-1.

ANME-2 showed a higher assimilation of methane, bicarbonate or acetate derived ^{13}C during respective incubation experiments. However, the assimilation rates were significant higher and thus the ANME-2 metabolism is more dependent on the presence of methane.

Both mat types showed highest assimilation of methanol derived ^{13}C into the archaeal lipids and demonstrate strong methylotrophic capabilities, especially in the absence of methane. This could be caused by an isotopic dilution effect of the unlabelled methane.

Archaeol could be a precursor for the GDGTs in ANME-1 dominated samples. Six isomers of a polyunsaturated C_{35}-ioprenoid hydrocarbon were found. These compounds could be involved in a hydrogen dependent methanogenesis and function as reversible hydrogen sink. A similar function of reversible hydrogen storage is also assumed for the PMIs.

The synthesis of *sn-2*-hydroxyarchaeol was mainly affected by the presence of methane. Crocetane revealed no explicit ^{13}C-assimilation throughout all incubation experiments supporting the assumption by Elvert et al. (2000) that crocetane is an ultimate product which is preserved in the environments.

4.3.2 Bacterial metabolisms among ANME-1 and -2 dominated mats

With different approaches, depending on the substrate, it was possible to gain more information about the metabolic potential within such mat systems. The used substrates are, with the exception of methane, possible metabolites derived from the methane carbon in natural methane fuelled systems. Acetate and CO_2 are also products after degradation processes in anaerobic systems. Additionally, acetate can be formed from carbon dioxide. The role of methanol is so far not well investigated

for marine sediments. However, some investigations demonstrated that methanol is a degradation product from pectin derived from an impact of algae to the sediment (Schink and Zeikus 1980, 1982). Furthermore, methyl sulphides e.g. methane thiol, DMDS (dimethyl disulphide) as secondary metabolites are formed in sediments with high sulphide concentrations and high organic content and may be generated through nucleophilic attack by sulphide on methyl groups (Mitterer, 2010). Here, methanol was tested as one representative compound.

The incubation experiments with ^{13}C-labelled methane (ML; Figures 4.12a, b; 4.13; 3.15a, b; Section 4.3.2.1) and ^{13}C-labelled bicarbonate (BcLM, BcL; Figures 4.12c, d; 4.13; 3.15c, d; Section 4.3.2.1) were conducted to determine (methane-dependent and independent) autotrophic growth of bacteria.

The addition of carbon isotopic labelled acetate (AcLM, AcL; Figures 4.12e, f; 4.17; 3.15e, f; Section 4.3.2.2) was conducted to demonstrate further chemoorgano-heterotrophic, chemolithoheterotrophic and mixotrophic life styles of the bacteria involved.

Methylotrophic or homoacetogenic capabilities of involved prokaryotes were tested with methanol (MeLM, MeL; Figures 4.12g, h; 4.21; 3.15g, h; Section 4.3.2.3).

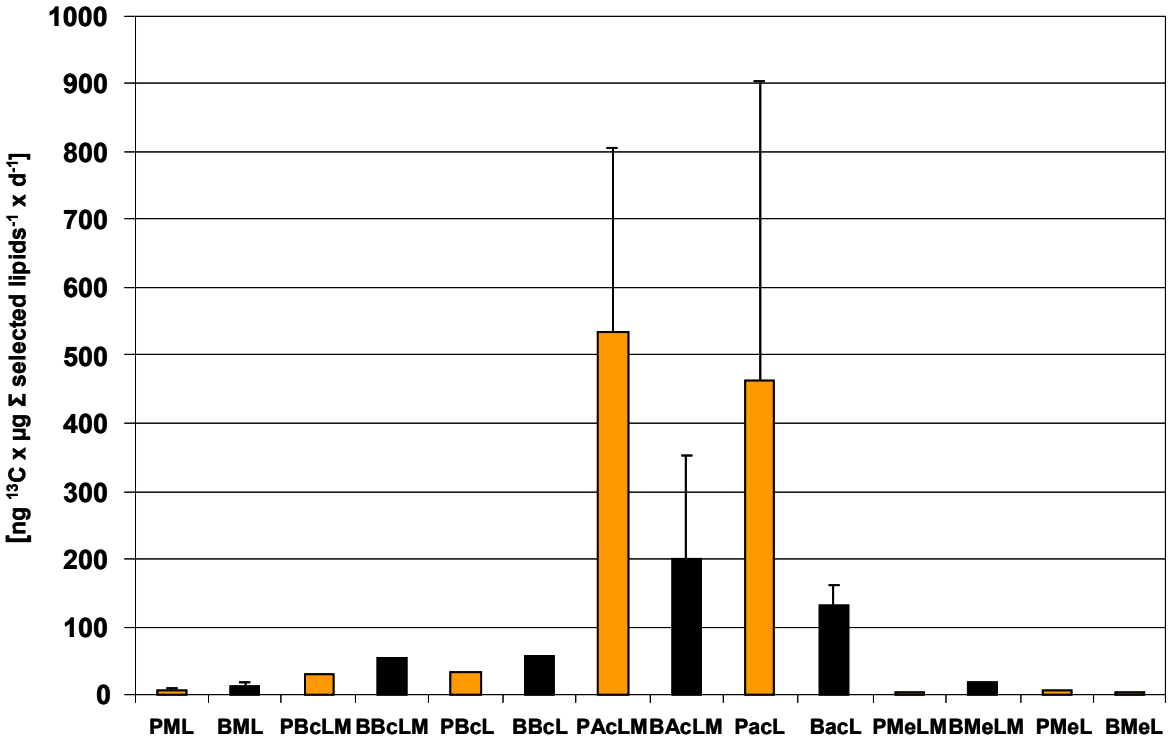

Figure 4.11: Total ^{13}C-assimilation rates into the bacterial lipids during the incubation experiments. The orange columns depict the pink mat samples, and the black columns the black mat samples. The rates were calculated for a 1µg fraction of selected (bacterial) lipids, for further details see also section 2.4.7.
Abbreviations: P - pink, B - black, ML - labelled methane, BcLM - labelled bicarbonate with methane, BcL - labelled bicarbonate, AcLM - labelled acetate with methane, AcL - labelled acetate, MeLM - labelled methanol with methane, MeL - labelled methanol

There are considerable differences between the two mat samples, and between incubation experiments which investigated autotrophic (ML, BcLM, BcL; Figure 4.12a-d; Section 4.3.2.1), heterotrophic (AcLM, AcL; Figure 4.12e, f; Section 4.3.2.2) and putative acetogenic (MeLM, MeL; Figure 4.12g, h; Section 4.3.2.3) metabolism. Figure 4.11 summarises the total daily ^{13}C-assimilation rates per 1 µg lipid fraction of selected bacterial lipids. At first glance, the ANME-1 associated bacterial community has pronounced heterotrophic capabilities (PAcLM, PAcL; Figure 4.11) compared to the ANME-2 dominated bacterial community. On the other hand, slightly enhanced uptakes into the lipid biomass of the ANME-2 associated community from methane and bicarbonate indicate a stronger autotrophic anabolism (BML, BAcLM, BAcL; Figure 4.11). Marginal, but remarkable uptake during experiments with labelled methanol in the presence of methane imply methylotrophic anabolism for ANME-2 associated bacteria. This indicates that in addition to AOM-dependent metabolism, other microbial processes (autotrophic and heterotrophic) have significant relevance for the associated bacteria in both communities. Moreover, the activity data (Figure 4.25) and carbon assimilation rates in concert support that ANME-1 relies much less on sulphate and bacterial partners (Sections 4.2, 4.4, 4.5.1) than ANME-2 communities, clearly hinting to different functioning of both communities.

Overall, the ^{13}C-assimilation patterns for bacterial lipids showed significant differences for ANME-1 dominated mat samples within all incubation experiments (Figure 4.12a, c, e, g). This indicates that the bacterial community were unequal influenced by the different substrates. Probably, different source organisms were responsible for the isotopic enrichment of considered compounds. Distinct assimilation patterns were observed within ANME-2 dominated mat types (Figure 4.12b, d, f, h). Nonetheless, the ANME-2 mat type exhibited similar patterns for incubation experiments with methane and bicarbonate (ML, BcLM, BcL; Figure 4.12b, d), but different for acetate and in particular for methanol (AcLM, AcL, MeLM; Figure 4.12f, h). This demonstrates a stable autotrophic community of sulphate reducing bacteria as major source organisms for all labelled fatty acids and non-isoprenoidal glycerol ethers. These sulphate reducers might be dominated by δ-Proteobacteria (SEEP-SRB1a-cluster; Boetius et al., 2000; Orphan et al., 2002; Knittel et al., 2005; Niemann et al., 2006; Lösekann et al., 2007; Schreiber et al., 2010).

Figure 4.12: ^{13}C-assimilation rates into the bacterial lipid biomarker compounds of ANME-1 (left) and -2 (right) dominated communities incubated with different ^{13}C-labelled substrates under different conditions. (a, b) ^{13}C-methane - ML, (c, d) ^{13}C-bicarbonate (black columns with methane - BcLM, white columns without methane in the headspace - BcL), (e, f) ^{13}C-acetate (black columns with methane - AcLM, chequered columns without methane in the headspace - AcL, white columns with methane and methyl fluoride - AcLMI, black-white stripped columns with methyl fluoride and without methane in the headspace - AcLI), (g, h) ^{13}C-methanol (black columns with methane - MeLM, white columns without methane in the headspace - MeL). The error bars result from replicate or triplicate measurements and show the maximum level of deviation of the rates. For experimental details see methods and table 2.1. * not analysed.

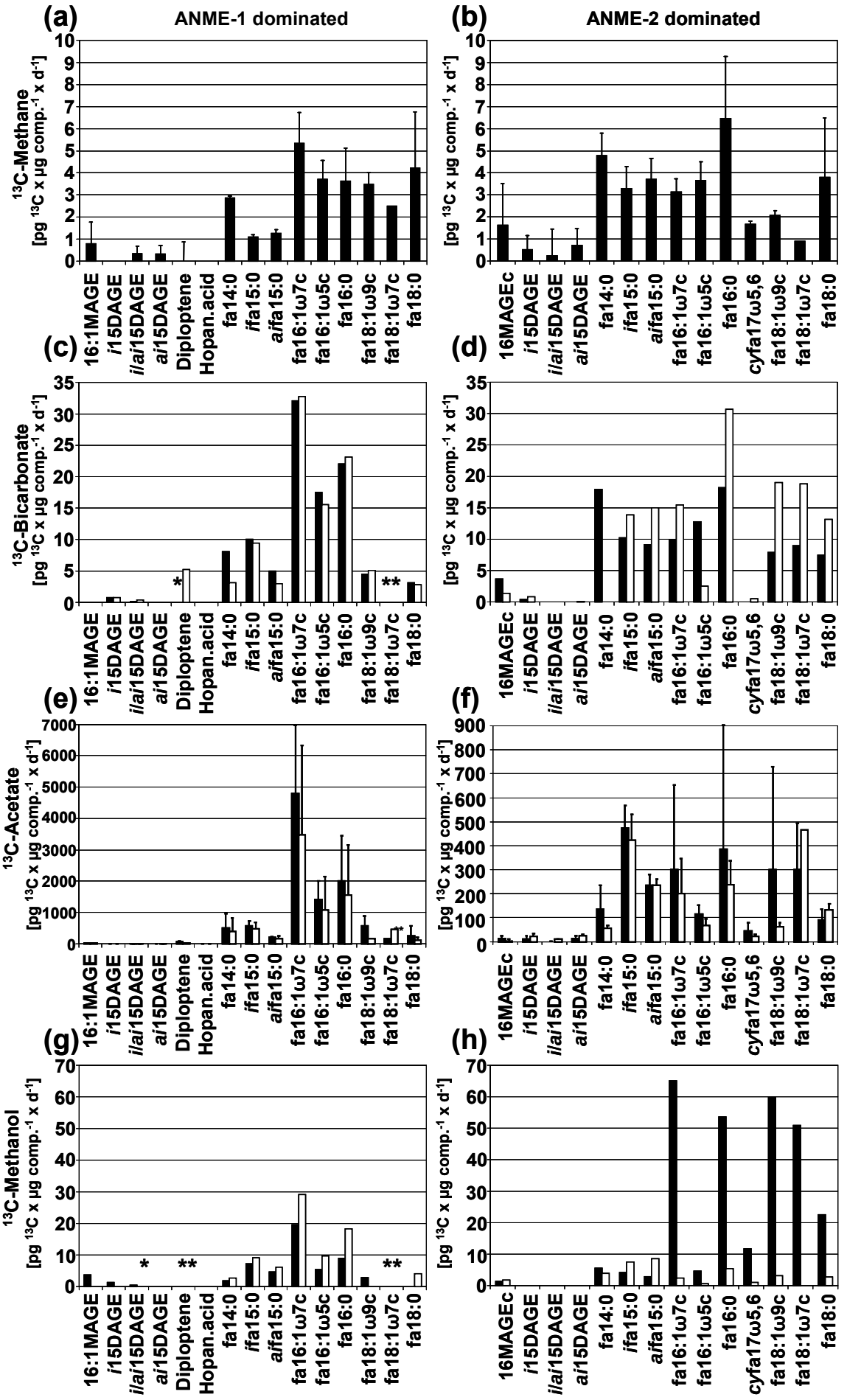
(a)
ANME-1 dominated
(b)
ANME-2 dominated
(c)
(d)
(e)
(f)
(g)
(h)
13C-Methane
13C-Bicarbonate
13C-Acetate
13C-Methanol
[pg 13C x µg comp.-1 x d-1]
16:1MAGE
i15DAGE
i/ai15DAGE
ai15DAGE
Diploptene
Hopan.acid
fa14:0
ifa15:0
afa15:0
fa16:1ω7c
fa16:1ω5c
fa16:0
fa18:1ω9c
fa18:1ω7c
fa18:0
16MAGEc
cyfa17ω5,6

4.3.2.1 Indications for autotrophy among bacteria

The autotrophic capabilities of the two distinct associated bacterial communities were investigated with labelled methane and labelled bicarbonate. The experiments clearly demonstrated lower total ^{13}C-assimilation rates from labelled methane compared to experiments with labelled bicarbonate. Probably an isotopic dilution effect with unlabelled bicarbonate was responsible for this observation, especially for ANME-1 associated bacteria (isotopic medium dilution effect; Section 4.2; Figures 4.3, 4.13).

The organisms capable to autotrophic growth do not necessarily depend on a methane-derived metabolism or sulphate reduction as mirrored by the methane-dependent sulphate reduction rates (Figures 4.25, 3.6; PBcL: 5.2 $\mu g\,^{13}C\,g_{TOC}^{-1}\,d^{-1}$, BBcL: 92 $\mu g\,^{13}C\,g_{TOC}^{-1}\,d^{-1}$). Although the sulphate reveals high amounts in the incubation medium (16 mM), and thus might be the main terminal electron acceptor (TEA) with the highest standard reduction potential ($E^{0'}$) in the system[iii]. Similar assimilation patterns and uptakes into specific compounds (Figures 4.12a-d, 4.13) indicate also further sulphate-independent metabolism or microorganisms in both mat samples. Although, the total daily ^{13}C-shifts were in the same range, the methane oxidation and sulphate reduction rates (Figure 4.25) were lower in pink mat samples. This similar activity, deduced by the ^{13}C-incorporation into the lipids (Figure 4.13) in both microbial communities indicates the presence of other autotrophic bacteria in ANME-1 samples. Homoacetogenic organisms (e.g. other autotrophic organisms), which also grow with bicarbonate have to be kept in mind, as they influence the observed assimilation patterns as they are also capable of growing on bicarbonate[iv] (MeLM, MeL; Figures 4.12g; see also Section 4.3.2.3).

Slight differences between the assimilation patterns of the two investigated bacterial communities (ANME-1 and -2 associated) within experiments with labelled methane or labelled bicarbonate (ML; BcLM, BcL; Figures 4.12a-d, 4.13) were observed. For bacterial compounds within ANME-1 dominated samples, the assimilation patterns are quite similar. This holds also true for compounds from ANME-2 dominated samples. As expected, the incorporations from labelled bicarbonate are significantly higher, due to the direct assimilation of carbon from bicarbonate.

The newly formed and the buffer carbonate can be incorporated by autotrophic SRB. In the pink mat samples the *anteiso*-pentadecanoic acid (*ai*a15:0) revealed considerable total assimilation rates from labelled methane (ML; Figure 3.13a) and from labelled bicarbonate in the presence of methane (BcLM, Figure 3.13c), although the assimilation rates were very low (ML, BcLM; Figures 4.12, 4.13). This can be explained by the very high concentration of this compound. This observation confirms previous assignments (Blumenberg et al., 2004) of this compound in ANME-1 dominated samples as diagnostic lipid biomarker for associated SRB. For all other

[iii] Standard redox potential ($E^{0'}$) of SO_4^{2-}/HS^-: -217 mV (Thauer et al., 1977)

[iv] $CH_3OH + 0.5\ HCO_3^- \rightarrow 0.75\ CH_3COO^- + H_2O;\ \Delta G^{0'} = -55$ KJ/ reaction (Thauer et al., 1977)
$4\ H_2 + HCO_3^- + H^+ \rightarrow CH_3COO^- + 4\ H_2O;\ \Delta G^{0'} = -104.6$KJ/ mol (Thauer et al., 1977)

fatty acids the assimilation rates were similar, during incubations with and without methane (BcLM, BcL; Figures 4.12c, 4.13, 3.15c). Furthermore, no sulphate reduction was measured in the absence of methane demonstrating the activity of other, rather methane-independent, autotrophic bacteria in the mats. However, the isotopic medium dilution effect (from the buffer carbonate) may contribute to slightly lower observed assimilation rates in the presence of methane.

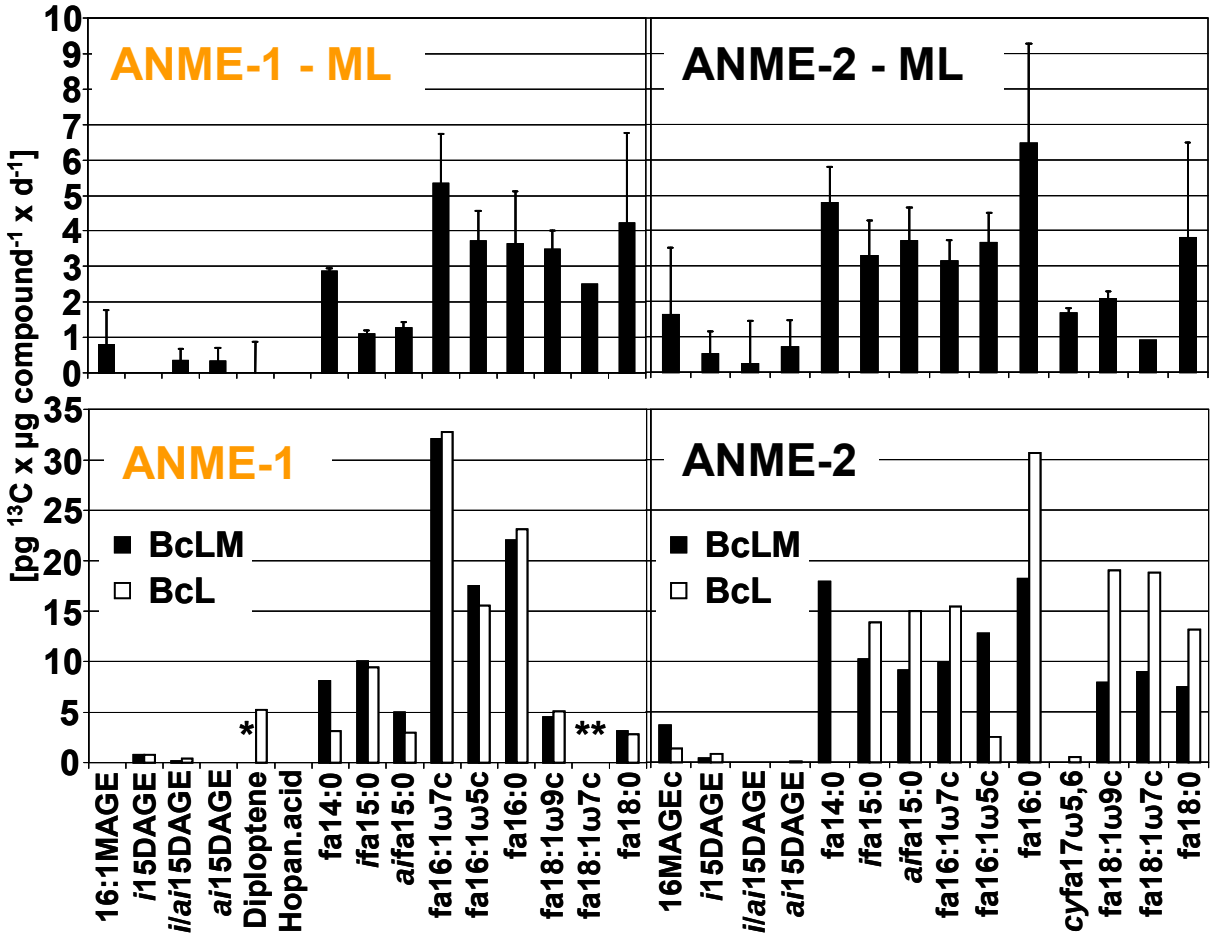

Figure 4.13: ^{13}C-assimilation rates into bacterial lipids from labelled substrates. AOM-dependent and autotrophic bacterial growth in pink (ANME-1 associated) and black (ANME-2 associated) mat. Abbreviations: ML - labelled methane, BcLM - labelled bicarbonate in the presence of methane, BcL - labelled bicarbonate. * - not analysed, for abbreviation of the lipids, see appendix A.5.

The ^{13}C-assimilation patterns for ANME-2 dominated samples for experiments with labelled methane (ML; Figures 4.12b, 4.13) were consistent with those of labelled bicarbonate (BcLM, BcL; Figures 4.12d, 4.13). These similar patterns support the activity of a stable autotrophic bacterial community, which is also active in the absence of methane (BcLM, BcL; Figure 4.12). The low uptakes in the presence of methane (BcLM; Figures 4.12, 4.13) can be best explained by the close association of respective source organisms to methanotrophic archaea (isotopic dilution effect, Section 4.2; Figure 4.13).

In ANME-2 dominated samples the ^{13}C-assimilation rate of fa16:1ω5c, diagnostic for sulphate-reducers in ANME-2 dominated communities (Elvert et al., 2003; Blumenberg et al., 2004), was in the same range with other lipids. However, growth

of the respective source bacteria especially depends on the presence of methane, which is indicated by the low assimilation of ^{13}C from labelled bicarbonate in the absence of methane (BcL; Figure 4.13). Moreover, the highest total assimilation per day (8 $pg^{13}C\ \mu g_{comp.}^{-1} d^{-1}$), measured for the fa16:1ω5c underlines this compound as diagnostic marker for SRB in AOM-settings. Very high assimilation rates into fa14:0 and fa16:0 within methane label experiments (ML; Figure 4.13) imply the majority of source organisms to be autotrophic. Tetradecanoic acid can be attributed to autotrophic, rather AOM-dependent source organisms not just for one but for both mat types, demonstrated by respective higher ^{13}C-assimilation rates in the presence of methane (ML, BcLM, BcL; Figures 4.12 a-d, 4.13). Moreover, direct associated δ-Proteobacteria within the ANME-2/DSS consortium were probably responsible for the assimilation of ^{13}C from labelled bicarbonate exclusively when methane was present (BcLM; Figures 4.13, 3.15d).

Very low assimilation rates into cyclopropyl-heptadecanoic acid (*cy*fa17:1ω5,6) during incubation experiments with labelled methane (ML, Figure 4.13) indicate a low synthesis rate of this compound under these experimental conditions. No ^{13}C-assimilation into the *cy*fa17:1ω5,6 (BcLM; Figure 4.13) was found when methane was present. This was unexpected; since this compound is commonly attributed to ANME-2 associated SRB (Elvert et al., 2003). If the source organisms are directly associated to ANME-2, this could indicate a dilution effect with unlabelled methane after its oxidation and a very low synthesis rate. The likelihood is that fa16:1ω5c and *cy*fa17:1ω5,6 have different source organisms.

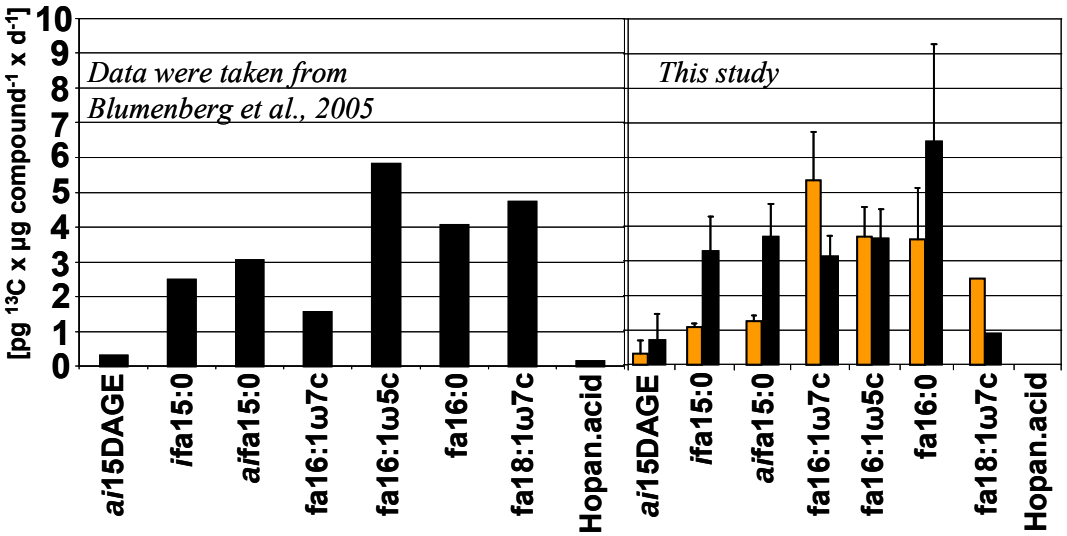

Figure 4.14: Comparison (with data taken from Blumenberg et al., 2005) of ^{13}C-assimilation rates into bacterial lipids from Black Sea mat samples. Left side: The data were taken from a study by Blumenberg et al. (2005) with a mixed microbial mat sample from the Black Sea, incubated with 7 % ^{13}C-labelled methane. **Right side:** The data were taken from this study, ANME-1 (orange columns) and ANME-2 dominated (black columns) mat samples were incubated with 25 % ^{13}C-labelled methane, respectively. For the abbreviation of the lipids see appendix A.5**.**

SRB (which belong mainly to the δ-Proteobacteria in the investigated samples) may have considerable impact on the autotrophic assimilation patterns. However, the molecular biological data of the pink and black mat samples, as well as those from

similar settings by other authors (Inagaki et al., 2006; Heijs et al., 2007; Wegener et al., 2008b; Jagersma et al., 2009; Bowles et al., 2011; Webster et al., 2011) exhibit several additional phyla, which may comprise potential anaerobic autotrophic members. Moreover as discussed later (Section 4.3.2.3), isotopic signals of homo-acetogenic bacteria may also serve to the observed assimilation patterns.

In previous studies Blumenberg et al. (2005) and Wegener et al. (2008a) demonstrated that methane and bicarbonate are important carbon sources for associated bacteria. This was confirmed in this study for both mat types.

The assimilation patterns found here (Figure 4.14) differ from those observed in experiments conducted by Blumenberg et al. (2005). Although the label of the substrate was lower, the respective assimilation rates into individual bacterial compounds were in the same range. Blumenberg and colleagues (2005) worked with mixed samples and a lower methane label. Remarkable is the very low assimilation rate into the fa16:1ω7c during incubation with 7 % labelled methane. The daily incurporation was about 1.5 pg^{13}C $\mu g_{comp.}^{-1}$. In this study, the daily incorporation was 5 in pink mats and 3 pg^{13}C $\mu g_{comp.}^{-1}$ for black mats. This indicates some differences in the bacterial composition or at least activity. The *ai*fa15:0 revealed 3 pg^{13}C $\mu g_{comp.}^{-1} d^{-1}$ in the incubations by Blumenberg et al. (2005) as observed in the black mat samples (this study). While Blumenberg et al. (2005) observed a daily assimilation of 6 pg^{13}C $\mu g_{comp.}^{-1}$ into the fa16:1ω5c during incubations with 7 % labelled methane, the daily incorporation within pink mat samples was 4 pg^{13}C $\mu g_{comp.}^{-1}$ (this study).

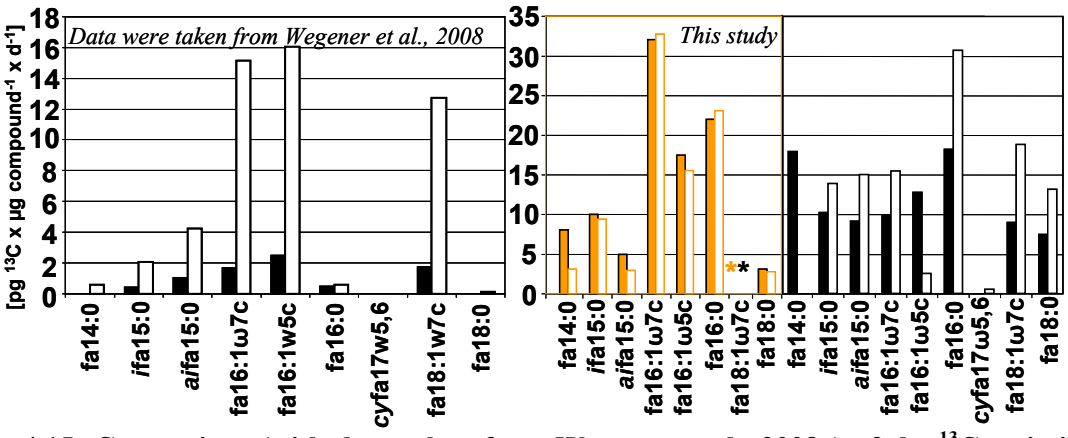

Figure 4.15: Comparison (with data taken from Wegener et al., 2008a) of the ^{13}C-assimilation rates into bacterial lipids from Black Sea mat samples. Left side: The data from a ^{13}C-labelleling study by Wegener et al. (2008a) were obtained from a mixed sample of a microbial mat from the Black Sea, incubated with 12 % ^{13}C-labelled methane (black columns) or 11 % ^{13}C-labelled bicarbonate and (unlabelled) methane in a flow-through incubation system (white columns). **Right side:** Data were taken from this study, ANME-1 associated bacteria with 20 % ^{13}C-labelled bicarbonate in the presence (orange filled columns) and in the absence of unlabelled methane (orange framed white columns) and ANME-2 associated bacteria with 20 % ^{13}C-labelled bicarbonate in the presence (black framed white columns) and absence of methane. * - not analysed, for abbreviation of the lipids, see appendix A.5**.**

Totally different assimilation patterns were determined by Wegener et al. (2008a) during incubation experiments with labelled bicarbonate in the presence of methane (Figure 4.15 - white columns). Daily incorporations about 15 and 16 pg^{13}C $\mu g_{comp.}^{-1}$

were measured for fa16:1ω5c and fa16:1ω7c, respectively. However, the respective daily ^{13}C-assimilations are consistent with those of this study, despite the two fold higher substrate label. This is shown by the fa16:1ω7c, which reveals in the study by Wegener et al. (2008a) daily incorporation of 15 pg^{13}C $\mu g_{comp.}^{-1}$ and in this study for pink mat samples approximately 33 pg^{13}C $\mu g_{comp.}^{-1}$ (PBcLM, PBcL). This also demonstrates that most of the source organisms grow rather methane independent autotrophic. All these discrepancies between the assimilation rates determined by Blumenberg et al. (2005), Wegener et al. (2008a) and in this study can be best explained with high diversity of the associated bacterial communities in the distinct samples. The sampling sites differ, too. While in this study experiments with sediment mats of nearly pure ANME-1 or -2 dominated samples from a depth of 180 m were conducted, Wegener and colleagues (2008) used rather mixed sediment samples from a depth of about 320 m. Blumenberg and colleagues performed incubation experiments with mixed mat samples from carbonate reef structures (230 m).

Figure 4.16 illustrates the possible methane and bicarbonate derived carbon fluxes as a simplified model. Methane is oxidised to bicarbonate by ANME-archaea as shown by the reduced assimilation rates into the bacterial lipids, when incubated with labelled methane (ML, Figures 4.11, 4.12a-d, 4.13) compared to incubations with labelled bicarbonate. The extracellular bicarbonate as well as methane can be incorporated into the archaeal lipids (Figures 4.4, 4.6). Furthermore, the bicarbonate can be reduced to methane by the archaea, as demonstrated by the methane generation during the experiments with labelled bicarbonate (Figure 4.25).

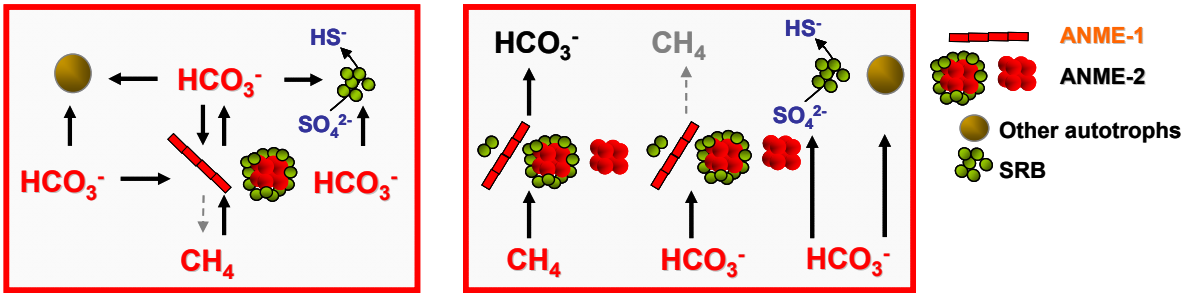

Figure 4.16: A simplified scheme of methane and bicarbonate metabolism modelled from the methane and bicarbonate derived ^{13}C-fluxes within both mat samples. Methane and bicarbonate derived carbon is incorporated into the archaeal lipids. Furthermore methane, after its oxidation by the ANME-archaea, as well as the bicarbonate derived carbon of the medium is incorporated into the bacterial lipids by autotrophic organisms. The SRB may have mainly influence on the bacterial assimilation patterns as predominant bacterial group and due to the experimental conditions (incubation medium). This carbon flux model includes other autotrophic growing bacteria, although no other electron donors have been added to the medium. Other potential candidates of autotrophic bacteria are homoacetogenic bacteria.

4.3.2.2 Indications for heterotrophy / mixotrophy among bacteria in AOM mats

Heterotrophic capabilities were demonstrated for both communities by the incorporation of ^{13}C derived from acetate (AcLM, AcL; Figures 4.12e, f, 4.17, 3.15e, f). Generally, incorporation of acetate-derived ^{13}C might also occur via cross feeding of CO_2 after acetate oxidation by bacteria or direct assimilation via acetyl-CoA. Nonetheless, a heterotrophic metabolism involved in energy generation and supplying electrons by an organic compound is possible. Unfortunately, it is not

possible to distinguish between a mixotrophic growth by sulphate reducing bacteria, other heterotrophic growing bacteria, or a direct incorporation into the lipids. However, it is assumed that most ^{13}C-labelled acetate is incorporated by (mixotrophic) SRB, since sulphate is the main electron acceptor. For a simplification of the discussion in the following sections the term heterotrophy will be used.

Only a little is known about the effect of acetate in AOM-performing communities. No incubation experiments with ^{13}C-labelled substrates were published, yet. This is the first time that the associated bacterial community has been investigated with isotopic labelled acetate.

In figure 4.17 the measured ^{13}C assimilation into the bacterial lipids are depicted and figure 4.18 illustrates a simplified model of acetate derived carbon fluxes during a heterotrophic metabolism in the two mat types (ANME-1 and -2 dominated).

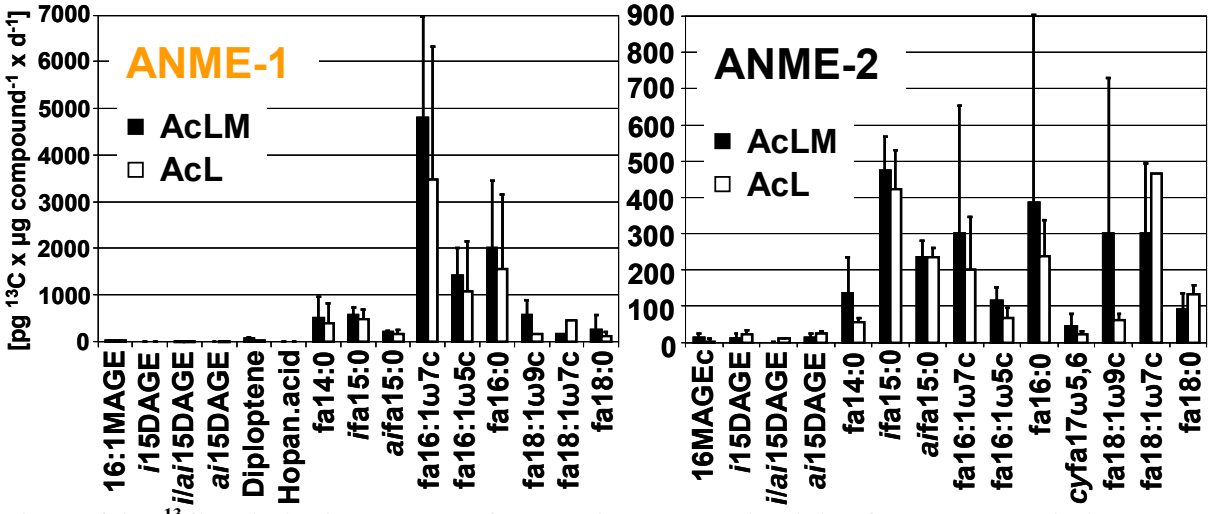

Figure 4.17: ^{13}C-assimilation patterns for associated bacterial lipids from acetate within the two investigated ANME-communities, ANME-1 and -2 dominated. Left side: ANME-1 associated bacterial lipids. **Right side:** ANME-2 associated bacterial lipids. Incubation experiments with ^{13}C-labelled acetate in the presence (black columns) and in the absence (white columns) of methane. For the abbreviation of the lipids see appendix A.5

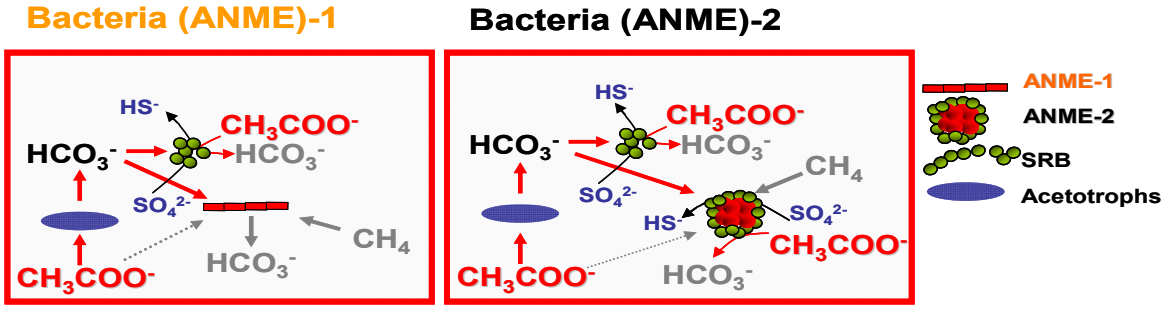

Figure 4.18: A simplified scheme of heterotrophic metabolism modelled from the acetate derived ^{13}C-fluxes within both mat samples. The acetate can be oxidised by acetate-oxidising bacteria and bicarbonate is formed. This bicarbonate can be assimilated by SRB or ANME-archaea. The SRB can also use acetate for sulphate reduction. Acetate can also be assimilated directly into the archaeal or bacterial lipids as building block.

Both AOM-performing microbial systems are quite similar. However, in the ANME-1 mat system, all processes are likely linked to the extracellular hydrogen concentration. The ANME-2 microbial system is an obligate syntrophic community.

The very high total ^{13}C-assimilation rates of acetate-derived carbon demonstrate a major anabolic effect of involved bacteria (AcLM, AcL; Figures 4.11; 4.12e, f, 4.17, 3.15e, f). This observation can be best explained with a direct uptake of acetate as building blocks for lipid biosynthesis, which are likely dominated by compounds of sulphate reducing bacteria. For most compounds, this appears to be independent of the addition of methane, implying a heterotrophic methane independent life style (AcLM, AcL; Figures 4.12e, f, 4.17). An autotrophic growth with CO_2 after acetate oxidation can be disregarded. A very high isotopic dilution effect (medium dilution effect; Section 4.2) led to lower labelling of the investigated compounds. Furthermore, low assimilation rates from ^{13}C-acetate or derived carbon into the fatty acids of ANME-2 associated bacteria point to lower heterotrophic capabilities (AcLM, AcL; Figures 4.11, 4.12f; 4.17).

The bacterial lipids of ANME-1 associated bacteria revealed about ten times higher assimilation rates from acetate-derived carbon, compared to bacteria associated to ANME-2 (AcLM, AcL; Figure 3.15e, f). These very high assimilation rates within incubation experiments with supplemented acetate for the ANME-1 associated bacterial community imply a stronger heterotrophic effect to the metabolism.

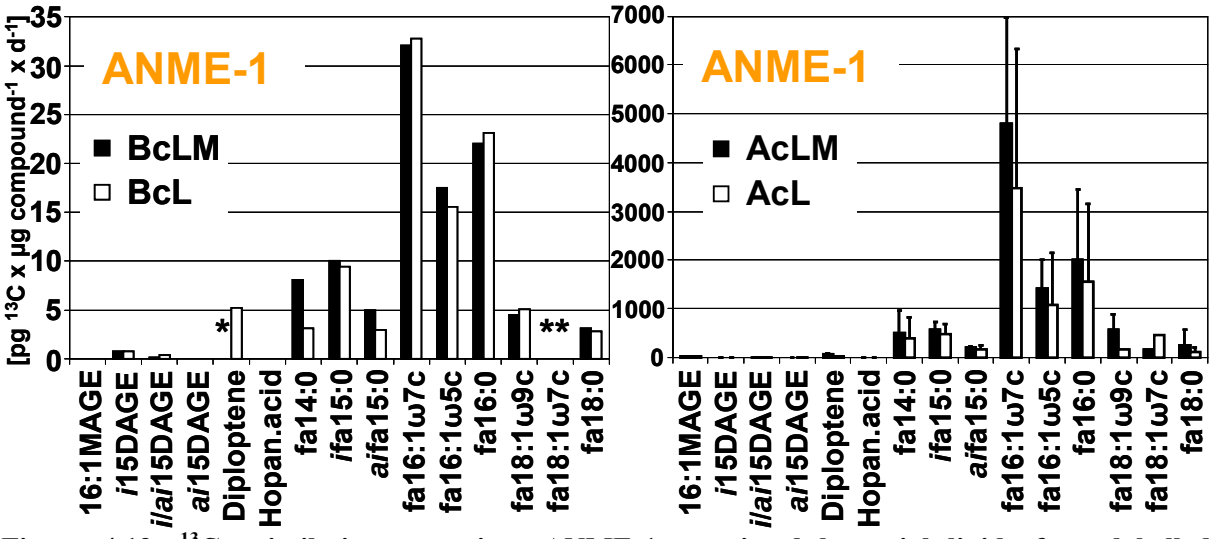

Figure 4.19: ^{13}C-assimilation rates into ANME-1 associated bacterial lipids from labelled substrates. Autotrophic (left) and heterotrophic (right) bacterial anabolism in pink mat samples (ANME-1 associated). Abbreviations: BcLM - labelled bicarbonate in the presence of methane (black columns), BcL - labelled bicarbonate (white columns), AcLM - labelled acetate in the presence of methane (black columns), AcL - labelled acetate (white columns). * - not analysed, for the abbreviation of the lipids, see appendix A.5

Nonetheless, mixotrophic SRB are likely to dominate the bacterial community as sources for these compounds. Figure 4.19 compare the lipid assimilation patterns of the ANME-1 associated bacteria. Similar patterns with other substrates give further evidence for mixotrophic SRB as source organisms and key players in these communities (Figure 4.19). Moreover, the assimilation rates from labelled acetate were two orders of magnitude higher than those with labelled bicarbonate. This implies obviously a direct incorporation of the acetate by a similar active bacterial community. In addition, high assimilation rates of fa16:1ω7c, fa16:1ω5c, and fa16:0,

imply a strong influence from heterotrophic source organisms (Figure 4.19). The fa16:1ω7c might be mainly influenced by heterotrophic organisms, due to very high daily ^{13}C-assimilation and uptakes, a daily uptake about 220 $\mu g\,^{13}C\,g_{TOC}^{-1}\,d^{-1}$ was measured during incubations with acetate in the absence of methane (AcL; Figure 3.15e). Notably, low assimilation rates observed into fa14:0, *i*fa15:0, *ai*fa15:0, and fa18:0 from ANME-1 dominated samples (AcLM, AcL; Figure 4.19) imply very low activity of the source organisms, when acetate was added. This was also confirmed by the low daily total uptake into the individual compounds, e.g. 4 $\mu g\,^{13}C\,g_{TOC}^{-1}$ for fa18:0 or 59 $\mu g\,^{13}C\,g_{TOC}^{-1}$ for *i*fa15:0 during incubations with acetate only (Figure 3.15e). The *ai*fa15:0 was already assigned to the associated SRB by Blumenberg et al. (2004). This could also be confirmed of data in this study (Section 4.3.2.1). The low assimilation rates (AcLM, AcL; Figure 4.19, e.g. *ai*fa15 196 $pg\,^{13}C\,\mu g_{comp.}^{-1}\,d^{-1}$ in the presence of methane) and daily ^{13}C-uptake (AcLM, AcL; Figure 4.15e, e.g. *ai*fa15:0: 107 $\mu g\,^{13}C\,g_{TOC}^{-1}$ in the presence of methane) demonstrate that the source organisms do not mainly depend on an autotrophic metabolism. Furthermore, similar observation for the fa14:0, very low assimilation and uptake rates, indicate a stronger autotrophic impact for the source organisms (during incubations with acetate only, fa14:0 revealed a daily assimilation rate of 395 $pg\,^{13}C\,\mu g_{comp.}^{-1}$ and a daily total uptake of 17 $\mu g\,^{13}C\,g_{TOC}^{-1}$). It is worth mentioning that no significant sulphate reduction during experiments without methane was observed.

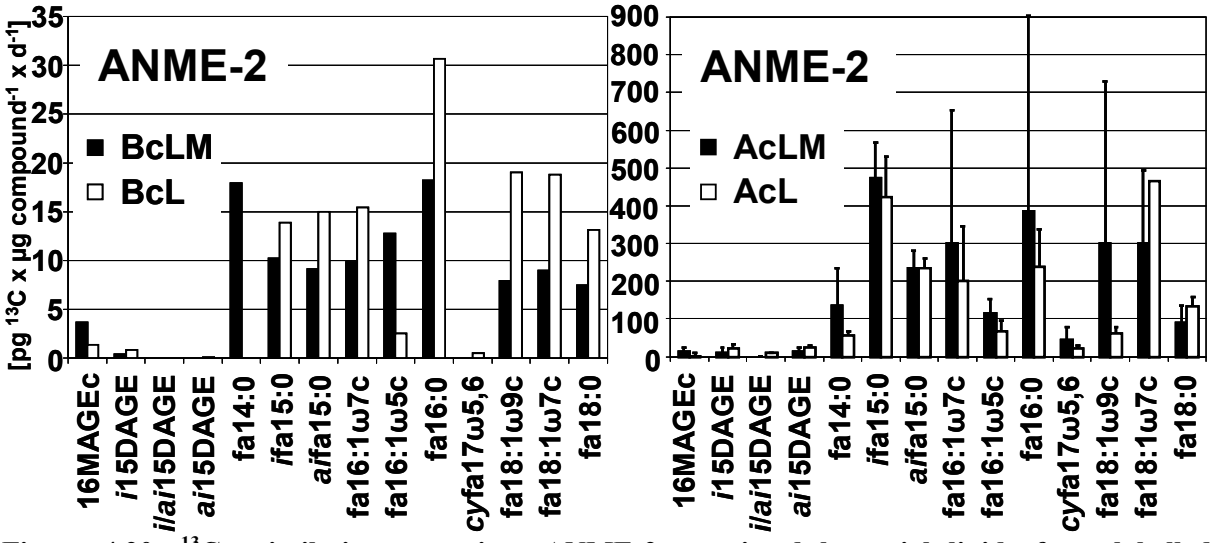

Figure 4.20: ^{13}C-assimilation rates into ANME-2 associated bacterial lipids from labelled substrates. Autotrophic (***left diagram***) and heterotrophic (***right diagram***) bacterial anabolism in pink mat samples (ANME-1 associated). Abbreviations: BcLM - labelled bicarbonate in the presence of methane (black columns), BcL - labelled bicarbonate (white columns), AcLM - labelled acetate in the presence of methane (black columns), AcL - labelled acetate (white columns). For the abbreviation of the lipids see appendix A.5.

Black mat samples exhibit significantly different assimilation patterns between incubations with labelled bicarbonate and acetate, implying a different community of active source organisms, probably with little impact of mixotrophic SRB (Figure 4.20). The experiments with ANME-2 dominated samples revealed very low assimilation rates into fa14:0, fa16:1ω5c, *cy*fa17:1ω5,6 and fa18:0 (AcLM, AcL; Figure 4.20). The

sulphate reduction was relative low without methane (~50 vs. 95 µmol $g_{TOC}^{-1} d^{-1}$, respectively without and with methane). Particularly, the fa14:0 revealed only 95 µg $^{13}C\, g_{TOC}^{-1}$ per day, when incubated with acetate and methane. These observations are coincident with results of labelling studies from labelled bicarbonate and methane, e.g. fa14:0 revealed 9 µg $^{13}C\, g_{TOC}^{-1} d^{-1}$ (BcLM; Figure 3.15). These compounds are apparently attributed to organisms, closely associated to ANME-2 within ANME-2/DSS consortia. For such compounds autotrophic incubation experiments by Blumenberg et al. (2005) and Wegener et al. (2008a) indicate a dominance of methane-dependent autotrophic source organisms. This is consistent with the findings for the autotrophic metabolism as discussed in section 4.3.2.1. Very high assimilation rates for *i*fa15:0, fa16:1ω7c, fa16:0, and fa18:1ω9*c* demonstrate the impact of a heterotrophic metabolism. Again, the fa16:1ω7c revealed high daily uptakes, about 500 µg $^{13}C\, g_{TOC}^{-1} d^{-1}$ during incubations with acetate in the absence of methane (AcL; Figure 3.16f). Figure 4.20 compares the lipid assimilation patterns of the ANME-2 associated bacteria.

Nauhaus et al. (2002, 2005) demonstrated for ANME-1 dominated communities that the sulphate reduction rates were decreased with acetate compared to incubations with methane, formate and hydrogen. Moreover they were in the same range in control experiments (without any supplementation). During incubation experiments with sediment samples from Hydrate Ridge (rather ANME-2 dominated) the sulphate reduction rates with acetate were in the same range with almost all substrates. Only the sulphate reduction in the presence of methane was two times higher. Acetate had no significant effect to sulphate reduction in particular for ANME-1 dominated samples. However the rates of sulphate reduction were increased compared to those with labelled bicarbonate during experiments with labelled acetate in this study.

Although in ANME-1 samples the assimilation patterns imply the occurrence of mixotrophic SRB, also the activity of other bacterial lineages most likely influences the assimilation patterns. Since the sulphate reduction was only marginal increased compared to experiments with bicarbonate and methane (PBcLM; Figure 4.25), and minor rates were observed without methane during incubations with acetate, other active bacterial lineages are probably also responsible for the observed patterns (Figures 4.12e, 4.19) during both experimental set ups (with labelled bicarbonate or labelled acetate). ANME-2 associated bacteria may be dominated by SRB, however, additional potential heterotrophic lineages were detected in ANME-2 dominated samples.

Bacteroidetes (e.g. Nedashkovskaya et al., 2007), Spirochetes (Canale-Parola, 1977), Chloroflexi, JS-1 (Yamada et al., 2005; Webster et al., 2011), and also Planctomycetes (Fürst et al., 1985, 2005) comprise species which have the ability to grow heterotrophically. Webster et al. (2011) did incubations with different concentrations with acetate and glucose to test heterotrophic capabilities of bacterial communities associated with the SMTZ at Aarhus Bay (rather ANME-1 dominated). They found high abundances of sequences related to Chloroflexi and JS-1 in the

samples and enrichments slurries of the sediments. Especially, JS-1 and chloroflexi-related bacteria were detected in methane-laden sediments by Inagaki et al. (2006) and by Blazejak and Schippers (2010) also in the sediments of the Black Sea.

Furthermore, the isolated nitrate-reducing *Caldithrix abyssi* (Miroshnichenko et al., 2003) exhibit heterotrophic capabilities (capable of growing under chemoorgano-heterotrophically as well as chemolithoheterotrophically conditions). Nucleic acid sequences related to *Caldithrix spp.* were found in both sample types (Figure 4.1).

4.3.2.3 Indications for homoacetogenic capabilities among bacteria

Incubation experiments with methanol were conducted to investigate potential homoacetogenic members of the two distinct bacterial communities in both sample types. This was the first time that potential homoacetogenic community members in AOM-settings were investigated. Incubations with methanol, TMA (trimethyl ammonium) or methyl sulphide were performed only to test the hypothesis of a potential electron shuttle or methanogenic capabilities of AOM-performing samples with focus on either the archaeal community or the close ANME/DSS-consortium (Nauhaus et al., 2002, 2005; Seifert et al., 2006; Moran et al., 2008). Methanol can be used by homoacetogenic organisms for acetate generation (Thauer et al., 1977; Diekert and Wohlfarth, 1994). For SRB a methanol dependent catabolism has only been described so far for some thermophilic Desulfofotomaculum strains and *Desulfovibrio carbinolicus* (Nanninga and Gottschal, 1986 and references herein). The reductive acetyl-CoA pathway is widespread in sulphate reducing bacteria. It was also detected in members of the DSS-cluster (Muyzer and Stams, 2008), to which the ANME-associated SRB also belong. Thus methanol-derived carbon can also be incorporated by organisms, which conduct the Ljungdahl-Wood pathway for the anabolism. However, a lower sulphate reduction or the incorporation into distinct lipids might be indicative of homoacetogenic source organisms.

Methanol showed different impact to both communities and distinct assimilation patterns under different conditions for ANME-2 associated bacteria (Figure 4.12g, h). The observed ^{13}C-incorporation from methanol can probably be linked to homo-acetogenic organisms, but an uptake after cross feeding from CO_2 can also explain the ^{13}C-enrichments of the lipids. The assimilation patterns for both samples are depicted in figure 4.21.

Figure 4.22 shows two models for methanol derived carbon fluxes in ANME-1 and -2 dominated communities. In particular within ANME-1 dominated mat types, acetogenic organisms could thrive on methanol and bicarbonate by forming acetate. Otherwise, SRB can also consume newly formed and ^{13}C enriched acetate (by methanol-derived ^{13}C), or incorporate methanol-derived ^{13}C after archaeal methanol disproportion. Finally, these isotopic signals (Figure 4.21) can be diluted by the uptake of methane-derived carbon after methane oxidation by the archaea.

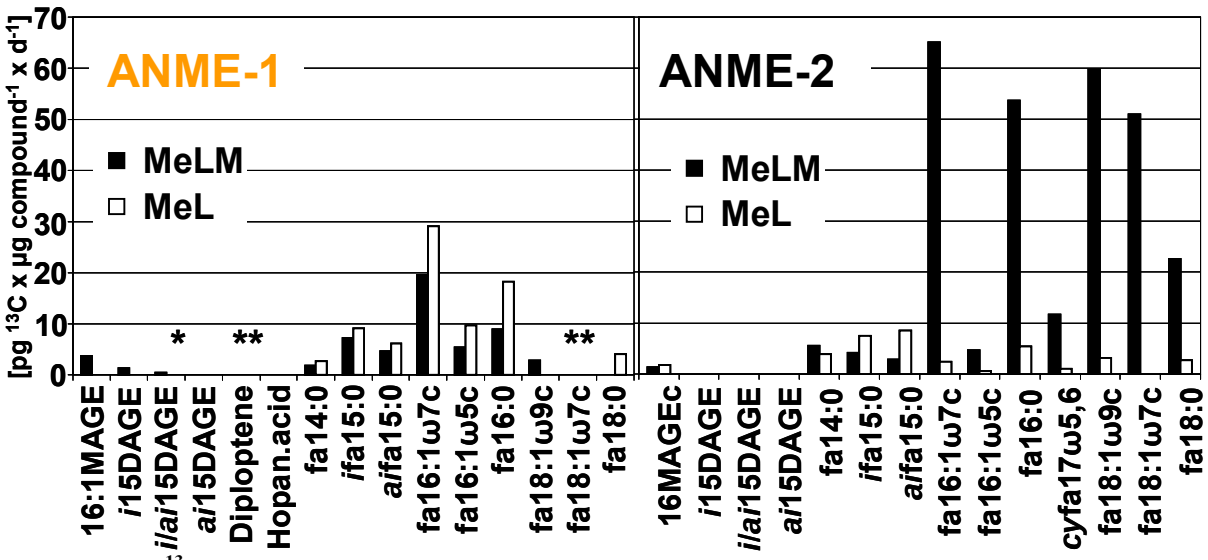

Figure 4.21: ^{13}C-assimilation rates into bacterial lipids in pink (ANME-1 associated) and black (ANME-2 associated) mats from labelled methanol. Left side: ANME-1 associated bacterial lipids. **Right side:** ANME-2 associated bacterial lipids. Incubation experiments with methanol in the presence (black columns) and in the absence (white columns) of methane. * - not analysed, for the abbreviation of the lipids see appendix A.5**.**

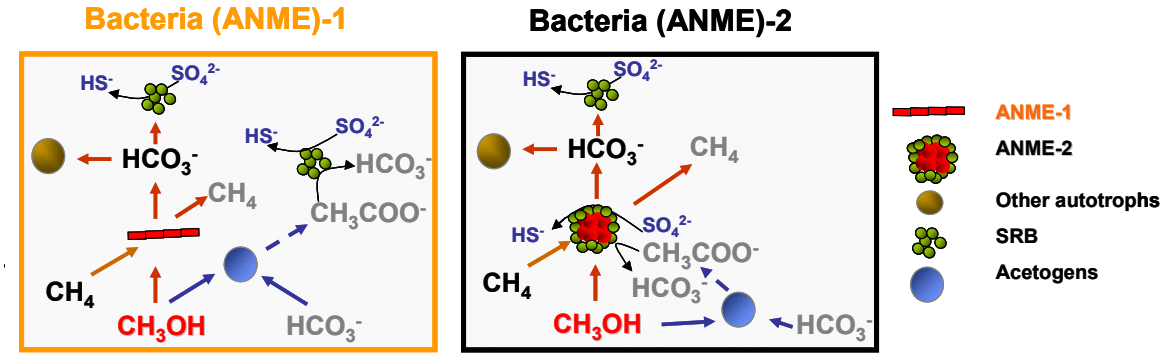

Figure 4.22: Carbon flux models for methanol derived carbon of ANME-1 and -2 dominated communities. ***Acetate*** can be generated from ***methanol*** and ***bicarbonate*** by homoacetogenic organisms ($CH_3OH + 0.5HCO_3^- \rightarrow 0.75CH_3COO^- + H_2O$; $\Delta G^{0'}$ = -55 KJ/ Reaction (Thauer et al., 1977)). This is shown for both mat samples. However the consortia structure influences the carbon flow and the respective ^{13}C-assimilation into the lipids of associated bacteria.
ANME-archaea generated ***methane*** most likely by a disproportion reaction of methanol. The formed bicarbonate or acetate can be incorporated into the lipid biomass via acetyl-CoA from SRB or other heterotrophic (acetate) or autotrophic (bicarbonate) bacteria.

Although the total ^{13}C-uptakes from methanol-derived carbon by bacterial compounds during incubations with and without methane for ANME-1 dominated samples were in the same range (MeLM, MeL; Figure 4.11), the assimilation rates into individual bacterial lipids were generally slightly lower with methane in the headspace. However, the observed assimilation patterns were quite similar. This can be best explained with a marginal dilution effect of newly formed CO_2 after methane oxidation (MeL, MeLM; Figures 4.12g, h, 4.21, 4.23) and indicates a rather AOM-independent autotrophic anabolism of the majority of the source organisms. A dilution effect by a huge amount of the respective lipids, not directly affected by methanol derived ^{13}C (isotopic lipid dilution effect) is assumed, because SRB were apparently not active during incubation experiments with methane. No sulphate

reduction was observed during experiments with methanol and methane for ANME-1 dominated samples, though marginal uptakes into the bacterial lipids were found (PMeLM; Figures 4.11, 4.12g, 4.25, 3.15g), implying the activity of other bacteria.

The ^{13}C-assimilation patterns from methanol are quite similar to those of incubations with labelled bicarbonate (BcLM; Figure 4.23) or labelled acetate (AcLM, AcL; Figure 4.19). The marginal assimilation rates into fa14:0, *i*fa15:0, *ai*fa15:0, fa16:1ω5*c*, and fa18:1ω9c hint to the influence of acetogenic bacteria (e.g. Spirochetes), associated within the community during the incubations with other substrates, since homoacetogenic organisms consume both, bicarbonate and methanol (Thauer et al., 1977; Diekert and Wohlfarth et al. 1994). This could explain that no sulphate reduction (Figure 4.25), but similar bacterial activity deduced from the ^{13}C-assimilation rates (Figure 4.23) was observed.

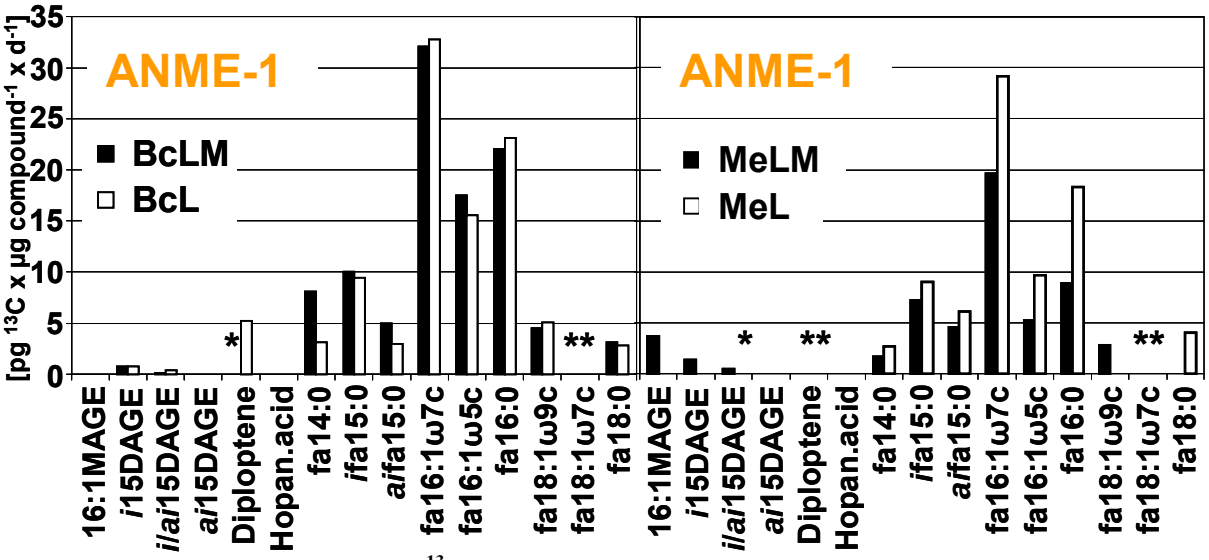

Figure 4.23: Comparison of the ^{13}C-assimilation patterns from ANME-1 associated bacterial lipids. The ^{13}C-incorporation into the bacterial lipids during incubation experiments with **labelled bicarbonate** (**left figure**; black column - in presence of methane; white columns - without methane) and **labelled methanol** (**right figure**; black column - in presence of methane; white columns - without methane) are shown, respectively. * - not analysed, for the abbreviation of the lipids see appendix A.5**.**

Apparently, SRB were totally out-competed by AOM-performing archaea and involved homoacetogenic bacteria with regard to methanol as substrate (MeLM; Figure 4.12g). The observed sulphate reduction within incubation experiments with added methanol in the absence of methane in ANME-1 dominated mat samples also demonstrate that sulphate reducing bacteria and ANME-1 are not closely associated. This underlines the facultative syntrophic consortia structure within ANME-1 communities.

Contrary, Nauhaus and colleagues (2005) measured no sulphate reduction, when only methanol was present. This demonstrates heterogeneity in the bacterial composition.

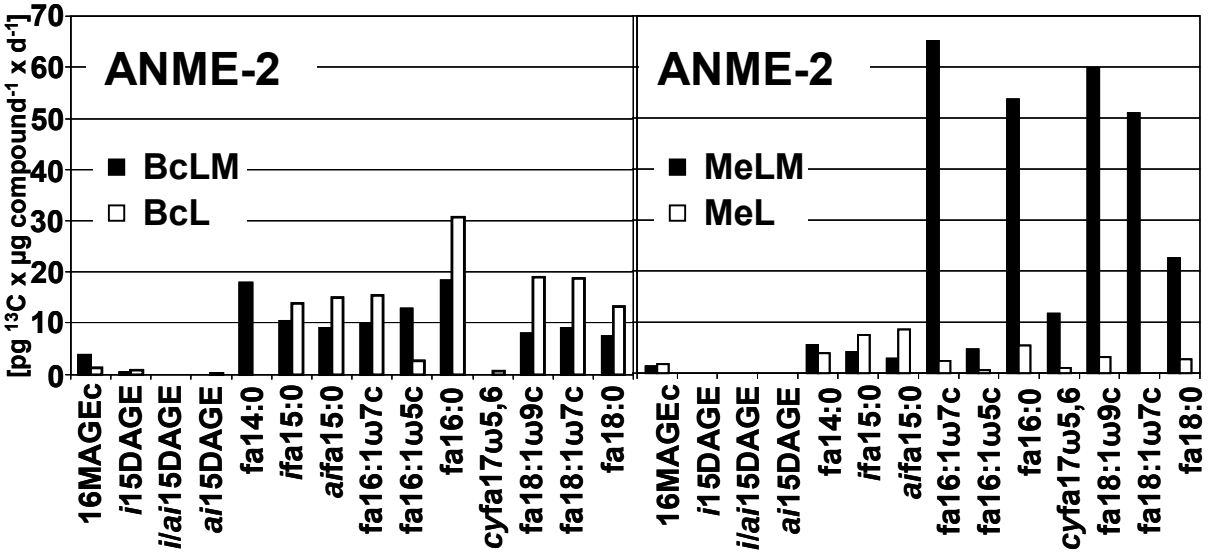

Figure 4.24: Comparison of the ^{13}C-assimilation patterns from ANME-2 associated bacterial lipids. The ^{13}C-incorporation into the bacterial lipids during incubation experiments with **labelled bicarbonate** (**left figure**; black column - in presence of methane; white columns - without methane) and **labelled methanol** (**right figure**; black column - in presence of methane; white columns - without methane) are shown. * - not analysed, for the abbreviation of the lipids see appendix A.5**.**

Figure 4.24 illustrates the assimilation patterns of ANME-2 associated bacterial lipids during incubations with labelled bicarbonate (left) and methanol (right). Methanol exhibits a major impact on the ANME-2 associated bacterial community during experiments with methane in the headspace. This intends a methane dependent anabolism by direct incorporation of methanol-derived ^{13}C by potential methane dependent acetogenic source organisms, or uptake of methanol derived ^{13}C after archaeal methanol disproportion. However, lower methane-independent metabolism was indicated by moderate ^{13}C-uptake without methane in the headspace (MeL; Figure 3.15h), for instance the *if*a15:0 revealed only 1 µg^{13}C g_{TOC}^{-1} per day. The assimilation patterns from labelled methane (ML; Figure 4.12b) or bicarbonate (BcLM, BcL; Figure 4.12d) differed significantly to that with carbon isotopic labelled methanol in ANME-2 dominated samples (Figure 4.24).

Considerable high ^{13}C-incorporation rates of methanol-derived carbon were found for fa16:1ω7c, fa16:0, fa18:1ω9c, fa18:1ω7c and fa18:0 (MeLM; Figure 4.12h). It is expected that acetogenic organisms might be out-competed by SRB under given experimental conditions. However, the very high total ^{13}C-assimilation rates (MeLM; Figure 3.15h) indicate a direct incorporation of labelled methanol. In this case, acetogenic organisms revealed an AOM-dependent activity. One explanation could be that homoacetogens use the hydrogen, supplied by AOM from ANME-2 which thrive without a close association to SRB.

Almost all carbon compounds might be assimilated after substrate oxidation by adjacent SRB in ANME-2/DSS consortia (Alperin and Hoehler, 2009). Very low assimilation rates into fa16:1ω7c (2.3 pg^{13}C $\mu g_{comp.}^{-1} d^{-1}$) and fa18:0 (2.6 pg^{13}C $\mu g_{comp.}^{-1} d^{-1}$; MeL; Figure 4.24) could be affected by close associated autotrophic sulphate reducing δ-Proteobacteria. The preferred incorporation into fa16:1ω5*c* in the presence of methane (MeLM; Figure 4.24) gives (indirect) evidence for a CO_2-

incorporation after methanol disproportion by ANME-2. This is also supported by considerable high assimilation rates into *cy*fa17:1ω5,6 ($pg^{13}C\ \mu g_{comp.}^{-1}d^{-1}$) in the presence of methane (MeLM; Figures 4.24). This fatty acid was already attributed to sulphate reducing δ-Proteobacteria (Elvert et al., 2003). However, the observed assimilation rates into *cy*fa17:1ω5,6 in the presence of methane (MeLM; Figure 4.24) could also be caused by acetogenic source organisms.

Those marginal assimilation rates for all other lipids, apparently not directly affected by a homoacetogenic metabolism (Figures 4.12g, h, 4.22) can be explained by restricted ^{13}C-labelled CO_2 availability (after methanol disproportion). The very low assimilation rates indicate a cross feeding after such an assumed disproportion reaction. Considering a disproportion effect with a ratio of 1:3 for CO_2- and CH_4-formation, the assimilation rates for some lipids (*i*fa15, *ai*fa15, fa16:1ω5) were similar to experiments with labelled bicarbonate (Figure 4.24). The maximum $\delta^{13}C$-value of the buffer carbonate after such a disproportion reaction might be about 2,000 ‰ (when 1/3 of the methanol was oxidised to CO_2). The enhanced ^{13}C-assimilation rates (*i*fa15, *ai*fa15) within incubation experiments without methane (MeL; Figure 4.12h) also underline the strong effect of bicarbonate (after methanol disproportion).

Homoacetogenic organisms were so far not well investigated in AOM settings. However, it may be possible that homoacetogenic bacteria oxidise acetate in a reverse reaction of acetogenesis to gain their energy (Hattori, 2008). During the reverse acetogenesis the produced hydrogen is consumed by the ANME-archaea, maintaining a low hydrogen concentration in the extracellular milieu. Lee and Zinder (1988) described homoacetogens in co-cultures with hydrogen scavenging methanogens that oxidise acetate.

Clostridia, Firmicutes, and Spirochetes were described in AOM-settings. These lineages comprise also bacteria with homoacetogenic capabilities. While Spirochetes and Clostridia were found in ANME-2 samples, in ANME-1 samples Spirochetes were detected (Figure 4.1).

Interestingly, molecular biological investigation of Planctomycetes revealed the enzymatically properties of a C_1-transfer to methanopterin and methanofuran (Chistoserdova et al., 2004). This could also explain the observed distinct assimilation patterns during incubations with methanol and methane of the black mat samples, even though these properties were assumed to be involved in a detoxification pathway of formaldehyde by the authors. However, this means that the Planctomycetes are dependent of the methane metabolism and use the reductive acetyl CoA-pathway.

Although methanol is not an adequate substrate for most SRB, it cannot be totally excluded from being responsible for the observed assimilation patterns. Clostridia were identified by molecular biological investigations. They also comprise species with sulphate reducing capabilities (Muyzer and Stams, 2008). Thus they may also be sources of the fatty acids, which revealed ^{13}C-assimilation from methanol.

Summary

Especially the incubation experiments with labelled bicarbonate underlines a facultative syntrophic consortia structure for ANME-1 dominated communities compared to a more obligate consortia structure for ANME-2/DSS.

Methane-independent autotrophic and heterotrophic capabilities were demonstrated for associated bacteria of both communities. Interestingly, bacteria associated to ANME-1 showed a very strong heterotrophic activity while bacteria associated to ANME-2 revealed a pronounced autotrophic metabolism.

In this study, first evidences were shown for acetogenic metabolism by compound specific stable isotope probing in both communities. This was demonstrated by the ^{13}C-assimilation from labelled methanol into bacterial lipids. Both communities showed distinct assimilation patterns. The patterns in ANME-1 dominated samples were similar, although no sulphate reduction was measured. In ANME-2 dominated samples considerable uptakes were observed when methane was present.

4.3.3 Potential sources of other bacterial lipid biomarkers

4.3.3.1 Mono- and dialkyl glycerol ethers (MAGEs, DAGEs)

MAGEs and DAGEs are commonly found in facultative anaerobic and specific thermophilic bacteria (Langworthy and Pond, 1986; Huber et al., 1992, 1996). However, few mesophilic bacteria appear to also be capable of their production, because methane-laden anoxic settings and soils (Rütters et al., 2002; Oppermann et al., 2010) are often enriched in those compounds. Moreover, 16MAGE were identified from cultured *Desulfosarcina variabilis* (Rütters et al., 2001). 15DAGEs are specific lipid biomarkers in AOM-settings, these ^{13}C-depleted lipids are attributed to sulphate reducing bacteria (Pancost et al., 2001; Michaelis et al., 2002). The high concentrations, very long residence times, and very low synthesis rates may cause the low assimilation rates which have already been reported in previous studies (Blumenberg et al., 2005; Jagersma et al., 2009). MAGEs and especially DAGEs revealed considerable amounts within the two sample types. Also in the approaches described in this study, MAGEs and DAGEs were much less labelled than co-occurring fatty acids.

Within ANME-1 consortia considerably high assimilation rates were determined for 16:1MAGE within experiments with ^{13}C-labelled methane (ML; Figure 3.13a). The *ai*15DAGE revealed only marginal uptake of ^{13}C from labelled methane and labelled acetate. Blumenberg et al. (2005) observed an average ^{13}C-assimilation of 0.3 pg^{13}C $\mu g_{comp.}^{-1} d^{-1}$ for the *ai*15DAGE during their incubation experiments with 7 % labelled methane (Figure 4.14). This was in the same range as the data of this study with between 0.3 pg^{13}C $\mu g_{comp.}^{-1} d^{-1}$ for pink mat samples (ML; Figure 4.14) and 0.07 pg^{13}C $\mu g_{comp.}^{-1} d^{-1}$ for black mat samples (ML; Figure 4.14). The very low δ^{13}C-shifts from 100 % labelled acetate support a very low synthesis rates, about

0.4 pg ^{13}C $\mu g_{comp.}^{-1} d^{-1}$ in pink mat samples and 14 pg ^{13}C $\mu g_{comp.}^{-1} d^{-1}$ in black mat samples (AcLM, AcL; Figure 4.12e, f). The daily ^{13}C-assimilation was of up to 21 pg ^{13}C $\mu g_{comp.}^{-1} d^{-1}$ into 16:1MAGE during incubations with labelled acetate (AcL; Figure 4.12e). This suggests that the compound is produced by sulphate reducing bacteria with mixotrophic capabilities. Only minor ^{13}C-assimilation rates were determined within ^{13}C-methanol incubation experiments of ANME-1 dominated mat samples for *i*15/*i*15DAGE and *i*15/*ai*15DAGE (MeLM, MeL; Figure 4.12g). Notably, ^{13}C-assimilation into the DAGEs was only found when methane was present. The respective source organisms were probably fed by CO_2 after methanol oxidation.

Among experiments with ANME-2 consortia considerably high uptakes from labelled methane into all mono- and dialkyl glycerol ether lipids were detected (0.1 µg ^{13}C $g_{TOC}^{-1} d^{-1}$ for *ai*15DAGE and 0.3 µg ^{13}C $g_{TOC}^{-1} d^{-1}$ for 16MAGEc), which gives evidence that SRB are main source organisms of these compounds (ML; Figure 3.15b). However, heterotrophic as well as mixotrophic (AcLM, AcL; Figure 3.15f) organisms could be also an adequate source. Since δ-Proteobacteria are the main organisms within the sulphate reducing community, members of this subclass are the most likely sources.

These very low synthesis rates can be explained with a very long residence time of relative stable compounds. Another explanation could be a different synthesis pathway. Previously, direct uptake of alkanes and alkenes were described by several authors for SRB (So et al., 2003; Cravo-Laureau et al., 2005; Grossi et al., 2007). Grossi et al. (2011, IMOG) investigated the synthesis of those lipids in sulphate reducing bacteria via incubation experiments with ^{13}C and deuterium labelled alkanes. They found a direct incorporation of those alkanes in the lipids.

Incubation experiments with labelled and perdeuterated alkanes will give further information to elucidate the respective source organisms. A higher labelling of these mono- and dialkyl glycerol ethers is expected, if the source organisms are still active in the AOM-performing microbial community and the synthesis is different to those of the fatty acids.

4.3.3.2 17β(H),21β(H)-Hop-22(29)-ene (Diploptene) and 17α(H),21β(H)-bishomohopanoic acid

Hopanoids comprise a class of pentacyclic terpenoid lipids (Härtner et al., 2005). These squalene derived lipids were found in the membranes of predominantly aerobic bacteria (Rohmer et al., 1992; Kannenberg and Poralla, 1999) and as geohopanoids in sediments; crude oils and slates (Mycke et al., 1987; Ourisson and Rohmer, 1992). Geohopanoids are considered as degradation products after diagenetic processes. However, biohopanoids were already found by other authors in anoxically grown cultures directly (Sinninghe Damsté et al., 2004; Härtner et al., 2005; Fischer et al., 2005; Blumenberg et al., 2006). In addition, there was indirect evidence for more widespread hopanoid sources, also from anaerobic bacteria (Thiel et al., 2003; Sinninghe Damsté et al., 2004). Thiel and colleagues (2003) found high concentrations of hopanoid derivatives in microbial mats from the Black Sea. The

highly depleted isotopic signature linked those compounds to anaerobic carbon cycling at methane seeps.

Diploptene and *17α(H),21β(H)*-bishomohopanoic acid were found in ANME-1 dominated samples.

No ^{13}C-uptake from methane (ML; Figure 4.12b) or methanol (MeLM, MeL; Figure 4.12c) was observed into diploptene. Considerable ^{13}C-assimilation rates of diploptene (AcLM, AcL; Figure 4.12m) can be interpreted as cross-feeding after acetate oxidation or a direct incorporation into the lipids. The ^{13}C-uptakes from bicarbonate support a rather autotrophic pathway. Diploptene revealed 0.2 μg^{13}C g_{TOC}^{-1} d^{-1} during incubation experiments with acetate (AcLM; Figure 3.15e). This is the first time that a ^{13}C-incorporation into diploptene from labelled bicarbonate and acetate in AOM-performing microbial systems was demonstrated, even though the assimilation and total uptake rates were very low (the daily ^{13}C-assimilation was 5.2 for incubations with bicarbonate, and 55.6 pg^{13}C $\mu g_{comp.}^{-1}$ during incubations with acetate and methane). Diploptene is most likely sourced by anaerobic organisms in AOM-settings. Certainly, diploptene is a very unspecific lipid biomarker. Thus, several source organisms can be responsible. The ^{13}C-uptake from acetate indicates also heterotrophic source organisms. The very high depletion in ^{13}C implies organisms associated to carbon cycling at methane seeps.

Blumenberg and colleagues (2009) extracted high amounts of diploptene from *Desulfovibrio bastinii* (strain DSMZ 16055T) grown under strictly anoxic conditions. Previous studies of the lipid content of isolates of the genus Desulfovibrio from Black Sea mats also revealed high amounts of diploptene (Blumenberg et al., 2006). These chemoorganotrophic prokaryotes are able to grow with various low-molecular weights organic compounds, using them as electron donors and carbon source, while degrading acetate incompletely (Castro et al., 2000). Thus, members of the genus Desulfovibrio could be a potential source and might have an important role in degradation processes in ANME-1 mats, feeding other bacterial and archaeal members with acetate. Probably they - and other abundant SRB - use bicarbonate as well as acetate as carbon source during mixotrophic growth in ANME-1 mats. However, Nauhaus et al. (2005) described enrichments of SRB during incubation experiments with elevated hydrogen pressures or concentrations of formate. They did not belong to the Desulfosarcina/ Desulfococcus-cluster as previously described for associated SRB, rather they are affiliated to the genus Desulfofrigus (Nauhaus, 2003). Thus, also other SRB have to be considered in complex AOM-performing bacterial community structures as potential sources.

17α(H),21β(H)-bishomohopanoic acid revealed high amounts in pink mat samples with very low δ^{13}C-values (Appendix A.4c, page 142). The δ^{13}C-values were comparable to other bacterial lipids in not incubated samples. The concentrations and isotopic composition were in the same range with those of previous studies (Thiel et al., 1999, 2003). This compound was previously described from samples from the Black Sea and was further tentatively excluded as remaining degradation products. The very high depletion in ^{13}C and high amounts argue against a diagenetic

degradation product of the isomers with a *αβ*-configuration (Thiel et al., 2003). However, no incorporation of ^{13}C from any labelled substrate was observed in this study. This gives evidence for organisms either in a dormant state or physiologically not directly linked to substrates of the conducted experiments. In addition, the high amount of *17α(H),21β(H)*-bishomohopanoic in the ANME-1 dominated mat type supports indigenous source organisms, because pink mats are usually covered by black mats and thus an allochthonous transport into the mat is very unlikely. Temporary mixing with oxic surface waters can not be totally excluded (Krüger et al., 2008). Thus, aerobic methanotrophic bacteria could be potential source organisms. Noticeable, marginal ^{13}C-uptakes into the bishomohopanoic acid were observed by Blumenberg (personal communication; Figure 4.14).

Usually, constitutional αβ or βα-isomers of hopanoids are considered as geological conformations. However, Rosa-Putra et al. (2001) found αβ and βα hopanoids in *Frankia spp.* Nonetheless, the bishomohopanoic acid is at least a biologically degradation product. Thus, the high concentrations and the considerable low incubation times may be a reason that no ^{13}C uptake was observed from any substrate.

4.3.3.3 Hentriacontatrien ($C_{31:3}$)

Three isomers of hentriacontatrien, a three fold unsaturated straight hydrocarbon, were found in ANME-2 dominated samples. C*is*-hentriaconta-9,15,22-triene was already attributed to Chloroflexi by van der Meer et al. (1999). Interestingly, heterotrophic Chloroflexi are key players in various marine environments including methane-settings (Inagaki et al., 2006), supporting the suggestion of heterotrophic growing *Chloroflexi* spp. in the Black Sea AOM-mat system as source for hentriacontatriene. The analysis of 16S rDNA accounted for 2 % of Chloroflexi in the ANME-2 dominated mats (Figure 4.1), where also considerable amounts of hentriacontatriene were observed. The mean concentrations were for the isomer $nC_{31:3}a$ about 23.7 $\mu g\, g_{TOC}^{-1}$ ± 39.4 (n = 19) and for the isomer $nC_{31:3}c$ about 168.3 $\mu g\, g_{TOC}^{-1}$ ± 247.9 (n = 19) (A.4d; page 143). Blazejak and Schippers (2010) detected high abundances of sequences of JS-1 and Chloroflexi-related bacteria by qPCR in the sediment of the Black Sea. However the physiological role in the sediments of the detected Chloroflexi-related bacteria remains unclear. Webster and colleagues (2011) described a high abundance of Chloroflexi and JS-1 in heterotrophic incubation experiments with slurry enrichments of sediments from the SMTZ, sampled at Aarhus Bay.

The assimilation rates of the three constitutional isomers of hentriacontatrien were lower than those of the fatty acids, e.g. while fa16:0 revealed a daily assimilation rate of 9.4 pg^{13}C $\mu g_{comp.}^{-1}$ during incubations with methane, for the isomer $C_{31:3}$b only 3 pg^{13}C $\mu g_{comp.}^{-1}$ was measured (after 64 days; ML; Table 4.2). Otherwise the ^{13}C-incorporation was stronger compared to those of the mono- and dialkyl glycerol ether lipids. For instance it was 1.5 pg^{13}C $\mu g_{comp.}^{-1} d^{-1}$ for the *ai*15DAGE (Table 4.2; ML64). The direct comparison of the assimilation rates between experiments with labelled bicarbonate and acetate exhibited similar ^{13}C-assimilations, if considered that the label of acetate was five fold higher. In addition, the comparison of the assimilation rates with other fatty acids during incubations with acetate implies a rather autotrophic anabolism or at least a very low heterotrophic metabolism. The isomer $C_{31:3}$c revealed an assimilation rate from labelled bicarbonate in the presence of methane of 7.8 pg^{13}C $\mu g_{comp.}^{-1} d^{-1}$ (BcLM; Table 4.2) and of 33.1 pg^{13}C $\mu g_{comp.}^{-1} d^{-1}$ from labelled acetate in the presence of methane (AcLM23; Table 4.2). There was no relation to the presence of methane. The assimilation rates where in the same range. The assimilation rates were relative low, considering the very high label of acetate (99.9 %) compared to the bicarbonate label (20 %).

Table 4.2: The daily ^{13}C-assimilation [pg^{13}C $\mu g_{comp.}^{-1} d^{-1}$] of the three isomers of hentriacontatrien ($C_{31:3}$a-c) during experiments with different ^{13}C-labelled substrates.
The table compares the assimilation rates of the three constitutional isomers of hentriacontatrien with other bacterial compounds. The notation of the samples is explained in Table 2.1. Numbers represent days of incubation. n.a. - not analysed

	Experiments									
Compounds	**ML64**	**ML135**	**BcLM**	**BcL**	**AcLM23**	**AcL23**	**AcL56**	**AcLM26**	**AcLMI26**	**AcLI26**
C31:3(a)	2.2	n.a.	n.a.	n.a.	2.4	3.5	n.a.	n.a.	n.a.	n.a.
C31:3(b)	3.0	2.4	n.a.	6.50	21.3	16.1	n.a.	53.1	26.5	22.7
C31:3(c)	1.4	1.7	7.76	6.36	33.1	28.0	30.5	84.4	40.0	36.0
16MAGE(c)	0.7	0.3	3.6	1.3	3.1	-3.3	8.2	26.1	1.4	0.3
i15DAGE	1.2	0.1	0.4	0.8	1.8	12.3	29.1	7.1	7.6	6.5
i/ai15DAGE	1.6	-0.2	-4.9	-3.4	-1.7	7.2	10.8	-3.1	-2.8	-4.3
ai15DAGE	1.5	0.0	-0.8	0.1	9.2	19.4	28.4	8.2	10.3	7.8
fa14:0	5.5	5.2	17.9	0.0	91.7	48.0	63.1	250.7	138.3	150.3
fa16:1ω5c	4.5	3.6	12.7	2.5	88.6	45.6	86.2	158.5	58.8	62.7
fa16	9.4	6.1	18.2	30.7	144.4	169.0	308.6	978.5	648.5	800.1

Nauhaus et al. (2007) found an unsaturated C_{31} hydrocarbon in ANME-2 dominated anoxic sediments from Hydrate Ridge. They attributed the C_{31}-polyene hydrocarbon to AOM-linked SRB. In contrast, they did not find any molecular biological evidence for *Chloroflexi spp.* (personal communication M. Elvert). Hentriacontatrien could be a new lipid biomarker for ANME-2 consortia. Although, this marker could also be derived from long-chain alkane wax-esters, the high depletion in ^{13}C and the observed ^{13}C-incorporation from labelled bicarbonate and acetate indicate a source organisms associated to the bacterial community. This compound can be diagnostic especially for ANME-2 dominated AOM-performing systems. The metabolism of the source organism depends apparently not directly on methane. Finally, the source organism remains unclear.

Summary

Among experiments with ANME-2 consortia considerably high uptakes from labelled methane into all mono- and dialkyl glycerol ether lipids were detected and give evidence that SRB are main source organisms of these compounds. Experiments with labelled acetate demonstrated also heterotrophic capabilities of the respective source organisms.

This is the first time that a ^{13}C-incorporation into diploptene from labelled bicarbonate and acetate in AOM-performing microbial systems was demonstrated, even though the assimilation and total uptake rates were very low. In the ANME-1 dominated sample, diploptene is most likely sourced by associated anaerobic organisms. The ^{13}C-uptake from acetate indicates also heterotrophic source organisms.

The high depletion in ^{13}C of hentriacontatrien and the observed ^{13}C-incorporation from labelled bicarbonate and acetate indicate a source organisms associated to the bacterial community. The metabolism of the source organism depends apparently not directly on methane. Although, the source organism remains unclear, this compound can be diagnostic especially for ANME-2 dominated AOM-performing systems.

4.4 General implications

4.4.1 Autotrophic and methanotrophic metabolisms in AOM-systems

Methane consumption and sulphate reduction were analysed to get further parameters for evaluating the metabolic capabilities. It was assumed that the methane decrease correspond to the methane consumption, or rather methane oxidation (Figure 4.25). A marginal hydrogen leakage during the incubation can not be ruled out completely and may leads to slight overestimation of the measured AOM-rates. The sulphate reduction and methane decrease rates were considerably different between both mat types under similar experimental conditions. In addition, they also vary between different experiments, especially for the ANME-1 mat type. The sulphate reduction and AOM-rates of ANME-1 communities are relatively low compared to similar incubation experiments with ANME-2 dominated communities (Figure 4.25).

Figure 4.26 illustrates the different physiological capabilities of the two ANME-clusters. While the physiology of ANME-1 depends rather on a facultative consortia structure, and thus more likely depends on the concentration of hydrogen or formate (due to similar electron potential, Section 4.2)[v], the ANME-2/DSS-consortia conduct a rather obligate syntrophic metabolism.

[v] Standard redox potential of CO_2/ formate ($E^{0'}$ = -432mV) and H^+/H_2 ($E^{0'}$ = -414mV) (Thauer et al., 1977)

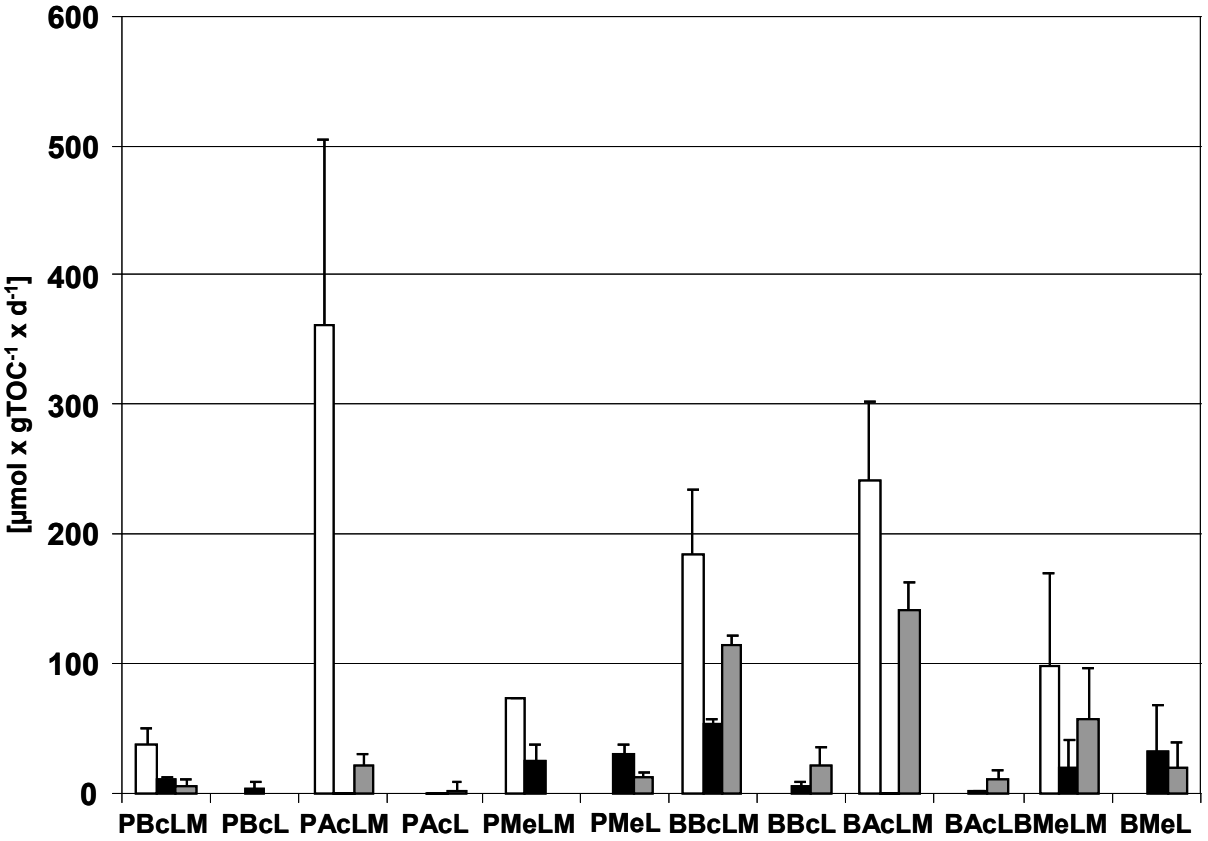

Figure 4.25: Comparison of AOM rates, methanogenesis and sulphate reduction rates.
The net AOM rates (white columns), the rates of methanogenesis (black columns), and the measured sulphate reduction rates (grey columns) during the different incubation experiments are shown. For ANME-1 dominated samples ***on the left side*** and ANME-2 dominated samples ***on the right side***. For the abbreviations of the incubation experiments see table 3.1

Autotrophic and methylotrophic methanogenesis were observed within the respective experiments. Furthermore, especially for ANME-1 dominated samples the sulphate reduction depends on the methane consumption as shown by the methane-dependent sulphate reduction rates (Figure 3.7). Probably, AOM is the main H_2-supplying process in the settings. The very high discrepancies argue against a direct coupling of AOM and sulphate reduction. Furthermore, evidence for homoacetogenic bacteria were given by the ^{13}C-assimilation into bacterial lipids whilst no sulphate reduction was detected (PMeLM; Figures 4.23, 4.25; Section 4.3.2.3). Previous investigations underline a very close consortia structure for ANME-2 in contrast to ANME-1 dominated samples (Figure 4.25; Section 4.2). Schreiber et al. (2010) observed in similar samples a high abundance of ANME-2/DSS consortia and only low amounts of single ANME-2 cells. This supports the consideration of a syntrophic metabolism, which is conducted by close consortia and may be reflected by the bacterial lipid assimilation patterns from black mat samples (Figures 4.3, 4.11, 4.12; Sections 4.2; 4.3.2.1).

The metabolism of ANME-1 is apparently not close linked to the sulphate reduction. This was demonstrated by the determined stoichiometry of 1:10 (SR:AOM; PBcLM; Figure 4.25). Other hydrogen consuming microorganisms, e.g. adjacent ANME-1 itself can affect the extracellular concentrations of hydrogen in the milieu.

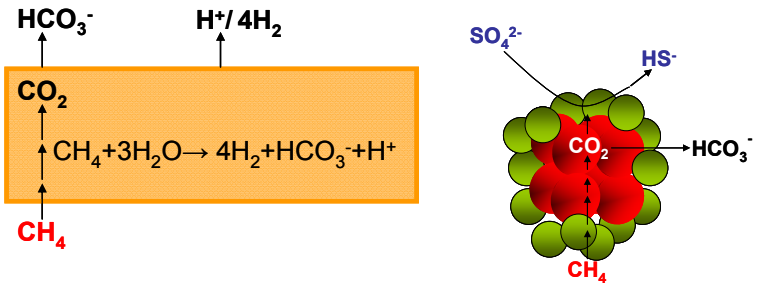

Figure 4.26: Different physiology of ANME-1 and -2.
Two distinct hypothesised physiological models are shown, those of a single ANME-1 cell (left) is compared to ANME-2/DSS consortia (right). The metabolism of ANME-1 is most likely triggered by the concentration of hydrogen. The metabolism of ANME-2 depends on a close, obligate syntrophic consortia structure between ANME-2 and SRB. The electron shuttle is unknown.

Thus, the concentration of hydrogen can probably be triggered by other organisms. Moreover, a metabolism of ANME-1 more adapted to very low hydrogen concentrations could be responsible for its physiology. ANME-1 are close affiliated to the order of the Methanomicrobiales, which lacks cytochromes and thus are able to conduct methanogenesis under very low concentrations of hydrogen (~10 Pa; Thauer et al., 2010). However, Meyerdierks and colleagues (2010) identified multiple multiheme *c*-type cytochromes and conclude that they are involved in an additional possible mode of electron transfer between ANME-1 and sulphate reducing bacteria.

During the incubation experiments with bicarbonate and methane (ML, BcLM), very low sulphate reduction rates were measured in ANME-1 dominated mat types (~5 µmol $g_{TOC}^{-1} d^{-1}$; PBcLM; Figure 4.25). However, the methane consumption rates exceeded the methane-dependent sulphate reduction by far with 37 µmol $g_{TOC}^{-1} d^{-1}$ (BcLM; Figure 4.25). The relative low sulphate reduction rates are coincident with molecular biological and geochemical data by Yanagawa et al. (2011), who demonstrated ANME-1 activity even in sulphate-depleted marine sediments. Further indications for sulphate-independent ANME-1 metabolism come from recent investtigations by Takeuchi et al. (2011). They confirmed the potential of anaerobic oxidation of methane from terrestrial freshwater subsurface environments by molecular biological investigations and $^{13}CH_4$-tracer experiments. They described the respective archaea as a new subgroup of ANME-1, able to grow without SRB. Several mechanisms have to be considered as alternatives, e.g. use of other terminal electron acceptors by associated bacteria or ANME-1 archaea itself (Barnes and Goldberg, 1976; Hoehler et al., 1994; Beal et al., 2009). It seems that sulphate as an important terminal electron acceptor in marine settings has minor relevance for ANME-1 in this study as well. Hallam et al. (2004) proposed that sulphur could be involved in a dissimilatory pathway by ANME-1. However, this was not confirmed, because the sulphate reduction and methane consumption rates were unequal (PBcLM; Figure 4.25). Furthermore, there were no findings of a dissimilatory sulphate reductase based on any metagenomic approach, as of yet (Hallam et al., 2004; Meyerdierks et al., 2005, 2010).

Figure 4.25 illustrates the net methane production for pink mat samples in the presence and absence of methane (PBcLM, PBcL - black columns; Figure 4.25). These data (see also Figures 3.2, 3.4, and 3.6) indicate a slightly higher methane generation in the presence of methane. Sulphate reduction was only observed when methane was present (PBcLM, PBcL - grey columns; Figure 4.25). This underlines a microbial system fuelled by methane. Methanogenesis and sulphate reduction are apparently influenced by the methane oxidation. Probably, ANME-1 archaea switch to autotrophic growth in the absence or at low concentrations of methane under given experimental conditions (even in the presence of sulphate). The enhanced methane generation (11.5 $\mu mol\, g_{TOC}^{-1} d^{-1}$; PBcLM) in the presence of methane indicates a coupling of AOM and methanogenesis. Further evidence comes from the observed ^{13}C-assimilation rates of the lipid biomarkers as discussed above (Section 4.3.1.3). The archaeal isoprenoid hydrocarbons revealed uptake especially in the presence of substrates linked to hydrogenotrophic methanogenesis. The observed high discrepancies between methane consumption and sulphate reduction rates in ANME-1 dominated mat samples argue against a strong coupling between the two processes. In contrast, sulphate reduction rates were directly dependent on AOM within standard incubation experiments (PBcLM; grey columns; Figure 4.25). Hoehler and colleagues (1994) already described this process as reverse methanogenesis under low H_2 conditions in marine sediments. They proposed that methane is converted to carbon dioxide and H_2 syntrophically under sulphate reducing conditions. In ANME-1 dominated communities, SRB are not directly associated to methanotrophic archaea (e.g. Blumenberg et al., 2004). Nonetheless, they also have to maintain a low hydrogen pressure. In marine AOM-environments SRB are a fundamental sink for hydrogen, accelerating the energy yield of CH_4-oxidation by reducing the hydrogen concentration in the (extracellular) system and favour the reverse pathway of methanogenesis (Hoehler et al., 1998). Figure 4.27 demonstrates potential metabolisms linked to hydrogen production and consumption within a facultative syntrophic consortium of ANME-1 and other hydrogen consuming microorganisms. In those consortia hydrogen produced by AOM and released into the extracellular milieu may be consumed by SRB, homoacetogens and (methanogenic) ANME-1.

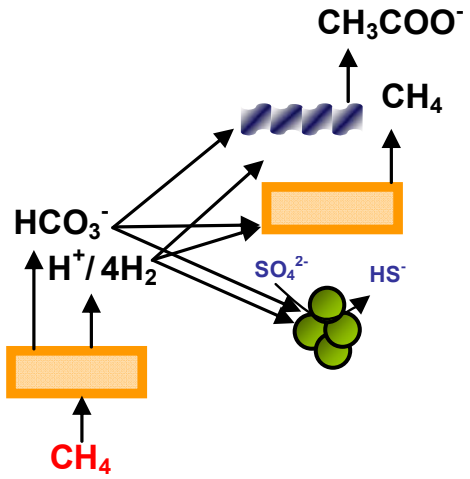

Figure 4.27: Model of hydrogen production and consumption within ANME-1 dominated microbial systems. ANME-1 produces hydrogen during AOM. This hydrogen can be consumed by other adjacent ANME-1 cells for autotrophic methanogenesis, by SRB and potential homoacetogenic bacteria.

Bowles and colleagues (2010) measured hydrogen concentrations in methane-rich seafloors. For gassy sediments with high methane concentrations (average 570 µM, ranging between 99.7 - 864.8 µM) they observed on average hydrogen concentration of 21.5 nM (ranging between 1.6

and 57.9 nM). Predominantly ANME-1 and SRB, not belonging to the DSS-cluster, were detected in those sediments. Moreover, they calculated the energy yield for a given average of hydrogen (14 nM) and methane (50 mM) concentrations the energy yield. They conclude that, under given environmental conditions hydrogenotrophic methanogenesis is more favorable than AOM. Lloyd et al. (2011) demonstrated the occurrence of ANME-1 in sediment layers below the sulfate methane transition zone (SMTZ) by molecular biological investigations, where methanogenesis usually takes place. Moreover, a simultaneous process of AOM and methanogenesis is possible, which maintain on the one hand a low hydrogen partial pressure in the environmental system. On the other hand, extracellular hydrogen is apparently produced and must be maintained by ANME-1 itself during AOM (e.g. by molecular hydrogen sinks like polyunsaturated hydrocarbons; see section 4.3). Presumably these two processes are divided by different ANME cells and do not occur simultaneously in one cell. These processes are apparently not directly coupled, due to kinetic constraints. The net energy yield would be $\Delta G^{0'} = 0$, if AOM and methanogenesis would be directly syntrophically linked[vi]. Rather the concentrations of hydrogen or formate influence the balance and the impact of energy yielding processes, conducted in those microbial systems. Holler and colleagues (2011b) described back fluxes during AOM and sulphate reduction, reaching 5 % and 13 % respectively. Interestingly, Meyerdierks and colleagues (2010) found nucleic sequences when encoding a putative [FeFe]-hydrogenase with metagenomic analysis. This was the first time a [FeFe]-hydrogenase was identified in archaea. Such hydrogenases produce reversible hydrogen and are responsible for hydrogen uptake in bacteria and lower eukaryotes. This enzyme operates contrary to [NiFe]-hydrogenases, which are more involved in hydrogen oxidation (Frey, 2002; Thauer et al., 2010 and references therein).

The occurrence of such a [FeFe]-hydrogenase in ANME-1 underlines the hypothesis discussed above, linking hydrogen production via AOM to hydrogen uptake for methanogenesis. Observations by House et al. (2009) are consistent with this explanation, since their results give additional evidence for a high heterogeneity in metabolism by wide carbon isotopic ranges, activity measurements by radiotracer analysis, and nanoSIMS measurements of ANME-1. Hydrogenotrophic methanogenesis was already observed by several authors for AOM-performing microbial communities (Seifert et al., 2006; Treude et al., 2007; Krüger et al., 2008; Orcutt et al., 2008; data in this work BcLM, BcL; Figure 4.25), but their observations were inconsistent. The data, summarised in figure 4.25, clearly demonstrate the occurrence of methanogenesis on different substrates independent of the presence of methane in particular for ANME-2 dominated samples (BBcLM; Figure 4.25). Experiments with similar samples from the Black Sea by different authors are shown in table 4.3, the rates of anaerobic methane oxidation (AOM), sulphate reduction (SR), methane production (MPR), and the ratio of AOM/ MPR are listed.

[vi] $HCO_3^- + 4\ H_2 + H^+ \rightarrow CH_4 + 3\ H_2O$ ($\Delta G^{'0} = -135.6$ kJ/mol; Thauer et al., 1977)
$CH_4 + 3\ H_2O \rightarrow HCO_3^- + 4\ H_2 + H^+$ ($\Delta G^{'0} = +135.6$ kJ/mol)

Table 4.3: Comparison of similar mat samples from the Black Sea
[a] Rates determined through measurements of headspace concentrations, [b] rates determined through measurements of sulphide concentrations, [c] rates determined through radiocarbon analysis ($H^{14}CO_3^-$, $^{14}CH_4$, $^{35}SO_4^{2-}$), [d] recalculated rates taken from Siegert (2010) (to transform the values from cm^3 to gdw they were multiplied with the factor 8.3, according to the consideration that 0.12 gdw mat is 1 cm^3 mat), [e] average AOM: 12.1, average MF: 4, average SRR: 7.5, [f] methane forming with H_2 in the headspace: ~2 µmol x gdw^{-1} x d^{-1} ± 0.5 (+CH_4/+SO_4^{2-}), ~0.2 µmol x gdw^{-1} x d^{-1} ± 0.2 (+CH_4/-SO_4^{2-}); methane forming without H_2 in the headspace: ~2 µmol x gdw^{-1} x d^{-1} ± 3 (+CH_4/+SO_4^{2-}), ~2 µmol x gdw^{-1} x d^{-1} ± 1.5 (+CH_4/-SO_4^{2-}), [g] methane forming with hydrogen in the headspace (80 %): 9.4 µmol x gdw^{-1} x d^{-1} ± 2.3; n.a. - not analysed, AOM - anaerobic oxidation of methane, SRR - sulphate reduction rates, MPR - methane production rates.

	Siegert, 2010[d]		**Krüger et al. 2008**		**Treude et al. 2007[e, f]**		**Seifert et al. 2006[g]**	**Michaelis et al. 2002**
	Samples from 2004, 180 m, sediment mats		Samples from 2004, 180 m, sediment mats		Samples from 2001, 230 m, carbonate reefs		Samples from 2001, 230 m, carbonate reefs	Samples from 2001, 230 m, carbonate reefs
[µmol $g_{dw}^{-1} d^{-1}$]	Pink mat	Black mat	Pink mat	Black mat	exp. 1a (mixed)	Exp. 1b (mixed)		
AOM	**4.17** ± 1.7[a]	**18.3** ± 5.8[a]	**~17**[a]	**~15**[a]	**20.9, 9.4, 8.2**[c]	**13.9, 12.4, 7.8**[c]	**20.9** ± 3.8[a]	**18** ± 12[c]
SRR	**0**	**4.17** ± 1.7[b]	**~5**[b]	**4.5** ± 0.3[b]	**n.a.**	**n.a.**	**n.a.**	**2.8** ± 0.6[b]
SRR + CH_4	**0.83** ± 0.8[b]	**16.7** ± 0.8[b]	**~22**[b]	**19.4** ± 3.3[b]	**10.9, 7.4, 4.3**[c]	**n.a.**	**9.1** ± 1.6[b]	**19** ± 1[c]; **34** ± 5.8[b]
MPR	**0.77** ± 0.7[a]	**0.9** ± 0.4[a]	**~2**[a]	**~5**[a]	**~8, ~3, ~2**[c]	**~2, ~1, ~1**[c]	**7** ± 1.5[a]	**n.a.**
AOM/MPR	**5.3**	**20.3**	**8.5**	**3**	**2.6, 3.1, 4.1**	**7, 12.4, 7.8**	**3**	**n.a.**

For most experiments the methane oxidation rates (AOM) are in the range between 12.4 and 19 µmol $g_{dw}^{-1} d^{-1}$. However the pink mat sample in this study, revealed lowest AOM-rates, about 4.2 µmol $g_{dw}^{-1} d^{-1}$. Measurements of AOM-rates by Treude et al. (2007) showed also slightly reduced rates of about 8 µmol $g_{dw}^{-1} d^{-1}$. The methane-dependent sulphate reduction rates (SRR+CH_4) are not in accordance with the methane oxidation rates. In particular for pink mat samples in this study, the rates are strongly diminished, contrary to black mat samples in similar experiments. This demonstrates the weak link between sulphate reduction and AOM in ANME-1 dominated samples. Most other experiments were conducted with rather mixed samples. Nonetheless, high discrepancies between AOM-rates and methane-dependent SR (SRR+CH_4) could indicate a predominance of ANME-1, likely with a lower extend of ANME-2/DSS consortia. The rates of methanogenesis were between 0.8 and 8 µmol $g_{dw}^{-1} d^{-1}$ (without methane). In the respective experiments of this study, the CO_2-reduction rates were similar in both mat samples (~0.8 µmol $g_{dw}^{-1} d^{-1}$). The observed rates of methanogenesis in the presence of methane (this study) were about five fold higher within ANME-2 samples (BcLM; Figure 4.25). Seifert et al. (2006) also demonstrated methane generation independent of the presence of methane. They determined within experiments with 16 mM sulphate in the presence of methane an average daily CO_2-reduction rate of 11 µmol $g_{dw}^{-1} d^{-1}$ ± 3.8 (MPR). Similar to the results of this study, the measured rates in the absence of methane were slightly reduced, 7 µmol $g_{dw}^{-1} d^{-1}$ (± 1.5). Interestingly, the rates were also slightly

higher in the presence of hydrogen (80 %; ~9.4 µmol $g_{dw}^{-1} d^{-1}$, ± 2.3). They worked with a mixed mat sample, dominated by ANME-1 communities. Treude et al. (2007) and Orcutt et al. (2008) showed only minor evidence for AOM-independent methanogenesis. Treude et al. (2007) demonstrated, that methanogenesis was coupled to the occurrence of methane and low concentrations of hydrogen. Interestingly, methanogenesis was decreased with added hydrogen, and no methanogenesis was observed within the incubations without methane. Based on these observations and on molecular biological data, which indicated the lack of non-ANME-methanogens, the authors assumed that CO_2-reduction was linked to AOM. Figure 4.28 illustrates a model within AOM-performing microbial systems. While methane oxidation has a positive effect on CO_2-reduction (Figure 4.28a, b), due to hydrogen supply, methane oxidation is inhibited by elevated concentrations of hydrogen (Figure 4.28c). Moreover, the processes are likely linked to the concentrations of sulphate, which affect the concentration of hydrogen negatively. Hence, this may reduce the rates of CO_2-reduction whilst the rates of methane oxidation increase due to thermodynamically preference of the oxidative metabolism (Figure 4.28b). If sulphate is absent or its concentration decreases, a higher induced threshold of hydrogen may positively affect the CO_2-reduction (Figure 4.28c).

Orcutt et al. (2008) showed that the inhibition of sulphate reduction with molybdate led to reduced rates of AOM and methanogenesis (in the presence of methane). The addition of hydrogen in the headspace led to increased rates of methanogenesis, while sulphate reduction was completely inhibited (Figure 4.28c). This experiment was conducted with a mixed culture (22 % ANME-1, <10 % ANME-2). The inhibition of sulphate reduction with molybdate and the elevated concentrations of hydrogen led to enhanced methanogenic activity in these samples under given experimental conditions. These findings support a link between SRB and ANME-1 over the extracellular hydrogen concentrations. Lower sulphate reduction leads to increased methanogenesis, due to a higher hydrogen availability for CO_2-reduction (Figure 4.28c). Feasible is that the metabolism of involved ANME-2 consortia was mainly affected and ANME-1 were responsible for the measured rates after switching to a rather methanogenic metabolism. This assumption would be consistent with observations by Treude et al. (2007), who maintained that methanogenesis only occurred in the presence of methane. Although relative high rates of CO_2-reduction were also observed during incubations with ANME-2 dominated samples when methane was present (Figure 4.25).

However, the decreased CO_2-reduction rates with added hydrogen cannot be clearly explained (Figure 4.28a). Considering a reverse process of methanogenesis, an elevated partial pressure of hydrogen is thermodynamically favorable for CO_2-reduction (Hoehler et al., 1998, 2001). Otherwise, the hydrogen could be consumed by other bacteria. Most likely hydrogen consumers in those systems are SRB (not closely associated), as described by Nauhaus et al. (2005) or homo-acetogenic bacteria (Section 4.3.2.3).

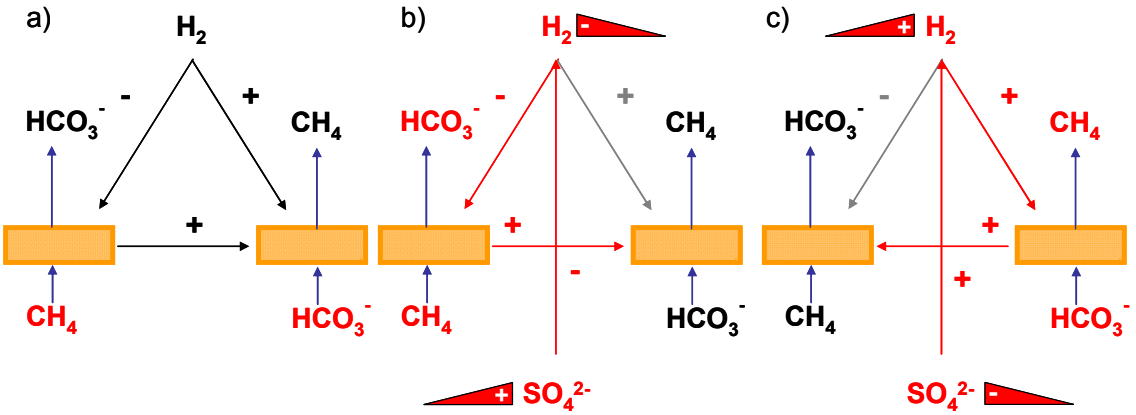

Figure 4.28: The anaerobic oxidation of methane and methanogenesis seems to be linked in sulphate depleted sediments. These two processes are apparently strongly influenced by the concentrations of hydrogen and sulphate. (a) A high concentration of hydrogen takes a positive effect on the CO_2-reduction, while increased hydrogen concentrations inhibit an methane oxidising metabolism in ANME-1. Moreover, methane oxidation leads to a enhanced hydrogen formation. (b) The concentration of sulphate takes effects on the metabolism of SRB, thus the threshold of hydrogen can be kept very low. This takes a positive effect on the methane oxidation by triggering the hydrogen concentration. Methane oxidation becomes energetically more favourable. (c) A low concentration or a decrease of the sulphate concentration has a positive increasing effect on the hydrogen threshold in the system, leading to more reducing conditions.

Nauhaus et al. (2005) found sulphate reduction rates with supplemented hydrogen similar to incubations with methane. They assumed, based on enrichments of SRB not belonging to the DSS-cluster that, the observed sulphate reduction was not maintained by SRB directly involved in AOM. Furthermore, they measured considerable sulphate reduction within control experiments without methane. Those data indeed indicated methane-independent sulphate reduction capabilities. Sulphate reduction is most likely dependent on metabolic processes carried out by other organisms. They might be responsible for hydrogen or formate production by fermentative processes. Interestingly, bromoethanesulfonate (BES), which inhibits methanogenesis, led to a nearly complete inhibition of methane-derived sulphate reduction for both mat sample types, but no potential electron shuttles were accumulated (Nauhaus et al., 2005). However, these findings are not contradictory to hydrogen as relevant compound involved in methanotrophic processes. Furthermore, the observations by Beal et al. (2009) underline that hydrogen is a relevant compound triggering the energy metabolism in the microbial system. Since hydrogen consuming bacteria reduce ferric iron (Fe^{3+}) or birnessite (Mn^{3+}, Mn^{4+}), and thus diminish the hydrogen level in the system, too (Hoehler et al., 1994). Nauhaus and colleagues (2005) tested both, Fe^{3+} and Mn^{4+} as electron acceptors with sediment samples from Hydrate Ridge. These samples were rather dominated by ANME-2/DSS consortia. Although they observed marginal reduction of these compounds, they did not detect methane oxidation by radiotracer investigations. These findings do not necessarily refute those electron acceptors involved in ANME-1 dominated microbial systems. Only little is known about the effect of hydrogen in AOM-performing systems. As mentioned above, only a few experiments considered elevated con-centrations of hydrogen (Nauhaus et al., 2005; Treude et al., 2007; Orcutt et al., 2008). But there are only few data about the *in-situ* concentration of

hydrogen within the medium during AOM (Hoehler et al., 1994). Webster et al. (2011) for instance measured the concentrations of hydrogen within heterotrophic incubation experiments. Thus, further investigations will resolve the function of hydrogen for AOM-performing communities and lead to deeper insights of AOM-physiology.

4.4.2 Acetate-dependent metabolisms in AOM-systems

The relevance of organisms other than sulphate reducing δ-Proteobacteria or of multiple biochemical pathways under the different experimental conditions also have to be considered as additional hydrogen consuming processes. It is probable that these hydrogen consuming processes regulate the biochemical properties of the entire community. The impact of homoacetogenic bacteria might also affect the AOM systems. But, although feasible, a possible H_2-transfer between acetate-oxidising homoacetogens and hydrogenotrophic methanogens is not well understood and for AOM settings so far not investigated. Such a syntrophic process leads to an enhanced CO_2-production (Lee and Zinder, 1988; Figure 4.29).

Furthermore, the reduced rates of methanogenesis in the presence of methane and acetate (PAcLM, PAcL; Figure 4.25) and an obviously higher rate of methane oxidation (362 $\mu mol\, g_{TOC}^{-1} d^{-1}$; PAcLM; Figure 4.25) give evidence for respective physiological processes in the AOM mats. Sulphate reduction rates reached highest levels for ANME-1 dominated mat samples within incubations supplemented with ^{13}C-acetate (PAcLM; Figure 4.25). The sulphate reduction under influence of acetate depends directly on methane as demonstrated by the sulphate reduction rates (PAcLM, PAcL; Figure 4.25). SRR were about 13.2 $\mu mol\, g_{TOC}^{-1} d^{-1}$ when methane was present and 2.4 $\mu mol\, g_{TOC}^{-1} d^{-1}$ without methane in the headspace. Thus the metabolism of the SRB apparently depends on methane. Remarkably, the sulphate reduction rates were much lower compared to measured methane decreases (Figure 4.25). This indicates a rather minor acetate-related activity of involved SRB in ANME-1 dominated mat samples. Usually sulphate reduction exceeds AOM in environmental settings. SRB are capable of using a broad spectrum of substrates from their environments (Bowles et al., 2010). Since the sulphate dependent oxidation of acetate[vii] and hydrogen[viii] are energetically in the same range under standard conditions, SRB can also gain their metabolic energy from acetate. In all likelihood, the SRB gain a part of their energy from acetate as shown by slightly higher SRR (PAcLM, PAcL; Figure 4.25). Otherwise, an acetate-dependent meta-

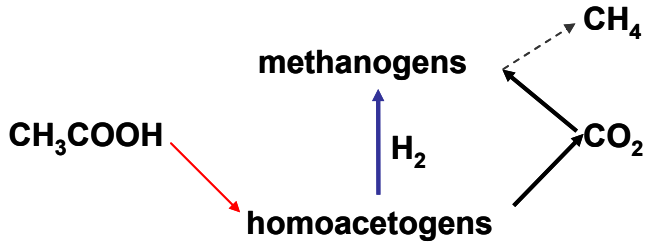

Figure 4.29: Scheme of substrate fluxes within a bacterial community of methanogenic archaea and acetate oxidising homoacetogenic bacteria.
Acetate is oxidised by homoacetogenic bacteria. During this oxidation process, hydrogen is shuttled from the homoacetogens to the methanogens. CO_2 and CH_4 are generated.

[vii] $3\ CH_3COOH + 4\ SO_4^{2-} + 5\ H^+ \rightarrow 4\ H_2S + 6\ HCO_3^-$; $\Delta G^{0'} = -126$ kJ/ mol (Konhauser, 2007)
[viii] $4\ H_2 + 4\ SO_4^{2-} \rightarrow H_2S + 2\ OH^- + 2\ H_2O$; $\Delta G^{0'} = -152$ kJ/mol (Konhauser, 2007)

bolism may lead to an enhanced sulphate reduction due to hydrogen transfer from ANME-archaea to the SRB. In addition, the methane oxidation was increased. The methyl group in acetate may be oxidised by the archaea instead of reduction. Such a process was shown by Phelps et al. (1985) in co-cultures of acetoclastic methanogens and *Desulfovibrio vulgaris*. The hydrogen transfer between both (for SRB, usually not able to use acetate or methanol as substrate) led to enhanced oxidation of acetate and methanol (Phelps et al., 1985; Figure 4.30). The very high carbon assimilation rates into bacterial lipids indicate a direct incorporation of acetate into the lipids (Figures 4.11, 4.12e, f; Section 4.3.2.2). The very high discrepancies between methane consumption and sulphate reduction rates also imply a rather uncoupled metabolism of ANME-1 to sulphate reduction (Orphan et al., 2002; Meyerdierks et al., 2010).

Nonetheless, acetate has apparently a strong effect on the metabolic balance of the investigated microbial community. The metabolic capabilities of involved ANME-1 could be inferred by acetate as substrate directly, hydrogen consuming SRB (mixotrophic life style), and under such experimental condition homoacetogenic bacteria (discussed in section 4.3.2.3). In euxinic culture experiments, Moran and colleagues (2007) showed for *Methanosarcina acetivorans* that methane was mainly converted to the methyl group of acetate under similar conditions. Several studies demonstrated that methanogenesis in the presence of acetate and sulphate was strongly inhibited (Achtnich et al., 1985; and references therein). In addition, Fukui et al. (1997) observed that SRB inhibited competitively the acetoclastic methanogenesis in coastal sediments due to a higher affinity of SRB to H_2. Thus, the equilibrium favours an oxidation process. Such an interspecies H_2-transfer was shown for methylotrophic substrates and was also assumed for acetate (Finke et al., 2007). This could also explain why no acetoclastic methanogenesis was determined during incubation experiments. Seifert et al. (2006) observed methane generation during incubations with acetate about 7.7 $\mu mol\, g_{dw}^{-1} d^{-1}$. This was in the same range with the CO_2-reductions rates (7 $\mu mol\, g_{dw}^{-1} d^{-1}$). However, it has to be considered that the concentrations of acetate in the performed experiments (AcLM, AcL, AcLMI, AcLI; Table 4.1) were much higher compared to previous published data for marine sediments (Fukui et al., 1997; Heuer et al., 2009).

All these considerations might also be true for ANME-2. The discrepancies between AOM and SR are lower within ANME-2 dominated samples compared to ANME-1 samples. The rates showed not such a strong fluctuation in ANME-2 samples during the experiments with bicarbonate and acetate (BBcLM, PAcLM; Figure 4.25). This may prevent a stronger influence of acetate to the bacterial system.

4.4.3 Methanol-dependent metabolism in AOM-systems

Methanol and other methylotrophic substrates, e.g. trimethylamine (TMA) or methyl sulfide may serve as methylotrophic substrates for methanotrophic archaea (Deppenmeier, 2002a, 2002b). Seifert and colleagues (2006) showed enhanced methanogenesis with TMA and methanol for Black Sea samples as well as Moran

and colleagues (2008) proposed methyl sulphides as inter-mediates in the anaerobic oxidation of methane. Therefore, methylotrophic capabilities of the ANME-clusters were investigated with methanol in the ^{13}C-labelling experiments. The isotopic analysis of the archaeal lipids revealed high assimilation rates and uptake from methanol (Figures 4.4, 4.5g, h).

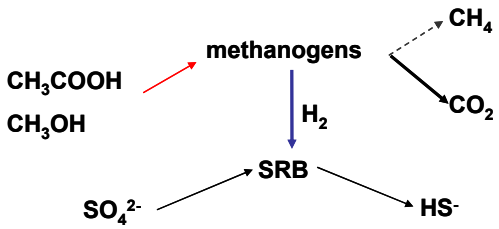

Figure 4.30: Scheme of substrate fluxes within a bacterial community of methanogenic archaea and (mixotrophic) SRB.
Acetate is oxidised by methanogens and SRB. During this oxidation process, hydrogen is shuttled from the methanogens to the SRB. CO_2 and CH_4 are generated.

In this study, rates up to 7.8 µmol $g_{dw}^{-1} d^{-1}$ of methylotrophic methanogenesis for both mat types were measured. Seifert and colleagues (2006) measured methane formation of 14.3 µmol $g_{dw}^{-1} d^{-1}$ from TMA and 12.1 µmol $g_{dw}^{-1} d^{-1}$ from methanol. The enhanced methylotrophic methanogenesis indicates that the involved ANME-clusters prefer methanol or methylated compounds under experimental conditions (MeLM, MeL; Figure 4.25). The metabolism with methanol[ix] leads to a higher energy yield and therefore might be a favourable substrate for methanogenesis in AOM settings as also found in conventional methanogenic environments (Deppenmeier, 2002a). Finke and colleagues (2007) demonstrated the effect of hydrogen-leakage on methylotrophic and hydrogenotrophic methanogenesis, also under sulphate reducing conditions. They showed for methylotrophic methanogens that the Gibbs free energy and the CO_2-production increased with decreasing hydrogen concentrations under sulphate reducing conditions. Their experiments demonstrated that hydrogen leakage occurs under sulphate reducing as well as methanogenic conditions. They also discussed that hydrogenotrophic methanogenesis becomes energetically favourable when the concentration of hydrogen decreases and methylotrophic methanogenesis becomes energetically unfavourable. Otherwise, when hydrogenotrophic methanogenesis is endergonic, the available energy by methyl conversion increases. Thus, these two kinds of methanogenesis are dependent on different factors, (i) hydrogen concentrations and (ii) sulphate reduction, as well as other abiotic factors like (iii) temperature and (iv) pH. Finke et al. (2007) suggested that hydrogen, produced by methylotrophic methanogens, was consumed by SRB under sulphate reducing conditions or driven by hydrogenotrophic methanogenesis.

Methylotrophic and hydrogenotrophic methanogenesis, as well as sulphate reduction and AOM, are apparently sensitive metabolic processes in the system. They depend on the disequilibrium of several electron donors (CH_4, H_2, CH_3X) and acceptors (HCO_3^-, SO_4^{2-}). Presumably, both investigated ANME-clusters can adapt their metabolism to varying conditions. They appear to be able to use bicarbonate, methane and methanol. Presumably, an enhanced hydrogen production (during anaerobic methane oxidation) leads to increased concentrations in the extracellular

[ix] $4\ CH_3OH \rightarrow 3\ CH_4 + CO_2 + 2\ H_2O$; $\Delta G^{0'} = -106$ kJ/mol (Deppenmeier, 2002b)

milieu. These elevated hydrogen concentrations have an inhibitory effect on the methyl transformation and methanogenesis from methanol might have driven exclusively in methane production (Meuer et al., 2002).

Interestingly, Mitterer (2010) proposed a model for simultaneous methylotrophic methanogenesis and sulphate reduction. Here, sulphate reduction has no inhibitory or competitive effect on methylotrophic methanogenesis. In contrast, enhanced sulphide concentration could lead to enhanced formation of methyl sulphides or TMA, feeding methylotrophic methanogenesis. Nonetheless, in this model, the influence of AOM was not much considered.

As already mentioned above, no sulphate reduction rates were determined with added methanol in the presence of methane during experiments with ANME-1 dominated samples (MeLM; Figure 4.25). In contrast, Nauhaus et al. (2005) observed such an inhibition effect without methane for ANME-1 dominated samples. However, it is not finally clear why sulphate reduction was inhibited during experiments without methane and what led to the differences between the both experiments (Nauhaus et al., 2005 vs. this study). Methanol is also an adequate substrate for homoacetogens (Cord-Ruwisch et al., 1988; Diekert and Wohlfarth, 1994). Therefore it is assumed that SRB associated to ANME-1 dominated samples in the methanol experiments were out-competed by methylotrophic archaea and probably associated homoacetogenic bacteria. This scenario, however, is not accompanied by dramatic changes in the lipid patterns (Figure 4.12). This suggests even in experiments with bicarbonate the acetogens may also be a part of the active bacterial community, thriving on bicarbonate. In the respective experiments, the activity of homoacetogenic bacteria might be enhanced by the addition of methanol. The correlating sulphate reduction rates again suggest the close association and strong (obligate) syntrophic capabilities of ANME-2 consortia, even under methylotrophic conditions (BMeLM; Figures 4.25, 3.7).

Summary

According to the physiology of the ANME-1, no strong coupling between ANME-1 archaea and SRB was indicated by high discrepancies between methane consumption and sulphate reduction rates.

For ANME-2 dominated samples a strong coupling between SRB and ANME-2 and a very strong adaptation to the presence of methane was demonstrated.

Hydrogen has probably an important impact to the ANME-1 community and the extracellular concentrations may affect the metabolism of ANME-1.

The electron shuttle between ANME-2 archaea and SRB remains unclear. However, hydrogen could also play an important role in the ANME-2/DSS consortia.

Both investigated mat types (ANME-1 and -2 dominated) revealed beside methanotrophic also significant methanogenic capabilities, independent of the presence of methane.

Both investigated mat samples exhibit highest rates of methylotrophic methanogenesis during this study. This implies strong methylotrophic capabilities.

In addition, microbial CO_2-reduction and methylotrophic methanogenesis are further microbial processes observed in both mat types. Their relevance *in-situ* within these microbial systems remains unclear. ANME-archaea, in particular those belong to the ANME-1 cluster are rather facultative methanotrophic archaea (Lloyd et al., 2011).

AOM, methanogenesis and sulphate reduction are apparently linked via the concentration of hydrogen, particularly in ANME-1 dominated mats. Thus, homoacetogenic bacteria may also influence the microbial system, at least under laboratory conditions.

4.5 Physiology of investigated ANME-clusters

4.5.1 ANME-1 physiology

The investigation of the ^{13}C-assimilation into archaeal lipid biomarkers and further studies of methanogenic capabilities demonstrate that ANME-1 do not necessarily need methane to thrive and their potential to switch between a methanogenic and a low but significant methanotrophic metabolism (> 30 % of the AOM rate) under experimental condition (Sections 4.3.1, 4.4). Moreover, it has to be considered that the processes of AOM and methanogenesis occur simultaneously in the mat systems (Figure 4.25). These findings are consistent with observations by other authors (Seifert et al., 2006; Treude et al., 2007; Orcutt et al., 2008; Lloyd et al., 2011; Holler et al., 2011b). Apparently, the metabolism of ANME-1 is not strongly linked to sulphate (Hoehler et al., 1994; Beal et al., 2009; Rossel et al., 2011; Takeuchi et al, 2011; Yanagawa et al., 2011; Lloyd et al., 2011), also underlined by the very low observed sulphate reduction compared to high methane consumption (Figure 4.25). Although, an overestimation of methane consumption due to small leakages can not be excluded, a strong discrepancy between both processes in ANME-1 associations is evident. According to FISH-investigations by several authors, no tight association between ANME-1 cells and SRB was observed (Michaelis et al., 2002; Blumenberg et al., 2004). These observations suggest a rather facultative syntrophic community. Potentially, hydrogen has an important relevance as electron shuttle in the system (Section 4.4.1).

Acetoclastic methanogenesis had no considerable impact on investigated ANME-1 samples (see discussion 4.4.2; Figure 4.25). Acetate is directly incorporated for the anabolism, as already proposed by Meyerdierks et al. (2010). Methanol, probably as well as other methylated (TMA, methyl sulphide) compounds, has an effect on the anabolism and catabolism shown by high carbon assimilation into archaeal lipids and considerable high rates of methanogenesis (Section 4.4.1). In this study those methylotrophic capabilities could be confirmed by relative high measured rates. Apparently, the presence or absence of methane did only reveal minor influence on

the methylotrophic capabilities (PMeLM, PMeL; Figure 4.25). Metagenomic analysis by Meyerdierks and colleagues (2010) of ANME-1 enrichments revealed typical biochemical properties of Methanomicrobiales. They found sequences encoding two putative cytoplasmatic heterodisulphide reductase complexes (HdrI and HdrII), supporting a hydrogenotrophic pathway of methanogenesis in addition to the results of a ^{13}C-labelling approach with bicarbonate (in this study). Nonetheless, Meyerdierks et al. (2010) found also sequences encoding putative enzymes involved in cytochrome shuttled electron transport and a so far not described [FeFe]-hydrogenase (for archaea). Usually, [FeFe]-hydrogenases produce reversible hydrogen and are responsible for hydrogen uptake in bacteria and lower eukaryotes. Interestingly, the second heterodisulphide reductase (also HdrII) seems to be associated with a methyl viologen reducing hydrogenase subunit (MvhD) and one β-subunit of a formate hydrogenase (FdhB). The function is unknown; however the subunit MvhD and FdhB may be involved in a ferredoxin reduction. Both, the MvhD and FdhB subunits are commonly used in electron transfer (Jormakka et al., 2003; Thauer et al., 2010). Moreover, the formate dehydrogenase subunit is described to link the subunit A with the membrane spanning subunit C of the Fdh complex (e.g. Jormakka et al., 2003). The electrons, transferred by the MvhD and FdhB subunits, are needed for the reduction of the heterodisulphide (CoM-S-S-CoB). In addition some subunits of a membrane-bound NADH:quinone oxidoreductase-like (Nuo-like) complex were identified. The Nuo-complex comprises subunits involved in proton shuttling through the membrane; particularly the subunits Nuo E and F associated with the membrane into the cell lumen bear a [2Fe-2S]-cluster, a flavin mononucleotide (FMN) and a [4Fe-4S]-cluster. Hence, the respective Nuo-like subunits E and F may be capable of oxidising also $F_{420}H_2$ as well transferring two protons via the FMN to the membrane spanning Nuo-like subunit LMN complex. These three subunits are presumably involved in proton shuttling. If this holds true, the reduction of the heterodisulphide at the HdrII is linked to the oxidation of $F_{420}H_2$ at the Nuo-like complex EF and protons can be shuttled out through the membrane spanning Nuo-like complex LMN. The MvdH and FdhB subunits could be responsible for the electron transfer within the enzyme complex.

The HdrII and the Nuo-like complex must not be close associated. The Nuo-like complex can be an analogue of the membrane bounded Eha or Ehb-complex. Ferredoxin can be oxidised at the Nuo-like complex after its reduction at the format dehydrogenase. Protons can also be shuttled out at this step. However, quinones usually associated with such a complex and other potential proton shuttle molecules are not well investigated or described for ANME-1 so far. Only Nauhaus and colleagues did incubations with ANME-2 dominated samples from Hydrate Ridge and added anthraquinone-2,6-disulfonate (AQDS), phenazine methosulfate, and phenazine ethosulfate. No effect on methane oxidation was observed. However, AQDS was reduced during the incubation experiments.

Also likely is a potential anabolic function of the Nuo-like complex, similar to the Ech-complex, detected in members of the Methanosarcinales. In Methanosarcinales

this complex was demonstrated to be involved in CO_2-reduction to formyl-methanofuran (energy metabolism), in reductive carboxylation reactions (e.g. pyruvate synthesis from acetyl-CoA), and in CO_2-reduction to CO (CO_2-assimilation) (Meuer et al., 2002). Relative high CO_2-incorporation was shown by the respective assimilation rates into archaeal lipids. Moreover the slightly reduced rates in the presence of unlabelled methane imply an isotopic dilution effect and underline (i) a simultaneous assimilation into the archaeal biomass of methane and carbon dioxide, and (ii) a possible function of the Nuo-like complex as analogue to the Ech complex. However, this must be proven in further biochemical investigations.

Meyerdierks et al. (2010) found evidence that cytochromes are involved in the metabolism of ANME-1. These cytochromes can be involved in electron shuttling, since members of the order of the Methanomicrobiales commonly do not have cytochromes and no membrane bound heterodisulphide reductase (HdrDE) was observed, as typically for Methanosarcinales. All these biochemical considerations lead to the assumption, that electron shuttling and further, so far not investigated metabolisms in ANME-1 might be involved. Thus, these observations have to be proven in further investigations, if those enzymes are involved in hydrogen or proton shuttling process or further substrate specific metabolisms are involved. The relevance of the multiheme c-type cytochromes, the [FeFe]-hydrogenase, the second putative heterodisulphide complex, and the membrane bounded subunits of the Nuo-like complex remains obscure, as of yet.

A detailed hypothetical biochemical scheme is depicted in the appendix (A.9a-c).

4.5.2 ANME-2 physiology

ANME-2 are closely affiliated to the order of the Methanosarcinales (Hallam et al., 2003; Knittel and Boetius, 2009). Methanosarcinales have a versatile substrate spectrum, capable of using CO_2 + H_2, acetate, methanol, and methylated C_1-compounds as methanogenic substrate (Deppenmeier, 2002a; Thauer et al., 2010). Similar ^{13}C-assimilation into archaeal lipids for experiments with labelled methane and labelled bicarbonate were detected, but only in the presence of methane (ML, BcLM, AcLM; Figure 4.5b, d). This clearly demonstrates the strong adaptation of ANME-2 to methane. Although many members of the Methanosarcinales perform methanogenesis from acetate, no significant rates of acetoclastic methanogenesis were observed, leading to the conclusion that, at least under given experimental conditions, ANME-2 revealed no considerable heterotrophic catabolism. Furthermore, as already discussed in sections 4.2 and 4.4.2, CO_2-reduction was apparently inhibited by the addition of acetate. Intriguingly, methanol exhibited a huge impact on the ANME-2 metabolism, as demonstrated by the highest overall ^{13}C-assimilation into lipids (MeLM, MeL; Table 3.2; Figure 3.14h) and considerable high rates of methylotrophic methanogenesis (BMeLM, BMeL; Figure 4.25). While the assimilation rates into the lipids were lower in the presence of methane (MeLM) compared to those in the absence (MeL), the rates of methanogenesis were

obviously independent of the presence of methane. They reached rates of methanogenesis up to 30 µmol $g_{TOC}^{-1} d^{-1}$ (or 7.8 µmol $g_{dw}^{-1} d^{-1}$).

Lower assimilation rates could be affected by a dilution effect of unlabelled methane or a competitive inhibition with methane (Sections 4.2, 4.4.3). Remarkable is the observed stoichiometry of sulphate reduction and methane consumption. It is nearly in a ratio of 1:2 (Figure 4.25). This was lower than observed in other studies (Nauhaus et al., 2002; Michaelis et al., 2002), which published a ratio of 1:1. This discrepancy can be best explained by an overestimation of methane consumption during the experiments due to losses of methane from the headspace. Otherwise, similar to ANME-1, a simultaneous process of methanogenesis and AOM, or electron shuttling to associated homoacetogenic bacteria may influence this observation. Additionally, a sulphate-independent metabolism could explain those effects, similar to those hypothesised for ANME-1 dominated samples (Sections 4.4.1, 4.5.1). Since sulphate-reduction of adjacent SRB would inhibit methanogenesis of ANME-2 within close consortia, it is possible that single cells of ANME-2 could instead gain their energy from a methanogenic catabolism (House et al., 2009; Alperin and Hoehler, 2009). This could explain the relative high rates of methane generation in the presence of methane and does not contradict the very low assimilation rates during the incubations without methane. If hydrogen is, despite all previous consideration the hydrogen shuttle, only the ANME-cells in close proximity to SRB are in direct competition with hydrogen consuming SRB. For single ANME cells higher concentration of hydrogen would be available. They apparently have similar physiological properties like ANME-1 archaea. However, the lipids biomarker data in this study demonstrate that ANME-2 archaea are presumably more adapted to sulphate-reducing conditions and have a higher affinity to methane (BcL, BcLM; Table 3.1; Figures 4.4, 4.25).

The calculated methane-dependent sulphate reduction, which correlates with measured sulphate reduction rates supports the close syntrophic relation between ANME-2 archaea and SRB (Boetius et al., 2000) and the strong dominance of SRB (in the black mat) under most experimental conditions within these consortia.

5. Conclusions

The metabolic effect of methane and other substrates (bicarbonate, acetate, methanol), also in the presence of methane, to AOM-performing communities was investigated. The ^{13}C-uptakes into bacterial and archaeal lipids within two different mat samples (ANME-1 and ANME-2 dominated) were determined. In addition, the sulphate reduction rates, methane decrease, and methane generation were measured and the isotopic composition of the methane in the headspace was determined.

Both investigated mat types (ANME-1 and -2 dominated) also revealed, along with methanotrophic, significant methanogenic capabilities, independent of the presence of methane. They exhibited similar methanogenic activity during similar incubation experiments. However, the rates of autotrophic methanogenesis were considerable enhanced for ANME-2 dominated samples when methane was present. Nonetheless, no or only weak catabolic effect of acetate for both ANME-clusters could be demonstrated. However, acetate was assimilated into the lipids. Furthermore, the minor autotrophic methane generation imply an inhibition effect of acetate. Moreover, the addition of acetate led to higher methane oxidation rates. No inhibition of the acetoclastic methanogenesis with methyl fluoride could be verified. The very high rates of methylotrophic methanogenesis and the assimilation of methanol derived ^{13}C into the archaeal lipids were shown and demonstrate strong methylotrophic capabilities.

According to the physiology of the ANME-1, no strong coupling between ANME-1 archaea and SRB was indicated by high discrepancies between methane consumption and sulphate reduction rates. Obviously, ANME-1 are able to switch easily between a methanogenic and a methanotrophic metabolism, depending on the culturing or environmental conditions. This was demonstrated by similar total daily $\Delta\delta^{13}C$ during incubation experiments with labelled methane and labelled bicarbonate in the presence of methane and slightly enhanced total daily $\delta^{13}C$-shifts with labelled bicarbonate (when no methane was present). Hydrogen (or formate) most likely has a big impact to the ANME-1 community and extracellular concentrations may affect the metabolism of ANME-1.

Archaeol could be a precursor for the GDGTs in ANME-1 dominated samples. This was shown by the similar ^{13}C-assimilation patterns obtained for the biphytanes and archaeol. Moreover, six isomers of a C_{35}-ioprenoid hydrocarbons were found, three tentatively head-to-tail linked straight structures, five to seven fold unsaturated. These compounds could be involved in a hydrogen dependent methanogenesis and function as reversible hydrogen sink. A similar function of reversible hydrogen storage is also assumed for the PMIs, indicated by very high synthesis rates of the PMI:4 and PMI:5 during the experiments with labelled methane or labelled bicarbonate, but only negligible synthesis rates from methanol.

Interestingly, both compound groups showed assimilation and thus synthesis in most experiments. For the experiments with methane and bicarbonate, it is assumed

that these compounds function as reversible hydrogen sink. Acetate has apparently no catabolic relevance, but is directly incorporated as building block. Methanol is probably disproportionated to methane and carbon dioxide. Hence, no hydrogen must be stored for a methylotrophic metabolism.

For ANME-2 dominated samples a strong coupling between SRB and ANME-2 was demonstrated by similar rates of sulphate reduction and methane consumption. In addition, a very strong adaptation to the presence of methane was demonstrated. The synthesis of *sn-2*-hydroxyarchaeol was mainly affected by the presence of methane.

The electron shuttle between ANME-2 archaea and SRB remains unclear. However, hydrogen could also play an important role in the consortia, at least with regard to general metabolic capabilities of the complex prokaryotic community associated to ANME-2.

Crocetane revealed no explicit ^{13}C-assimilation throughout all incubation experiments supporting the assumption by Elvert et al. (2000) that crocetane is an ultimate product which is preserved in the environments.

Especially the incubation experiments with bicarbonate underlines a facultative syntrophic consortia structure for ANME-1 compared to a more obligate consortia structure for ANME-2/DSS. This is in accordance with several FISH-investigations of similar samples (e.g. Boetius et al., 2000; Michaelis et al., 2002).

Methane-independent autotrophic and heterotrophic capabilities were demonstrated for associated bacteria of both communities. Interestingly, bacteria associated to ANME-1 showed a very strong heterotrophic activity while bacteria associated to ANME-2 revealed a pronounced autotrophic metabolism.

The lipid biomarker investigations give a first evidence for further homoacetogenic metabolism in both communities, demonstrated by ^{13}C-assimilation from labelled methanol into bacterial lipids. Both communities showed distinct assimilation patterns. Interestingly, the patterns in ANME-1 dominated samples were similar, although no sulphate reduction was measured. In ANME-2 dominated samples considerable uptakes were observed when methane was present.

Figure 5.1 extends a basic model of sulphate-related AOM, as proven in previous SIP studies (Blumenberg et al., 2005; Wegener et al., 2008a; Jagersma et al., 2009). It shows additional carbon fluxes and further metabolic capabilities. Bicarbonate has a central role after methane in such anaerobic systems. It is probably involved in chemolithoautotrophic metabolism with several electron acceptors like sulphate, ferric iron and manganese (Hoehler et al., 1994; Beal et al., 2009). Further evidence for chemolithoheterotrophic and chemoorganoheterotrophic metabolisms were demonstrated by acetate labelling experiments. Probably a mixotrophic metabolism of SRB plays an important part within the communities. In this study, first evidences were shown for acetogenic metabolism by compound specific stable isotope probing and sulphate reduction rates. These organisms could also be responsible for maintaining a low hydrogen pressure in the extracellular milieu. Hence, the additional

hydrogen consumption during acetogenesis leads also to a disequilibrium which is thermodynamically beneficial for the anaerobic oxidation of methane.

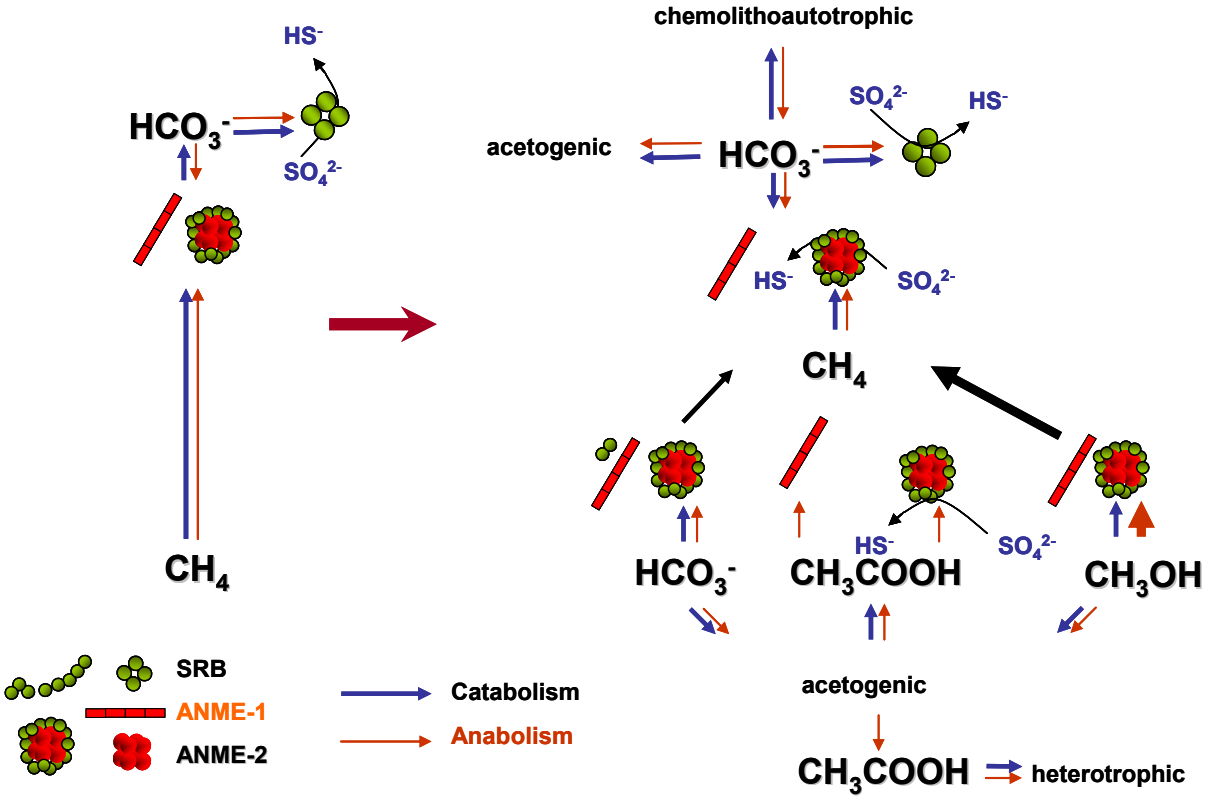

Figure 5.1: Extended model of carbon fluxes in the microbial AOM-performing communities. The model on the left side, confirmed by several previous studies was extended during this work (right side). Although the principle carbon fluxes within the two distinct ANME-consortia are quite similar and thus, summarised as simplified scheme. There are also some differences between the consortia as already shown by previous studies. For example the consortia structures differ significantly. This may have influence on further metabolic processes within the consortia. Nevertheless, beside methane also bicarbonate has a central function within those AOM-performing consortia. Apparently SRB, ANME (itself), acetogenic, and probably other chemolithoautotrophic organisms use bicarbonate for their anabolism. Homoacetogenic bacteria gain also their energy from autotrophic acetogenesis. Acetate only has a low impact on the archaea, but appreciable influence on the bacterial lipid anabolism. Furthermore methanol has considerable relevance as substrate for methylotrophic archaea, most likely ANME and homoacetogenic bacteria.

In addition, microbial CO_2-reduction and methylotrophic methanogenesis are further microbial processes observed in both mat types. Their relevance *in-situ* within these microbial systems remains unclear. ANME-archaea, in particular those belonging to the ANME-1 cluster, are rather facultative methanotrophic archaea (Lloyd et al., 2011).

AOM, methanogenesis and sulphate reduction are apparently linked via the concentration of hydrogen, particularly in ANME-1 dominated mats. Thus, homoacetogenic bacteria may also influence the microbial system, at least under laboratory conditions.

Further investigations should reveal the biochemistry of ANME, in particular the set of enzymes in ANME-1 with respect to hydrogen or formate metabolism; including electrochemical consideration of the enzyme and coenzyme system. Investigations of

cytochromes and quinones may lead to deeper insights of electron transport, at least in membrane bound respiratory oxidoreductase systems.

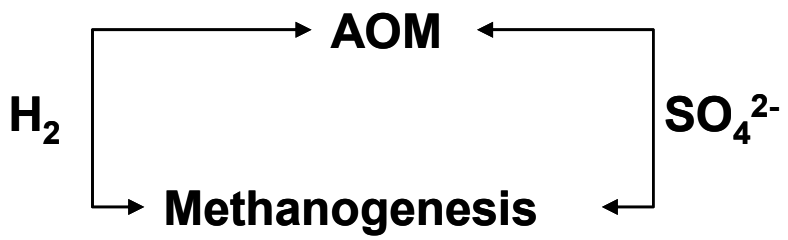

Figure 5.2: Relation between AOM, methanogenesis, sulphate and hydrogen.
The processes of methanogenesis and AOM seem to be triggered by the concentrations of hydrogen and sulphate.

If the ANME-1 consortium is rather facultative the role of hydrogen, sulphate, sulphide, and formate has to be elucidated in additional incubation experiments (Figure 5.2). Further investigations with focus on methylotrophic capabilities of ANME-1 and their role in sulphate depleted sediment layers may lead to a deeper understanding of the physiology of ANME-1 and its role in the global methane turnover.

The occurrence and the function of homoacetogenic bacteria, particularly as hydrogen consumers and acetate suppliers, and the role of further autotrophic organisms may lead to a complex understanding of the microbial consortia. Nevertheless, heterotrophic organisms are probably important key players in organic rich sediments. Further efforts to understand the anaerobic degradation of complex molecules will be of interest to evaluate the impact of methane as main carbon source in cold seeps or vent systems, and its fade in a complex microbial system, which may function as a natural filter for methane emitted from marine sediments.

References:

Achtnich, C., Schuhmann, A., Wind, T. and Conrad, R. (1995). Role of interspecies H_2 transfer to sulfate and ferric iron-reducing bacteria in acetate consumption in anoxic paddy soil. FEMS Microbiology Ecology **16**(1): 61-69.

Alperin, M. J. and Hoehler, T. M. (2009). Anaerobic methane oxidation by archaea/sulfate-reducing bacteria aggregates:1. Thermodynamic and physical constraints. American Journal of Science **309**(10): 869-957.

Anderson, I., Ulrich, L. E., Lupa, B., Susanti, D., Porat, I., Hooper, S. D., Lykidis, A., Sieprawska-Lupa, M., Dharmarajan, L., Goltsman, E., Lapidus, A., Saunders, E., Han, C., Land, M., Lucas, S., Mukhopadhyay, B., Whitman, W. B., Woese, C., Bristow, J. and Kyrpides, N. (2009). Genomic Characterization of Methanomicrobiales Reveals Three Classes of Methanogens. Plos One **4**(6): e5797.

Bapteste, E., Brochier, C. and Boucher, Y. (2005). Higher-level classification of the Archaea: evolution of methanogenesis and methanogens. Archaea **1**(5): 353-363.

Barnes, R. O. and Goldberg, E. D. (1976). Methane production and consumption in anaerobic marine sediments. Geology **4**: 297-300.

Beal, E. J., House, C. H. and Orphan, V. J. (2009). Manganese- and Iron-dependent marine methane oxidation. Science **325**(5937): 184-187.

Biddle, J. F., Lipp, J. S., Lever, M. A., Lloyd, K. G., Sørensen, K. B., Anderson, R., Fredricks, H. F., Elvert, M., Kelly, T. J., Schrag, D. P., Sogin, M. L., Brenchley, J. E., Teske, A., House, C. H. and Hinrichs, K.-U. (2006). Heterotrophic Archaea dominate sedimentary subsurface ecosystems off Peru. Proceedings of the National Academy of Sciences of the United States of America **103:** 3846-3851.

Blazejak, A. and Schippers, A. (2010). High abundance of JS-1-and Chloroflexi-related Bacteria in deeply buried marine sediments revealed by quantitative, real-time PCR. FEMS Microbiology Ecology **72**(2): 198-207.

Blumenberg, M., Seifert, R., Reitner, J., Pape, T. and Michaelis, W. (2004). Membrane lipid patterns typify distinct anaerobic methanotrophic consortia. Proceedings of the National Academy of Sciences of the United States of America **101**(30): 11111-11116.

Blumenberg, M., Seifert, R., Nauhaus, K., Pape, T. and Michaelis, W. (2005). In vitro study of lipid biosynthesis in an anaerobically methane-oxidizing microbial mat. Applied and Environmental Microbiology **71**(8): 4345-4351.

Blumenberg, M., Krüger, M., Nauhaus, K., Talbot, H. M., Oppermann, B. I., Seifert, R., Pape, T. and Michaelis, W. (2006). Biosynthesis of hopanoids by sulfate-reducing bacteria (genus Desulfovibrio). Environmental Microbiology **8**(7): 1220-1227.

Blumenberg, M., Seifert, R., Petersen, S. and Michaelis, W. (2007). Biosignatures present in a hydrothermal massive sulfide from the Mid-Atlantic Ridge. Geobiology **5**(4): 435-450.

Blumenberg M., Oppermann., B.I., Guyoneaud, E. and Michaelis, W. (2009). Hopanoid production by Desulfovibrio bastinii isolated from oilfield formation water. FEMS Microbiology Letters **293**: 73-78.

Boetius, A., Ravenschlag, K., Schubert, C. J., Rickert, D., Widdel, F., Gieseke, A., Amann, R., Jorgensen, B. B., Witte, U. and Pfannkuche, O. (2000). A marine microbial consortium apparently mediating anaerobic oxidation of methane. Nature **407**(6804): 623-626.

Boschker, H. T. S., Nold, S. C., Wellsbury, P., Bos, D., de Graaf, W., Pel, R., Parkes, R. J. and Cappenberg, T. E. (1998). Direct linking of microbial populations to specific biogeochemical processes by ^{13}C-labelling of biomarkers. Nature **392**: 801-805.

Bouloubassi, I., Aloisi, G., Pancost, R. D., Hopmans, E., Pierre, C. and Sinninghe Damsté, J. S. (2006). Archaeal and bacterial lipids in authigenic carbonate crusts from eastern Mediterranean mud volcanoes. Organic Geochemistry **37**(4): 484-500.

Bowles, M. W., Samarkin, V. A., Bowles, K. M. and Joye, S. B. (2011). Weak coupling between sulfate reduction and the anaerobic oxidation of methane in methane-rich sea floor sediments during *ex-situ* incubation. Geochimica et Cosmochimica Acta **75**(2): 500-519.

Braissant, O., Decho, A. W., Dupraz, C., Glunk, C., Przekop, K. M. and Visscher, P. T. (2007). Exopolymeric substances of sulfate-reducing bacteria: Interactions with calcium at alkaline pH and implication for formation of carbonate minerals. Geobiology **5**: 401-411.

Brissette, J. L., Cabacungan, E. A. and Pieringer, R. A. (1986). Studies on the antibacterial activity of dodecylglycerol. Its limited metabolism and inhibition of glycerolipid and lipoteichoic acid biosynthesis in *Streptococcus mutans* BHT. Journal of Biological Chemistry **261**(14): 6338-6345.

Brocks, J. J. and Pearson, A. (2005). Building the biomarker tree of life. Molecular Geomicrobiology **59**: 233-258.

Brocks, J.J. and Grice, K. (2011). Biomarkers (molecular fossils), in: Reitner, J., Thiel, V. (Eds.), Encyclopedia of Geobiology. Springer, pp. 147-167.

Buser, H. R., Arn, H., Guerin, P. and Rauscher, S. (1983). Determination of double bond position in mono-unsaturated acetates by mass spectrometry of dimethyl disulfides adducts. Analytical Chemistry **55**: 818-822.

Caillon, E., Lubochinsky, B. and Rigomier, D. (1983). Occurence of dialkyl ehter phospholipids in *Stigmatella aurantiaca* DW4. Journal of Bacteriology **153**(3): 1348-1351.

Canale-Parola, E. (1977). Physiology and evolution of spirochetes. Bacteriological Reviews **41**(1): 181-204.

Castro, H. F., Williams, N. H. and Ogram, A. (2000). Phylogeny of sulfate-reducing bacteria. FEMS Microbiology Ecology **31**: 1-9.

Chappe, B., Michaelis, W. and Albrecht, P. (1980). Molecular fossils of Archaebacteria as selective degradation products of kerogen. Douglas A. G. and Maxwell J. R. (Eds.). Advances in Organic Geochemistry, Pergamon Press Oxford (1980)**:** 265-274.

Chappe, B., Albrecht, P. and Michaelis, W. (1982). Polar Lipids of Archaebacteria in Sediments and Petroleums. Science **217**(4554): 65-66.

Chistoserdova, L., Vorholt, J. A., Thauer, R. K. and Lidstrom, M. E. (1998). C-1 transfer enzymes and coenzymes linking methylotrophic bacteria and methanogenic Archaea. Science **281**(5373): 99-102.

Chistoserdova, L., Jenkins, C., Kalyuzhnaya, M. G., Marx, C. J., Lapidus, A., Vorholt, J. A., Staley, J. T. and Lidstrom, M. E. (2004). The enigmatic Planctomycetes may hold a key to the origins of methanogenesis and methylotrophy. Molecular Biology and Evolution **21**(7): 1234-1241.

Chistoserdova, L., Vorholt, J. A. and Lidstrom, M. E. (2005). A genomic view of methane oxidation by aerobic bacteria and anaerobic archaea. Genome Biology **6**(2).

Conrad, R. (1999). Contribution of hydrogen to methane production and control of hydrogen concentrations in methanogenic soils and sediments. FEMS Microbiology Ecology **28**(3): 193-202.

Conrad, R. and Klose, M. (1999). How specific is the inhibition by methyl fluoride of acetoclastic methanogenesis in anoxic rice field soil? FEMS Microbiology Ecology **30**(1): 47-56.

Cord-Ruwisch, R. (1985). A quick method for the determination of dissolved and precipitated sulfides in cultures of sulfate-reducing bacteria. Journal of Microbiological Methods **4**(1): 33-36.

Cord-Ruwisch, R., Seitz, H.-J. and Conrad, R. (1988). The capacity of hydrogenotrophic anaerobic bacteria to compete for traces of hydrogen depends on the redox potential of the terminal electron acceptor. Archives of Microbiology **149**(4): 350-357.

Craig, H. (1954). Carbon 13 in plants and the relationships between carbon 13 and carbon 14 variations in nature. Journal of Geology **62**(2): 115-149.

Cravo-Laureau, Grossi, V., Raphel, D., Matheron, R. and Hirschler-Réa, A. (2005). Anaerobic *n*-alkane metabolism by a sulfate-reducing bacterium, *Desulfatibacillum aliphaticivorans* train CV2803^{T}. Applied and Environmental Microbiology **71**(7): 3458-3467.

De Rosa, M. and Gambacorta, A. (1988). The lipids of archaebacteria. Progress in Lipid Research **27**(3): 153-175.

del Giorgio, P. A. and Duarte, C. M. (2002). Respiration in the open ocean. Nature **420**(6914): 379-384.

DeLong, E. F., King, L. L., Massana, R., Cittone, H., Murray, A., Schleper, C. and Wakeham, S. G. (1998). Dibiphytanyl ether lipids in nonthermophilic Crenarchaeotes. Applied and Environmental Microbiology **64**(3): 1133-1138.

DeLong, E. F. (2000). Resolving a methane mystery. Nature **407**(6804): 577-579.

Deppenmeier, U. (2002a). The unique biochemistry of methanogenesis. Progress in Nucleic Acid Research and Molecular Biology **71**: 223-283.

Deppenmeier, U. (2002b). Redox-driven proton translocation in methanogenic Archaea. Cellular and Molecular Life Sciences **59**(9): 1513-1533.

Dickens, G. R., Castillo, M. M. and Walker, J. C. G. (1997). A blast of gas in the latest Paleocene: Simulating first-order effects of massive dissociation of oceanic methane hydrate. Geology **25**(3): 259-262.

Diekert, G. and Wohlfarth, G. (1994). Metabolism of homoacetogens. Antonie van Leeuwenhoek **66**(1): 209-221.

Dijkstra, P., Dalder, J., Selmants, P. C., Hart, S. C., Koch, G. W., Schwartz, E. and Hungate, B. A. Modeling soil metabolic processes using isotopologue pairs of position-specific ^{13}C-labeled glucose and pyruvate. Soil Biology and Biochemistry **43**(9): 1848-1857.

Drake, H. L., Gößner, A. S. and Daniel, S. L. (2008). Old Acetogens, New Light. Annals of the New York Academy of Sciences **1125**(1): 100-128.

Dumont, M. G. and Murrell, J. C. (2005). Stable isotope probing - linking microbial identity to function. Nature Reviews Microbiology **3**(6): 499-504.

Dumont, M. G., Radajewski, S. M., Miguez, C. B., McDonald, I. R. and Murrell, J. C. (2006). Identification of a complete methane monooxygenase operon from soil by combining stable isotope probing and metagenomic analysis. Environmental Microbiology **8**(7): 1240-1250.

Dupraz, C. and Visscher, P. T. (2005). Microbial lithification in marine stromatolites and hypersaline mats. Trends in Microbiology **13**(9): 429-438.

Elvert, M., Suess, E. and Whiticar, M. J. (1999). Anaerobic methane oxidation associated with marine gas hydrates. Superlight C-isotopes from saturated and unsaturated C20 and C25 irregular isoprenoids. Naturwissenschaften **86**(6): 295-300.

Elvert, M., Suess, E., Greinert, J. and Whiticar, M. J. (2000). Archaea mediating anaerobic methane oxidation in deep-sea sediments at cold seeps of the eastern Aleutian subduction zone. Organic Geochemistry **31**: 1175-1187.

Elvert, M., Boetius, A., Knittel, K. and Jorgensen, B. B. (2003). Characterization of specific membrane fatty acids as chemotaxonomic markers for sulfate-reducing bacteria involved in anaerobic oxidation of methane. Geomicrobiology Journal **20**(4): 403-419.

Ettwig, K. F., Shima, S., Van De Pas-Schoonen, K. T., Kahnt, J., Medema, M. H., Op Den Camp, H. J. M., Jetten, M. S. M. and Strous, M. (2008). Denitrifying bacteria anaerobically oxidize methane in the absence of Archaea. Environmental Microbiology **10**(11): 3164-3173.

Ettwig, K. F., Butler, M. K., Le Paslier, D., Pelletier, E., Mangenot, S., Kuypers, M. M. M., Schreiber, F., Dutilh, B. E., Zedelius, J., de Beer, D., Gloerich, J., Wessels, H., van Alen, T., Luesken, F., Wu, M. L., van de Pas-Schoonen, K. T., den Camp, H., Janssen-Megens, E. M., Francoijs, K. J., Stunnenberg, H., Weissenbach, J., Jetten, M. S. M. and Strous, M. (2010). Nitrite-driven anaerobic methane oxidation by oxygenic bacteria. Nature **464**(7288): 543-548.

Ferry, J. G. (1999). Enzymology of one-carbon metabolism in methanogenic pathways. FEMS Microbiology Reviews **23**(1): 13-38.

Ferry, J. G. (2010). How to Make a Living by Exhaling Methane. Annual Review of Microbiology **64:** 453-473.

Finke, N., Hoehler, T. M. and Jorgensen, B. B. (2007). Hydrogen 'leakage' during methanogenesis from methanol and methylamine: implications for anaerobic carbon degradation pathways in aquatic sediments. Environmental Microbiology **9**(4): 1060-1071.

Fischer, W. W., Summons, R. E. and Pearson, A. (2005). Targeted genomic detection of biosynthetic pathways: anaerobic production of hopanoid biomarkers by a common sedimentary microbe. Geobiology **3**(1): 33-40.

Frey, M. (2002). Hydrogenases: Hydrogen-activating enzymes. Chembiochem A European Journal Of Chemical Biology **3**(2-3): 153-160.

Friedrich, M. W., Pommerenke, B., Seifert R., Krüger M. (2007). Unexpected Microbial Diversity in Anaerobically Methane-oxidizing Mats of the Black Sea. AGU Fall Meeting 2007 - San Francisco, USA (2007). Abstract: #B51D-06

Fürst, J. A. (1995). The Planctomycetes: emerging models for microbial ecology, evolution and cell biology. Microbiology **141**(7): 1493-1506.

Fürst, J. A. (2005). Intracellular compartmentation in Planctomycetes. Annual Review of Microbiology. **59:** 299-328.

Fukui, M., Suh, J., Yonezawa, Y. and Urushigawa, Y. (1997). Major substrates for microbial sulfate reduction in the sediments of Ise Bay, Japan. Ecological Research **12**(2): 201-209.

Goñi, M. A. and Eglinton, T. I. (1996). Stable carbon isotopic analyses of lignin-derived CuO oxidation products by isotope ratio monitoring gas chromatography mass spectrometry (irm-GC-MS). Organic Geochemistry **24**(6-7): 601-615.

Grossi, V., Cravo-Laureau, C., Méou, A., Raphel, D., Garzino, F. and Hirschler-Réa, A. (2007). Anaerobic 1-Alkene Metabolism by the Alkane- and Alkene-Degrading

Sulfate Reducer *Desulfatibacillum aliphaticivorans* Strain CV2803^T. Applied and Environmental Microbiology **73**(24): 7882-7890.

Grossi V., Hirschler-Réa A., Schaeffer P. Cravo-Laureau C (2011). Bacterial formation of(di)ether lipids: a state of the art. 25th International Meeting on Organic Geochemistry 2011 – Interlaken, Switzerland (2011). Book of Abstracts, p104.

Hallam, S. J., Girguis, P. R., Preston, C. M., Richardson, P. M. and DeLong, E. F. (2003). Identification of methyl coenzyme M reductase A (mcrA) genes associated with methane-oxidizing archaea. Applied and Environmental Microbiology **69**(9): 5483-5491.

Hallam, S. J., Putnam, N., Preston, C. M., Detter, J. C., Rokhsar, D., Richardson, P. M. and DeLong, E. F. (2004). Reverse methanogenesis: Testing the hypothesis with environmental genomics. Science **305**(5689): 1457-1462.

Hanson, R. S. and Hanson, T. E.(1996). Methanotrophic bacteria. Microbiological Reviews **60**(2): 439-471.

Härtner, T., Straub, K. L. and Kannenberg, E. (2005). Occurrence of hopanoid lipids in anaerobic *Geobacter* species. FEMS Microbiology Letters **243**(1): 59-64.

Hattori, S. (2008). Syntrophic acetate-oxidizing microbes in methanogenic environments. Microbes and Environments **23**(2): 118-127.

Hayes, J. M. (1993). Factors controlling C-13 contents of sedimentary organic-compounds - principles and evidence. Marine Geology **113**(1-2): 111-125.

Hayes, J. M. (2001). Fractionation of carbon and hydrogen isotopes in biosynthetic processes. Stable Isotope Geochemistry **43**: 225-277.

Heijs, S. K., Aloisi, G., Bouloubassi, I., Pancost, R. D., Pierre, C., Sinninghe Damsté, J. S., Gottschal, J. C., van Elsas, J. D. and Forney, L. J. (2006). Microbial community structure in three deep-sea carbonate crusts. Microbial Ecology **52**(3): 451-462.

Heijs, S. K., Haese, R. R., van der Wielen, P., Forney, L. J. and van Elsas, J. D. (2007). Use of 16S rRNA gene based clone libraries to assess microbial communities potentially involved in anaerobic methane oxidation in a Mediterranean cold seep. Microbial Ecology **53**(3): 384-398.

Heuer, V. B., Pohlman, J. W., Torres, M. E., Elvert, M. and Hinrichs, K.-U. (2009). The stable carbon isotope biogeochemistry of acetate and other dissolved carbon species in deep subseafloor sediments at the northern Cascadia Margin. Geochimica et Cosmochimica Acta **73**(11): 3323-3336.

Hinrichs, K. U., Hayes, J. M., Sylva, S. P., Brewer, P. G. and DeLong, E. F. (1999). Methane-consuming archaebacteria in marine sediments. Nature **398**(6730): 802-805.

Hinrichs, K.-U., Summons, R. E., Orphan, V. J., Sylva, S. P. and Hayes, J. M. (2000). Molecular and isotopic analysis of anaerobic methane-oxidizing communities in marine sediments. Organic Geochemistry **31**: 1685-1701.

Hinrichs, K.-U. and Boetius, A. (2002). The anaerobic oxidation of methane: new insights in microbial ecology and biogeochemistry. Wefer, G., Billet, D., Hebbeln D. et al. (Eds.). Ocean Margin Systems, Heidelberg, Springer-Verlag**:** 457-477.

Hoefs, M. J. L., Schouten, S., De Leeuw, J. W., King, L. L., Wakeham, S. G. and Sinninghe Damsté, J. S. (1997). Ether lipids of planktonic archaea in the marine water column. Applied and Environmental Microbiology **63**(8): 3090-3095.

Hoehler, T. M., Alperin, M. J., Albert, D. B. and Martens, C. S. (1994). Field and laboratory studies of methane oxidation in an anoxic marine sediment: Evidence for a methanogen-sulfate reducer consortium. Global Biogeochemical Cycles **8**(4): 451-463.

Hoehler, T. M., Alperin, M. J., Albert, D. B. and Martens, C. S. (1998). Thermodynamic control on hydrogen concentrations in anoxic sediments. Geochimica et Cosmochimica Acta **62**(10): 1745-1756.

Hoehler, T. M., Alperin, M. J., Albert, D. B. and Martens, C. S. (2001). Apparent minimum free energy requirements for methanogenic archaea and sulfate-reducing bacteria in an anoxic marine sediment. FEMS Microbiology Ecology **38**(1): 33-41.

Holler, T., Widdel, F., Knittel, K., Amann, R., Kellermann, M. Y., Hinrichs, K.-U., Teske, A., Boetius, A. and Wegener, G. (2011a). Thermophilic anaerobic oxidation of methane by marine microbial consortia. ISME Journal **5**(12): 1946-1956.

Holler, T., Wegener, G., Niemann, H., Deusner, C., Ferdelman, T. G., Boetius, A., Brunner, B. and Widdel, F. (2011b). Carbon and sulfur back flux during anaerobic microbial oxidation of methane and coupled sulfate reduction. Proceedings of the National Academy of Sciences of the United States of America doi: 10.1073/pnas.1106032108

Holzer, G., Oró, J. and Tornabene, T. G. (1979). Gas chromatographic-mass spectrometric analysis of neutral lipids from methanogenic and thermoacidophilic bacteria. Journal of Chromatography **186**: 795-809.

Holzer, G. U., Kelly, P. J. and Jones, W. J. (1988). Analysis of lipids from a hydrothermal vent methanogen and associated vent sediment by supercritical fluid chromatography. Journal of Microbiological Methods **8**(3): 161-173.

Horita, J. and Berndt, M. E. (1999). Abiogenic Methane Formation and Isotopic Fractionation Under Hydrothermal Conditions. Science **285**(5430): 1055-1057.

House, C. H., Orphan, V. J., Turk, K. A., Thomas, B., Pernthaler, A., Vrentas, J. M. and Joye, S. B. (2009). Extensive carbon isotopic heterogeneity among methane seep microbiota. Environmental Microbiology **11**(9): 2207-2215.

Huber, R., Rossnagel, P., Woese, C. R., Rachel, R., Langworthy, D. E. and Stetter, K. O. (1996). Formation of ammonium from nitrate during chemolithoautotrophic growth of the extremely thermophilic bacterium *Ammonifex degensii* gen. nov. sp. nov. Systematic and Applied Microbiology **19**: 40-49.

Huber, R., Wilharm, T., Huber, D., Trincone, A., Burggraf, S., König, H., Rachel, R., Rockinger, I., Fricke, H. and Stetter, K. O. (1992). *Aquifex pyrophilus* gen. nov. sp. nov., represents a novel group of marine hyperthermophilic hydrogen-oxidizing bacteria. Systematic and Applied Microbiology **15**: 340-351.

Imkamp, F. and Müller, V. (2001). Acetogenic Bacteria. eLS, John Wiley & Sons, Ltd.

Inagaki, F., Nunoura, T., Nakagawa, S., Teske, A., Lever, M., Lauer, A., Suzuki, M., Takai, K., Delwiche, M., Colwell, F. S., Nealson, K. H., Horikoshi, K., D'Hondt, S. and Jorgensen, B. B. (2006). Biogeographical distribution and diversity of microbes in methane hydrate-bearing deep marine sediments, on the Pacific Ocean Margin. Proceedings of the National Academy of Sciences of the United States of America **103**(8): 2815-2820.

IPCC (2007) The Physical Science Basis. Contribution of Working Group I to the Fourth Assessment Report of the Intergovernmental Panel on Climate Change. In: Solomon, S. *et al.* (Eds.). Cambridge University Press, Cambridge, United Kingdom and New York, NY, USA, pp. 996.

Jagersma, G. C., Meulepas, R. J. W., Heidkamp-de Jong, I., Gieteling, J., Klimiuk, A., Schouten, S., Sinninghe Damsté, J. S., Lens, P. N. L., and Stams A. J. M. (2009). Microbial diversity and community structure of a highly active anaerobic methane-oxidizing sulfate-reducing enrichment. Environmental Microbiology **11** (12): 3223-3232.

Jormakka, M., Byrne, B. and Iwata, S. (2003). Formate dehydrogenase – a versatile enzyme in changing environments. Current Opinion in Structural Biology **13**(4): 418-423.

Kannenberg, E. L. and Poralla, K. (1999). Hopanoid biosynthesis and function in bacteria. Naturwissenschaften **86**(4): 168-176.

Kasting, J. F. (2005). Methane and climate during the Precambrian era. Precambrian Research **137**(3-4): 119-129.

Kellermann M. Y., Wegener G., Lin Y.-S., Yoshinaga M. Y., Holler T., Elvert M., Hinrichs K.-U. (2011). Tracing ^{13}C-labelled inorganic carbon into intact polar lipids of thermophilic anaerobic methanotrophs provides new insights into pathways of archaeal lipid biosynthesis. 25th International Meeting on Organic Geochemistry 2011 – Interlaken, Switzerland. Book of Abstracts, p. 135.

Klenk, H.-P., Clayton, R. A., Tomb, J.-F., White, O., Nelson, K. E., Ketchum, K. A., Dodson, R. J., Gwinn, M., Hickey, E. K., Peterson, J. D., Richardson, D. L., Kerlavage, A. R., Graham, D. E., Kyrpides, N. C., Fleischmann, R. D., Quackenbush, J., Lee, N. H., Sutton, G. G., Gill, S., Kirkness, E. F., Dougherty, B. A., McKenney, K., Adams, M. D., Loftus, B., Peterson, S., Reich, C. I., McNeil, L. K., Badger, J. H., Glodek, A., Zhou, L., Overbeek, R., Gocayne, J. D., Weidman, J. F., McDonald, L., Utterback, T., Cotton, M. D., Spriggs, T., Artiach, P., Kaine, B. P., Sykes, S. M., Sadow, P. W., D'Andrea, K. P., Bowman, C., Fujii, C., Garland, S. A., Mason, T. M., Olsen, G. J., Fraser, C. M., Smith, H. O., Woese, C. R. and Venter, J. C. (1997). The complete genome sequence of the hyperthermophilic, sulphate-reducing archaeon *Archaeoglobus fulgidus*. Nature **390**(6658): 364-370.

Knittel, K., Lösekann, T., Boetius, A., Kort, R. and Amann, R. (2005). Diversity and distribution of methanotrophic archaea at cold seeps. Applied and Environmental Microbiology **71**(1): 467-479.

Knittel, K. and Boetius, A. (2009). Anaerobic Oxidation of Methane: Progress with an Unknown Process. Review of Microbiology **63:** 311-334.

Koga, Y., Nishihara, M., Morii, H. and Akagawa-Matsushita, M. (1993). Ether polar lipids of methanogenic bacteria: structures, comparative aspects, and biosyntheses. Microbiological Reviews **57**(1): 164-182.

Koga, Y. and Morii, H. (2005). Recent advances in structural research on ether lipids from archaea including comparative and physiological aspects. Bioscience Biotechnology and Biochemistry **69**(11): 2019-2034.

Kohnen, M. E. L., Schouten, S., Sinninghe Damsté, J. S., de Leeuw, J. W., Merritt, D. A. and Hayes, J. M. (1992). Recognition of Paleobiochemicals by a Combined Molecular Sulfur and Isotope Geochemical Approach. Science **256**(5055): 358-362.

Konhauser K. (2007). Introduction to Geomicrobiology. Blackwell Science.

Krüger, M., Meyerdierks, A., Glockner, F. O., Amann, R., Widdel, F., Kube, M., Reinhardt, R., Kahnt, J., Bocher, R., Thauer, R. K. and Shima, S. (2003). A conspicuous nickel protein in microbial mats that oxidize methane anaerobically. Nature **426**(6968): 878-881.

Krüger, M., Blumenberg, M., Kasten, K., Wieland, A., Layla, K., Klock, J.-H., Michaelis, W. and Seifert, R. (2008). A novel, multi-layered methanotrophic microbial mat system growinig on the sediment of the Black Sea. Environmental Microbiology **10**(8): 1934-1947.

Krull, E. S. and Retallack, G. J. (2000). $\delta^{13}C$ depth profiles from paleosols across the Permian-Triassic boundary: Evidence for methane release. Geological Society of America Bulletin **112**(9): 1459-1472.

Kvenvolden, K. A. (1998). A primer on the geological occurrence of gas hydrate. Geological Society, London, Special Publications **137**(1): 9-30.

Kvenvolden, K. A. and Rogers, B. W. (2005). Gaia's breath - global methane exhalations. Marine and Petroleum Geology **22**(4): 579-590.

Langworthy, T. A. (1977). Long-chain diglycerol tetraethers from *Thermoplasma acidophilum*. Biochimica et Biophysica Acta **487**(1): 37-50.

Langworthy, T. A. and Pond, J. L. (1986). Archaebacterial ether lipids and chemotaxonomy. Systematic and Applied Microbiology **7**(2-3): 253-257.

Lee, M. J. and Zinder, S. H. (1988). Isolation and Characterization of a Thermophilic Bacterium Which Oxidizes Acetate in Syntrophic Association with a Methanogen and Which Grows Acetogenically on H_2-CO_2. Applied Environmental Microbiology **54**(1): 124-129.

Lloyd, K. G., Alperin, M. J. and Teske, A. (2011). Environmental evidence for net methane production and oxidation in putative ANaerobic MEthanotrophic (ANME) archaea. Environmental Microbiology: **13**(9): 2548-2564.

Lösekann, T., Knittel, K., Nadalig, T., Fuchs, B., Niemann, H., Boetius, A. and Amann, R. (2007). Diversity and Abundance of Aerobic and Anaerobic Methane Oxidizers at the Haakon Mosby Mud Volcano, Barents Sea. Applied Environmental Microbiology **73**(10): 3348-3362.

Madigan, M.T., Martinko, J.M., Parker, J., (2002) *Biology of Microorganisms*. Prentice Hall International, Englewood Cliffs, N.J., USA.

Manefield, M., Whiteley, A. S., Ostle, N., Ineson, P. and Bailey, M. J. (2002). Technical considerations for RNA-based stable isotope probing: an approach to associating microbial diversity with microbial community function. Rapid Communications in Mass Spectrometry **16**(23): 2179-2183.

Manquin, B. P., Morgan, J. A., Ju, J. Y., Muller-Spath, T. and Clark, D. S. (2004). Production of C_{35} isoprenoids depends on H_2 availability during cultivation of the hyperthermophile Methanococcus jannaschii. Extremophiles **8**(1): 13-21.

Martin, W. F. (2012). Hydrogen, metals, bifurcating electrons, and proton gradients: The early evolution of biological energy conservation. FEBS Letters **586**(5): 485-493.

McDonald, I. R., Radajewski, S. and Murrell, J. C. (2005). Stable isotope probing of nucleic acids in methanotrophs and methylotrophs: A review. Organic Geochemistry **36**(5): 779-787.

Meuer, J., Kuettner, H. C., Zhang, J. K., Hedderich, R. and Metcalf, W. W. (2002). Genetic analysis of the archaeon Methanosarcina barkeri Fusaro reveals a central role for Ech hydrogenase and ferredoxin in methanogenesis and carbon fixation. Proceedings of the National Academy of Sciences of the United States of America **99**(8): 5632-5637.

Meulepas, R. J. W., Jagersma, C. G., Khadem, A. F., Stams, A. J. M. and Lens, P. N. L. (2010). Effect of methanogenic substrates on anaerobic oxidation of methane and sulfate reduction by an anaerobic methanotrophic enrichment. Applied Microbiology and Biotechnology **87**(4): 1499-1506.

Meyerdierks, A., Kube, M., Lombardot, T., Knittel, K., Bauer, M., Glockner, F. O., Reinhardt, R. and Amann, R. (2005). Insights into the genomes of archaea mediating the anaerobic oxidation of methane. Environmental Microbiology **7**(12): 1937-1951.

Meyerdierks, A., Kube, M., Kostadinov, I., Teeling, H., Glöckner, F. O., Reinhardt, R. and Amann, R. (2010). Metagenome and mRNA expression analyses of anaerobic methanotrophic archaea of the ANME-1 group. Environmental Microbiology **12**(2): 422-439.

Michaelis, W., Albrecht, P. (1979). Molecular fossils of archaebacteria in kerogen. Naturwissenschaften **66**(8): 420-422.

Michaelis, W., Seifert, R., Nauhaus, K., Treude, T., Thiel, V., Blumenberg, M., Knittel, K., Gieseke, A., Peterknecht, K., Pape, T., Boetius, A., Amann, R., Jørgensen, B. B., Widdel, F., Peckmann, J., Pimenov, N. V. and Gulin, M. B. (2002). Microbial reefs in the Black Sea fueled by anaerobic oxidation of methane. Science **297**(5583): 1013-1015.

Miller, T. L. and Wolin, M. J. (1985). *Methanosphaera stadtmaniae* gen-nov, sp-nov - A species that forms methane by reducing methanol with hydrogen. Archives of Microbiology **141**(2): 116-122.

Miroshnichenko, M. L., Kostrikina, N. A., Chernyh, N. A., Pimenov, N. V., Tourova, T. P., Antipov, A. N., Spring, S., Stackebrandt, E. and Bonch-Osmolovskaya, E. A. (2003). *Caldithrix abyssi* gen. nov., sp nov., a nitrate-reducing, thermophilic, anaerobic bacterium isolated from a Mid-Atlantic Ridge hydrothermal vent, represents a novel bacterial lineage. International Journal of Systematic and Evolutionary Microbiology **53**: 323-329.

Mitterer, R. M. (2010). Methanogenesis and sulfate reduction in marine sediments: A new model. Earth and Planetary Science Letters **295**(3-4): 358-366.

Moran, J. J., House, C. H., Thomas, B. and Freeman, K. H. (2007). Products of trace methane oxidation during nonmethyltrophic growth by Methanosarcina. Journal of Geophysical Research **112**(G2): 1-7.

Moran, J. J., Beal, E. J., Vrentas, J. M., Orphan, V. J., Freeman, K. H. and House, C. H. (2008). Methyl sulfides as intermediates in the anaerobic oxidation of methane. Environmental Microbiology. **10**(1), 162–173.

Muyzer, G. and Stams, A. J. M. (2008). The ecology and biotechnology of sulphate-reducing bacteria. Nature Reviews Microbiology **6**(6): 441-454.

Mycke, B., Narjes, F. and Michaelis, W. (1987). Bacteriohopanetetrol from Chemical Degradation of an Oil-Shale Kerogen. Nature **326**(6109): 179-181.

Nanninga, H. J. and Gottschal, J. C. (1986). Isolation of a sulfate-reducing bacterium growing with methanol. FEMS Microbiology Letters **38**(2): 125-130.

Nauhaus, K. (2003). Mikrobiologische Studien zur anaeroben Oxidation von Methan (AOM). PhD-Thesis, Universität Bremen, Fachbereich Biologie/Chemie.

Nauhaus, K., Boetius, A., Krüger, M. and Widdel, F. (2002). In vitro demonstration of anaerobic oxidation of methane coupled to sulphate reduction in sediment from a marine gas hydrate area. Environmental Microbiology **4**(5): 296-305.

Nauhaus, K., Treude, T., Boetius, A. and Krüger, M. (2005). Environmental regulation of the anaerobic oxidation of methane: a comparison of ANME-I and ANME-II communities. Environmental Microbiology **7**(1): 98-106.

Nauhaus, K., Albrecht, M., Elvert, M., Boetius, A. and Widdel, F. (2007). In vitro cell growth of marine archaeal-bacterial consortia during anaerobic oxidation of methane with sulfate. Environmental Microbiology **9**(1): 187-196.

Nedashkovskaya, O. I., Kim, S. B., Hoste, B., Shin, D. S., Beleneva, I. A., Vancanneyt, M. and Mikhailov, V. V. (2007). *Echinicola vietnamensis* sp. nov., a member of the phylum Bacteroidetes isolated from seawater. International Journal of Systematic and Evolutionary Microbiology **57**(4)**:** 761-763.

Neufeld, J. D., Dumont, M. G., Vohra, J. and Murrell, J. C. (2007). Methodological Considerations for the Use of Stable Isotope Probing in Microbial Ecology. Microbial Ecology **53**(3): 435-442.

Niemann, H., Lösekann, T., de Beer, D., Elvert, M., Nadalig, T., Knittel, K., Amann, R., Sauter, E. J., Schluter, M., Klages, M., Foucher, J. P. and Boetius, A. (2006). Novel microbial communities of the Haakon Mosby mud volcano and their role as a methane sink. Nature **443**(7113): 854-858.

Niemann, H. and Elvert, M. (2008). Diagnostic lipid biomarker and stable carbon isotope signatures of microbial communities mediating the anaerobic oxidation of methane with sulphate. Organic Geochemistry **39**(12): 1668-1677.

Nunoura, T., Oida, H., Miyazaki, J., Miyashita, A., Imachi, H. and Takai, K. (2008). Quantification of mcrA by fluorescent PCR in methanogenic and methanotrophic microbial communities. FEMS Microbiology Ecology **64**(2): 240-247.

Nunoura, T., Oida, H., Toki, T., Ashi, J., Takai, K. and Horikoshi, K. (2006). Quantification of mcrA by quantitative fluorescent PCR in sediments from methane seep of the Nankai Trough. FEMS Microbiology Ecology **57**(1): 149-157.

Oppermann, B. I., Michaelis, W., Blumenberg, M., Frerichs, J., Schulz, H. M., Schippers, A., Beaubien, S. E. and Krüger, M. (2010). Soil microbial community changes as a result oflong-term exposure to a natural CO_2 vent. Geochimica et Cosmochimica Acta **74**(9): 2697-2716.

Orcutt, B., Boetius, A., Elvert, M., Samarkin, V. and Joye, S. B. (2005). Molecular biogeochemistry of sulfate reduction, methanogenesis and the anaerobic oxidation of methane at Gulf of Mexico cold seeps. Geochimica et Cosmochimica Acta **69**(17): 4267-4281.

Orcutt, B., Samarkin, V., Boetius, A. and Joye, S. (2008). On the relationship between methane production and oxidation by anaerobic methanotrophic communities from cold seeps of the Gulf of Mexico. Environmental Microbiology **10**(5): 1108-1117.

Oremland, R. S. and Polcin, S. (1982). Methanogenesis and sulfate reduction - competitive and noncompetitive substrates in estaurine sediments. Applied and Environmental Microbiology **44**(6): 1270-1276.

Orphan, V. J., House, C. H., Hinrichs, K. U., McKeegan, K. D. and DeLong, E. F. (2001a). Methane-consuming archaea revealed by directly coupled isotopic and phylogenetic analysis. Science **293**(5529): 484-487.

Orphan, V. J., Hinrichs, K. U., Ussler, W., Paull, C. K., Taylor, L. T., Sylva, S. P., Hayes, J. M. and Delong, E. F. (2001b). Comparative analysis of methane-oxidizing archaea

andsulfate-reducing bacteria in anoxic marine sediments. Applied and Environmental Microbiology **67**(4): 1922-1934.

Orphan, V. J., House, C. H., Hinrichs, K. U., McKeegan, K. D. and DeLong, E. F. (2002). Multiple archaeal groups mediate methane oxidation in anoxic cold seep sediments. Proceedings of the National Academy of Sciences of the United States of America **99**(11): 7663-7668.

Ourisson, G. and Rohmer, M. (1992). Hopanoids. 2. Biohopanoids: a novel class of bacterial lipids. Accounts of Chemical Research **25**: 403-408.

Pachiadaki, M. G., Lykousis, V., Stefanou, E. G. and Kormas, K. A. (2010). Prokaryotic community structure and diversity in the sediments of an active submarine mud volcano (Kazan mud volcano, East Mediterranean Sea). FEMS Microbiology Ecology **72**(3): 429-444.

Pancost, R. D., Bouloubassi, I., Aloisi, G., Sinninghe Damsté, J. S. and Medinaut Shipboard Sci, P. (2001). Three series of non-isoprenoidal dialkyl glycerol diethers in cold-seep carbonate crusts. Organic Geochemistry **32**(5): 695-707.

Pancost, R. D., Hopmans, E. C. and Sinninghe Damsté, J. S. (2001). Archaeal lipids in Mediterranean cold seeps: molecular proxies for anaerobic methane oxidation. Geochimica et Cosmochimica Acta **65**(10): 1611-1627.

Pancost, R. D. and Sinninghe Damsté, J. S. (2003). Carbon isotopic compositions of prokaryotic lipids as tracers of carbon cycling in diverse settings. Chemical Geology **195**(1-4): 29-58.

Penning, H. and Conrad, R. (2006). Effect of Inhibition of Acetoclastic Methanogenesis on Growth of Archaeal Populations in an Anoxic Model Environment. Applied Environmental Microbiology **72**(1): 178-184.

Pernthaler, A., Dekas, A. E., Brown, C. T., Goffredi, S. K., Embaye, T. and Orphan, V. J. (2008). Diverse syntrophic partnerships from-deep-sea methane vents revealed by direct cell capture and metagenomics. Proceedings of the National Academy of Sciences of the United States of America **105**(19): 7052-7057.

Phelps, T. J., Conrad, R. and Zeikus, J. G. (1985). Sulfate-Dependent Interspecies H_2 Transfer between Methanosarcina barkeri and Desulfovibrio vulgaris during Coculture Metabolism of Acetate or Methanol. Applied Environmental Microbiology **50**(3): 589-594.

Radajewski, S., Ineson, P., Parekh, N. R. and Murrell, J. C. (2000). Stable-isotope probing as a tool in microbial ecology. Nature **403**: 646-649.

Raghoebarsing, A. A., Pol, A., van de Pas-Schoonen, K. T., Smolders, A. J. P., Ettwig, K. F., Rijpstra, W. I. C., Schouten, S., Sinninghe Damsté, J. S., Op den Camp, H. J. M., Jetten, M. S. M. and Strous, M. (2006). A microbial consortium couples anaerobic methane oxidation to denitrification. Nature **440**(7086): 918-921.

Ragsdale, S. W. and Pierce, E. (2008). Acetogenesis and the Wood–Ljungdahl pathway of CO_2 fixation. Biochimica et Biophysica Acta **1784**(12): 1873-1898.

Reeburgh, W. S. (1976). Methane Consumption in Cariaco Trench Waters and Sediments. Earth and Planetary Science Letters **28**(3): 337-344.

Reeburgh, W. S., Ward, B. B., Whalen, S. C., Sandbeck, K. A., Kilpatrick, K. A. and Kerkhof, L. J. (1991). Black Sea methane geochemistry. Deep-Sea Research **38**: S1189-S1210.

Reeburgh, W. S. (2007). Oceanic methane biogeochemistry. Chemical Reviews **107**(2): 486-513.

Reitner, J., Peckmann, J., Reimer, A., Schumann, G. and Thiel, V. (2005). Methane-derived carbonate build-ups and associated microbial communities at cold seeps on the lower Crimean shelf (Black Sea). Facies **51**: 71-84.

Ring, M. W., Schwaer, G., Thiel, V., Dickschat, J. S., Kroppenstedt, R. M., Schulz, S. and Bode, H. B. (2006). Novel iso-branched ether lipids as specific markers of developmental sporulation in the myxobacterium *Myxococcus xanthus*. Journal of Biological Chemistry **281**(48): 36691-36700.

Roberts, Z. E., Meldrum, F. C. and Pancost, R. D. (2008). The archaeal lipid composition of partially lithified cold seep mats. Organic Geochemistry **39**(8): 1000-1006.

Rohmer, M., Bisseret, P. and Neunlist, S. (1992). The hopanoids, prokaryotic triterpenoids and precursors of ubiquitous molecular fossils. J. M. Moldowan, P. Albrecht and R. P. Philp (Eds.). Biological Markers in Sediments and Petroleum, Prentice-Hall, Englewood Cliffs**:** 1-17.

Rosa-Putra, S., Nalin, R., Domenach, A.-M. and Rohmer, M. (2001). Novel hopanoids from *Frankia* spp. and related soil bacteria - Squalene cyclization and significance of geological biomarkers revisited. European Journal of Biochemistry **268**: 4300-4306.

Rossel, P. E., Lipp, J. S., Fredricks, H. F., Arnds, J., Boetius, A., Elvert, M. and Hinrichs, K.-U. (2008). Intact polar lipids of anaerobic methanotrophic archaea and associated bacteria. Organic Geochemistry **39**(8): 992-999.

Rossel, P. E., Elvert, M., Ramette, A., Boetius, A. and Hinrichs, K.-U. (2011). Factors controlling the distribution of anaerobic methanotrophic communities in marine environments: Evidence from intact polar membrane lipids. Geochimica et Cosmochimica Acta **75**(1): 164-184.

Rütters, H., Sass, H., Cypionka, H. and Rullkötter, J. (2001). Monoalkylether phospholipids in the sulfate-reducing bacteria *Desulfosarcina variabilis* and *Desulforhabdus amnigenus*. Archives of Microbiology **176**: 435-442.

Rütters, H., Sass, H., Cypionka, H. and Rullkötter, J. (2002). Microbial communities in a Wadden Sea sediment core - clues from analyses of intact glyceride lipids, and released fatty acids. Organic Geochemistry **33**: 803-816.

Rütters, H., Sass, H., Cypionka, H. and Rullkötter, J. (2002). Phospholipid analysis as a tool to study complex microbial communities in marine sediments. Journal of Microbiological Methods **48**(2-3): 149-160.

Sakai, S., Imachi, H., Hanada, S., Ohashi, A., Harada, H. and Kamagata, Y. (2008). *Methanocella paludicola* gen. nov., sp. nov., a methane-producing archaeon, the first isolate of the lineage 'Rice Cluster I', and proposal of the new archaeal order Methanocellales ord. nov. International Journal of Systematic and Evolutionary Microbiology **58**(4): 929-936.

Sakai, S., Takaki, Y., Shimamura, S., Sekine, M., Tajima, T., Kosugi, H., Ichikawa, N., Tasumi, E., Hiraki, A. T., Shimizu, A., Kato, Y., Nishiko, R., Mori, K., Fujita, N., Imachi, H. and Takai, K. (2011). Genome Sequence of a Mesophilic Hydrogenotrophic Methanogen Methanocella paludicola, the First Cultivated Representative of the Order Methanocellales. Plos One **6**(7): e22898.

Sakata, S., Hayes, J. M., McTaggart, A. R., Evans, R. A., Leckrone, K. J. and Togasaki, R. K. (1997). Carbon isotopic fractionation associated with lipid biosynthesis by a cyanobacterium: Relevance for interpretation of biomarker records. Geochimica et Cosmochimica Acta **61**(24): 5379-53889.

Scheller, S., Goenrich, M., Boecher, R., Thauer, R. K. and Jaun, B. (2010). The key nickel enzyme of methanogenesis catalyses the anaerobic oxidation of methane. Nature **465**(7298): 606-608.

Schink, B. and Zeikus, J. G. (1980). Microbial methanol formation - a major end product of pectin metabolism. Current Microbiology **4**(6): 387-389.

Schink, B. and Zeikus, J. G. (1982). Microbial ecology of pectin decomposition in anoxic lake-sediments. Journal of General Microbiology **128** (FEB): 393-404.

Schouten, S., Hopmans, E. C., Pancost, R. D. and Sinninghe Damsté, J. S. (2000). Widespread occurrence of structurally diverse tetraether membrane lipids: Evidence for the ubiquitous presence of low-temperature relatives of hyperthermophiles. Proceedings of the National Academy of Sciences of the United States of America **97**(26): 14421-14426.

Schouten, S., Wakeham, S. G., Hopmans, E. C. and Sinninghe Damsté, J. S. (2003). Biogeochemical evidence that thermophilic archaea mediate the anaerobic oxidation of methane. Applied and Environmental Microbiology **69**(3): 1680-1686.

Schreiber, L., Holler, T., Knittel, K., Meyerdierks, A., Amann,R. (2010). Identification of the dominant sulfate-reducing bacterial partner of anaerobic methanotrophs of the ANME-2 clade. Environmental Microbiology **12**(8): pp. 2327-2340(2314).

Seifert, R., Nauhaus, K., Blumenberg, M., Krüger, M. and Michaelis, W. (2006). Methane dynamics in a microbial community of the Black Sea traced by stable carbon isotopes in vitro. Organic Geochemistry **37**(10): 1411-1419.

Sherwood Lollar, B., Westgate, T. D., Ward, J. A., Slater, G. F. and Lacrampe-Couloume, G. (2002). Abiogenic formation of alkanes in the Earth's crust as a minor source for global hydrocarbon reservoirs. Nature **416**: 522-524.

Shima, S., Krüger, M., Weinert, T., Demmer, U., Kahnt, J., Thauer, R. K. and Ermler, U. (2011). Structure of a methyl-coenzyme M reductase from Black Sea mats that oxidize methane anaerobically. Nature **481**(7379): 98-101

Siegert, M. (2010). Methanogenic hydrocarbon degradation and methane oxidation in benthic microbial communities. PhD-Thesis, Gottfried Leibniz Universität Hannover, Naturwissenschaftliche Fakultät.

Simoneit, B. R. T. (2002). Molecular indicators (biomarkers) of past life. Anatomical Record **268**(3): 186-195.

Sinensky, M. (1974). Homeoviscous Adaptation - A Homeostatic Process that Regulates the Viscosity of Membrane Lipids in *Escherichia coli*. Proceedings of the National Academy of Sciences of the United States of America **71**(2): 522-525.

Sinninghe Damsté, J. S., Rijpstra, W. I. C., Hopmans, E. C., Prahl, F. G., Wakeham, S. G. and Schouten, S. (2002). Distribution of membrane lipids of planktonic Crenarchaeota in the Arabian Sea. Applied and Environmental Microbiology **68**(6): 2997 - 3002.

Sinninghe Damsté, J. S., Rijpstra, I. C., Schouten, S., Fuerst, J. A., Jetten, M. S. M. and Strous, M. (2004). The occurrence of hopanoids in planctomycetes: implications for the sedimentary biomarker record. Organic Geochemistry **35**(5): 561-566.

Sinninghe Damsté, J. S., Rijpstra, W. I. C., Hopmans, E. C., Weijers, J. W. H., Foesel, B. U., Overmann, J. and Dedysh, S. N. (2011). 13,16-Dimethyl Octacosanedioic Acid (iso-Diabolic Acid), a Common Membrane-Spanning Lipid of Acidobacteria Subdivisions 1 and 3. Applied and Environmental Microbiology **77**(12): 4147-4154.

Sirevag, R., Buchanan, B. B., Berry, J. A. and Troughton, J. H. (1977). Mechanisms of CO_2 fixation in bacterial photosynthesis studied by the carbon isotope fractionation technique. Archives of Microbiology **112**: 35-38.

So, C. M., Phelps, C. D. and Young, L. Y. (2003). Anaerobic Transformation of Alkanes to Fatty Acids by a Sulfate-Reducing Bacterium, Strain Hxd3. Applied and Environmental Microbiology **69**(7): 3892-3900.

Sørensen, K. B., Finster, K. and Ramsing, N. B. (2001). Thermodynamic and kinetic requirments in anaerobic methane oxidizing consortia exlude hydrogen, acetate, and methanol as possible electron shuttles. Microbial Ecology **42**(1): 1-10.

Stadnitskaia, A., Muyzer, G., Abbas, B., Coolen, M. J. L., Hopmans, E. C., Baas, M., van Weering, T. C. E., Ivanov, M. K., Poludetkina, E. and Sinninghe Damsté, J. S. (2005). Biomarker and 16S rDNA evidence for anaerobic oxidation of methane and related carbonate precipitation in deep-sea mud volcanoes of the Sorokin Trough, Black Sea. Marine Geology **217**(1-2): 67-96.

Stams, A. J. M. and Plugge, C. M. (2009). Electron transfer in syntrophic communities of anaerobic bacteria and archaea. Nature Review Microbiology **7**(8): 568-577.

Strittmatter, A., W, Liesegang, H., Rabus, R., Decker, I., Amann, J., Andres, S., Henne, A., Fricke, W. F., Martinez-Arias, R., Bartels, D., Goesmann, A., Krause, L., Pühler, A., Klenk, H.-P., Richter, M., Schüler, M., Glöckner, F. O., Meyerdierks, A., Gottschalk, G. and Amann, R. (2009). Genome sequence of *Desulfobacterium autotrophicum* HRM2, a marine sulfate reducer oxidizing organic carbon completely to carbon dioxide. Environmental Microbiology **11:** 1038-1055.

Strous, M. and Jetten, M. S. M. (2004). Anaerobic oxidation of methane and ammonium. Annual Review in Microbiology **58**: 99-117.

Sturt, H. F., Summons, R. E., Smith, K., Elvert, M. and Hinrichs, K.-U. (2004). Intact polar membrane lipids in prokaryotes and sediments deciphered by high-performance liquid chromatography/electrospray ionization multistage mass spectrometry - new biomarkers for biogeochemistry and microbial ecology. Rapid Communications in Mass Spectrometry **18**(6): 617-628.

Summons, R. E., Jahnke, L. L. and Roksandic, Z. (1994). Carbon isotopic fractionation in lipids from methanotrophic bacteria: Relevance for interpretation of the geochemical record of biomarkers. Geochimica et Cosmochimica Acta **58**(13): 2853-2863.

Takano, Y., Chikaraishi, Y., Ogawa, N. O., Nomaki, H., Morono, Y., Inagaki, F., Kitazato, H., Hinrichs, K.-U. and Ohkouchi, N. (2010). Sedimentary membrane lipids recycled by deep-sea benthic archaea. Nature Geoscience **3**:858-861.

Takeuchi, M., Yoshioka, H., Seo, Y., Tanabe, S., Tamaki, H., Kamagata, Y., Takahashi, H. A., Igari, S., Mayumi, D. and Sakata, S. (2011). A distinct freshwater-adapted subgroup of ANME-1 dominates active archaeal communities in terrestrial subsurfaces in Japan. Environmental Microbiology **13**(12): 3206-3218.

Teske, A., Hinrichs, K.-U., Edgcomb, V., de Vera Gomez, A., Kysela, D., Sylva, S. P., Sogin, M. L. and Jannasch, H. W. (2002). Microbial diversity of hydrothermal sediments in the Guaymas Basin: Evidence for anaerobic methanotrophic communities. Applied and Environmental Microbiology **68**(4): 1994-2007.

Thauer, R. K. (1998). Biochemistry of methanogenesis: a tribute to Marjory Stephenson: 1998 Marjory Stephenson Prize Lecture. Microbiology **144**(9): 2377-2406.

Thauer, R. K., Jungermann, K. and Decker, K. (1977). Energy-conservation in chemotropic anaerobic bacteria. Bacteriological Reviews **41**(1): 100-180.

Thauer, R. K., Kaster, A.-K., Seedorf, H., Buckel, W. and Hedderich, R. (2008). Methanogenic archaea: ecologically relevant differences in energy conservation. Nature Review Microbiology **6**(8): 579-591.

Thauer, R. K., Kaster, A. K., Goenrich, M., Schick, M., Hiromoto, T. and Shima, S. (2010). Hydrogenases from Methanogenic Archaea, Nickel, a Novel Cofactor, and H_2 Storage. Annual Review of Biochemistry **79**: 507-536.

Thauer, R. K. and Shima, S. (2008). Methane as fuel for anaerobic microorganisms. Incredible Anaerobes: from Physiology to Genomics to Fuels **1125**: 158-170.

Thiel, V., Blumenberg, M., Pape, T., Seifert, R. and Michaelis, W. (2003). Unexpected occurrence of hopanoids at gas seeps in the Black Sea. Organic Geochemistry **34**(1): 81-87.

Thiel, V., Jenisch, A., Wörheide, G., Löwenberg, A., Reitner, J. and Michaelis, W. (1999). Mid-chain branched alkanoic acids from "living fossil" demosponges: A link to ancient sedimentary lipids? Organic Geochemistry **30**(1): 1-14.

Thiel, V., Peckmann, J., Seifert, R., Wehrung, P., Reitner, J. and Michaelis, W. (1999). Highly isotopically depleted isoprenoids: Molecular markers for ancient methane venting. Geochimica et Cosmochimica Acta **63**(23/24): 3959-3966.

Tornabene, T. G., Langworthy, T. A., Holzer, G. and Oró, J. (1979). Squalenes, phytanes and other isoprenoids as major neutral lipids of methanogenic and thermoacidophilic "archaebacteria". Journal of Molecular Evolution **13**: 73-83.

Tornabene, T. G., Wolfe, R. S., Balch, W. E., Holzer, G., Fox, G. E. and Oró, J. (1978). Phytanyl-glycerol ethers and squalenes in the archaebacterium *Methanobacterium thermoautotrophicum*. Journal of Molecular Evolution **11**(259-266): 259-266.

Treude, T., Knittel, K., Blumenberg, M., Seifert, R. and Boetius, A. (2005). Subsurface microbial methanotrophic mats in the Black Sea. Applied and Environmental Microbiology **71**(10): 6375-6378.

Treude, T., Orphan, V., Knittel, K., Gieseke, A., House, C. H. and Boetius, A. (2007). Consumption of methane and CO_2 by methanotrophic microbial mats from gas seeps of the anoxic Black Sea. Applied and Environmental Microbiology **73**(7): 2271-2283.

Valentine, D. L. and Reeburgh, W. S. (2000). New perspectives on anaerobic methane oxidation. Environmental Microbiology **2**(5): 477-484.

Valentine, D. L. (2002). Biogeochemistry and microbial ecology of methane oxidation in anoxic environments: A review. Antonie van Leeuwenhoek **81**(1-4): 271-282.

Valentine, D. L., Sessions, A. L., Tyler, S. C. and Chidthaisong, A. (2004). Hydrogen isotope fractionation during H_2/CO_2 acetogenesis: hydrogen utilization efficiency and the origin of lipid-bound hydrogen. Geobiology **2**(3): 179-188.

van der Meer, M. T. J., Schouten, S., Ward, D. M., Geenevasen, J. A. J. and Sinninghe Damsté, J. S. (1999). All-*cis* hentriaconta-9,15,22-triene in microbial mats formed by the phototrophic prokaryote Chloroflexus. Organic Geochemistry **30**(12): 1585-1587.

Vorholt, J., Kunow, J., Stetter, K. O. and Thauer, R. K. (1995). Enzymes and coenzymes of the carbon monoxide dehydrogenase pathway for autotrophic CO_2-fixation in *Archaeoglobus lithotrophicus* and the lack of carbon monoxide dehydrogenase in the heterotrophic *A. profundus*. Archives of Microbiology **163**(2): 112-118.

Wahlen, M. (1993). The global methane cycle. Annual Review of Earth and Planetary Sciences **21**: 407-426.

Webster, N. S. and Hill, R. T. (2001). The culturable microbial community of the Great Barrier Reef sponge *Rhopaloeides odorabile* is dominated by an α-Proteobacterium. Marine Biology **138**: 843-851.

Webster, G., Yarram, L., Freese, E., Köster, J., Sass, H., Parkes, R. J. and Weightman, A. J. (2007). Distribution of candidate division JS1 and other Bacteria in tidal sediments of the German Wadden Sea using targeted 16S rRNA gene PCR-DGGE. FEMS Microbiology Ecology **62**(1): 78-89.

Webster, G., Sass, H., Cragg, B. A., Gorra, R., Knab, N. J., Green, C. J., Mathes, F., Fry, J. C., Weightman, A. J. and Parkes, R. J. (2011). Enrichment and cultivation of prokaryotes associated with the sulphate–methane transition zone of diffusion-controlled sediments of Aarhus Bay, Denmark, under heterotrophic conditions. FEMS Microbiology Ecology: **77**(2): 248-263.

Wegener, G., Niemann, H., Elvert, M., Hinrichs, K.-U. and Boetius, A. (2008). Assimilation of methane and inorganic carbon by microbial communities mediating the anaerobic oxidation of methane. Environmental Microbiology **10**(9): 2287–2298.

Wegener, G., Shovitri, M., Knittel, K., Niemann, H., Hovland, M. and Boetius, A. (2008b). Biogeochemical processes and microbial diversity of the Gullfaks and Tommeliten methane seeps (Northern North Sea). Biogeosciences **5**(4): 1127-1144.

Weijers, J. W. H., Schouten, S. and Sinninghe Damsté, J. S. (2007). Bacterial tetraether membrane lipids in soils and their application in palaeoenvironmental studies. Geochimica et Cosmochimica Acta **71**(15): A1098-A1098.

Welander, P. V. and Metcalf, W. W. (2005). Loss of the mtr operon in Methanosarcina blocks growth on methanol, but not methanogenesis, and reveals an unknown methanogenic pathway. Proceedings of the National Academy of Sciences of the United States of America **102**(30): 10664-10669.

Whiticar, M. J. (1999). Carbon and hydrogen isotope systematics of bacterial formation and oxidation of methane. Chemical Geology **161**: 291-314.

Widdel, F. and Bak, F. (1992). Gram negative mesophilic sulfate-reducing bacteria. Balows, A., Trüper, H. G., Dworkin, M., Harder, W. and Schleifer, K.-H. (Eds.). The Prokaryotes New York, Springer**:** 3352-3378.

Woese, C. R. and Olsen, G. J. (1986). Archachaebacterial phylogeny - perspectives on the urkingdoms. Systematic and Applied Microbiology **7**(2-3): 161-177.

Wood, H. (1991). Life with CO or CO_2 and H_2 as a source of carbon and energy. The FASEB journal **5**(2): 156-163.

Yamada, T., Sekiguchi, Y., Imachi, H., Kamagata, Y., Ohashi, A. and Harada, H. (2005). Diversity, localization, and physiological properties of filamentous microbes

belonging to Chloroflexi subphylum I in mesophilic and thermophilic methanogenic sludge granules. Applied and Environmental Microbiology **71**(11): 7493-7503.

Yanagawa, K., Sunamura, M., Lever, M. A., Morono, Y., Hiruta, A., Ishizaki, O., Matsumoto, R., Urabe, T. and Inagaki, F. (2011). Niche Separation of Methanotrophic Archaea (ANME-1 and-2) in Methane-Seep Sediments of the Eastern Japan Sea Offshore Joetsu. Geomicrobiology Journal **28**(2): 118-129.

VII. Appendix

A.1 Medium for sulphate-reducing bacteria (Widdel and Bak, 1992), modified by Krüger (Black Sea Medium)

The incubation experiments with labelled ^{13}C-methane were conducted by the BGR. The media for all other experiments were prepared in this work.

A.1.1 Trace Element Solution (SL 10) - 1 l

Compounds	Weight [mg]	Concentration [mM]
HCl	12.5 ml (37.5 %)	
$FeCl_2 \times 4H_2O$	2100	0.01
$ZnCl_2$	30	0.22
$MnCl_2 \times 4H_2O$	100	0.505
H_3BO_3	190	0.3
$CoCl_2 \times 6H_2O$	24	0.116
$CuCl_2 \times 2H_2O$	2	0.012
$NiCl_2 \times 6H_2O$	144	0.061
$Na_2MoO_4 \times 2H_2O$	36	0.202
ad H_2O dest.	1000 ml	

At first, $FeCl_2$ was dissolved in HCl. This solution was dissolved in water, followed by the dissolution of the other salts. The trace element solution was sterilely filtered.

A.1.2 $NaHCO_3$ Solution - 30 mM

30 ml deionised water was fumigated with nitrogen and shook at first of all. Than 2.52 g $NaHCO_3$ were added. This solution was fumigated with CO_2 and autoclaved.

A.1.3 Basal Medium

Compounds	Concentration [mM]
$MgSO_4 \times 7H_2O$	16.23
KBr	0.756
KCl	8.85
$CaCl_2 \times 2H_2O$	1.02
$MgCl_2 \times 6H_2O$	15.25
NaCl	318
ad H_2O dest.	

The salts were dissolved in distilled water and autoclaved at 121 °C for 30 minutes. After autoclavation, the solution was fumigated with N_2/CO_2 (90:10). The solution has a salinity of about 2.4 %.

A.1.4 N+P-Solution - 1 l

Compounds	Weight [g]	Concentration [mM]
NH_4Cl	4	75
KH_2PO_4	5	37

The N+P-Solution was fumigated with nitrogen and CO_2.

A.1.5 Vitamine-Solution - 1 l

A.1.5.1 NaP-Buffer - 100 ml

0.356 g Na_2HPO_4 and 0.27 g NaH_2PO_4 were dissolved in 100 ml NaP-buffer in distilled water (pH 7.1). The solution was sterilely filtered.

A.1.5.2 Thiamine-Solution

10 mg Thiamine (vitamine B1) were dissolved in 100ml NaP-buffer (25 mM, pH 3.4 - 3.7). The solution was sterilely filtered.

A.1.5.3 Vitamine B12 (Cyanocobalamine) - Solution

5 mg vitamine B12 were dissolved in distilled water. The solution was autoclaved.

A.1.5.4 Riboflavin

5 mg Riboflavin were resolved in 100 ml acetate (20 mM). The solution was autoclaved.

A.1.5.5 Selenite / Wolframate - Solution - 1l

Compounds	Weight [mg]	Concentration [mM]
NaOH	400	10
$Na_2WO_4x\ 2H_2O$	8	0.033
$Na_2SeO_3\ x\ 5H_2O$	6	0.023

The solution was autoclaved.

A.1.5.6 5-Vitamine-Solution - 1 l

Compounds	Weight [mg]	Cocnentration [mM]
NaP-buffer (20 mM)	100 ml	2
4-Aminobenzoat	4	0.022
D (+) Biotin	1	0.004
Nicotinsäure	10	0.081
Calcium D (+) panthothenat	5	0.023
Pyridoxamine dihydrochlorid	15	0.062
Lipoic acid	5	0.024

The solution was sterilely filtered.

A.1.5.7 Na_2S-Solution - 1 M

24 g $Na_2S\ x\ 9\ H_2O$ were dissolved in 100 ml anaerobic water (fumigated with N_2 and CO_2). The solution was autoclaved.

A.2 Correction of the $\delta^{13}C$-values of the biphytanes and C_{35}-isoprenoid hydrocarbons

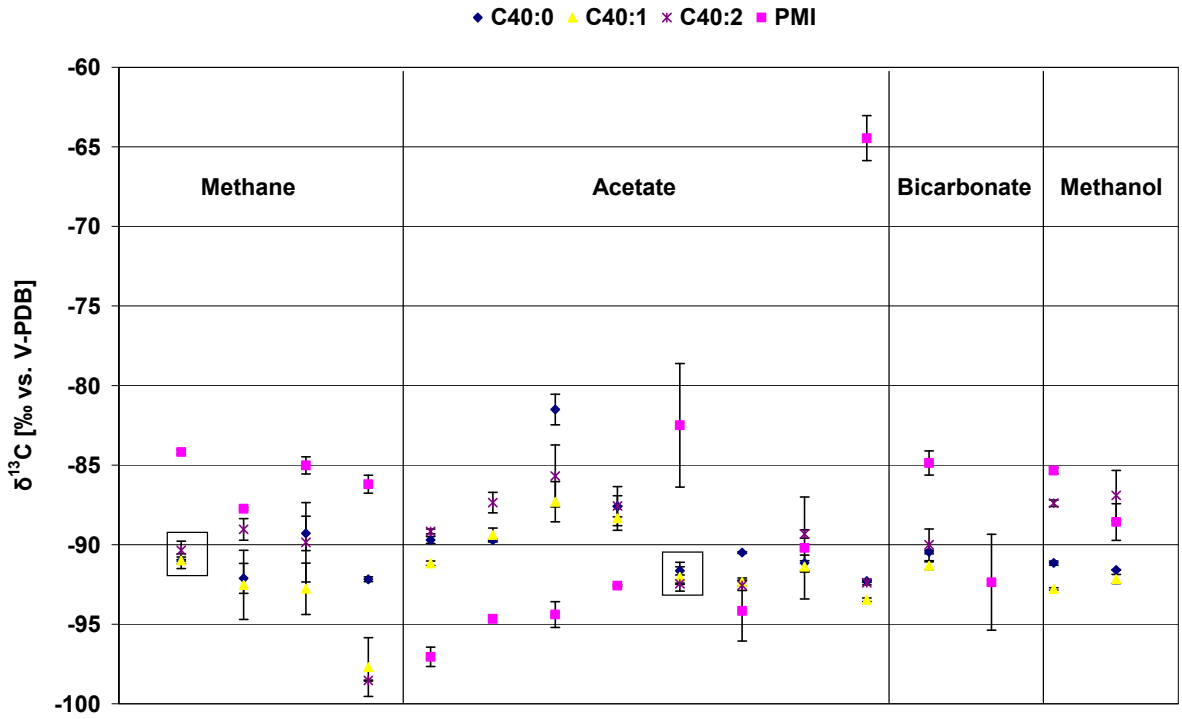

Figure A.2a: Correlation between the three isomers of the biphytanes and the saturated PMI. $\delta^{13}C$-values measured for the three isomers of the biphytanes are correlated to those of PMI within all experiments. The $\delta^{13}C$-values of the biphytanes, extracted from not incubated controls, are framed by the boxes.

Table A.2b: Corrected $\delta^{13}C$-values of the biphytanes.
Then notation of the samples is explained in Table 2.1. Numbers represent days of incubation.

Sample/ Compound	ML64	ML135	ML378	AcLM23	AcL23	AcLM56	AcL56	AcLM26	AcLMI26	BcLM	MeLM	MeL
C40:0	-95.7	-93.0	-94.2	-105.0	-102.7	-102.4	-100.6	-102.2	-98.2	-92.9	-93.3	-96.6
C40:1	-95.9	-93.2	-94.4	-105.2	-102.8	-102.6	-100.7	-102.3	-98.4	-93.0	-93.5	-96.7
C40:2	-95.8	-93.1	-94.3	-105.1	-102.7	-102.5	-100.6	-102.2	-98.3	-92.9	-93.4	-96.6

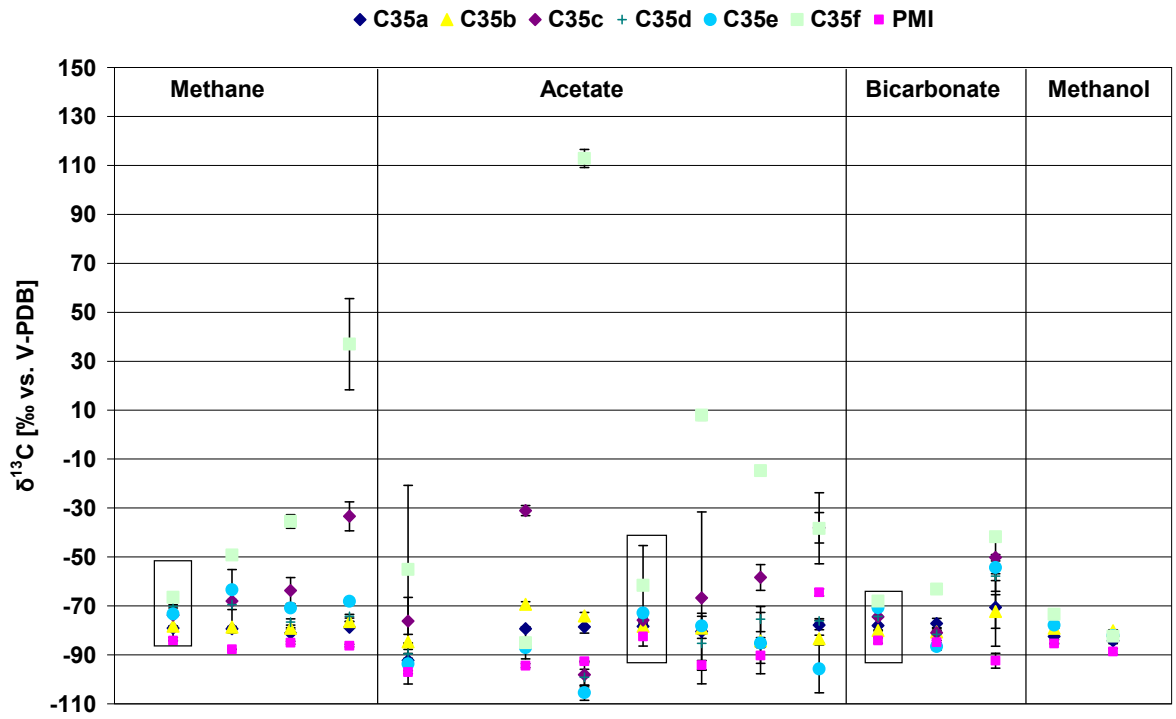

Figure A.2c: Correlation between the six isomers of the C_{35}-isoprenoid hydrocarbons and the saturated PMI. δ^{13}C-values measured for the six isomers of the C_{35}-isoprenoid hydrocarbons are correlated to those of PMI within all experiments. The δ^{13}C-values of the C_{35}-isoprenoid isomers, extracted from not incubated controls, are framed by the boxes.

Table A.2d: Corrected δ^{13}C-values of the C_{35}-isoprenoid hydrocarbons.
Then notation of the samples is explained in Table 2.1. Numbers represent the days of incubation.

Sample/ Compound	ML64	ML135	ML378	AcLM23	AcLM56	AcL56	AcLM26	AcLMI26	BcLM	BcL	MeLM	MeL
C35(a)	-82.6	-79.9	-81.1	-91.9	-89.2	-87.4	-89.0	-85.1	-79.7	-87.2	-80.2	-83.4
C35(b)	-83.0	-80.3	-81.4	-92.3	-89.6	-87.8	-89.4	-85.4	-80.1	-87.6	-80.6	-83.8
C35(c)	-78.8	-76.1	-77.3	-88.1	-85.4	-83.6	-85.2	-81.3	-75.9	-83.4	-76.4	-79.6
C35(d)	-77.2	-74.5	-75.7	-86.5	-83.9	-82.0	-83.6	-79.7	-74.3	-81.8	-74.8	-78.0
C35(e)	-76.4	-73.7	-74.9	-85.7	-83.1	-81.2	-82.8	-78.9	-73.5	-81.0	-74.0	-77.2
C35(f)	-69.5	-66.8	-68.0	-78.8	-76.2	-74.3	-75.9	-72.0	-66.6	-74.1	-67.1	-70.3

A.3 Calibration of the IRMS with a pure methane standard (100 %)

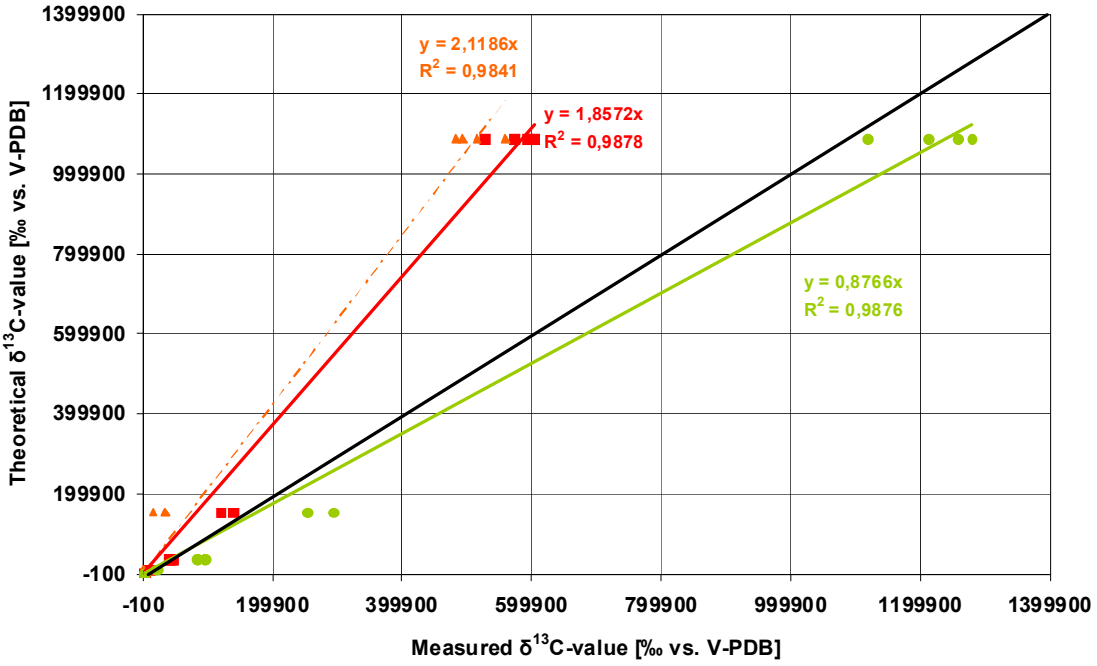

Figure A.3a: Calibration of the IRMS with a pure methane standard (100 %). Red squares show the measured δ^{13}C-values. Orange triangles describe the calculated regression. Green circles illustrate the corrected δ^{13}C-values multiplied with the correction value of 2.1186. The orange dotted line shows the regression.

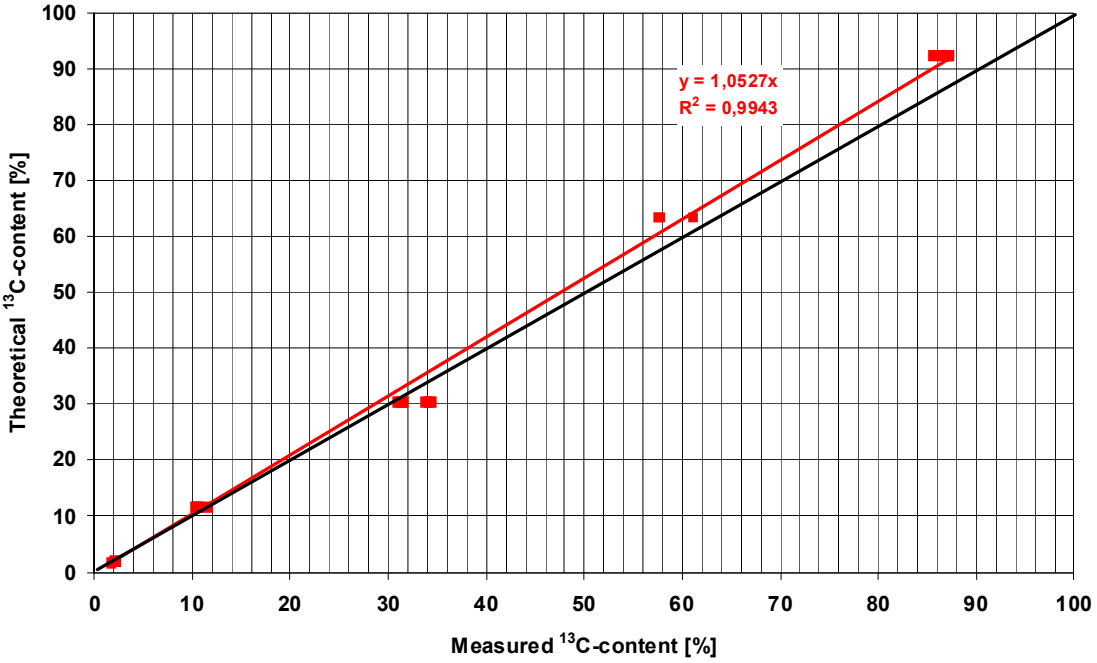

Figure A.3b: Calculation of ^{13}C-proportion [%] from the measured δ^{13}C-values. Red squares show ^{13}C-proportion [%] calculated from the corrected δ^{13}C-values.

A.4.1 Measured isotopic values [‰ vs. V-PDB] of the lipid biomarker molecules after incubation with different labelled substrates

Table A.4a: Measured isotopic values [‰ vs. V-PDB] of the lipid biomarker molecules from ANME-1 dominated communities after incubation with different labelled substrates ($^{13}CH_4$, $H^{13}CO_3^-$, $^{13}CH_3{}^{13}COO^-$, $^{13}CH_3OH$). n.a. - not analysed, * - acetate and methyl fluoride

Compound	$\delta^{13}C_{t0}$	$^{13}CH_4$			$H^{13}CO_3^- + CH_4$	$H^{13}CO_3^-$	$^{13}CH_3{}^{13}COO^- + CH_4$			$^{13}CH_3{}^{13}COO^- + CH_4 + CH_3F$	$^{13}CH_3{}^{13}COO^-$			$^{13}CH_3OH + CH_4$	$^{13}CH_3OH$
	[‰ vs. V-PDB]	$\delta^{13}C_{t64}$	$\delta^{13}C_{t135}$	$\delta^{13}C_{t378}$	$\delta^{13}C_{t64}$	$\delta^{13}C_{t64}$	$\delta^{13}C_{t23}$	$\delta^{13}C_{t26}$	$\delta^{13}C_{t56}$	$\delta^{13}C_{t26}$	$\delta^{13}C_{t23}$	$\delta^{13}C_{t26}$*	$\delta^{13}C_{t56}$	$\delta^{13}C_{t26}$	$\delta^{13}C_{t26}$
PMI:4	-83.7	-62.7	-13.7	97.0	-56.8	-79.5	-53.7	-52.0	35.1	-65.9	n.a.	-73.2	-55.2	-82.1	-80.6
PMI:5	-93.0	-25.4	69.0	276.5	-34.1	-55.6	114	119	395	40.7	n.a.	6.7	20.7	-22.8	9.1
C_{35}a	-85.4	-79.3	-81.1	-78.7	-77.2	-70.5	-92.3	-80.5	-79.3	-85.3	n.a.	-77.8	-78.6	-82.5	-84.2
C_{35}b	-87.9	-78.7	-79.2	-76.4	-80.6	-72.3	-84.7	-79.0	-69.4	-84.3	n.a.	-83.4	-74.0	-79.1	-80.1
C_{35}c	-91.0	-68.0	-63.7	-33.4	-80.9	-50.2	-76.2	-66.8	-31.1	-58.3	n.a.	-38.1	-98.1	n.a.	n.a.
C_{35}d	-91.0	-69.4	-76.6	-74.2	-81.6	-57.8	-89.6	-85.3	-85.7	-75.4	n.a.	-76.1	-99.2	-77.5	-81.7
C_{35}e	-90.3	-63.4	-70.8	-68.1	-86.5	-54.3	-93.6	-78.1	-87.0	-85.2	n.a.	-95.7	-105.4	-77.8	-82.0
C_{35}f	-79.1	-49.2	-35.5	36.9	-63.2	-41.7	-55.1	8.0	-85.0	-14.7	n.a.	-38.3	112.9	-73.5	n.a.
Archaeol	-78.2	-67.1	-45.9	-25.0	-37.6	-64.8	-48.6	-58.2	165	-74.2	-66.1	-76.7	-19.9	1454	3037
Archaeol:1	-73.8	-79.3	-59.9	-34.8	-78.7	-75.6	-61.1	-71.8	110	-81.2	-77.9	-81.2	-32.7	51.5	748
Biphytane	-70.2	-92.1	-89.3	-92.2	-90.5	n.a.	-89.7	-90.5	-81.5	-91.1	-89.7	-92.3	-87.6	-91.2	-91.6
Biphytane:1	-73.3	-92.5	-92.8	-97.7	-91.3	n.a.	-91.2	-92.3	-87.3	-91.4	-89.4	-93.5	-88.3	-92.8	-92.2
Biphytane:2	-66.5	-89.0	-89.9	-98.5	-90.0	n.a.	-89.2	-92.6	-85.7	-89.3	-87.4	-92.4	-87.6	-87.4	-86.9
16:1 MAGE	-95.9	-85.5	-98.0	-70.9	-101.0	-105.2	-72.1	-20.8	-28.6	-93.3	-49.8	-88.5	-57.2	-87.3	-100.7
***i/i*15DAGE**	-80.5	-80.4	-83.6	-80.1	-80.9	-81.0	-85.6	-86.8	-56.8	-83.4	-83.2	-84.4	-62.9	-82.4	-90.8
***i/ai*15DAGE**	-89.2	-84.9	-87.3	-84.8	-88.3	-87.2	-88.7	-89.8	-65.0	-87.1	-85.9	-87.5	-57.4	-88.2	n.a.
***ai/ai*15DAGE**	-88.0	-83.6	-85.8	-87.9	-87.9	-87.7	-88.1	-88.1	-79.0	-87.6	-85.8	-86.8	-73.9	-88.4	-90.4
Diploptene	-60.0	-69.3	-62.2	-29.0	n.a.	-34.0	22.8	150	143	174.1	n.a.	33.9	16.2	n.a.	n.a.
Hopanoic acid	-72.1	-73.5	-74.1	-76.5	-73.7	-73.6	-74.3	-73.5	-80.2	-74.1	-72.4	-72.6	-91.3	-73.6	-73.9
fa14:0	-72.6	-55.6	-37.1	23.0	-25.4	-54.5	167	2367	1966	2135	110	1489	3655	-68.5	-66.4
***i*fa15:0**	-85.0	-78.2	-73.0	-46.4	-23.7	-27.1	1163	1652	2162	1846	639	1562	3203	-64.9	-60.5
***ai*fa15:0**	-83.5	-75.8	-66.6	-47.7	-52.7	-64.8	283	489	808	477	159	442	1040	-70.9	-67.3
fa16:1ω7c	-56.1	-28.5	-3.6	183.1	117	121	7652	21251	24041	15028	3119	12809	40516	-23.1	-0.7
fa16:1ω5c	-65.2	-44.0	-29.9	93.2	29.1	17.7	1700	4961	7774	4840	598	5062	10284	-60.4	-50.1
fa16:0	-67.6	-36.7	-29.7	16.1	65.8	72.3	1710	9335	8924	7822	802	4374	16065	-41.5	-19.4
fa18:1ω9c	-73.7	-56.6	-24.6	46.9	-42.4	-44.1	801	2187	1939	882	241	730	n.a.	-63.2	-70.0
fa18:1ω7c	-77.8	n.a.	-47.2	n.a.	n.a.	n.a.	n.a.	n.a.	755	n.a.	n.a.	n.a.	2346	n.a.	n.a.
fa18	-73.3	-45.5	-42.0	-16.2	-73.7	-73.6	107	1438	28.1	396	-25.3	148	817	-66.3	-50.7

Table A.4b: Measured isotopic values [‰ vs. V-PDB] of the lipid biomarker molecules from ANME-2 dominated communities after incubation with different labelled substrates ($^{13}CH_4$, $H^{13}CO_3^-$, $^{13}CH_3{}^{13}COO^-$, $^{13}CH_3OH$). n.a, - not analysed, * - acetate and methyl fluoride

Compound	$\delta^{13}C_{t0}$	$^{13}CH_4$			$H^{13}CO_3^- + CH_4$	$H^{13}CO_3^-$	$^{13}CH_3{}^{13}COO^- + CH_4$			$^{13}CH_3{}^{13}COO^- + CH_4 + CH_3F$	$^{13}CH_3{}^{13}COO^-$			$^{13}CH_3OH + CH_4$	$^{13}CH_3OH$
	[‰ vs. V-PDB]	$\delta^{13}C_{t64}$	$\delta^{13}C_{t135}$	$\delta^{13}C_{t378}$	$\delta^{13}C_{t64}$	$\delta^{13}C_{t64}$	$\delta^{13}C_{t23}$	$\delta^{13}C_{t26}$	$\delta^{13}C_{t56}$	$\delta^{13}C_{t26}$	$\delta^{13}C_{t23}$	$\delta^{13}C_{t26}{}^*$	$\delta^{13}C_{t56}$	$\delta^{13}C_{t26}$	$\delta^{13}C_{t26}$
Crocetane	-108.5	-106.9	-106.9	-99.8	-106.0	-107.3	-114.7	-105.5	-99.3	-109.4	-117.0	-109.2	-112.0	-105.8	-107.7
PMI:4	-104.9	-67.3	-20.1	66.3	13.6	-108.1	24.7	31.9	13.0	-91.0	-98.0	-103.4	-92.9	-108.0	-106.8
PMI:5	-80.7	23.5	199	465	n.a.	-105.0	272	102	443	-3.6	-53.0	-72.4	-46.5	-66.1	47.9
Archaeol	-112.0	-96.2	-79.6	-30.6	-78.5	-103.2	-81.6	-47.2	-35.8	-94.0	-106.2	-96.1	-86.7	61.0	1107
HO-Archaeol	-113.8	-106.9	-104.7	-87.5	-94.8	-109.2	-113.4	-94.7	-105.3	-112.1	-116.5	-114.0	-115.3	-31.5	352
$C_{31:3}$a	-76.8	-64.2	n.a.	n.a.	n.a.	n.a.	-73.7	n.a.	n.a.	n.a.	-69.3			n.a.	n.a.
$C_{31:3}$b	-86.0	-68.7	-57.1	n.a.	n.a.	-47.1	-47.4	40.6	n.a.	-22.4	-52.5	-31.4		n.a.	n.a.
$C_{31:3}$c	-86.3	-78.4	-65.8	n.a.	-37.3	-45.4	-17.1	117.3	n.a.	12.2	-27.8	2.6	68.8	n.a.	n.a.
16MAGE c	-78.8	-74.4	-36.7	-32.1	-66.0	-79.6	-72.2	-25.6	-62.2	-83.9	-85.6	-86.6	-61.6	-84.1	-82.8
***i/i*15DAGE**	-88.6	-81.4	-87.9	-85.7	-92.1	-89.4	-84.8	-77.6	-32.9	-76.3	-62.9	-78.9	-27.7	-96.2	-94.5
***i/ai*15 DAGE**	-82.6	-82.1	-94.3	-99.8	-102.0	-93.4	-95.0	-81.2	-86.8	-80.5	-76.4	-83.9	-68.8	-98.7	-96.3
***ai/ai*15 DAGE**	-90.5	-81.6	-90.4	-83.6	-97.9	-92.9	-71.2	-73.9	-36.9	-69.1	-50.0	-75.0	-31.0	-96.8	-94.9
fa14:0	-90.4	-58.2	-27.0	33.8	15.1	-89.2	102	507	239	238	10.0	267	232	-76.3	-80.2
***i*fa15:0**	-99.4	-73.7	-63.8	-13.2	-42.4	-21.1	1047	1122	1803	1244	957	1205	1701	-92.2	-84.3
***ai*fa15:0**	-93.6	-65.7	-54.5	14.5	-40.7	-6.1	504	438	941	373	438	463	1022	-86.8	-73.5
fa16:1ω7c	-86.1	-64.6	-47.2	0.5	-31.1	1.8	157	1616	299	1018	119	1163	1481	65.8	-82.8
fa16:1ω5c	-86.1	-59.9	-41.8	10.7	-11.6	-71.1	99.3	290	421	53.4	9.3	62.5	354	-74.9	-84.4
fa16:0	-79.2	-35.6	-15.8	41.6	26.2	99.1	212	2292	97	1478	264	1850	1507	46.9	-67.3
***cy*fa17ω5,6**	-91.5	-80.9	-72.5	-35.5	-91.3	-87.2	-20.4	102	18	-84.7	-34.5	-118.2	-0.3	-62.8	-88.1
fa18:1ω9c	-88.8	-75.3	-64.2	-23.5	-41.0	23.6	35.4	1832	159	1314	7.2	1345	286	54.4	-79.6
fa18:1ω7c	-84.0	-78.7	-72.8	n.a.	-32.0	25.3	n.a.	962	755.1	882	n.a.	721	2347	35.5	-95.8
fa18	-85.3	-34.0	-27.5	-30.4	-42.7	-9.6	221	106	521	145	38.4	239	699	-33.1	-80.0

A.4.2 Concentrations [$\mu g\, g_{TOC}^{-1}$] of the lipid biomarker molecules after incubation with different labelled substrates

Table A.4c: Concentrations [$\mu g\, g_{TOC}^{-1}$] of the lipid biomarker molecules from ANME-1 dominated communities after incubation with different labelled substrates ($^{13}CH_4$, $H^{13}CO_3^-$, $^{13}CH_3{}^{13}COO^-$, $^{13}CH_3OH$). n.a. - not analysed, * - acetate and methyl fluoride

Compound	$^{13}CH_4$			$H^{13}CO_3^-$ + CH_4	$H^{13}CO_3^-$	$^{13}CH_3{}^{13}COO^-$ + CH_4			$^{13}CH_3{}^{13}COO^-$ + CH_4 + CH_3F	$^{13}CH_3{}^{13}COO^-$			$^{13}CH_3OH$ + CH_4	$^{13}CH_3OH$
	C_{t64}	C_{t135}	C_{t378}	C_{t64}	C_{t64}	C_{t23}	C_{t26}	C_{t56}	C_{t26}	C_{t23}	C_{t26}	C_{t56}	C_{t26}	C_{t26}
PMI:4	19.3	15.3	57.0	56.6	74.2	54.8	47.0	42.6	62.4	49.4	28.9	43.8	49.1	118.2
PMI:5	1.9	2.5	5.3	4.6	5.6	3.9	3.3	2.1	4.8	3.0	2.4	2.1	2.1	7.1
C_{35}a	5.7	6.2	13.8	12.9	16.8	19.2	10.4	14.7	12.6	19.5	6.9	15.1	1.2	31.1
C_{35}b	21.7	20.8	55.2	65.1	84.8	60.6	49.0	46.2	63.0	60.0	32.4	49.0	10.3	126.8
C_{35}c	0.9	1.3	3.5	5.0	7.7	4.3	3.4	2.5	6.3	4.1	2.4	3.0	35.0	n.a.
C_{35}d	5.1	4.2	11.4	11.5	16.4	13.5	8.6	9.7	11.5	12.7	6.0	10.9	n.d.	28.6
C_{35}e	4.9	2.9	9.1	12.8	13.1	12.4	9.1	9.3	8.6	12.7	6.6	10.2	11.1	28.8
C_{35}f	27.5	2.6	6.2	11.1	10.7	7.9	7.3	6.6	9.3	8.7	5.5	7.0	4.7	n.a.
Archaeol	54.6	382.9	116.0	451.1	295.1	197.2	347.2	32.7	207.1	224.8	332.1	72.7	307.6	303.2
Archaeol:1	53.7	393.4	110.7	276.7	223.9	132.0	257.3	21.9	160.3	138.7	250.5	47.3	224.4	171.9
Biphytane	1020.5	912.7	388.1	1189.7	2056.8	425.2	927.5	692.2	1217.2	4209.2	1084.4	1379.8	460.0	746.2
Biphytane:1	865.7	772.0	332.6	944.7	1844.7	437.3	736.6	620.9	987.7	4162.1	1005.6	1274.3	405.5	594.8
Biphytane:2	563.0	910.5	108.3	281.4	550.5	127.9	198.9	186.4	283.8	1301.5	285.3	430.3	104.2	160.1
16:1MAGE	4.4	3.1	1.7	58.0	21.1	13.5	1.4	2.9	0.5	5.0	3.9	2.8	35.7	32.8
***i*/i15DAGE**	11.3	80.8	21.1	122.2	35.1	40.5	41.4	6.3	24.9	45.7	40.1	8.2	52.5	49.3
***i/ai*15DAGE**	23.9	196.0	60.5	222.0	104.2	94.6	125.3	18.0	75.1	113.1	122.3	23.3	129.5	127.7
***ai/ai*15DAGE**	70.9	510.7	154.5	595.7	338.7	275.0	382.0	51.4	241.9	318.3	382.1	70.8	393.1	396.1
Diploptene	0.7	3.9	3.8	n.a.	4.9	0.8	n.a.	2.5	3.7	2.1	0.4	2.6	n.a.	n.a.
Hopanoic acid	734.0	516.3	511.5	712.8	671.3	452.8	517.4	508.9	511.4	496.6	524.1	414.5	514.0	387.2
fa14:0	133.7	76.8	119.8	89.1	84.9	78.2	77.6	39.0	84.4	66.8	79.0	39.0	71.6	45.2
ifa15:0	347.3	238.2	307.6	340.8	321.4	91.3	253.7	141.7	281.6	85.3	262.3	141.7	248.1	169.2
aifa15:0	1319.8	861.0	1057.0	919.3	797.0	359.3	667.4	497.2	735.2	321.6	675.1	497.2	649.8	455.0
fa16:1w7c	180.6	79.5	97.3	130.2	128.9	24.0	111.7	80.8	152.0	22.4	118.0	80.8	96.8	75.5
fa16:1w5c	162.9	107.0	170.2	139.9	140.2	44.3	52.9	57.9	116.1	39.0	105.7	57.9	91.0	62.8
fa16:0	355.8	134.2	174.0	151.5	136.4	159.2	122.7	97.2	123.4	147.8	160.6	97.2	115.9	78.1
fa18:1w9c	413.9	275.6	458.0	50.5	62.7	114.0	212.5	56.5	258.2	101.8	218.1	56.5	343.7	255.8
fa18:1w7c	n.a.	28.9	77.6	n.a.	n.a.	4.1	n.a.	116.1	n.a.	n.a.	n.a.	116.1	n.a.	n.a.
fa18	182.7	53.6	157.2	712.8	671.3	111.0	46.5	30.8	47.9	96.7	136.3	30.8	49.8	46.1

Table A.4d: Concentrations [$\mu g\, g_{TOC}^{-1}$] of the lipid biomarker molecules from ANME-2 dominated communities after incubation with different labelled substrates ($^{13}CH_4$, $H^{13}CO_3^-$, $^{13}CH_3{}^{13}COO^-$, $^{13}CH_3OH$). n.a. - not analysed, * - acetate and methyl fluoride

Compound	$^{13}CH_4$			$H^{13}CO_3^-$ + CH_4	$H^{13}CO_3^-$	$^{13}CH_3{}^{13}COO^-$ + CH_4			$^{13}CH_3{}^{13}COO^-$ + CH_4 + CH_3F	$^{13}CH_3{}^{13}COO^-$			$^{13}CH_3OH$ + CH_4	$^{13}CH_3OH$
	C_{t64}	C_{t135}	C_{t378}	C_{t64}	C_{t64}	C_{t23}	C_{t26}	C_{t56}	C_{t26}	C_{t23}	C_{t26}*	C_{t56}	C_{t26}	C_{t26}
Crocetane	26.6	402.3	304.6	170.6	650.1	183.3	100.4	232.1	233.7	114.7	489.8	222.6	114.9	143.9
PMI:4	27.0	106.0	166.2	279.8	937.3	152.8	136.4	180.3	338.0	90.2	665.1	172.5	153.2	208.2
PMI:5	5.8	27.0	19.2	n.a.	56.4	27.6	7.9	31.9	19.0	15.8	38.2	32.6	6.4	8.8
Archaeol	1287.2	1418.4	890.0	1469.7	1257.0	1164.6	227.2	745.3	4601.7	697.2	1143.3	665.9	903.1	1105.8
HO-Archaeol	4549.9	1937.4	2757.3	5398.1	4183.5	3207.9	691.4	2358.9	10004.5	1925.1	4394.8	2105.8	3604.5	4009.8
$C_{31:3}$a	3.2	n.a.	n.a.	13.1	151.0	15.5	5.9	3.1	9.9	5.9	42.9	4.0	2.4	0.7
$C_{31:3}$b	6.7	7.5	n.a.	78.0	354.8	56.7	40.5	3.5	58.5	15.7	201.1	8.1	4.7	3.8
$C_{31:3}$c	5.4	5.2	n.a.	264.7	280.9	225.8	175.2	4.3	170.9	47.9	909.3	17.0	8.1	7.4
16MAGE(c)	79.7	88.3	297.5	42.4	58.1	141.7	280.5	496.7	1706.0	141.8	353.3	540.3	480.2	474.5
***i/i*15DAGE**	18.5	55.8	34.6	179.5	79.9	66.0	13.8	38.0	351.4	39.1	102.8	32.8	73.9	87.4
***i/ai*15DAGE**	83.33	53.2	39.3	217.2	51.4	69.6	9.4	45.7	225.4	43.8	55.5	38.5	75.2	55.8
***ai/ai*15DAGE**	96.1	161.9	119.9	211.6	155.1	200.3	27.8	138.2	857.2	131.6	218.2	119.6	127.6	164.5
fa14:0	131.9	856.1	830.4	513.7	686.1	669.6	354.6	2105.1	530.7	1425.3	523.8	965.3	372.3	482.3
ifa15:0	198.2	807.5	816.6	862.3	1116.2	521.3	520.9	1944.7	773.4	1327.6	752.2	907.8	583.5	759.6
aifa15:0	269.5	1149.8	1065.6	912.7	1229.5	663.9	555.1	2512.6	827.7	1921.0	819.3	1189.8	644.7	851.2
fa16:1w7c	973.7	2016.1	2100.7	1788.3	2247.7	1220.9	1048.8	4145.4	1576.6	3931.8	1374.8	2005.8	1129.4	1438.7
fa16:1w5c	1071.8	3238.8	2874.8	3400.9	4075.9	2573.5	2123.2	8329.5	3009.8	6560.2	2484.7	3924.8	2291.2	2878.7
fa16:0	498.5	649.1	663.7	682.3	754.7	717.9	389.4	1701.9	576.5	2122.9	542.8	817.7	424.0	538.2
cyfa17w5,6	413.0	1489.5	700.3	119.2	521.6	2600.8	133.7	1602.6	367.9	1775.1	386.8	814.6	175.4	367.6
fa18:1w9c	726.0	1271.2	1581.6	497.3	641.4	1037.0	314.2	3937.4	443.7	2486.2	415.2	1352.4	372.5	426.0
fa18:1w7c	244.2	25.6	n.a.	311.4	274.0	n.a.	189.4	60.7	230.0	n.a.	206.5	116.1	n.a.	n.a.
fa18	336.7	58.6	173.1	398.6	347.0	288.0	162.1	351.2	252.1	520.6	226.5	158.9	229.3	254.8

A.5 Abbreviations of investigated lipids

Croc.: crocetane *(2,6,11,15-tetramethylhexadecane)*
PMI:x: x-fold unsaturated 2,6,10,15,19-pentamethylicosene
HO-Arch.: *sn-2*-hydroxyarchaeol *(2-O-3-hydroxyphytanyl-3-O-phytanyl-sn-glycerol)*
Arch.: archaeal *(2,3-di-O-phytanyl-sn-glycerol)*
Arch:1: unsaturated archaeal *(2-O-3-phytenyl-3-O-phytanyl-sn-glycerol or 2-O-phytanyl-3-O-3-phyentyl-sn-glycerol)*
$C_{35:X}$ tentatively determined as *2,6,10,14,18,22,26*-heptmethyloctacosane (a, d = 5, b, e =6, c, f = 7 fold unsaturated)
$C_{40:0}$: straight biphytane after ether cleavage of GDGT *(3,7,11,15,18,22,26,30-octamethyl-dotriacontane)*
$C_{40:1}$: monopentacyclic biphytane after ether cleavage of GDGT 1-(1,5,8,12,16,20-hexamethyldocosyl)-3-(4-methylhexyl)-cyclopentane
$C_{40:2}$: dipentacyclic biphytane after ether cleavage of GDGT 1,1'-(1,5,8,12-tetramethyl-1,12-dodecandiyl)-bis[3-(4-methylhexyl)]-cyclopentane
16MAGE(x) (x: a, b, c) undetermined isomers of 1-*O*-hexadecyl-*sn*-glycerol,
16:1MAGE: unsaturated 1-*O*-hexadecyl-*sn*-glycerol
15DAGE: *1,2-di-O*-pentadecyl-*sn*-glycerol ethers (*i: iso*, *ai*: *anteiso*)
fa14:0: tetradecanoic acid
***i*fa15:0**: ω13-methyl tetradecanoic acid
***ai*fa15:0**: *ω12*-methyl tetradecanoic acid
fa16:1ω7c, **fa16:1ω5c**: *cis*-ω7- and *cis*-ω5-hexadecenoic acids
fa16:0: hexadecanoic acid
***cy*fa17:1ω5,6**: *ω5,6*-heptadecanoic acid
fa18:1ω9c, **fa18:1ω7c**: *cis*-ω9-, *cis-ω7*-octadecanoic acid
fa18:0: octadecanoic acid
hopan. acid: 17α(H),21β(H)-bishomohopanoic acid
$C_{31:3}$(a, b, c) - hentriacontatrien, constitutional isomers a-c

A.6 Abbreviations of the notation

ML - labelled methane
BcLM - labelled bicarbonate with methane
BcL - labelled bicarbonate
AcLM - labelled acetate with methane
AcL - labelled acetate
AcLMI - labelled acetate with methane and methyl fluoride
AcL - labelled acetate with methyl fluoride
MeLM - labelled methanol with methane
MeL - labelled methanol

A.7 Mass spectra of the compounds $C_{35:6}$b, $C_{35:7}$c, $C_{35:6}$e, $C_{35:7}$f

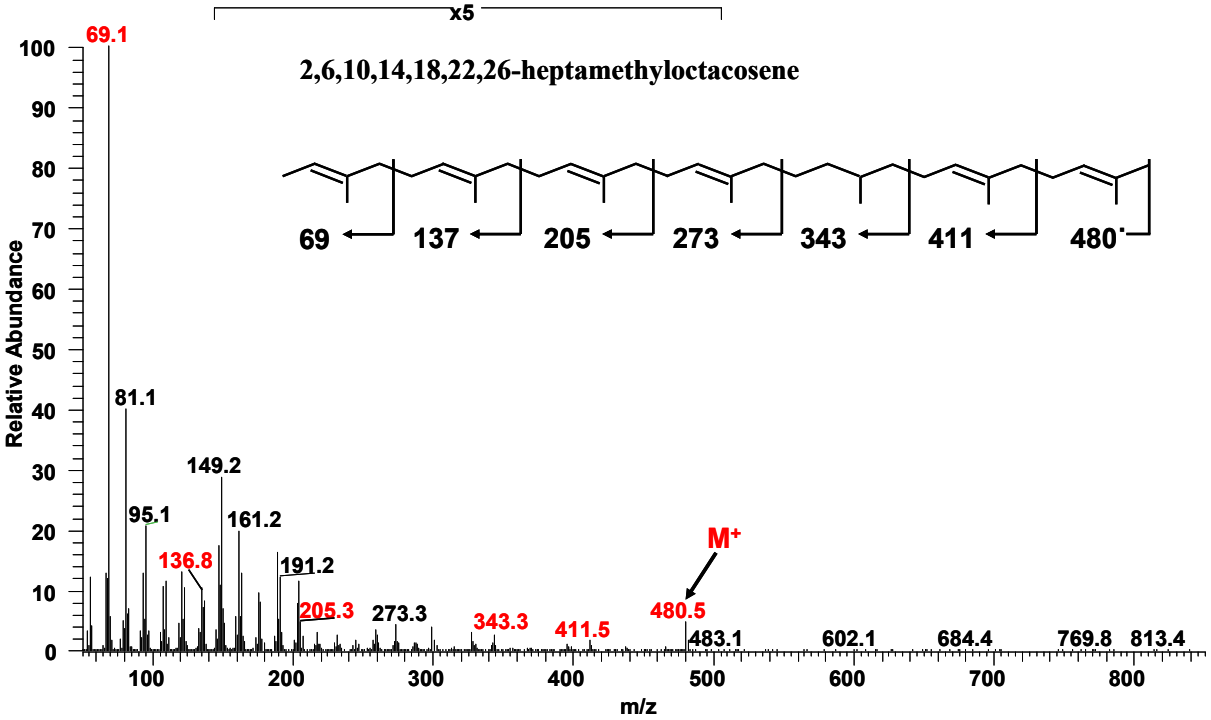

Figure A.7a: Spectrum of the C_{35}-isoprenoid hydrocarbon isomer $C_{35:6}$b with six double bonds. The spectrum was revealed with a GC-MS in the EI modus with -70 eV.

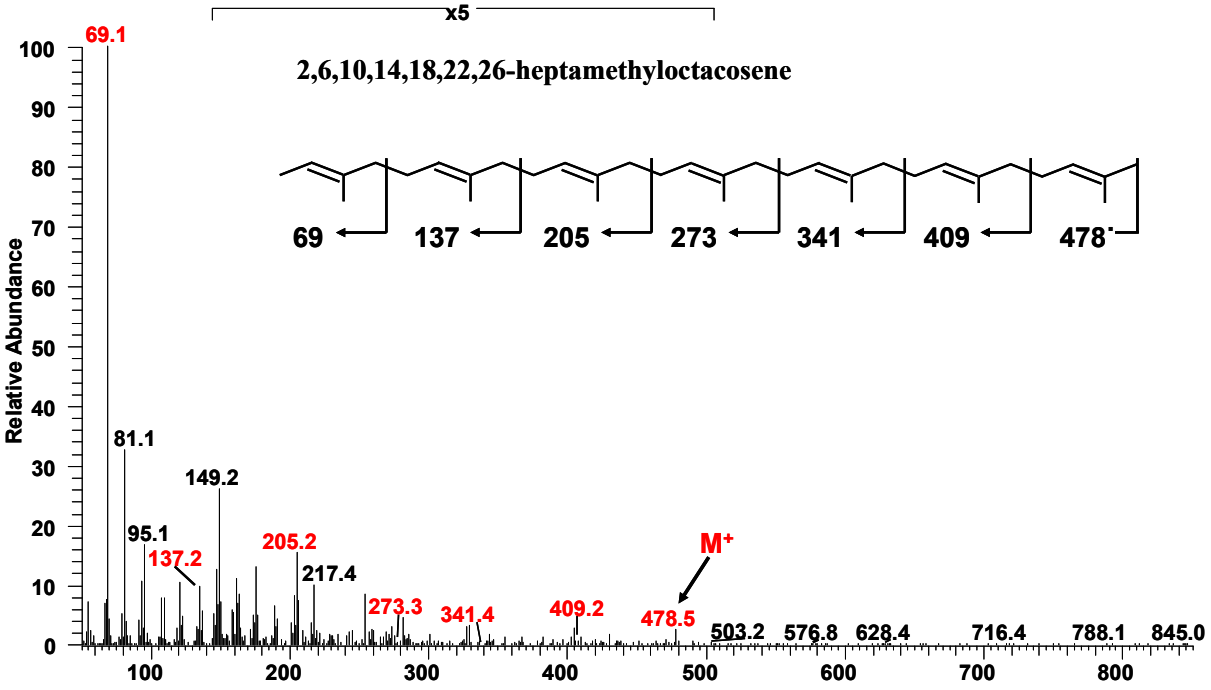

Figure A.7b: Spectrum of the C_{35}-isoprenoid hydrocarbon isomer $C_{35:7}$c with seven double bonds. The spectrum was revealed with a GC-MS in the EI modus with -70 eV.

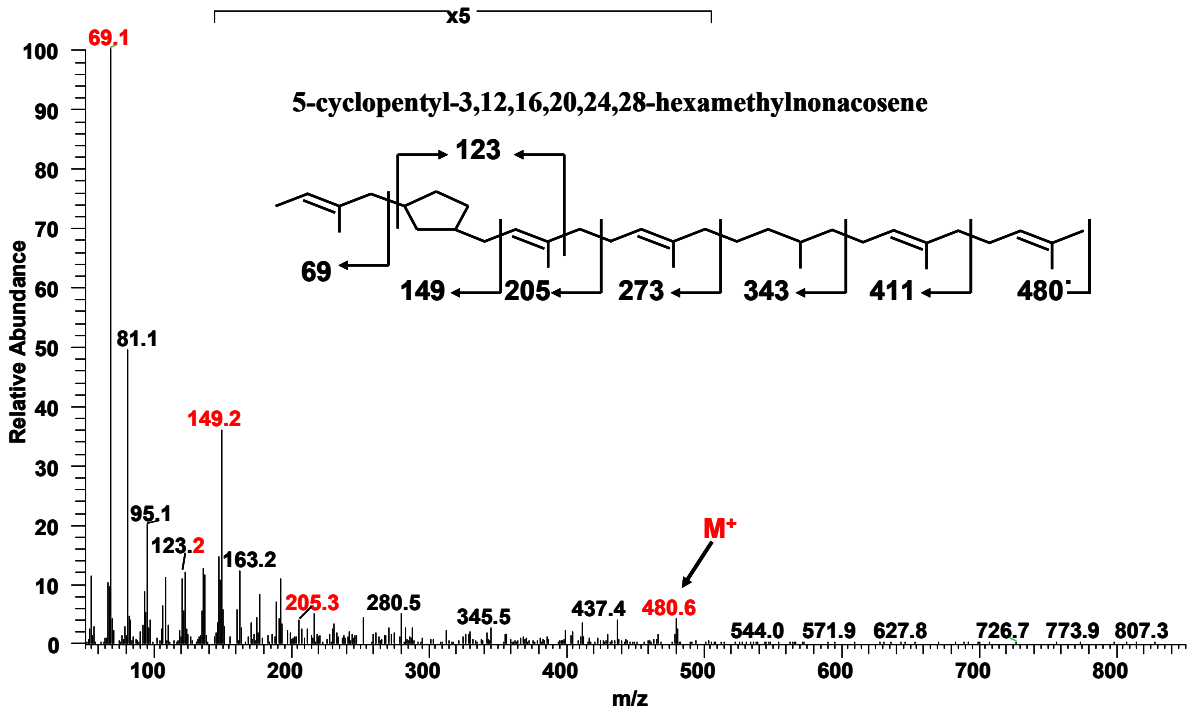

Figure A.7c: Spectrum of the C_{35}-isoprenoid hydrocarbon isomer $C_{35:6}$e with five double bonds, bearing one additional pentacyclic ring structure. The spectrum was revealed with a GC-MS in the EI modus with -70 eV.

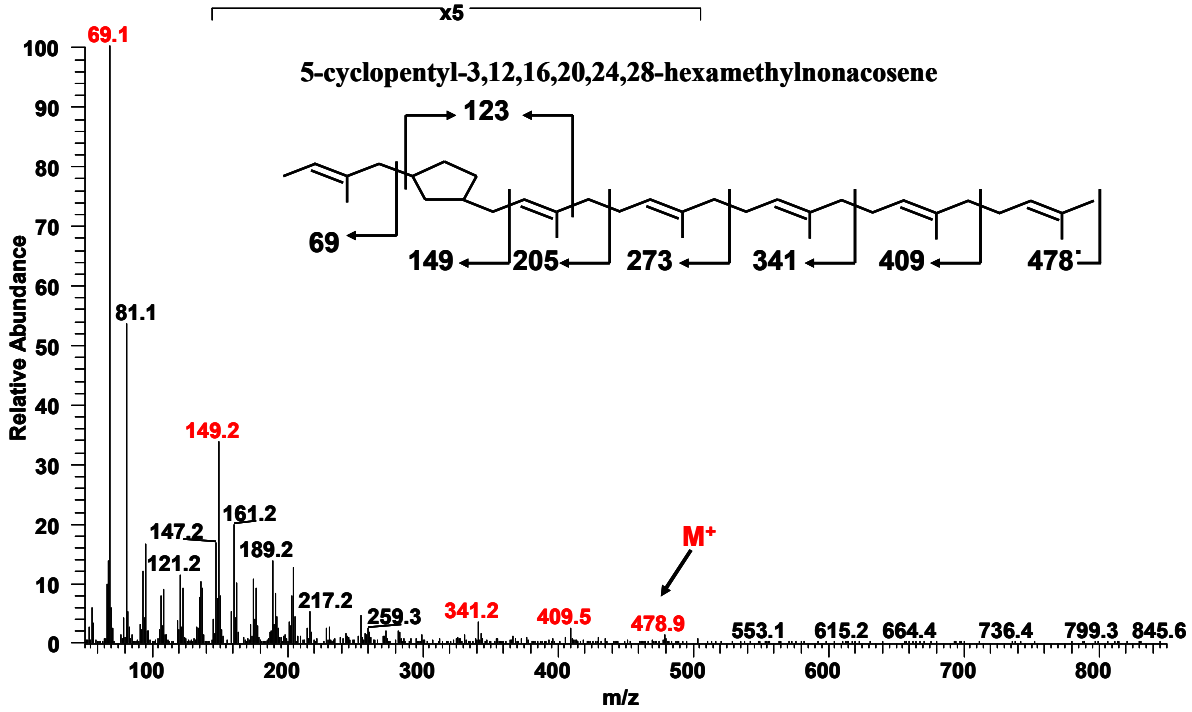

Figure A.7d: Spectrum of the C_{35}-isoprenoid hydrocarbon isomer $C_{35:7}$f with six double bonds, bearing one additional pentacyclic ring structure. The spectrum was revealed with a GC-MS in the EI modus with -70 eV.

A.8 Scheme of traced carbon fluxes within the mat samples

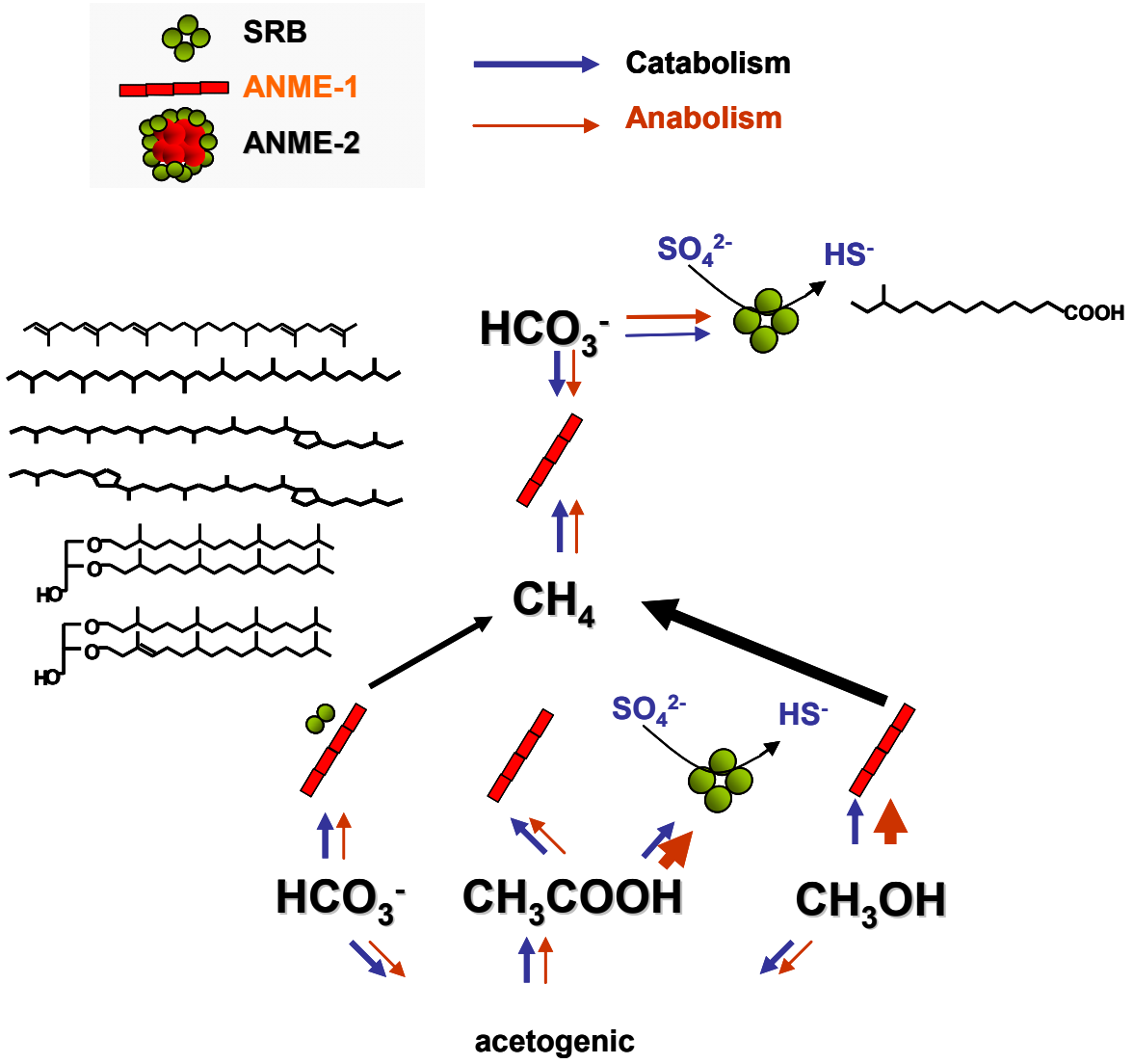

Figure A.8a: Scheme of traced carbon fluxes within the ANME-1 dominated samples. Lipid biomarkers for ANME-1 archaea were the three constitutional isomers of the biphytanes and archaeol, specific lipid for the SRB was the *ai*fa15.
Label experiments with methane demonstrate the methanotrophic metabolism of the ANME archaea and the following uptake of the methane derived ^{13}C after methane oxidation into bacterial lipids. Autotrophic metabolism was measured with labelled bicarbonate. Heterotrophic metabolism was traced with acetate. Methanol was a methylotrophic substrate for the archaea and gives evidence for homoacetogenic metabolism. Methane formation was also determined for the different substrates.

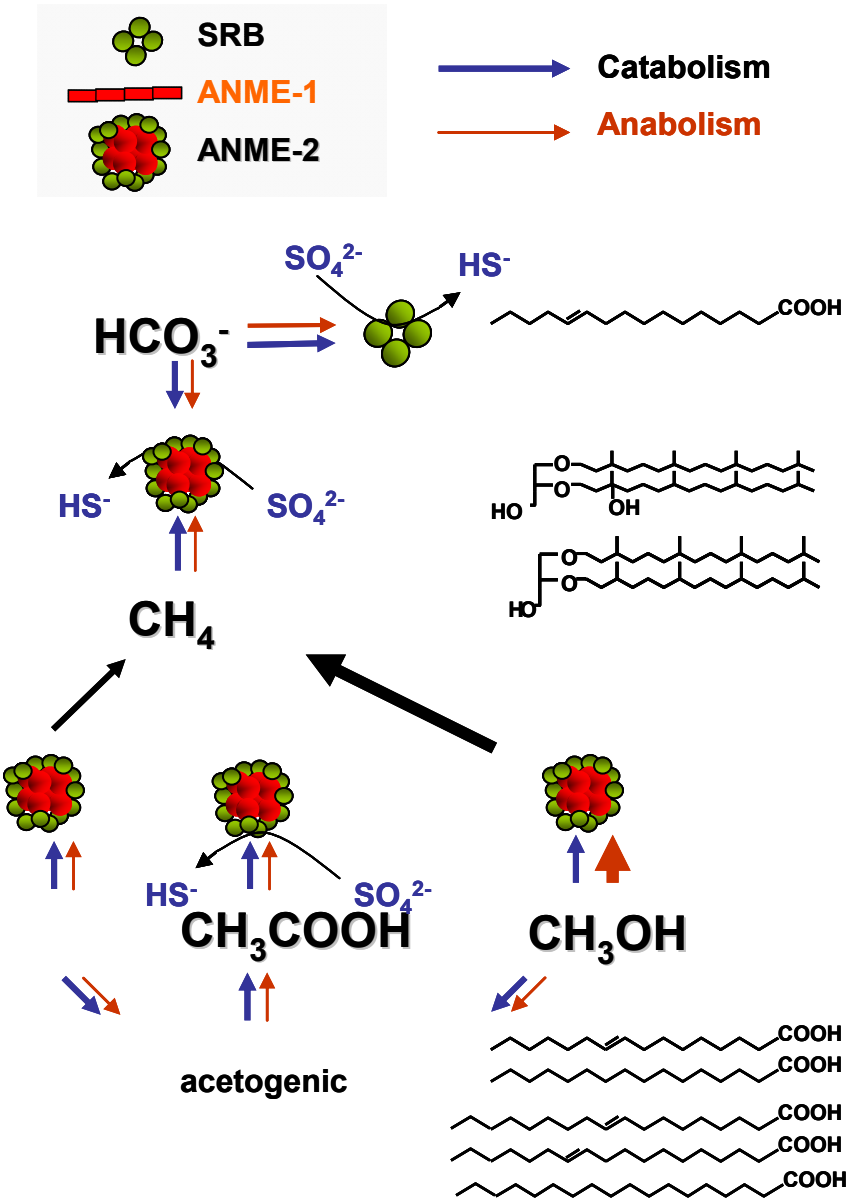

Figure A.8b: Scheme of traced carbon fluxes within the ANME-2 dominated samples. Lipid biomarkers for ANME-2 archaea were archaeol and *sn-2*-hydroxyarchaeol; specific lipid for the SRB was the *cis*-ω5-fa16:1. The *cis*-ω7-fa16:1, fa16:0, *cis*-ω9-fa18:1, *cis*-ω7-fa18:1 and fa18:0 seems to be sourced by methanol fed organisms.
Label experiments with methane demonstrate the methanotrophic metabolism of the ANME archaea and the following uptake of the methane derived ^{13}C after methane oxidation into bacterial lipids. Autotrophic metabolism was measured with labelled bicarbonate. Heterotrophic metabolism was traced with acetate. Methanol was a methylotrophic substrate for the archaea and gives evidence for homoacetogenic metabolism. Methane formation was also determined for the different substrates.

A.9: The biochemistry of ANME-1

The biochemistry, based on the consideration of a reverse methanogenic metabolism with methane (A.9a) and two different methanogenic substrates (A.9b, A.9c) is modelled.

The catabolic (red arrows) and the potential anabolic (green arrows) branch are depicted, influenced by the different substrates. The methane oxidation pathway linked to the methyl-H_4MPT leads to a possible anabolic branch. The methyl group of acetate is transferred by the H_4MPT after the first step in methane oxidation. The Nuo-like complex is most likely involved in the anabolic branch.

The reduction of the CO_2 introduces the CO-group to the acetyl-CoA (Figure A.9a). The possibility that new formed acetate can be a possible electron shuttle under high methane concentrations (Valentine et al., 2002) remains still open. The pathway with methanol as substrates is quite similar (Figure A.9b). Probably, acetate inhibits parts of the anabolic branch, and is introduced into biomass directly via the aceyl-CoA-synthase (Figure A.9c).

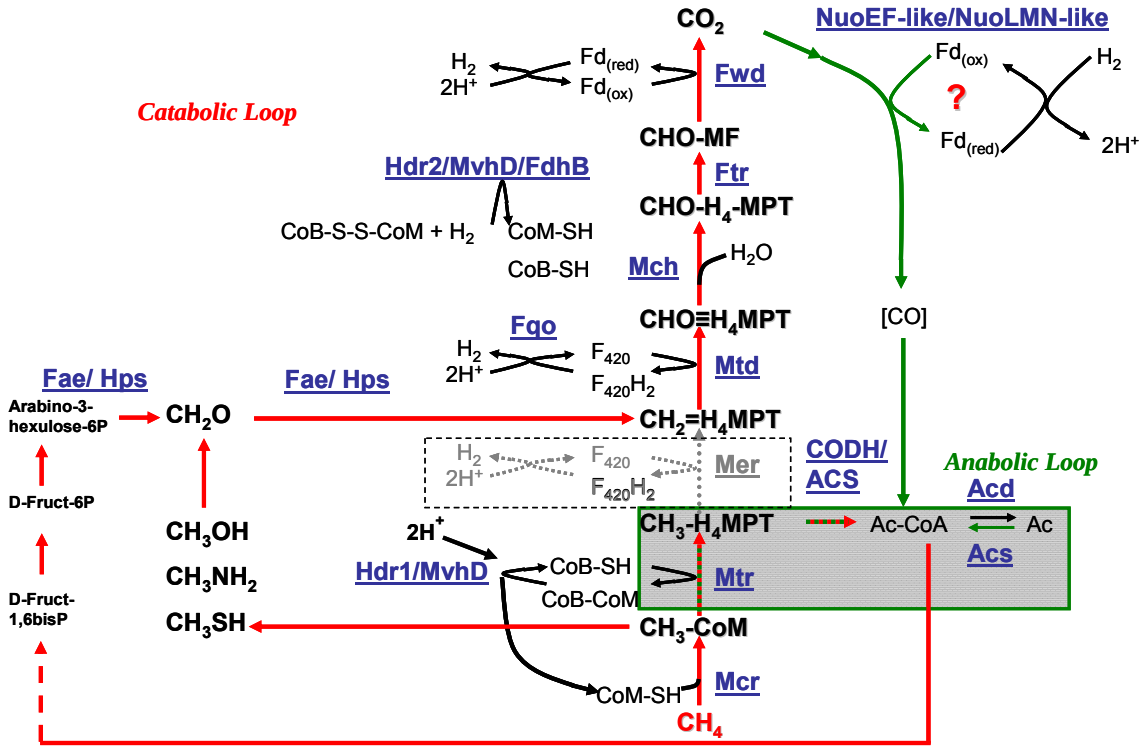

Figure A.9a: The biochemistry of ANME-1 (after Meyerdierks et al., 2009) with methane as substrate; red arrows describe the catabolic relevant pathway, green arrows illustrates the branches of the anabolic pathway.
Ech - energy-converting hydrogenase, Ftr - formylmethanofuran:H_4SPT formyltransferase, Mch - methenyl-H_4SPT cyclohydrolase, Mtd - Methylene-H_4SPT dehydrogenase, Frh - F_{420}-reducing hydrogenase, Mer - methylene-H_4SPT reductase, Mtr - methyl-H_4SPT:HS-CoM methyltransferase, Mcr - methyl coenzym M reductase, Hdr - heterodisulphide reductase, Vho - methanophenazine reducing hydrogenase, Fpo - energy-converting $F_{420}H_2$ dehydrogenase complex, MePH - methanophenazine, Ac - acetate, Ac-Pi - phosphorylated, Ac-CoA - acetyl-coenzym A, Fd_{red} - reduced ferredoxin, Fd_{ox} - oxidised ferredoxin, Fae/ Hps - formaldehyde activating enzyme/ hexulose-6-phosphate synthase, nuo-like NADH:quinone oxidoreductase, HdrI and HdrII - two nucleic acid deduced cytoplasmatic heterodisulphide reductases.

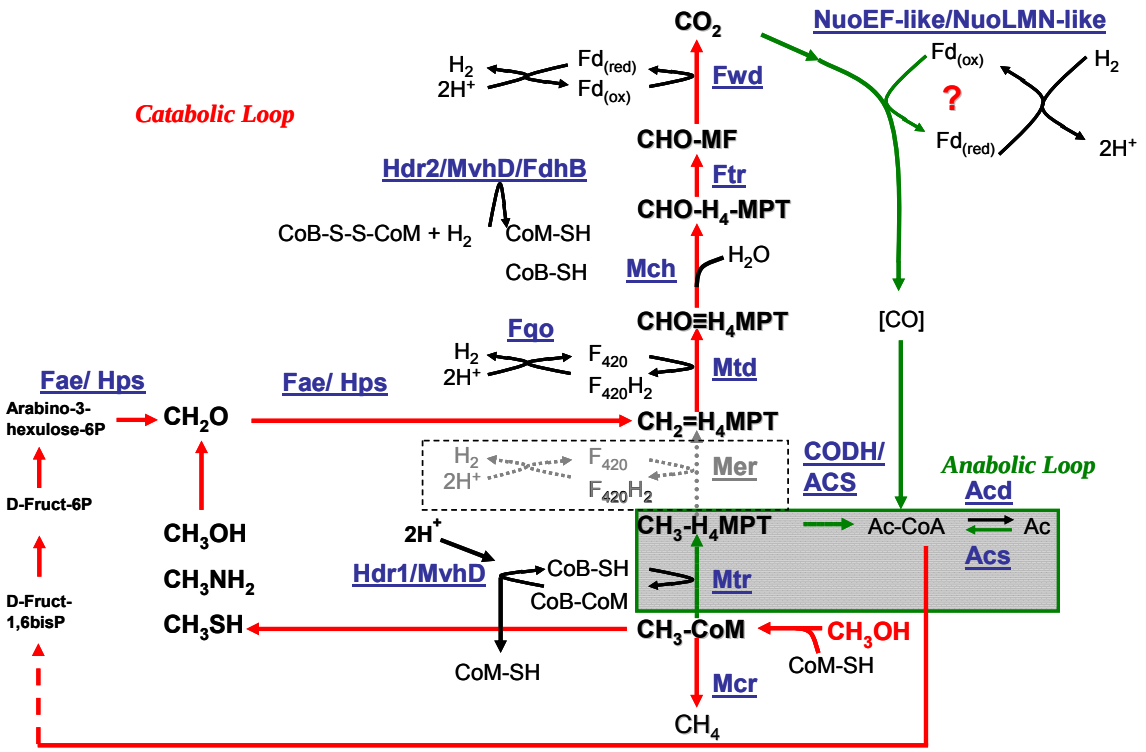

Figure A.9b: The biochemistry of ANME-1 (after Meyerdierks et al., 2009) with methanol as substrate; red arrows describe the catabolic relevant pathway, green arrows illustrates the branches of the anabolic pathway.

Ech - energy-converting hydrogenase, Ftr - formylmethanofuran:H_4SPT formyltransferase, Mch - methenyl-H_4SPT cyclohydrolase, Mtd - Methylene-H_4SPT dehydrogenase, Frh - F_{420}-reducing hydrogenase, Mer - methylene-H_4SPT reductase, Mtr - methyl-H_4SPT:HS-CoM methyltransferase, Mcr - methyl coenzym M reductase, Hdr - heterodisulphide reductase, Vho - methanophenazine reducing hydrogenase, Fpo - energy-converting $F_{420}H_2$ dehydrogenase complex, MePH - methanophenazine, Ac - acetate, Ac-Pi - phosphorylated, Ac-CoA - acetyl-coenzym A, Fd_{red} - reduced ferredoxin, Fd_{ox} - oxidised ferredoxin, Fae/ Hps - formaldehyde activating enzyme/ hexulose-6-phosphate synthase, nuo-like NADH:quinone oxidoreductase, HdrI and HdrII - two nucleic acid deduced cytoplasmatic heterodisulphide reductases.

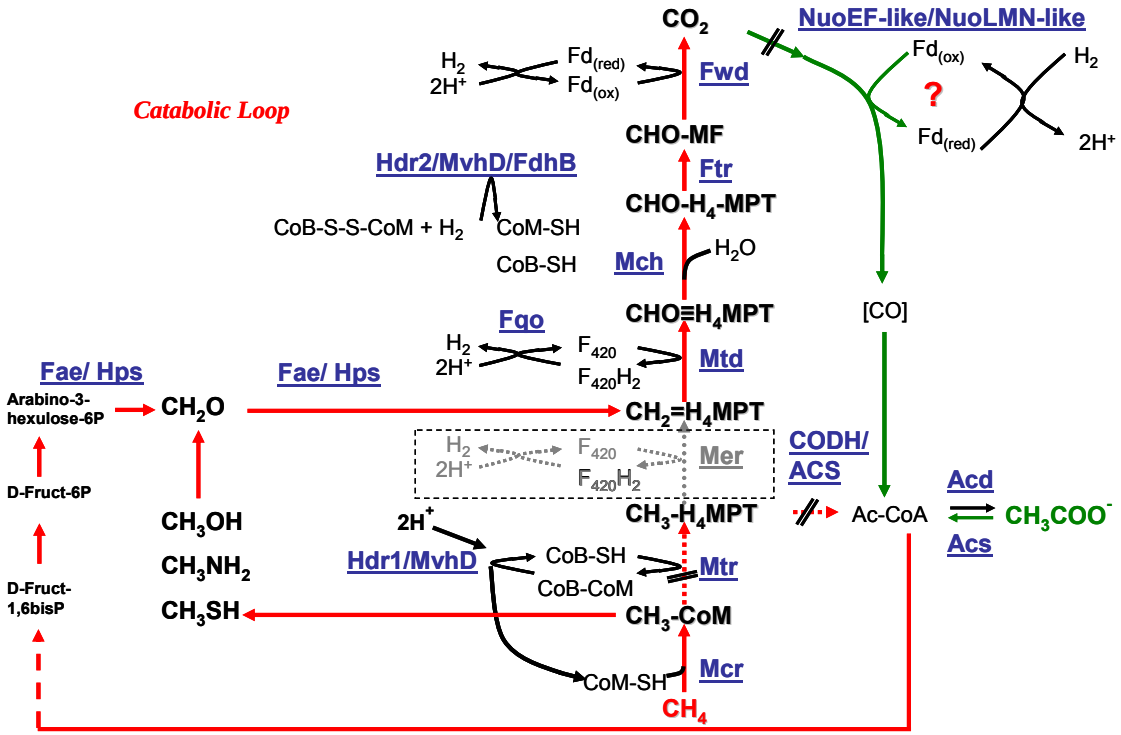

Figure A.9c: The biochemistry of ANME-1 (after Meyerdierks et al., 2009) with methane and acetate as substrates; red arrows describe the catabolic relevant pathway, green arrows illustrates the branches of the anabolic pathway.
Ech - energy-converting hydrogenase, Ftr - formylmethanofuran:H_4SPT formyltransferase, Mch - methenyl-H_4SPT cyclohydrolase, Mtd - Methylene-H_4SPT dehydrogenase, Frh - F_{420}-reducing hydrogenase, Mer - methylene-H_4SPT reductase, Mtr - methyl-H_4SPT:HS-CoM methyltransferase, Mcr - methyl coenzym M reductase, Hdr - heterodisulphide reductase, Vho - methanophenazine reducing hydrogenase, Fpo - energy-converting $F_{420}H_2$ dehydrogenase complex, MePH - methanophenazine, Ac - acetate, Ac-Pi - phosphorylated, Ac-CoA - acetyl-coenzym A, Fd_{red} - reduced ferredoxin, Fd_{ox} - oxidised ferredoxin, Fae/ Hps - formaldehyde activating enzyme/ hexulose-6-phosphate synthase, nuo-like NADH:quinone oxidoreductase, HdrI and HdrII - two nucleic acid deduced cytoplasmatic heterodisulphide reductases.

A.10 Figure captions

A.11 Table captions

A.12 Equations

Acknowledgements/ Danksagung

Zunächst möchte ich Ihnen, Hr. Michaelis für die Bereitstellung und Betreuung dieser interessanten Arbeit danken, sowie für die Möglichkeit anhand der mir gegebenen Aufgabenstellung mich wissenschaftlich und persönlich weiter zu entwickeln und daran zu wachsen. Des Weiteren danke ich Ihnen für das Vertrauen und die Geduld in mich und meine Arbeit.

Ich möchte Dir danken Martin, für die umfangreiche Betreuung, den technischen und fachlichen Beistand und darüber hinaus für vieles mehr am Rande dieser Arbeit.

Vielen Dank Richard, für die vielen hilfreichen und gehaltvollen Diskussionen, die dieser Arbeit sicherlich noch mal eine ganz besondere Qualität verliehen haben. An dieser Stelle sei auch nochmals für die weitere finanzielle Unterstützung, die mir am Ende dieser Arbeit zu Teil wurde, gedankt.

Ralf und Sabine kann ich meinen Dank nur schwer in Worte fassen, für all die technische Hilfestellung bei den manchmal doch schwierigen technischen Herausforderungen an Mensch und Maschine. Frauke danke ich für die Unterstützung bei der Analyse der Bulkproben.

Mirjam Perner danke ich für die Kontaktherstellung, die ja letztlich mir die Teilnahme an diesem Projekt ermöglicht und zu dieser Arbeit geführt hat.

Birte, Arja, Berit, Peggy, Sabrina, Imke, Tanja, Jan, Caesar, Stephan, Sascha, Stefan, Philip, Ingo, Yu, Enno, Frank, sowie allen weiteren Nachbarn auf dem Flur in der 10. Etage möchte ich für das angenehme Arbeitsumfeld sowie eure Unterstützung danken.

Ein besonderer Dank für das Korrekturlesen geht an dich Katy.

Euch, all meinen Freunden, gilt mein größter Dank. Denn Ihr wart immer da. In allen Zeiten gabt Ihr mir den nötigen Rückhalt, aus eurer Freundschaft schöpfte ich immer wieder neuen Mut und neue Kraft, immer wieder bereit zum Optimismus. Vielen Dank!

Ich danke meiner Familie.

Curriculum Vitae

Personal Details

Date of Birth: 12 December 1977

Place of Birth: Dortmund

Education

12 / 2010 - 08 / 2012 Associated member of the (LEXI) Graduate School for C_1-Chemistry in Resource and Energy Management

11 / 2004 - 12 / 2008 University of Hamburg, Biology, Diplom

1. Major subject: Microbiology, **2. Major subject:** Genetics and Molecular Biology

Diplom thesis: Purification and over expression of a new homoserine lactonase from Metagenomics

02 / 2000 - 06 / 2002 Education as hotel specialist at the Hilton Hotel Dortmund

11 / 1997 - 09 / 1999 Ruhr University of Bochum, Biology, undergraduate

08 / 1988 - 05 / 1997 Immanuel-Kant-Gymnasium, secondary school, Dortmund

Professional Experience

05 / 2008 - 08 / 2012 PhD-Candidate, Advisor: Prof. Dr. W. Michaelis, Institute of Biogeochemistry and Marine Chemistry, University of Hamburg

Additional Professional Experiences (Internships)

03 / 2006 - 04 / 2006 Schülke and Mayr, Hamburg, Research and Development, Department BioScience (S2-Laboratory)

Topic: DIN EN 13704 Quantitative suspension test for the evaluation of sporicidal activity of chemical disinfectants used in food, industrial, domestic and institutional areas

Professional Training and Qualifications

05 / 2009 Gerstel user seminar 2009 for GC/MS and LC/MS in Hamburg

10 / 2008 - 03 / 2009 Basic Course in Scanning Electron Microscopy

09 / 2008	Varian, Darmstadt - 1200 LC/ MS Single- and Triple Quadrupol training
10 / 2005 - 03 / 2006	Examined courses in Bioinformatics, MSc level
10 / 2005	Accomplished examination of the 'Eingeschränkte Sachkunde nach § 5 Chemikalien-Verbotsverordnung (BGBI I S. 867)'

Professional Experience outside Science

04 / 2003 - 09 / 2004	Commis de rang in Raffles Hotel Vier Jahreszeiten, Restaurant Jahreszeiten Grill, Hamburg
08 / 2002 - 03 / 2003	Commis de rang in Restaurant Landhaus Scherrer, Hamburg
07 / 2002	Demi chef de rang at Hilton Hotel Dortmund, Restaurant L´Oliva and Rhapsody

Publications

Contributions to Conferences and Meetings

Bertram S, Blumenberg M, Michaelis W, Krüger M, and Seifert R. Tracing carbon fluxes within two distinct microbial mats in anaerobically methane oxidising mats by stable isotope probing. 3rd Summer School - Graduate School C_1-Chemistry in Resource and Energy Management 2012 - Hamburg, Germany (Oral)

Bertram S, Blumenberg M, Michaelis W, Siegert M, Krüger M, und Seifert R. Umsetzung und Bildung von Methan in anaeroben mikrobiellen Lebensgemeinschaften aus dem Schwarzen Meer. New Years Reception and Inauguration of the Graduate School C_1-Chemistry in Resource and Energy Management 2012 - Hamburg, Germany (Poster)

Bertram S, Blumenberg M, Michaelis W, Seifert R, Siegert M, Krüger M. Carbon fluxes in phylogenetically distinct AOM performing microbial consortia. 25th International Meeting on Organic Geochemistry 2011 - Interlaken, Switzerland (oral) - Book of Abstracts, p. 138

Bertram S, Blumenberg M, Seifert R, Siegert M, Krüger M, and Michaelis W. Novelties on the carbon fluxes in different AOM performing microbial consortia. North German Meeting on Organic Geochemistry 2011 - Bremen, Germany (Poster)

Bertram S, Blumenberg M, Seifert R, Siegert M, Krüger M, and Michaelis W. Novelties on the carbon fluxes in different AOM performing microbial consortia. Gordon Research Conference - Geobiology 2011 Ventura, CA, USA (Poster)

Bertram S, Oppermann B I, Blumenberg M, Michaelis W, Krüger M und Seifert R. Rekonstruktion von Kohlenstoffflüssen aus ^{13}C-markierten Substraten in anaerob methanoxidierenden Konsortien. New Years Reception and Inauguration of the Graduate School C_1-Chemistry in Resource and Energy Management 2011 - Hamburg, Germany (Poster)

Bertram S, Siegert M, Blumenberg M, Seifert R, Krüger M, and Michaelis W. Carbon fluxes in different AOM performing microbial consortia. North German Meeting on Organic Geochemistry 2010 - Hamburg, Germany (oral)

Bertram S, Siegert M, Blumenberg M, Seifert R, Krüger M, Michaelis W. Carbon fluxes in anaerobically methane-oxidising microbial mats revealed by Stable Isotope Probing. 3rd VAAM 2010, International Meeting in Hannover, Germany (Poster) - Book of Abstracts, p. 78

Bertram S, Herrlich S, Blumenberg M, Michaelis W und Seifert W. Identifikation von Kohlenstoffflüssen in anaeroben Methan oxidierenden Matten durch Markierungs-experimente mit stabilen Isotopen. New Years Reception and Inauguration of the Graduate School C_1-Chemistry in Resource and Energy Management 2010 - Hamburg, Germany (Poster)

Bertram S, Siegert M, Weitbrecht K, Blumenberg M, Seifert R, Krüger M, Friedrich M W, and Michaelis W. Carbon fluxes in anaerobically methane-oxidising microbial mats revealed by Stable Isotope Probing (SIP). 24th International Meeting on Organic Geochemistry 2009 - Bremen, Germany (Poster) - Book of Abstracts, p. 125

Manuscripts / Articles in Peer-Reviewed Journals

Carbon fluxes within ANME-1 and -2 dominated microbial mat systems from the Black. Bertram S, Blumenberg M, Michaelis W, Siegert M, Krüger M, and Seifert R. - in preparation

Methanogenic capabilities of ANME archaea deduced from ^{13}C-labeling approaches. Bertram S, Blumenberg M, Michaelis W, Siegert M, Krüger M, and Seifert R. - in preparation